Quantitative Magnetic Resonance Spectroscopy of Brain Metabolites and Macromolecules at Ultra-High Field

Dissertation

der Mathematisch-Naturwissenschaftlichen Fakultät

der Eberhard Karls Universität Tübingen

zur Erlangung des Grades eines

Doktors der Naturwissenschaften

(Dr. rer. nat.)

vorgelegt von

Saipavitra Venkateshwaran Murali Manohar

aus Srirangam, Indien

Tübingen

2021

Gedruckt mit Genehmigung der Mathematisch-Naturwissenschaftlichen Fakultät der Eberhard Karls Universität Tübingen.

Tag der mündlichen Qualifikation:	13.08.2021
Dekan:	Prof. Dr. Thilo Stehle
1. Berichterstatter:	Prof. Dr. Anke Henning
2. Berichterstatter:	Prof. Dr. Fritz Schick

Erklärung:

Ich erkläre, dass ich die zur Promotion eingereichte Arbeit mit dem Titel:

“Quantitative Magnetic Resonance Spectroscopy of Brain Metabolites and Macromolecules at Ultra-High Field”

selbständig verfasst, nur die angegebenen Quellen und Hilfsmittel benutzt und wörtlich oder inhaltlich übernommene Stellen als solche gekennzeichnet habe. Ich versichere an Eides statt, dass diese Angaben wahr sind und dass ich nichts verschwiegen habe. Mir ist bekannt, dass die falsche Abgabe einer Versicherung an Eides statt mit Freiheitsstrafe bis zu drei Jahren oder mit Geldstrafe bestraft wird.

Declaration:

I hereby declare that I have produced the work entitled:

“Quantitative Magnetic Resonance Spectroscopy of Brain Metabolites and Macromolecules at Ultra-High Field*”,*

submitted for the award of a doctorate, on my own (without external help), have used only the sources and aids indicated and have marked passages included from other works, whether verbatim or in content, as such. I swear upon oath that these statements are true and that I have not concealed anything. I am aware that making a false declaration under oath is punishable by a term of imprisonment of up to three years or by a fine.

Tübingen, den _____ _____

Datum Unterschrift

Acknowledgements

I am immensely grateful to my research supervisor, Prof. Anke Henning for giving me the opportunity to do this research. This PhD thesis would have never been accomplished without her invaluable guidance, constant support and encouragement over these years. Further, I would to like to thank my co-supervisor Prof. Fritz Schick for his advice and fruitful discussions on the thesis. I would also like to extend my gratitude to Prof. Klaus Scheffler for providing me access to the state-of-the-art facilities of the ultra-high field department and for accepting to be one of the examiners. I am also thankful to Prof. Daniela Thorwarth for being an examiner of the thesis.

I take this opportunity to acknowledge the financial support from the European Union's CDS-QUAMRI and ERC grants. Thanks also to the IT, bureaucratic and administrative support at the Max Planck Institute: Tina, Mihai, Jihen, Katrin, Jacqueline and all the other administrative staff; they all made my PhD life easier.

I am very thankful to all my former and current colleagues and friends at the Max Planck Institute. My heartfelt thanks to Andreas, Ioannis, Andrea, Tingting, Sahar, and, Paul: I learnt a lot from them in the initial years of my PhD. I am extremely grateful to Tamas and Andrew for their huge support both personally and at work; and for some of the best scientific discussions I had during my PhD. I wish to express my thanks to Nikolai, Ole, Johanna, Theresia, and Loreen who were always there – be it technical support, or as a co-pilot for scans, or for a nice little chat.

Getting through my dissertation required more than academic support, and I have many people to thank for being with me throughout. I would like to thank Oliver Burkhardt, Lena and Andreas Herpich who opened both their home and heart to me when I first arrived in Tuebingen. I cannot begin to express my gratitude and appreciation for the friendship of Andrew and Nicole and for the memorable times spent together.

Most importantly, none of this could have happened without my supportive family. To my mother and my husband – it would be an understatement to say that, as a family, we have experienced some vicissitudes; you both were always by my side, and I am forever grateful for your unceasing encouragement. To my father who would have loved to see me in the position where I am today, I am forever indebted.

Abbreviations, symbols, and units

AFP	Adiabatic full passage
BPP theory	Bloembergen-Purcell-Pound theory
^{13}C	Carbon
CSF	Cerebrospinal fluid
CSD	Chemical shift displacement
DF	Downfield
DIR	Double inversion recovery
DANN	Deoxyribonucleic Acid
FAST(EST)MAP	Fast, automatic shim technique using echo-planar signal readout using mapping along projections
FID-MRSI	Free induction decay – magnetic resonance spectroscopic imaging
GM	Gray matter
^{1}H	Proton
IR	Inversion recovery
LASER	Localization by adiabatic selective refocusing
MC	Metabolite cycling
MM	Macromolecule
MRI	Magnetic resonance imaging
MRS	Magnetic resonance spectroscopy
NMR	Nuclear magnetic resonance
^{31}P	Phosphorus
PRESS	Point resolved spectroscopy
RF	Radiofrequency
RNA	Ribonucleic Acid
SAR	Specific absorption rate
semiLASER	semi localization by adiabatic slice selective refocusing
SNR	Signal-to-noise ratio
SPECIAL	Spin echo full intensity acquired localized
STEAM	Stimulated echo acquisition mode
1D	One dimensional

2D	Two dimensional
3D	Three dimensional
$\boldsymbol{B_0}$	Static magnetic field
B_1^+	RF transmit field
δ	Chemical shift
FWHM	Full width at half maximum
$\boldsymbol{\gamma}$	Gyromagnetic ratio
h	Planck's constant
Hz	Hertz
$\boldsymbol{I}$	Nuclear spin angular momentum
kg	Kilogram
mmol	Millimoles
m	Magnetic quantum number
MHz	Mega Hertz
ms	Milliseconds
$\boldsymbol{\mu}$	Magnetic moment
ppm	Parts per million
σ	Shielding constant
T	Tesla
T_1	Longitudinal relaxation time
T_2	Transversal relaxation time
TE	Echo time
TI	Inversion time
TR	Repetition time
T_2^{eff}	Effective transversal relaxation time
$\boldsymbol{\tau}$	Torque
UHF	Ultra high field
WM	White matter
$\boldsymbol{\omega_o}$	Larmor frequency

Abstract

Proton magnetic resonance spectroscopy (^{1}H MRS) in the human brain is a non-invasive technique capable of aiding the investigation of the neurochemical composition. The clinical importance of ^{1}H MRS can be seen in pathological diagnosis, understanding disease mechanisms or in treatment monitoring.

Reliable detection and quantification of metabolites is of paramount importance in establishing potential biomarkers for several neurological pathologies. Furthermore, broad macromolecular resonances underlying metabolite peaks in a proton spectrum also hold a wealth of information. These macromolecular resonances originate from amino acids within cytosolic peptides and proteins. Some studies in the past have even discussed their clinical relevance in pathologies such as acute multiple sclerosis, glioma, and traumatic encephalopathy. However, the characteristics of these macromolecular resonances are yet to be fully explored. In-depth knowledge about the macromolecules could open up a new horizon of potential biomarkers for neurological diseases. In addition, characterizing macromolecular resonances may help the MR community answer some of the lingering research questions such as identifying the biological background of the individual macromolecular peaks, assigning macromolecular peaks to particular amino acids, and investigating other contributions to the macromolecular signal such as sugars, DNA or RNA.

Detection capabilities of MRS have increased to a great extent with increasing static magnetic field. Ultra-high field (≥7 T) MRS benefits from increased signal-to-noise ratio (SNR) and improved spectral resolution. There is also constant development in localization techniques and quantification methods to accurately measure concentrations of metabolites and macromolecules with lower signal-to-noise ratio and complex spectral pattern due to J-coupling.

The first part of the thesis focuses on characterizing the physical properties of macromolecular resonances in the human brain at 9.4 T and understanding their contribution to the metabolite spectrum. T_2 relaxation times are calculated and a quantitative linewidth analysis is performed to understand the degree of overlap and J-

coupling effects in the observed macromolecular peaks. Moreover, a novel double inversion recovery method is proposed to determine T_1 relaxation times of individual macromolecular resonance lines.

The second part of the thesis focuses on quantification of metabolites in the human brain at 9.4 T using one-dimensional and two-dimensional MRS techniques. Metabolite concentrations are reported in millimoles/kg after correcting for T_1- and T_2-weighting effects and the tissue composition. The concentration values measured from both the acquisition techniques were compared against each other and to literature.

Zusammenfassung

Die Protonen-Magnetresonanzspektroskopie (^{1}H-MRS) ist eine nicht-invasive Technik, die die Untersuchung der neurochemischen Zusammensetzung des menschlichen Gehirns ermöglicht. Bedeutende klinische Anwendungen von ^{1}H-MRS ergaben sich in der Diagnose von Erkrankungen, in dem Verständnis von Krankheitsmechanismen oder in der Behandlungsüberwachung.

Die zuverlässige Erkennung und Quantifizierung der Metaboliten ist von größter Bedeutung, um Biomarker für verschiedene neurologische Krankheiten zu etablieren. Zusätzlich enthalten Makromoleküle, die in dem Protonen-Spektrum breite Spektrallinien unter dem Metaboliten-Spektrum bilden, zahlreiche, wertvolle Informationen. Die Spektrallinien der Makromoleküle stammen von Aminosäuren aus Proteinen und Peptiden des Cytosols. Frühere Studien haben die klinische Relevanz von Makromolekülen in Erkrankungen wie Multiple Sklerose, Tumoren oder chronisch-traumatische Enzephalopathie gezeigt. Jedoch müssen mehrere Charakteristiken der Makromoleküle noch erforscht werden. Ein tiefgehendes Verständnis der Makromoleküle könnte dabei die Entdeckung neuer Biomarker für neurologische Krankheiten ermöglichen. Zusätzlich kann die Charakterisierung der makromolekularen Spektrallinien helfen folgende offene Fragen der MR Spektroskopie zu beantworten: den biologischen Ursprung der einzelnen makromolekularen Spektrallinien, die Zuordnung der makromolekularen Spektrallinien zu einzelnen Aminosäuren sowie die Untersuchung von anderen möglichen Beiträgen zum Signal der Makromoleküle wie z.B. verschiedene Zucker, DNA oder RNA.

Die Sensitivität von MRS wurde durch stärkere Magnetfelder erheblich verbessert. MRS Messungen am Ultrahochfeld (≥7 T) profitieren von einem höheren Signal-Rausch-Verhältnis und einer höheren spektralen Auflösung. Zusätzlich wurden Lokalisierungsmethoden und Quantifizierungsmethoden weiterentwickelt, die es ermöglichen, die Konzentrationen auch der Metaboliten und Makromoleküle akkurat zu bestimmen, die ein kleines Signal-Rausch-Verhältnis haben oder komplexere spektrale Muster aufgrund von J-Kopplung aufweisen.

Im Fokus des ersten Teils dieser Doktorarbeit steht die Charakterisierung der physikalischen Eigenschaften der makromolekularen Spektrallinien und die Frage, wie diese das Metaboliten-Spektrum beeinflussen. Dazu wurden Spektren am 9.4 T im menschlichen Gehirn aufgenommen, um hiermit T_2 Relaxationszeiten zu bestimmen bzw. Linienbreiten quantitativ zu analysieren. Diese Analysen liefern Erkenntnisse über die spektrale Überlappung und J-Kopplungseffekte, die man in den makromolekularen Spektrallinien beobachtet. Zusätzlich wird eine neue „double inversion recovery“ Methode vorgestellt, um damit die T_1 Relaxationszeiten von einzelnen makromolekularen Spektrallinien zu bestimmen.

Der zweite Teil dieser Doktorarbeit beschäftigt sich mit der Quantifizierung von den Metaboliten des menschlichen Gehirns am 9.4 T mittels ein- und zweidimensionaler MRS Methoden. Die Konzentrationen der Metaboliten werden in mmol/kg berichtet. Hierbei wurden T_1- und T_2-Gewichtungen korrigiert sowie die Zusammensetzung des gemessenen Gewebes berücksichtigt. Die resultierenden Konzentrationen, die mittels der zwei Methoden gemessen wurden, werden untereinander sowie mit weiterer Literatur verglichen.

Contents

1 Synopsis

1.1 Introduction

Nuclear magnetic resonance (NMR) spectroscopy is a sought-after technique often used to understand the three-dimensional structure of molecules, to determine concentrations of certain molecules present in a complex mixture or to observe chemical reactions and binding of different components to each other. It is used in a wide range of applications including chemistry, medicine, geology, biology and so on.

An atomic nucleus, composed of protons and neutrons, possesses certain important physical properties such as mass, electric charge, magnetism and spin. Out of these physical properties, the NMR technique exploits nuclear magnetism and nuclear spin. The nucleus in a strong external static magnetic field is perturbed by a weak oscillating magnetic field. Resonance occurs when the frequency of the oscillating field matches the frequency of the nucleus that depends on the static magnetic field strength, chemical environment of the nucleus, and magnetic properties of the nucleus. The energies absorbed correspond to the radiofrequency (RF) part of the electromagnetic spectrum.

Extending the application of NMR to in vivo tissues, single voxel magnetic resonance spectroscopy (MRS) allows for non-invasive detection and quantification of the concentrations of neurochemicals and metabolites in biological tissues. More specifically, the complex biochemical changes contributing to metabolism in the human brain tissues are extremely intriguing. MRS enables both neuroscientific and clinical researchers to understand the metabolic processes in the in vivo healthy human brain, respective changes in case of pathological conditions and during treatment monitoring.

This chapter focuses on familiarizing with the most important concepts of NMR/MRS and concludes with introducing the primary goals of this thesis. The introductory chapter attempts to cover only the basic concepts of NMR/MRS that would aid in understanding the scientific work presented here. For a more thorough explanation of the NMR/MRS spin physics in classical and quantum mechanical perspectives and for the derivations of

the equations used, referring to the textbooks by de Graaf[1], Keeler[2], and Levitt[3] is suggested.

1.1.1 Larmor frequency

An intrinsic property possessed by the nucleus is angular momentum. The nuclear spin angular momentum ($\boldsymbol{I}$) is often denoted as nuclear spin. It is a vector quantity with both magnitude and direction. According to quantum mechanics, angular momentum is quantized.

Protons and neutrons have $I = 1/2$. Nuclei with even numbers of both protons and neutrons have $I = 0$ whereas nuclei containing odd number of both protons and neutrons have $I = 1$. For the other nuclei with odd-even or even-odd numbers of protons and neutrons respectively have half integral values of I. When nuclei have $I = 0$, the nuclei are said to be NMR silent. However, the nuclei are said to be NMR active when I has half-integral or integral values. Out of these nuclei, the NMR behavior of the half-integral nuclear spins is easier to understand and detect because of their spherically distributed electric charge.

Each nuclear spin is associated with a nuclear magnetic moment $\boldsymbol{\mu}$**.** When placed in an external static magnetic field ($\boldsymbol{B_0}$) $\boldsymbol{\mu}$ experience a torque (r) and precess about the $\boldsymbol{B_0}$ axis at a frequency given by

$$m_0 = -\gamma \boldsymbol{B_0} \qquad (1)$$

where m_0 is the angular frequency, famously known as the Larmor frequency, and γ the gyromagnetic ratio which is a constant for a given nucleus. Figure 1 shows a proton spin precessing around an external static magnetic field $\boldsymbol{B_0}$.

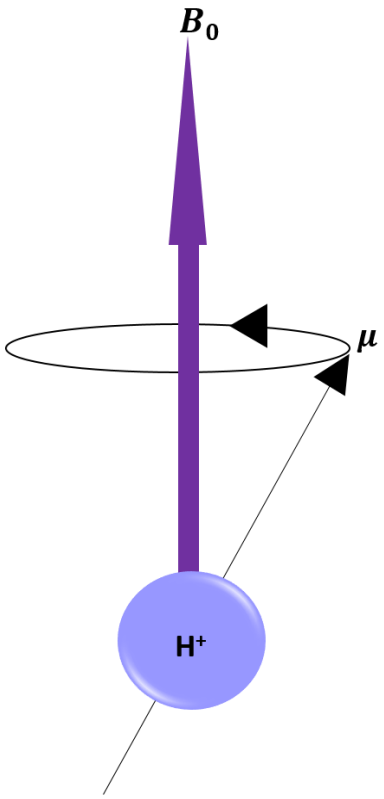

Figure 1: *A proton spin precessing in an external magnetic field* $\boldsymbol{B_0}$*. The Larmor frequency* m_0 *is proportional to* $\boldsymbol{B_0}$*. Gyromagnetic ratio* γ *of a proton is positive; therefore, it undergoes a negative precession according to Equation 1.*

For in vivo MRS, detection of metabolically valuable and MR-visible nuclei such as ^{1}H, ^{13}C and ^{31}P are feasible. Among them proton (^{1}H) MRS is quite a popular technique due to the high natural abundance (>99.9%) of proton nucleus and its high γ and thus sensitivity. Therefore, ^{1}H MRS allows for the detection of a large number of brain metabolites.

1.1.2 Energy levels

In general, spectroscopy techniques exploit the energy difference between quantized energy states and detect the frequency absorbed by the object. The number of nuclear spin states for nuclear spin I is given by $2I + 1$. In the absence of external field, the nuclear spin states are degenerate. However, for example, in the presence of an external magnetic field, the nuclear spin states have different energies. This is called the Zeeman

effect and the splitting of the energy levels in the presence of a magnetic field is known as Zeeman splitting.

Considering proton ($I = 1/2$), there are two possible energy levels corresponding to the two nuclear spin states. These two spin states are known as parallel or spin-up (α) and anti-parallel or spin-down (β) depending on their orientation with the external magnetic field. This is illustrated in Figure 2.

Borrowing concepts from quantum mechanics, the energy corresponding to the magnetic quantum states are given by

$$E_m = -m \frac{h}{2\pi} \gamma B_0 \qquad (2)$$

where m is the magnetic quantum number and can take $2I + 1$ values between $-I$ and $+I$ in steps of 1.

More specifically, in NMR electromagnetic waves in the RF range of 10-800 MHz are absorbed by the spins when there is an induced energy difference created by the external static magnetic field ($\boldsymbol{B_0}$) in a nucleus between the parallel and anti-parallel nuclear spin states. This energy difference ΔE between the quantized states is given by the Planck relation:

$$\Delta E = h\nu \qquad (3)$$

where h is the Planck's constant and ν is the absorbed frequency.

The energy of a magnetic dipole moment $\boldsymbol{\mu}$ when placed in an external static magnetic field is given by

$$E = -\boldsymbol{\mu}.\boldsymbol{B_0} = -\mu B_0 \cos\theta \qquad (4)$$

where θ is the angle between $\boldsymbol{\mu}$ and $\boldsymbol{B_0}$. Therefore, E is minimum when $\theta = 0°$ and maximum when $\theta = 180°$. Therefore, classically speaking E can take any value between $+\mu B_0$ to $-\mu B_0$ since $\boldsymbol{\mu}$ can assume any orientation between $0°$ and $180°$. However, it is not true since the resonance condition for magnetic resonance spectroscopy cannot be

derived that way. Therefore, a quantum mechanical treatment is necessary ($\Delta E = h\nu$). That way it can be explained why the angle θ between $\boldsymbol{\mu}$ and $\boldsymbol{B_0}$ is also quantized.

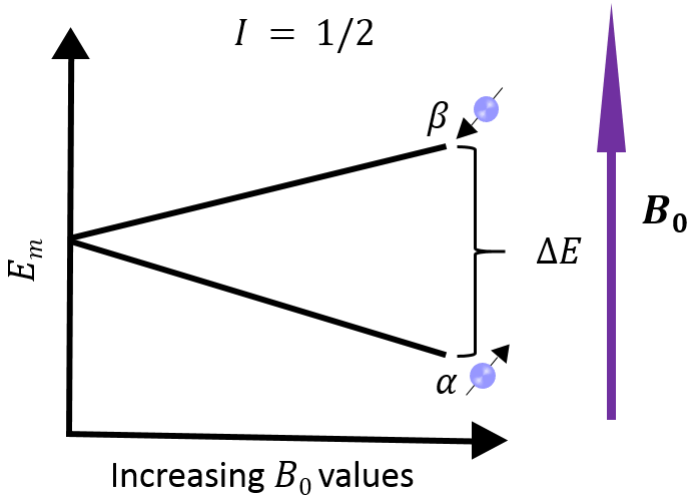

Figure 2: *Spin energy level diagram for a proton ($I = 1/2$). Therefore, there are two possible magnetic quantum numbers (m = -1/2, +1/2) and therefore two possible energy states corresponding to m. The energy level difference between the two spin states α and β corresponds to energy in the RF range.*

When the spin transitions from $m = +1/2$ (α) to $-1/2$ (β) state (Figure 2), the energy difference is given by

$$\Delta E = \gamma \frac{h}{2\pi} B_0 \qquad (5)$$

Therefore, the resonance occurs when

$$\nu = \frac{\gamma}{2\pi} B_0 \qquad (6)$$

with ν being the Larmor frequency in Hz. The resonance condition is satisfied by applying RF energy equal to the Larmor frequency, which is then absorbed by the spins. This will result in a resonance line in the nuclear magnetic resonance spectrum at the given frequency ν.

Moreover, cosine of the angle between $\boldsymbol{\mu}$ and $\boldsymbol{B_0}$ is given by

$$\cos\theta = \frac{m}{\sqrt{I(I+1)}} \qquad (7)$$

which indicates θ = 54.75° relative to the z-axis for protons (I = 1/2). This means that the protons are distributed on the surface of the two cones (with $\boldsymbol{\mu}$ parallel or anti-parallel to $\boldsymbol{B_0}$) rotating about the static field $\boldsymbol{B_0}$ at ν. We have seen that the energy of interaction between the magnetic moment of the nucleus and the external static magnetic field ($\boldsymbol{B_0}$) is dependent on the angle θ between them (Equation 4). Therefore, in order to have the preferred minimum energy the spins align with the applied field. The population difference between the two spin states is given by the Boltzmann equation[1].

The nuclear spin angular momentum can point in any possible direction and the direction of the spin angular momentum is known as the spin polarization. For nuclei with $\gamma > 0$ (such as ^{1}H), magnetic moment $\boldsymbol{\mu}$ of the nucleus points in the same direction as the spin polarization and for nuclei with $\gamma < 0$, magnetic moment of the nucleus points in the opposite direction to the spin polarization. In the absence of an external magnetic field, the magnetic moments in a sample point in all possible directions. However, despite the random thermal motion of the molecules, the magnetic moments are aligned over time in such a way that the average over the sample is parallel to the external magnetic field. This is represented by a bulk magnetization vector denoted by $\boldsymbol{M}$ which is the sum of all magnetic moments. There are slightly more spins aligned parallel to the magnetic field than anti-parallel to the field making the total net magnetization the so-called macroscopic magnetization - parallel to the static magnetic field. Since there is no net component along the transverse XY plane, the net macroscopic magnetization is parallel to +Z-axis and is called the longitudinal magnetization $\boldsymbol{M_0}$.

An RF transmitter/receiver system (transceiver) is used for generating an oscillating magnetic field ($\boldsymbol{B_1}$) along the XY-plane. This results in the initial longitudinal magnetization $\boldsymbol{M_0}$ experiencing a torque. Hence, the macroscopic magnetization vector rotates towards the transverse XY-plane in the case of a 90° excitation RF pulse or rotates towards the antiparallel state –Z in the case of a 180° inversion RF pulse. At this point, the external magnetic field $\boldsymbol{B_0}$ acts on the nuclear spins in order to attain a phase

coherence between a large number of spins in the sample under investigation resulting in a detectable net transverse magnetization $\boldsymbol{M_{XY}}$. This magnetization rotates about the $\boldsymbol{B_0}$ field at Larmor frequency inducing an electromotive force (emf) in the receiver coil, thereby detecting the NMR/MRS signal.

1.1.3 Chemical shift

Depending on the chemical environment of the nucleus, the effective magnetic field experienced by the spin of the nucleus is given by $\boldsymbol{B}$ is not the same as the external magnetic field $\boldsymbol{B_0}$ (Figure 3).

$$\boldsymbol{B} = \boldsymbol{B_0}\,(1 - \sigma) \qquad (8)$$

In this equation σ is known as the shielding constant.

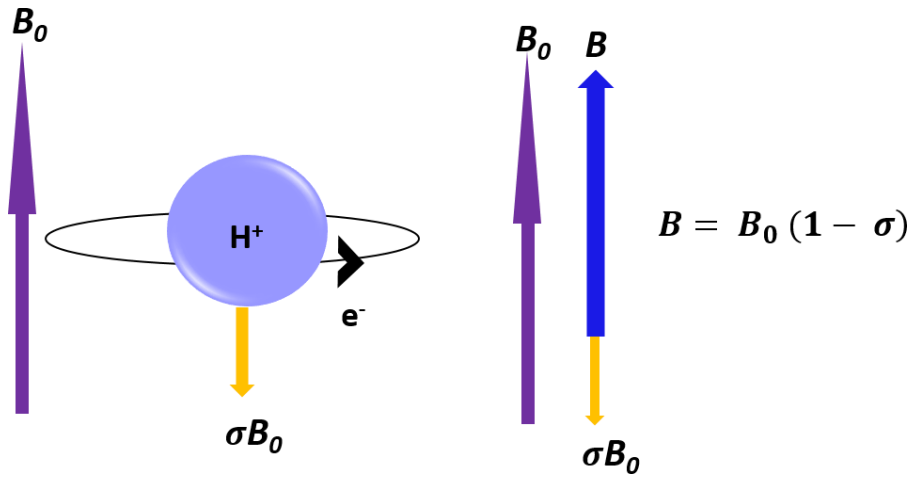

Figure 3: *A proton is shielded by the electron orbital thereby making it experience not* $\boldsymbol{B_0}$*, but a slightly lower field strength* $\boldsymbol{B}$*.*

Therefore, the resonance condition becomes

$$\nu = \gamma \frac{h}{2\pi} B_0\,(1 - \sigma) \qquad (9)$$

The resonance frequency not only depends on the gyromagnetic ratio and external static magnetic field, but also on the chemical environment of the nucleus. This is termed as chemical shift. As an example, a more shielded proton will experience a larger $\sigma \boldsymbol{B_0}$, therefore a lower field $\boldsymbol{B}$. This results in a decrease in the difference between the energy states α and β. Consequently, it gives rise to a signal in the lower frequency range. On the other hand, a more deshielded proton results in a signal in the higher frequency range. In a ^{1}H MRS spectrum, protons from aliphatic chains resonate at lower frequencies (upfield); and protons that belong to aromatic rings, amide or amine groups resonate at higher frequencies (downfield) as shown in Figure 4.

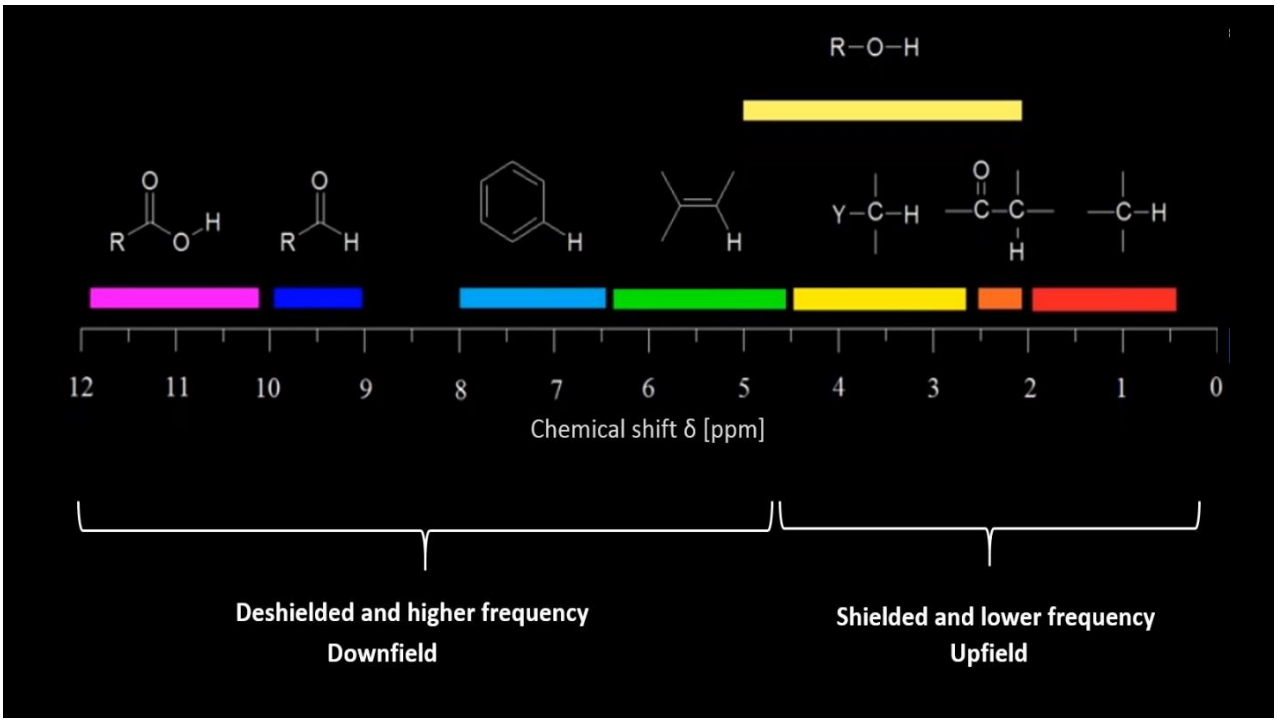

Figure 4*: A proton spectral range from 0 to 12 ppm is depicted here with aliphatic chains resonating at lower frequency (upfield) and aromatic rings, amide or amine groups resonating at higher frequency (downfield). Two protons belonging to the water molecule resonate close to 4.7 ppm. The ppm scale is preferred for plotting NMR/MRS spectra as it is field strength independent which makes the proton spectrum of a particular sample comparable across different field strengths. (Courtesy: American Medical Colleges and Khan Academy, www.khanacademy.org CC BY-NC-SA 3.0)*

From Equation 9 it can be observed that the resonance frequency ν is dependent on external static magnetic field B_0. So comparing NMR spectra across different field strengths becomes tedious when the chemical shift is expressed in hertz (Hz). In order to avoid the field strength dependence, chemical shift scale in parts per million (ppm) was introduced. The chemical shift scale requires a reference compound such as 2.2-dimethyl-2-silapentane-5-sulfonate (DSS) whose chemical shift has been assigned chemical shift $\delta = 0$ ppm.

The position of a peak in a spectrum is taken as the frequency separation between the peak of interest and reference peak divided by the frequency of the reference peak. Chemical shift δ in ppm is therefore defined as

$$\delta = \frac{\nu - \nu_{ref}}{\nu_{ref}} \times 10^6 \qquad (10)$$

where ν is the resonance frequency of a spectral line representing the molecule of interest and ν_{ref} is the frequency of a spectral line from a reference compound. Traditionally, the lower frequency resonances are displayed to the right of the water resonance (known as upfield) in the ^{1}H MRS spectrum and higher frequency resonances to the left of the water resonance (known as downfield) in the spectrum (Figure 4).

1.1.4 J-coupling

J-coupling or scalar coupling is a phenomenon that occurs as a result of indirect magnetic interaction between two nuclei and their spins which is brought about by the electron spins contributing to the chemical bonds between the nuclei. The effect can be seen in the spectrum as splitting of peaks into multiplets in the NMR spectrum. The spacing between the peaks in the multiplet is given by the coupling constant J. The J-coupling constant is independent of the external magnetic field and is reported in Hz.

The hyperfine interactions between the nuclear spin and the electron spin is governed by Fermi contact. The s-electrons play a significant role in this interaction since they have a finite probability of being at the nucleus. According to Fermi contact, the nuclear and the electron spins favor an anti-parallel arrangement. Therefore, four nuclear spin

combinations (and hence four corresponding energy levels) are possible for a coupled spin system containing two nuclei as shown in Figure 5. Introducing Pauli exclusion principle which states that two or more fermions (particles with half integral spins) cannot occupy the same quantum state within a same quantum system. Therefore, the interacting bonding electrons need to be antiparallel. These rules influence the energy level of the coupled spin system resulting in changes in the energy levels. Compared to energy levels of a non-coupled spin system, in a coupled system, high-energy $\beta\beta$ state is energetically less favorable. Therefore, there is an increase in the energy level of $\beta\beta$ state. Similarly, there is an increase in the energy level of the $\alpha\alpha$ state. $\alpha\beta$ and $\beta\alpha$ states have antiparallel electron spins leading to more favorable with a decrease in their energy levels. A more thorough explanation of the energy levels is given in the text book by de Graaf[1].

The multiplicity of the peak is given by the $n + 1$ empirical rule where n is the number of hydrogens attached to the immediate neighboring carbon atom. It means that the number of line splitting of a peak can be predicted as one more than the number of hydrogens attached to the immediately neighboring carbon atom. Additionally, the relative heights of the subpeaks are given by the binomial coefficients of Pascal's triangle.

There is a rapid decrease in the J-coupling effect with increasing number of bonds and the effect can be ignored for four or more bonds. Considering an AX spin system where A and X are two coupled nuclei, if $|\nu_A - \nu_X| \gg J_{AX}$ then the system is known as a weakly coupled system. The spectrum corresponding to a weakly coupled system is known as a first-order spectrum. If the frequency difference is about the same order as the coupling constant J_{AB}, then the spin system AB where A and B are two coupled nuclei is known as a strongly coupled system. In such a spin system, $\alpha\beta$ and $\beta\alpha$ spin states are mixed leading to more complicated spectral pattern since both peak intensities and frequencies are perturbed. The outer peaks are lesser in amplitude and in the so-called roof effect with an imaginary roof forming from the outer to inner resonances. These spectra are also referred to as second-order spectra. Since J-coupling is field strength independent, higher external static magnetic field improves the spectral dispersion and reduces strong coupling effects thereby simplifying second-order spectral pattern.

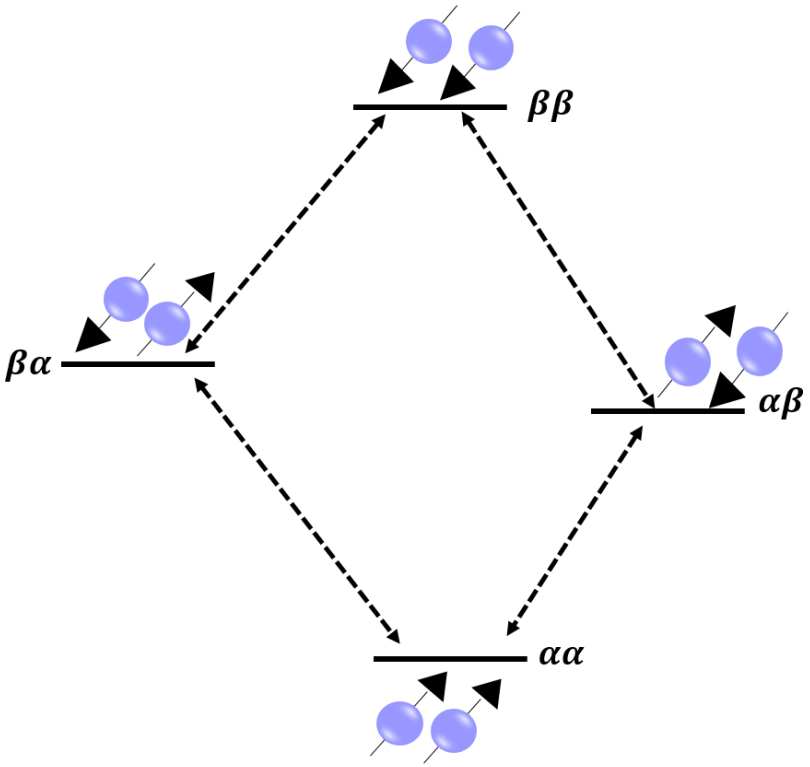

Figure 5: *In an uncoupled spin system, there are two possible energy states corresponding to parallel and anti-parallel spin states as shown in Figure 2. Here* ***t****he figure shows energy level diagram of a weakly coupled AX spin system. There are four possible combinations of parallel and anti-parallel spin states for both nuclei which correspond to four different energy levels. Four transitions are allowed with respect to spin quantum number* $m = \pm 1$ *(single quantum coherences). Therefore, the corresponding spectrum would contain four resonance lines at* $\nu_A + J_{AX}/2$, $\nu_A - J_{AX}/2$, $\nu_X + J_{AX}/2$, *and* $\nu_X - J_{AX}/2$, *where* ν_A *and* ν_X *are resonance frequencies corresponding to non-coupled A and X spin systems and* J_{AX} *is the J-coupling constant. In addition,* $m = 0 \; or \; \pm 2$ *(zero and double quantum coherences) are also allowed resulting in two more transitions. But they are not observable directly*[4]*.*

Magnetically equivalent nuclei (such as protons within an isolated CH_3 group) have identical scalar coupling constants with a third non-equivalent nucleus (such as an additional CH group in the molecule) whereas for chemically equivalent nuclei, the scalar

coupling constant of the two nuclei with the third nucleus is different. All magnetically equivalent nuclei are also chemically equivalent and chemically equivalent nuclei do not show first-order splitting in the spectrum.

The concept of J-coupling is used in multi-dimensional spectroscopy[5–7] (section 1.1.7 and 1.3). The coupled spin systems undergo J-evolution with increasing echo time TE. Therefore, an incremental delay in the pulse sequence is introduction for J-coupling to undergo evolution. A thorough quantum mechanical treatment using product operator formalism is necessary to explain the scalar coupling evolution and it is beyond the scope of this thesis. Therefore, it is suggested to refer to the text books of Levitt[3] and Keeler[2] to understand about the concept of J-evolution. In principle, the magnetization vector of the coupled spins oscillates between in-phase and anti-phase terms in the transverse XY plane and this leads to what is observed as J-evolution and inversion of the J-coupled resonances in the spectrum. The spectral peaks are fully inverted by 180° when $TE = 1/J$.

1.1.5 T_1 and T_2 relaxation times

The concepts of T_1 and T_2 relaxation are essential to understand even a basic NMR experiment. A single RF pulse or a sequence of different RF pulses perturbs the spins thereby causing a change in the net magnetization.

T_1 relaxation time (also known as spin-lattice relaxation or longitudinal relaxation) is the time that it takes to return the longitudinal net magnetization to its equilibrium M_0 which is parallel to the external static magnetic field B_0. The recovered magnetization at time t is given by

$$M_Z(t) = M_0(1 - e^{-t/T_1}) \qquad (11)$$

When $t > 5T_1$, $M_Z(t) = M_0$. Therefore, the knowledge of metabolite specific T_1 relaxation times is necessary to optimize the data acquisition parameters such as the flip angle and repetition time TR for a spectroscopy experiment. A repetition time TR that is short in comparison to $5T_1$ gives the spectrum a T_1-weighting. Moreover, it is important to

correct for T_1 relaxation effects for accurate concentration estimates of metabolites and the calculation of chemical exchange rates. T_1 relaxation times are dependent on external magnetic field and get longer with increasing static magnetic field strength B_0. T_1 relaxation time in vivo is also tissue-specific and dependent on temperature.

T_1 relaxation times are measured using inversion recovery techniques or using a progressive saturation approach with a repetition time series. This results in the spectral signal sweeping a range of magnetizations from positive to negative. Fitting the resulting signal to inversion recovery equation or to Equation 11 with $t = TR$, T_1 relaxation times can be calculated. Section 1.2 describes the use of a double inversion recovery sequence for measuring T_1 relaxation times of the macromolecular peaks.

T_2 relaxation is the exponential decay process of the transverse magnetization with time. It is also known as transverse relaxation or spin-spin relaxation. T_2 relaxation time is the time taken by the transverse magnetization M_{XY} to fall to 37% (1/e) of its initial value. For a simple spin-echo sequence, the transverse magnetization at a specific time t is given by

$$M_{XY}(t) = M_{XY}(0)e^{-t/T_2} \qquad (12)$$

The relationship between echo time $t = TE$ and T_2 relaxation time is an exponential curve according to Equation 12 and it is used to measure the T_2 relaxation times in section **1.2** and 1.3. A non-zero TE gives a T_2-weighting to the spectrum. Various factors contributing to the exponential decay of the NMR signal include microscopic magnetic susceptibility differences, dipole-dipole interaction, chemical shift anisotropy, molecular translation, fluid flow, J-coupling and chemical exchange. T_2 relaxation times decrease with increasing field strength.

The Lorentzian linewidth component of the spectral peaks arise from the T_2 relaxation. The T_2 component contributing to linewidth of the peaks is metabolite/resonance-specific. On the other hand, the linewidth component arising from B_0 inhomogeneities is identical to all the spins present in the sample/voxel of interest. The B_0 inhomogeneities originate

from microscopic and macroscopic susceptibility effects as well as tissue compartment effects[8] contributing to the Gaussian linewidth component.

Bloembergen-Purcell-Pound (BPP) theory[9] explains the relaxation of pure substances in a magnetic field. However, the relaxation phenomenon gets more complex in in vivo samples. The relaxation times are also shown to vary with pathological or physiological changes. Unlike the metabolites, relaxation times of water have been studied in detail and they are governed by a principle known as dipole-dipole interaction. Their relaxation property is explained as a result of the fast exchange of free bulk water and the bound water near macromolecular surfaces.

Molecules undergo translational, rotational and vibrational motion. Out of these, frequencies corresponding to the rotational motion are in the MHz range thereby having an impact on the MR signal. Smaller molecules rotate faster compared to larger molecules. Also, as temperature increases, increase in the kinetic energy of the molecules make them rotate faster. Therefore, with increasing tumbling rate, both T_1 and T_2 relaxation times increase. Therefore, for larger macromolecules with shorter tumbling rates, T_1 and T_2 relaxation times are shorter compared to those of metabolites.

In vivo, T_1 relaxation times are predominantly tissue specific. On the other hand, in addition to being field strength specific, T_2 relaxation times are also sequence specific depending primarily on whether the sequence employs adiabatic pulses or not. For instance, the adiabatic pulses cause a spin-locking effect[10] which suppresses the evolution of spins to some extent for the pulse duration. Furthermore, T_2 relaxation times are not only tissue specific, but they are also specific to the region of the brain since they depend on the iron content[11].

Analyzing relaxation times can also lead to spectral assignment of unknown compounds in sample mixtures. In the later sections, the necessity of knowing T_1 and T_2 relaxation times of water and metabolites for the quantification of metabolites in comparable units (molar or molal) is emphasized.

1.1.6 Bloch equations

Looking at the macroscopic magnetization gives an equation of motion from the classical mechanics point of view. Bloch proposed a set of equations for the time dependence of the net magnetization during an NMR experiment involving RF pulses. The bulk magnetization $\boldsymbol{M}$ experiences a torque and therefore precesses around the external static magnetic field $\boldsymbol{B_0}$:

$$\frac{d\boldsymbol{M}(t)}{dt} = \boldsymbol{M}(t) \times \gamma \boldsymbol{B}(t) \qquad (13)$$

The magnetic field $\boldsymbol{B}(t)$ is time dependent when RF pulses are applied. The vector $\boldsymbol{M}$ has three components: M_x and M_y which are the transverse components and M_z which is the longitudinal component. Solving the cross product yields

$$\frac{dM_x(t)}{dt} = \gamma[M_y(t)B_z(t) - M_z(t)B_y(t)]) \qquad (14)$$

$$\frac{dM_y(t)}{dt} = \gamma[M_z(t)B_x(t) - M_x(t)B_z(t)] \qquad (15)$$

$$\frac{dM_z(t)}{dt} = \gamma[M_x(t)B_y(t) - M_y(t)B_x(t)] \qquad (16)$$

Bloch assumed the spins to relax differently in the transverse (spin-spin relaxation) and longitudinal planes (spin-lattice relaxation); however, the Bloch equations follow first order kinetics. Considering the relaxation process where T_1 and T_2 are relaxation time constants, the relaxation terms become

$$(-\frac{M_x(t)}{T_2}, -\frac{M_y(t)}{T_2}, -\frac{M_z(t) - M_0}{T_1})$$

Therefore, accounting for relaxation in Equations 14, 15, and 16 and since $B_z(t)$ in the laboratory frame is B_0, the Bloch equations in the laboratory frame are written as

$$\frac{dM_x(t)}{dt} = \gamma[M_y(t)B_0 - M_z(t)B_y(t)] - \frac{M_x(t)}{T_2} \quad (17)$$

$$\frac{dM_y(t)}{dt} = \gamma[M_z(t)B_x(t) - M_x(t)B_0] - \frac{M_y(t)}{T_2} \quad (18)$$

$$\frac{dM_z(t)}{dt} = \gamma[M_x(t)B_y(t) - M_y(t)B_x(t)] - \frac{M_z(t) - M_0}{T_1} \quad (19)$$

Considering a rotating frame (x', y', z') with frequency ω around the static magnetic field $B_0 = -\gamma\omega_0$,

$$M'_x = M_x \cos\omega t + M_y \sin\omega t \quad (20)$$

$$M'_y = M_y \cos\omega t - M_y \sin\omega t \quad (21)$$

$$M'_z = M_z \quad (22)$$

the equations above transform as follows:

$$\frac{dM'_x(t)}{dt} = [-(\omega_0 - \omega)M'_y(t) - \gamma M'_z(t)B'_y(t)] - \frac{M'_x(t)}{T_2} \quad (23)$$

$$\frac{dM'_y(t)}{dt} = [(\omega_0 - \omega)M'_x(t) + \gamma M'_z(t)B'_x(t)] - \frac{M'_y(t)}{T_2} \quad (24)$$

$$\frac{dM'_z(t)}{dt} = \gamma[M'_x(t)B'_y(t) - M'_y(t)B'_x(t)] - \frac{M'_z(t) - M_0}{T_1} \quad (25)$$

A detailed derivation can be found in the paper by Bloch[12]. The Bloch equations are used in section 1.2.2 to determine the longitudinal magnetizations of MM peaks for different combinations of inversion times in a double inversion recovery sequence to find optimal sequence parameters to measure T_1 relaxation times of MM.

1.1.7 Single voxel spectroscopy techniques

Application of concepts from physics in medicine has been of immense importance. The branch of medical physics has grown tremendously and yielded diagnostic, therapeutic

and theranostic methods. Magnetic resonance imaging (MRI) and spectroscopy are used for diagnostic purposes and for monitoring treatment response. Single voxel proton MRS is a non-invasive technique that has complemented MRI by providing a means to detect and quantify concentrations of metabolites in the human brain. About 18 brain metabolites can be detected at ultra-high field (UHF) (≥ 7 T) using this technique[13]. MRS is used to not only understand the regular metabolism in the human brain, but also in establishing biomarkers for diagnostics and therapy response monitoring in a range of pathologies in the human brain, therefore proving to be clinically useful[14]. Quite contrasting to MRI, in MRS, one aims to suppress tissue water and fat signal, and measure the concentrations of metabolites. The sensitivity of ^{1}H MRS allows for detection of metabolites with concentrations in the millimolal range. Therefore, ^{1}H MRS provides more specificity since this technique can detect several metabolite peaks of interest. Figure 6 a) shows ^{1}H MRS spectrum acquired at 9.4 T.

The most common in vivo spectroscopy pulse sequences for single voxel localization are PRESS[15], STEAM[16], semiLASER[17,18], LASER[19] and SPECIAL[20] . They differ from each other with respect to type and number of radiofrequency pulses needed for 3D localization, the resulting chemical shift displacement and SNR. Typically, the most suited pulse sequence is chosen for a study depending on the metabolites of interest, hardware constraints and feasibility of acquisition duration and other parameters such as TE, TR and number of averages required to yield a good quality spectrum. A recent experts' consensus article[21] compares the pulse sequences based on various characteristics and recommends sequences for different situations such as lower/higher field strengths, reducing chemical shift displacement and to overcome inhomogeneous B_1^+ fields. Another interesting review article by Landheer et al.,[22] describes the pulse sequences more theoretically and elaborates the trade-offs between them.

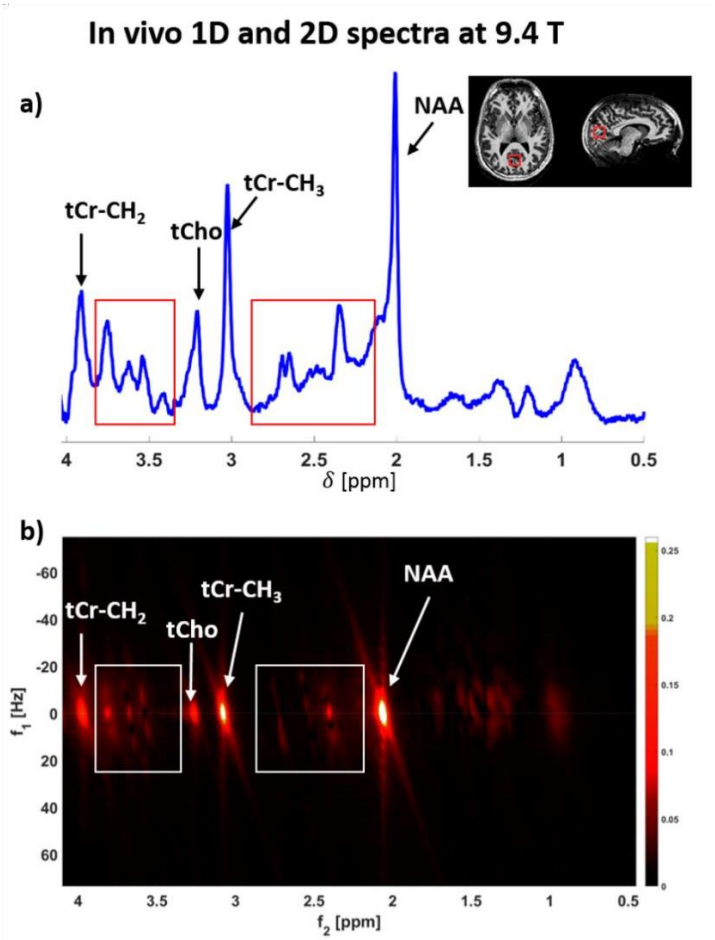

Figure 6: *a) Proton spectrum acquired in vivo in the human brain at 9.4 T using a one-dimensional metabolite-cycled semiLASER sequence with an inlay showing the voxel placement in an anatomical image. A gray matter rich voxel of interest in the occipital lobe was chosen. The spectrum shows regions of severe spectral overlap highlighted with red boxes in the spectrum. These regions contain spectral peaks from J-coupled metabolites such as aspartate, glutamine, glutamate and myo-inositol. b) A in vivo human brain two-dimensional J-resolved metabolite-cycled semiLASER spectrum acquired from the same voxel shows well-resolved spectral patterns of these metabolites with J-coupled spin systems across the indirect dimension f_1. The spectral range containing most metabolites with J-coupled spin systems are shown with white boxes. In both a) and b) major singlet resonance lines of metabolites such as NAA, tCr and tCho are labeled to serve as spectral landmarks for comparison between the two figures. Further explanation about the sequences and acquisition parameters are given in section 3.*

UHF pose several technical challenges[13] and they have to be addressed in order to reap the benefits offered by UHF. Some of the challenges include B_1^+ inhomogeneity[23], and increased chemical shift displacement effect. In this thesis, semiLASER[17] (semi localization by adiabatic selective refocusing) sequence is used for localization. The semiLASER[24] sequence employed 90° sinc pulse of 8000 Hz bandwidth for excitation. Higher bandwidth adiabatic full passage (AFP) pulses (pulse duration: 3.5 ms; bandwidth: 8000 Hz) can minimize chemical shift displacement thereby improving the localization of the voxel of interest. In addition, adiabatic pulses are also relatively insensitive to B_1^+ inhomogeneity. This helps overcome the B_1^+ field inhomogeneity especially at UHF. Even though LASER offers better localization since it uses adiabatic pulses also for excitation as well, semiLASER allows shorter TEs since it has lesser number of RF pulses. This is beneficial since T_2 relaxation times of metabolites are shorter at UHF compared to lower field strengths, therefore using a shorter TE sequence is better. The sequence is described in detail in Giapitzakis et al[24].

Another important aspect of acquiring MRS data is a water suppression scheme. Water molecule is present in abundance in the human brain resulting in a huge water peak at ~4.7 ppm in the ^{1}H spectrum. Therefore, it is essential to suppress the water peak in order to detect metabolites that are present in millimolal range. The water suppression also needs to be robust in order to avoid any baseline distortions or water tails affecting the detection of metabolites closer to 4.7 ppm. However, water suppression techniques[25,26] uses a combination of RF pulses which increases RF power deposition at UHF. Therefore, metabolite-cycling (MC) technique was proposed[27] which is an alternative to using water suppression techniques. The MC technique[24] used in this thesis employed an asymmetric adiabatic inversion pulse. The MC inversion pulse preceeded the semiLASER localization[24]. It works by selectively alternatively inverting the upfield and the downfield part of the proton spectrum (upfield and downfield parts are inverted in the odd and even numbered acquisitions respectively). Therefore, adding the even and odd numbered acquisitions gives the water spectrum and their difference results in the metabolite spectrum. The inversion of the upfield and the downfield part of the spectrum

without affecting the water peak also enables detection of some of the peaks that exchange their proton with water[28].

Using proper preprocessing steps (such as averaging, eddy current correction, RF coil combination, frequency and phase drift correction, etc.,) in order to reconstruct the raw data from the MRI scanner is just as important as choosing the appropriate pulse sequence with optimized parameters for a study. This is aptly illustrated in experts' consensus recommendations on preprocessing, analysis and quantification in single voxel MRS[29].

As a next step, in order to quantify the concentrations of metabolites, a linear combination of simulated basis spectra are fit to model the acquired spectrum. There are several software packages such as LCModel[30], FiTAID[31] or jMRUI[32], which perform spectral fitting. The most preferred way to generate the basis spectra for individual metabolites is using software tools such as Vespa[33] by performing density matrix calculations on the spin-system of the metabolites that are expected to be observed in the acquired spectrum. All the acquisition parameters are taken into consideration. Major metabolites observed in the in vivo neurochemical profile are N-acetyl aspartate (NAA), NAA glutamate (NAAG), γ-aminobutyric acid (GABA), aspartate (Asp), creatine (Cr), glutamate (Glu), glutamine (Gln), glutathione (GSH), glucose (Glc), glycerophosphocholine (GPC), glycine (Glyc), myo-inositol (mI), scyllo-inositol (Scy), lactate (Lac), phosphocreatine (PCr), phosphocholine (PCho), phosphoethanolamine (PE), and taurine (Tau). These are typically included as basis vectors in the basis set. The acetyl and aspartate moieties of NAA is represented as NAA(CH_3) and NAA(CH_2) respectively. The total creatine singlets at 3.028 and 3.925 ppm are given as tCr(CH_3) and tCr(CH_2) respectively. tCho corresponds to total choline combining PCho and GPC. The resulting relative concentrations from the spectral fitting are often converted to molar or molal units after correcting for various factors that are described in detail in section 1.1.8.

Several challenges are encountered when one attempts to perform spectral fitting due to complex spectral patterns and severe overlap of peaks in a proton spectrum acquired using the techniques/pulse sequences discussed so far. It becomes difficult to distinguish

some peaks of metabolic importance such as GABA, Gln, Glu, Lac, etc., since these peaks appear as multiplets and also overlap with other metabolite peaks.

One technique to acquire well-resolved MR spectroscopy data is by utilizing 1D MRS at ultra-high field strength (UHF)[13] since it benefits from higher SNR and increased spectral resolution. Therefore, acquisition of spectra at UHF helps distinguishing metabolites with lower SNR peaks and/or J-coupled spin systems better.

Another technique used by the NMR community to reduce spectral overlap is multi-dimensional spectroscopy[34,35]. Among these multi-dimensional spectroscopy techniques that exist, two-dimensional J-resolved spectroscopy is shown to be feasible and also to be promising in vivo[36–38]. The principle of 2D J-resolved spectroscopy[7] exploits the concept of J-evolution and the consequential amplitude and phase modulation of spectral pattern. It simply consists of a series of signals acquired with different TEs encoding the indirect f_1 dimension. The direct f_2 dimension consists the chemical shift and J-coupling information as in 1D MR spectroscopy experiments. The second dimension (f_1) in two-dimensional J-resolved spectrum contains J-coupling information. After a Fourier transformation in both dimensions, the spectrum displays the J-coupling information in the indirect dimension eliminating the overlap of J-coupled resonances. Figure 6 a) and b) illustrates a spectral comparison between 1D and 2D MC-semiLASER spectra (section 1.3) acquired in vivo from the human brain at 9.4 T. In this thesis, quantification of metabolites using one-dimensional MRS and two-dimensional MRS semiLASER localization at UHF is compared in section 1.3.

1.1.8 Quantification of metabolites

The relative metabolite concentrations obtained from the fitting software are not directly comparable between various time points measured during treatment monitoring or across different acquisition methods, field strengths, or vendors. Hence, it is necessary to introduce correction factors in order to convert these relative concentrations to standard comparable values such as molal or molar units. To perform the corrections a reference of known concentration is essential. Several approaches[39–47] exist in order to measure the concentrations of metabolites. One such method uses the internal water signal as the

reference[48]. This thesis uses the quantification formula described in detail by Gasparovic et al.,[48] to calculate the concentration values in millimoles/kg (millimolal) using the internal water referencing method. The concentrations of metabolites are obtained after correcting for the fractional tissue compositions and T_1 and T_2 corrections for both water and metabolite signals.

The quantification values are reported after applying the necessary correction factors (unless stated otherwise) for determining concentrations using the internal water referencing method. For external concentration reference methods certain factors such as coil loading, RF homogeneity, temperature differences need to be considered. While using internal water referencing method, the unsuppressed water spectrum is acquired from the same voxel as the metabolites. Since the metabolite signal and water signal are acquired similarly, internal water referencing is advantageous in comparison to external concentration references.

In order to estimate the fractional tissue compositions, this work uses segmentation of acquired high-resolution MP2RAGE[49] images into WM, GM and CSF (white-matter, gray matter and cerebrospinal fluid) using Statistical Parametric Mapping 12 (SPM 12) [50] software. Later the tissue fractions were calculated using an in-house written script in Python (v3.7). Finally, the concentrations of metabolites were calculated using the formula[48] given below:

$$[\mathrm{M}]_{mmolal} = [\mathrm{M}]_{\mathrm{obs}} \times conc_{pure\_H2O} \times \frac{2}{1+\mathrm{Fs}} \times \frac{(\mathrm{f_{GM}} \times R_{H2O\_GM} + \mathrm{f_{WM}} \times R_{H2O\_WM} + \mathrm{f_{CSF}} \times R_{H2O\_CSF})}{(1-\mathrm{f_{CSF}}) \times R_M} \quad (26)$$

$$\text{where } f_y = \frac{f_{y\_vol} \times a_y}{f_{GM\_vol} \times a_{GM} + f_{WM\_vol} \times a_{WM} + f_{CSF\_vol} \times a_{CSF}}$$

where y corresponds to either GM, WM or CSF; f_{y_vol} is the fraction of the respective tissue type determined by segmentation; a_{GM}, a_{WM}, a_{CSF} (78%, 65%, 97% respectively) are the relative densities of MR-visible water for the given tissue type; The pure water concentration (55,510 millimolal) is used along with the MR visible fractions of water in GM, WM, and CSF.

$R_{H2O\_y} = \exp\left[-\frac{TE}{T2_{H2O\_y}}\right]\left[1-\exp\left[-\frac{\mathrm{TR}}{T1_{H2O_y}}\right]\right]$ is the relaxation correction factor for each water compartment y. $T1_{H2O_y}$ and $T2_{H2O\_y}$ are the T_1 and T_2 relaxation times of water in the compartment y.

$R_M = \exp\left[-\frac{TE}{T2_M}\right]\left[1-\exp\left[-\frac{\mathrm{TR}}{T1_M}\right]\right]$ is the relaxation correction term for metabolites (section 1.3). For macromolecules R_M was replaced by R_{MM} as the macromolecular spectra were acquired using double inversion recovery (DIR) the relaxation (section 1.2.3). The relaxation correction term for macromolecules is given by $R_{MM} = [1 - 2e^{\frac{TI2}{T_1}} + 2e^{-(\frac{TI1+TI2}{T_1})}]\exp\left[-\frac{TE}{T2_{MM}}\right]\left[1-\exp\left[-\frac{\mathrm{TR}}{T1_{MM}}\right]\right]$. The denominator $1 - f_{CSF}$ was implemented for partial-volume correction. The factor $\frac{2}{1+\mathrm{Fs}}$ was introduced to correct for the multiplication of even-numbered acquisitions with the scaling factor (F_s), originating from the metabolite-cycling data processing. $[\mathrm{M}]_{\mathrm{obs}}$ is the concentration obtained from LCModel (section 1.2 and 1.3.2) or ProFit 2.0 (section 1.3.3). For metabolite concentrations (section 1.3), number of protons contributing to the metabolite peaks were accounted. However, for macromolecules since the proton contributions to each macromolecular peak is not known, the proton contribution was not corrected (section 1.2.3).

1.1.9 Macromolecules

Broad macromolecular resonances underlie narrow higher intensity metabolite resonance lines in short TE ^{1}H MR spectra. Macromolecules (MMs) between 0.5 and 4.5 ppm are attributed to mobile methyl, methylene, and methine groups of amino acids from cytosolic peptides and proteins[51]. Several studies at field strengths between 1.5 to 3 T have highlighted the clinical relevance of MMs in aging[52] and in pathologies such as traumatic encephalopathy[53], Kennedy's disease[54], acute multiple sclerosis[55], and glioma[56]. Figure 7 shows a MM spectrum (summed from eleven healthy volunteers) acquired at 9.4 T (section 1.2). Due to increased spectral dispersion, SNR, and resolution, more MM peaks are distinguishable at ultra-high field[57]; hence, it is possible to more accurately characterize the behavior of individual MM peaks.

On the other hand, the well-resolved underlying MM spectrum at UHF often distorts the metabolite spectrum. Therefore, characterizing MM peaks additionally improves accuracy in quantifying metabolite concentrations. Various techniques have been used to handle MM signals in metabolite spectra. Cudalbu et al.,[58] suggested that using prior information from experimentally acquired MM spectra may prove to be the best solution at UHF.

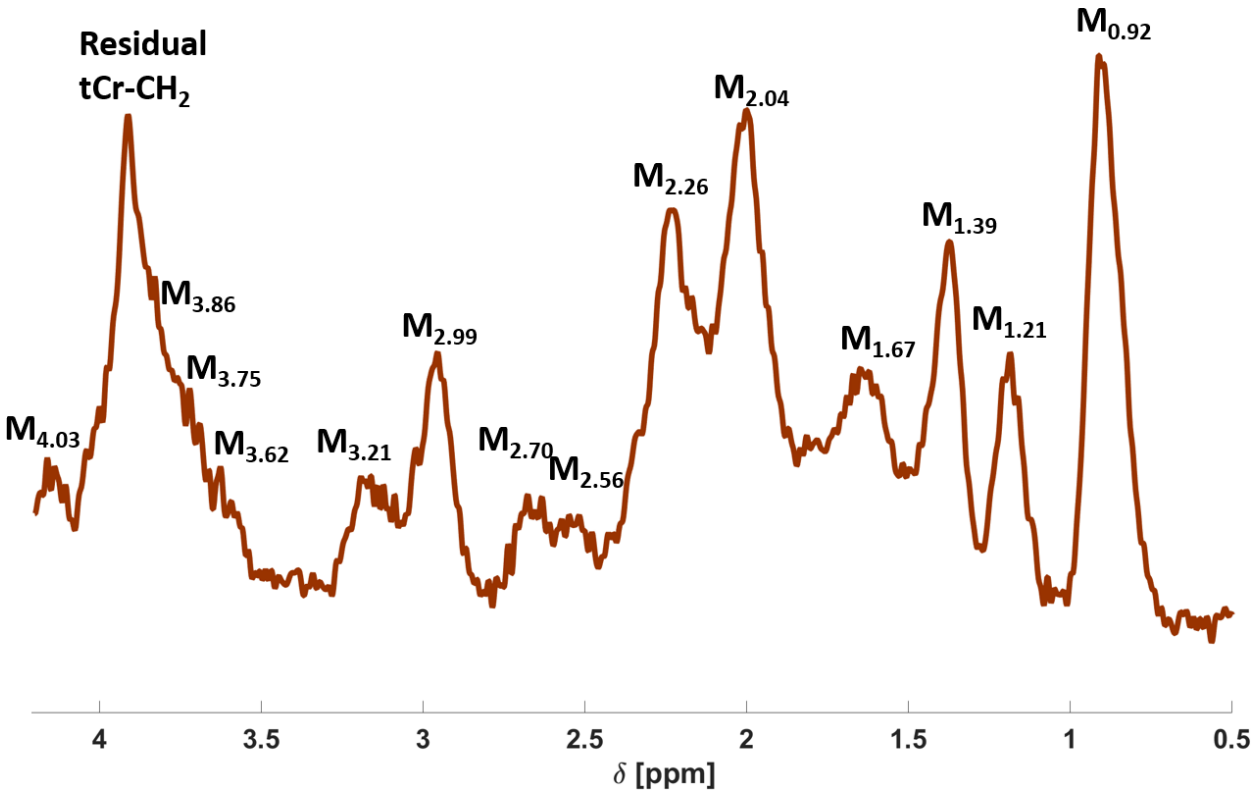

Figure 7: *Macromolecular spectrum summed from eleven healthy volunteers acquired from a gray matter rich voxel in the human brain using a double inversion recovery MC-semiLASER sequence[59] with inversion times set to 2360 and 625 ms at 9.4 T. Further details are provided about acquisition set up and parameters in section 1.2. The MM peaks are labeled as $M_{X.XX}$ where the subscript X.XX represents the chemical shift of the MM peak in ppm. A sharper metabolite residual tCr-CH_2 peak is seen at 3.925 ppm.*

Macromolecules have shorter T_1 relaxation times when compared to metabolites[57]. Exploiting this difference in T_1 relaxation times MM spectra are acquired using inversion recovery methods. The chosen inversion time (TI) determines the T_1-weighting of the

MRS spectrum. In addition, MMs have shorter T_2 relaxation times compared to metabolites. Therefore, some studies use longer TE spectra are acquired in order to avoid the MM contribution to the proton spectrum. However, it results in SNR loss for shorter T_2 and J-coupled metabolites.

1.1.10 Objectives and outcome of doctoral research

Reliable detection and quantification of the concentration of metabolites and macromolecules in the human brain using proton single voxel spectroscopy at an ultra-high field strength of 9.4T was the prime goal of this thesis. Increased spectral dispersion and SNR at UHF provides better detection and distinction of the metabolite peaks[13]. However, this also implies that the MM peaks are more distinguishable at UHF, which may negatively impact the accuracy and precision of metabolite concentration estimates. Furthermore, the MM spectrum itself contains potentially clinically relevant information. This makes it necessary to characterize and understand the contribution of MM peaks better. Therefore, the first part of this thesis focuses on characterizing the relaxation times of MMs (Publication 1, Publication 2) and to quantify their brain tissue concentrations (Publication 2). This work helps in accounting for the contribution of MMs in the metabolite spectrum and to understand the nature of MMs. The effective T_2 relaxation times (T_2^{eff}) of MMs (Publication 1) are reported for gray and white matter-rich voxels in the human brain at 9.4 T. The T_2^{eff} relaxation times were calculated for MM peaks from an echo time series of a double inversion recovery (DIR) metabolite-cycled (MC) semiLASER sequence. In Publication 2, T_1 relaxation times of MM peaks for gray and white-matter rich (GM and WM respectively) voxels are calculated by using a novel DIR technique. These two publications helped in understanding the sequence and scan parameter dependency of the contribution of MMs to the metabolite spectrum and led to the development of a respective simulated relaxation corrected sequence specific MM model[60] (co-author paper not a part of this thesis).

The second part of the thesis focuses on quantifying the concentrations of brain metabolites (Publication 1, Publication 3) reliably. This is done using two different single

voxel spectroscopy localization techniques namely one-dimensional (Publication 1) and two-dimensional spectroscopy (Publication 3) and comparing their performance. The MC semiLASER sequence was used for acquiring one dimensional spectroscopy data from a GM-rich voxel in the occipital lobe. In addition, a two-dimensional J-resolved MC semiLASER sequence with a maximum echo sampling scheme was developed and used to acquire two-dimensional spectroscopy data from a GM-rich voxel in the occipital lobe as well. MM contributions to the metabolite spectra in both 1D and 2D MC semiLASER were accounted for by including experimentally acquired 1D and 2D MM spectra using 1D and 2D double inversion recovery MC semiLASER respectively. T_1 relaxation times[61] (co-author paper not part of this thesis) and T_2 relaxation times of metabolites (Publication 1) were determined and used in the correction factors to obtain concentration values.

This thesis is written in a cumulative form and includes three publications that arose during my PhD work. The results from Publication 1, Publication 2, and Publication 3 are summarized and presented here. The full articles as published in peer reviewed journals are appended in this thesis and can be found in Chapter 5.

1.2 Characterization and Quantification of Macromolecules

The broad macromolecular peaks underlying the metabolite spectrum in ^{1}H MRS experiments with short echo time are often viewed as a distortion due to the negative impact on the quantification accuracy and precision of metabolite concentrations. Therefore, characterizing these macromolecular peaks is necessary in understanding their influence in quantifying metabolite concentrations in dependence of sequence parameters. Moreover, several studies[52–54,58,62] have highlighted the clinical importance of MMs since respective changes have been detected in various pathologies in the rat brain and human brain. Hence, in order to understand the mechanisms behind different pathologies and to improve the diagnostic capability for several diseases of clinical relevance by establishing potential biomarkers, assimilation of MMs and their behavior is essential. A recent consensus article about MRS visible MM[57] also emphasized that the knowledge of T_1 and T_2 relaxation times of individual peaks at different field strengths is necessary. In the following sections, characterization of T_2 (Publication 1) and T_1 (Publication 2) relaxation times of MM peaks in GM- and WM-rich voxels at 9.4 T is described in detail. Finally, the concentration of MM peaks (Publication 2) in the human brain are reported after correcting for tissue fractions of the respective voxels and for the tissue type specific relaxation effects.

1.2.1 T_2 relaxation times of macromolecules

Introduction

At the time when this study was performed, T_2 relaxation times of all individual MM peaks detectable in the human brain have not been reported at any field strength to the best of our knowledge. The T_2 relaxation times of MM peaks have been reported in the rat brain[63–66] at 4.0, 9.4, 11.7, and 17.2 T and for the non-overlapping $M_{0.92}$ peak in the human brain at 2.1 T by Behar et al[67]. Therefore, the primary goal of this study was to measure the effective T_2 relaxation times (T_2^{eff}; includes the J-evolution effects) of individual MM peaks in both GM- and WM-rich voxels in the human brain at 9.4 T. Another interesting aspect of this study is a quantitative analysis of the actual full width at half maximum

FWHM ($\Delta_{1/2}$) of the MM peaks compared to the respective contributions by T_2 relaxation times, micro-susceptibility and macro-susceptibility as well as chemical shift anisotropy effects.

Study design

In this study, eleven and five healthy volunteers participated for data acquisition in the GM- and WM-rich voxels respectively. A 2 × 2 × 2 cm^3 GM-rich voxel was chosen in the occipital lobe and a WM-rich voxel of same dimensions was chosen in the occipital-parietal transition. A home-built coil with 8 transmit and 16 receive channels[68] was used for the study, by driving power to only the bottom three channels for the single-voxel spectroscopy experiments as described in Giapitzakis et al[24].

First- and second-order B_0 shimming using FAST(EST)MAP[69] (acronym for fast, automatic shim technique using echo-planar signal readout using mapping along projections), and voxel-based power calibration[70,71] were performed. A non-linearly spaced TE series (TE: 25, 32, 40, 52, and 60 ms) of MM spectra was acquired using a DIR[59] MC semiLASER sequence (TR: 10 s, Averages per TE: 32, transmit reference frequency: 2.4 ppm) to estimate the T_2^{eff} of MM peaks.

All raw data were preprocessed with in-house written software in MATLAB (version 2016a; MathWorks, Natrick, MA) as described in Publication 1. MM spectral fitting was performed in LCModel V6.3-1L[30] using simulated Voigt lines. The following MM peaks were included in the basis set: $M_{0.92}$, $M_{1.21}$, $M_{1.39}$, $M_{1.67}$, $M_{2.04}$, $M_{2.26}$, $M_{2.56}$, $M_{2.70}$, $M_{2.99}$, $M_{3.21}$, $M_{3.62}$, $M_{3.75}$, $M_{3.86}$, $M_{4.03}$, and $M_{4.17}$ where the corresponding subscripts indicate their chemical shifts in ppm. For the fitting of the MM peaks, the chemical shifts and $\Delta_{1/2}$ were systematically varied to achieve minimum possible standard deviation of the T_2^{eff} relaxation time values among subjects, to maximize R^2 values, and to minimize the mean Cramer-Rao lower bounds. After considering the above-mentioned criterions, the values chosen by Lopez et al[63] best suited the data. Hence, these chemical shifts and $\Delta_{1/2}$values, with minor deviations were used as input for the spectral fitting model. Creatine (tCr-CH_2) metabolite residual was subtracted by adding a narrower Voigt peak

at 3.925 ppm. More information on basis set creation can be found in the appended Publication 1.

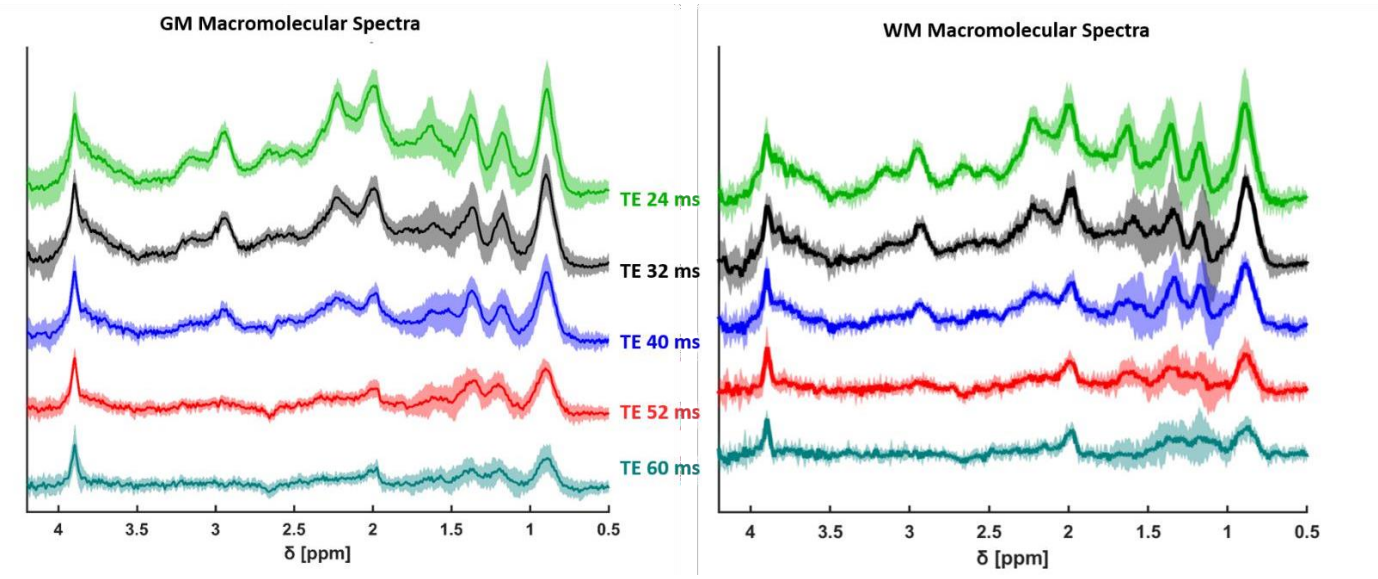

Figure 8: *Echo time series (TE: 24, 32, 40, 52, and 60 ms from top to bottom) macromolecular spectra from GM- and WM-rich voxels. The MM spectra shown here are summed from all the healthy volunteers for the respective voxels. The figure has been adapted from Publication 1.*

To calculate the T_2^{eff} relaxation of MM peaks, the resulting concentrations of MM peaks across the TE series were fit to a mono-exponential decay for the individual subject data and spectra summed across all volunteers. The mean coefficient of determination R^2 was used to evaluate the goodness of the exponential fits.

The FWHM of the MM peaks were extracted from the LCModel .coord files. The contribution of T_2^{eff} relaxation times to $\Delta_{1/2}$ was calculated as $(\pi T_2^{eff})^{-1}$. The residual linewidth was calculated as

$$\Delta\nu_{residual} = \Delta_{1/2} - (\pi T_2^{eff})^{-1} - \Delta\nu_{singlet} \qquad (27)$$

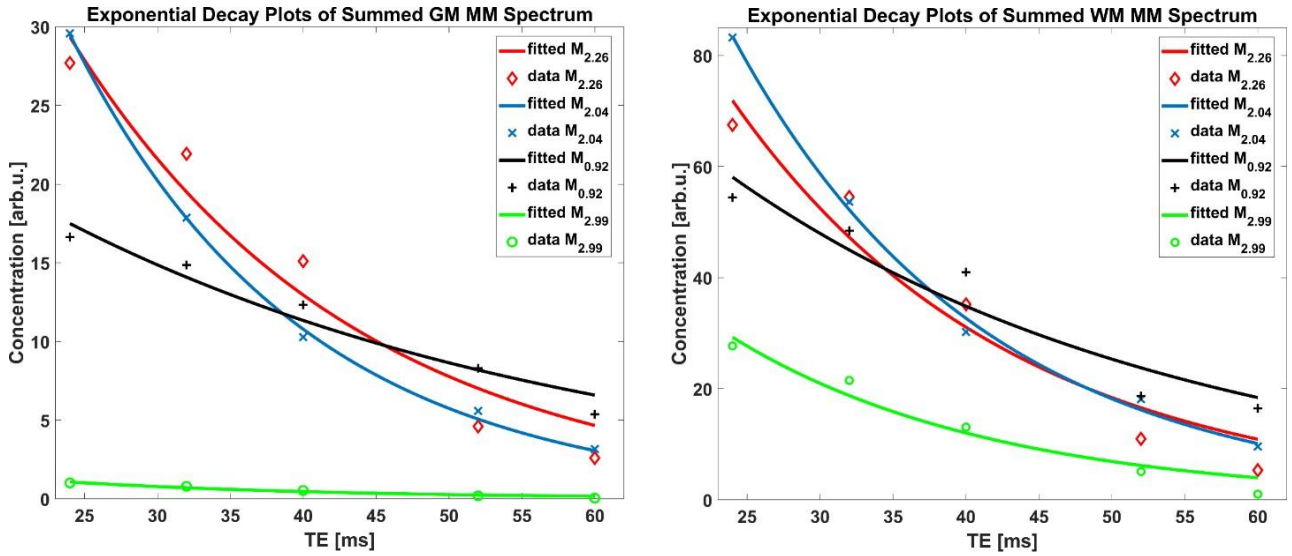

Figure 9: *Exponential decay plots of $M_{0.92}$, $M_{2.04}$, $M_{2.26}$ and $M_{2.99}$ from MM spectra summed for all healthy volunteers for GM- and WM-rich voxels. The scatter points show the fitted concentrations for the respective TEs and the line shows the exponential decay fit. The y-axis has arbitrary units. Therefore, conclusions should not be drawn about the differences between GM and WM plots. The figure is adapted from Publication 1.*

The B_0 components deduced from the tCr(CH_2) residual as

$$\Delta\nu_{singlet} = \Delta_{1/2} - (\pi T_2^{eff})^{-1} \approx \Delta\nu_{micro} + \Delta\nu_{macro} \qquad (28)$$

The values of $\Delta\nu_{micro}$, $\Delta\nu_{macro}$ represent the microscopic and macroscopic susceptibility components respectively.

Results

Figure 8 shows the TE series of MM spectra from GM- and WM-rich voxels. The shaded area represents the standard deviation in the signal between subjects illustrating the high reproducibility of the data quality. The exponential decay fits for $M_{0.92}$, $M_{2.04}$, $M_{2.26}$ and $M_{2.99}$ peaks in the GM- and WM-rich voxels are shown in Figure 9. The LCModel fit residual was minimum and showed minimal structured noise indicating a good fit quality for all individual data from GM- and WM-rich voxels (Publication 1). $M_{2.70}$ is observed to undergo J-evolution and it attains full inversion between TE = 52 and TE = 60 ms. In order

to account for this effect in fitting, the $M_{2.70}$ peak was simulated as a negative peak at the aforementioned TEs.

The T_2^{eff} relaxation times calculated from fits of the individual subject data and the across subjects summed spectra were in good agreement. The box plots of the T_2^{eff} relaxation times are given in Figure 10. The values lie between 13 and 37 ms for GM-rich voxels and between 13 and 40 ms for WM-rich voxels. The mean R^2 values of the exponential decay fits were above 0.70 for all MM peaks except $M_{4.03}$.

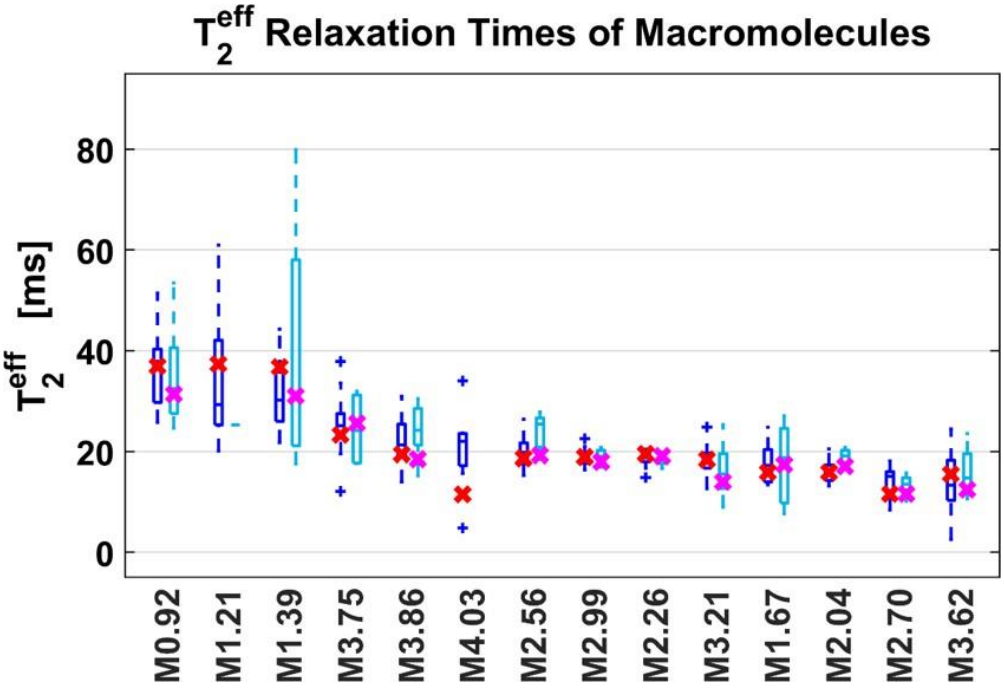

Figure 10: *The boxplots show T_2^{eff} relaxation times calculated for 14 MM peaks in GM-rich (dark blue) and WM-rich (light blue) voxels. Horizontal lines inside the boxes indicate median values (50% quartile). The boundaries at the bottom and the top represent 25 and 75 % quartiles respectively. Red and magenta crosses represent the $T^{eff,sum}{}_2$ relaxation times calculated for the subject-wise summed spectrum from GM- and WM-rich voxels respectively. The figure is adapted from Publication 1.*

The measured $\Delta_{1/2}$ of the MM peaks ranged between 35 and 85 Hz across all TEs. However, the contribution of T_2^{eff} relaxation times $(\pi T_2^{eff})^{-1}$ calculated were between 4

and 30 Hz. The $\Delta\nu_{residual}$ for MM peaks calculated after using the $\Delta\nu_{singlet}$ of tCr(CH_2) varied between 10 and 60 Hz (Figure 11).

Discussion

T_2^{eff} relaxation time values are comparable between the GM- and WM-rich voxels in the occipital lobe and the occipital-parietal transition respectively. These values are brain region specific as the difference in T_2 relaxation times is primarily governed by the iron concentrations across the human brain as shown by Hasan et al[11].

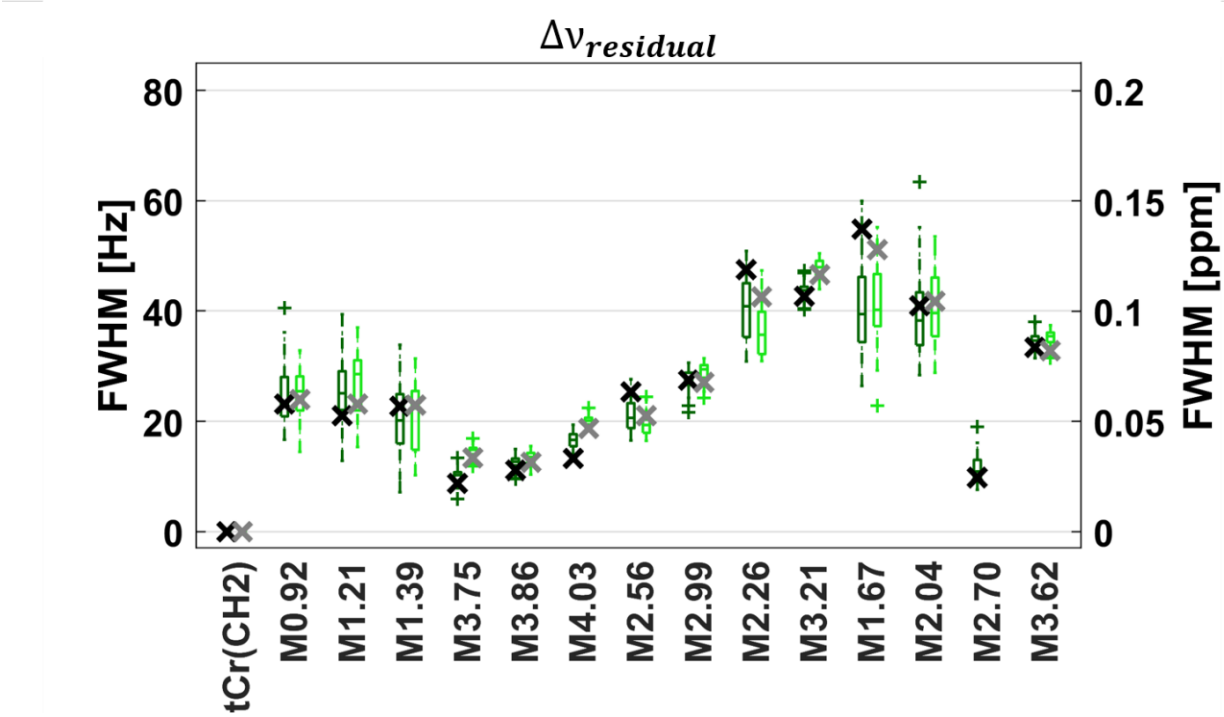

Figure 11: *Residual linewidths calculated using Equation 27 for the MM peaks and metabolite residual tCr(CH_2) at 3.925 ppm. The figure is adapted from Publication 1.*

Table 1 shows a comparison of T_2^{eff} relaxation time values across field strengths. Most MM peaks show a mild B_0 dependence. As discussed in the MM experts' consensus article[57], even though the T_2^{eff} relaxation times tend to decrease with field strength, they have a very mild B_0 dependence. $M_{0.92}$ peak shows maximum deviation from the field strength trend since T_2^{eff} relaxation times at 9.4 T is slightly higher than T_2^{eff} reported at

3 T[72,73]. In addition, Hoefemann et al[72] reported lower T_2^{eff} relaxation times for $M_{1.22}$ and $M_{1.43}$ peaks combined. The T_2^{eff} relaxation times of MMs obtained from this study was utilized also to develop the relaxation corrected MM simulation model[60]. In addition, the knowledge of T_2^{eff} relaxation times of MMs was essential to optimize the acquisition parameters in the two-dimensional spectroscopy study (Publication 3).

The linewidth of the MM peaks were not explained by contribution of the T_2 relaxation times and the microsusceptibility and macrosusceptibility effects. The $\Delta\nu_{residual}$ values for the MM peaks (Figure 11) varied consistently between 10 and 60 Hz for both GM- and WM-rich voxels indicating the magnitude of chemical shift anisotropy, potential spectral overlap and/or J-evolution components for each MM peak is similar between different tissue types. These peaks could originate from amino acids[74] which, depending on the larger protein structure they belong to, can have different chemical shifts, but are distributed around a main resonance frequency for the bulk of protein peaks.

Conclusion

In this study, for the first time, T_2^{eff} relaxation times of 14 individual MM peaks ranging from 13 to 45 ms were measured in both GM- and WM-rich voxels. The T_2^{eff}relaxation times follow the decreasing trend of T_2 relaxation times with increasing B_0 field strength. The T_2^{eff} relaxation time values were utilized to quantify the concentrations of the MMs in human brain tissue (section 1.2.3) and for the development of a generalized relaxation-corrected MM simulation model for accurate quantification of metabolite concentrations[60]. Finally, this work quantitatively shows the contribution of T_2^{eff}relaxation times and B_0 components to the linewidths of the MM peaks and demonstrates a substantial additional contribution by chemical shift anisotropy, potential spectral overlap and J-coupling components to the residual linewidth of amino acid proton groups.

T_2 relaxation times of macromolecular peaks in the human brain [ms]					
Study	**Murali-Manohar (2020) Publication 1**		**Landheer (2020)[73]**	**Hoefemann (2020)[72]**	**Behar (1994)[67]**
B0 (T)	9.4		3	3	2.1
Sequence	DIR-semiLASER		DIR-semiLASER	2DJ-IR MC-PRESS	ISIS
Echo Time (ms)	24 - 60		20.1 - 62.1	20 - 95	19.4 - 145.2
Repetition Time (ms)	10000		2000	3000 - 4000	3300
Region of Interest	Occipital lobe		Occipital and frontal lobe (GM-rich)	Occipital lobe (GM-rich)	Occipital lobe (mixed)
	GM-rich	WM-rich			
M0.94	36 ± 7	35 ± 10	27 ± 2	21	44 ± 4
M1.22	34 ± 13	25 ± 0	39 ± 13	19	
M1.43	32 ± 7	40 ± 24	18 ± 4		
M1.70	18 ± 4	18 ± 8	17 ± 3	27	
M1.81				19	
M1.9	16 ± 2	19 ± 2	14 ± 1		
M2.05					
M2.07					
M2.17	18 ± 2	18 ± 1	20 ± 2		
M2.27				24	
M2.36					
M2.47					
M2.57	20 ± 3	24 ± 3	26 ± 4		
M2.74	14 ± 3	13 ± 2		16	
M2.97	19 ± 2	19 ± 1	21 ± 4	[35]	
M3.00					
M3.09				[35]	
M3.21	18 ± 3	16 ± 5	18 ± 5		
M3.26-3.28				[35]	
M3.4-3.6	14 ± 6	16 ± 5	21 ± 2	24	
M3.71	25 ± 7	25 ± 7			
M3.79					
M3.87	22 ± 5	24 ± 7		34	
M3.97	21 ± 8				
M4.20					

Table 1: *T_2 relaxation times of macromolecular peaks from Publication 1 and from previous studies performed at other field strengths. The T_2 relaxation times given with square brackets indicate that the values reached the maximum limits set in the FitAid software used for spectral fitting. The table is adapted from the MM consensus article[57] (co-author publication).*

1.2.2 T_1 relaxation times of macromolecules

Introduction

Estimating T_1 relaxation times can help elucidate the exchange dynamics and can lead to spectral assignments. Previous literature reported T_1 relaxation times of MMs in the human brain for MM spectra as a whole[75], only for the non-overlapping MM peak at ~0.94 ppm[63,67,76] or for groups of MM peaks[72]. The T_1 relaxation times of individual MM peaks are yet to be reported at any field strength in vivo. Therefore, the prime goal of this study is to report T_1 relaxation times of individual MM peaks.

Inversion recovery (IR) techniques are often utilized as a reliable method for acquiring MM spectra. This method exploits the difference in the T_1 relaxation times between MMs and metabolites[57]. MM peaks are known to have faster T_1 relaxation times compared to those of metabolites. In order to determine T_1 relaxation times of MM peaks, it is necessary to suppress the metabolite signal while still sweeping through a range of magnetizations for the MM peaks. A range of longitudinal magnetization of MM peaks is necessary to plot the T_1 relaxation curve. Even though single IR sequences are popular to acquire MM spectra, in the case of characterizing T_1 relaxation times for all individual MM peaks a single IR technique would be a difficult choice due to eventual contribution from metabolites. More specifically, using a single IR technique would result in metabolite signal contaminating the inversion series MM spectra at most of the TIs; consequently, making it challenging to estimate the T_1 relaxation times of most MM peaks with a sufficient range of longitudinal magnetization. As a result, a DIR technique was chosen for this study as it allowed flexibility for more consistent metabolite nulling while allowing for the observation of a range of different magnetizations of MM peaks simultaneously. Moreover, using a DIR technique proved to be advantageous as this approach is shown to be insensitive to inhomogeneity of the transmit field B_1^+.

Depending on the chosen inversion time (TI) and repetition time (TR), the use of IR techniques results in a T_1-weighting of the MM peaks. Therefore, it is likely that using T_1-weighted MM spectra to account for MM contribution while fitting metabolite spectra will influence quantitative accuracy. This is because the metabolite spectra are typically

acquired without inversion pulses, and thus often also with a shorter TR. Hence, it is necessary to characterize the T_1-relaxation behavior of the MM peaks for improved metabolite spectral fitting and accurate quantification of both MMs and metabolites.

Study design

Exhaustive Bloch simulations (section 1.1.6) assuming a single proton spin were performed in order to determine a range of longitudinal magnetization values for MM signals ranging from negative to positive M_Z, which are required to calculate T_1 relaxation times of the MM peaks. The magnetization vector (M(x,y,z)) was calculated for the actual inversion pulse shape implemented at the 9.4 T MRI scanner and the inversion times TI_1 and TI_2 as depicted in the DIR scheme (Figure 12). The ratio of the available magnetization following a DIR block to the initial magnetization (M_Z/M_0) was calculated for the inversion pulse with a frequency offset ranging from -2000 to 2000 Hz, which is equal to the actual bandwidth of the pulse.

For the Bloch simulations, T_1 relaxation times of metabolites and MMs were considered from previous in vivo results at 9.4 T[77] and at 7 T[75] respectively. TI_1/TI_2 combinations were chosen such that the corresponding spectra had minimal metabolite residual while sweeping a range of longitudinal magnetizations for MM peaks. Finally, the resultant TI_1/TI_2 combinations were further tested in vivo to ensure good quality MM spectra with minimal residual metabolite contributions.

Eleven healthy volunteers participated in the study. All measurements were performed on a 9.4T Siemens Magnetom whole-body MRI scanner using a home-built 8Tx/16Rx coil[68]. A 2 × 2 × 2 cm^3 voxel was placed spanning the longitudinal fissure of the occipital lobe for GM measurements, and a voxel was placed within the left occipital-parietal transition for WM measurements. Second-order B_0 shimming with FAST(EST)MAP[69,78] and voxel-based power calibration[70] were performed.

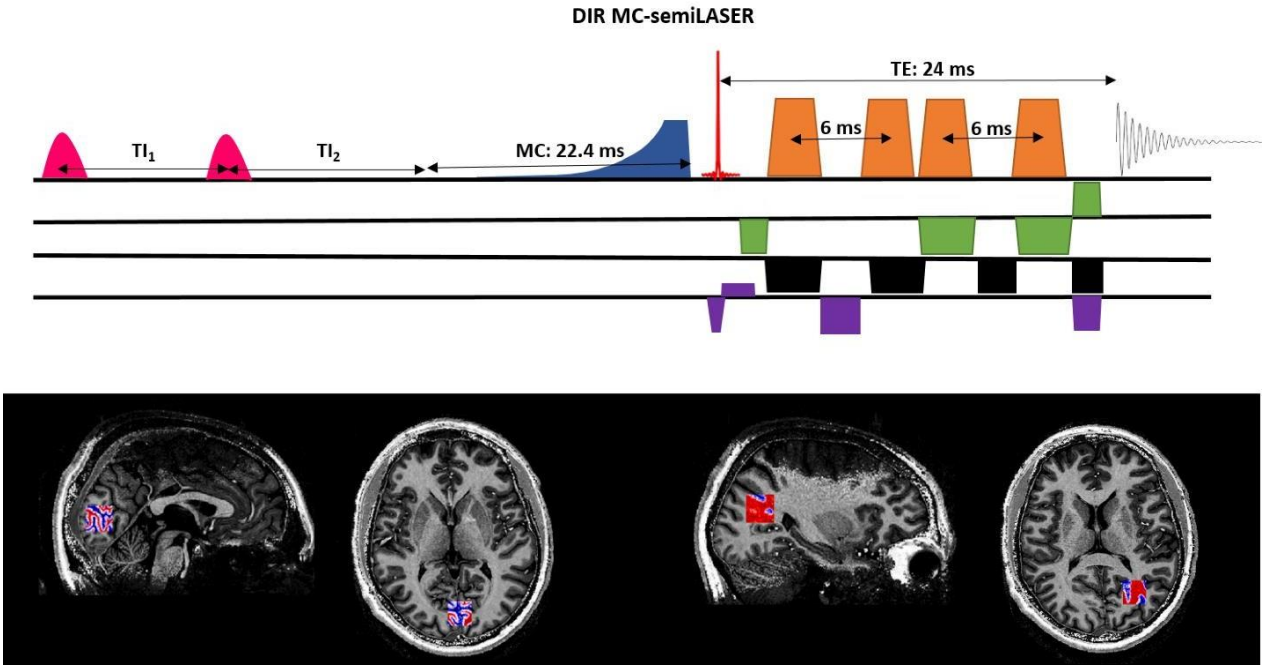

Figure 12: *(Top) Schematic pulse sequence diagram of the double inversion recovery metabolite-cycled semiLASER localization. Eleven different combination of inversion times TI_1/TI_2 were employed to obtain a range of magnetization values for the MM peaks with almost nulled metabolite signal. (Bottom) GM- and WM-rich voxels in the occipital lobe and occipital-parietal transition respectively. The figure is adapted from Publication 2.*

A DIR MC semiLASER[59] (TE: 24 ms, TR: 8000 ms, averages per TI_1/TI_2 combination: 32, transmit reference frequency: 2.4 ppm) sequence was used to acquire MM data. 11 MM spectra were acquired per subject with 11 different TI_1/TI_2 combinations chosen (TI_1/TI_2: 2360/625, 2150/600, 2000/575, 1900/550, 1800/525, 1050/238, 1300/80, 1200/20, 1250/20, and 1300/20 ms). Additional unsuppressed water signals (averages: 16, transmit reference frequency: 4.7 ppm) were acquired without MC. All MM raw data were processed as described in Publication 2 and then the preprocessed spectra were fitted in LCModel (v6.3-1L)[30] using CHSIMU simulated Voigt lines to fit 13 MM peaks. Tailored basis sets corresponding to each TI_1/TI_2 combination were established with adjusted phases to consider metabolite residuals.

The individual LCModel concentrations from all subjects sorted by TI_1/TI_2 combinations were fitted to the DIR signal equation

$$S = \frac{a}{2}\left(1 - 2e^{\frac{-TI_2}{T_1}} + 2e^{-\left(\frac{TI_1+TI_2}{T_1}\right)}\right) \qquad (29)$$

to determine T_1 relaxation times for each of the MM peaks. The differences in T_1 relaxation times between GM- and WM-rich voxels were evaluated using Welch's t-test ($\alpha = 0.05$) for all 13 MM peaks. Adjusted *P*-values were calculated using the Bonferroni correction to account for multiple comparisons.

Results

Metabolite-nulled MM spectra were acquired from GM- and WM-rich voxels with the 11 chosen TI_1/TI_2 combinations encompassing a range of magnetizations. All the spectral fits showed good quality with minimal fit residue, which lacked structured noise (Figure 13). Figure 14 shows $M_{0.92}$ peak amplitudes fitted to Equation 29. Figure 15 reports the T_1 relaxation times of MM peaks from GM- and WM-rich voxels. Additionally, since T_1 relaxation times are mostly tissue-type but not brain region dependent, T_1 relaxation times for pure GM- and WM-voxels are also reported assuming a linear relationship between T_1 relaxation time and the contribution of tissue-type.

The T_1 relaxation times of MM peaks range from 204 to 510 ms and 253 to 564 ms in GM- and WM-rich voxels respectively. Significant differences in T_1 relaxation times between GM- and WM-rich voxels are denoted in Figure 15 by an asterisk: $*P<0.0038$.

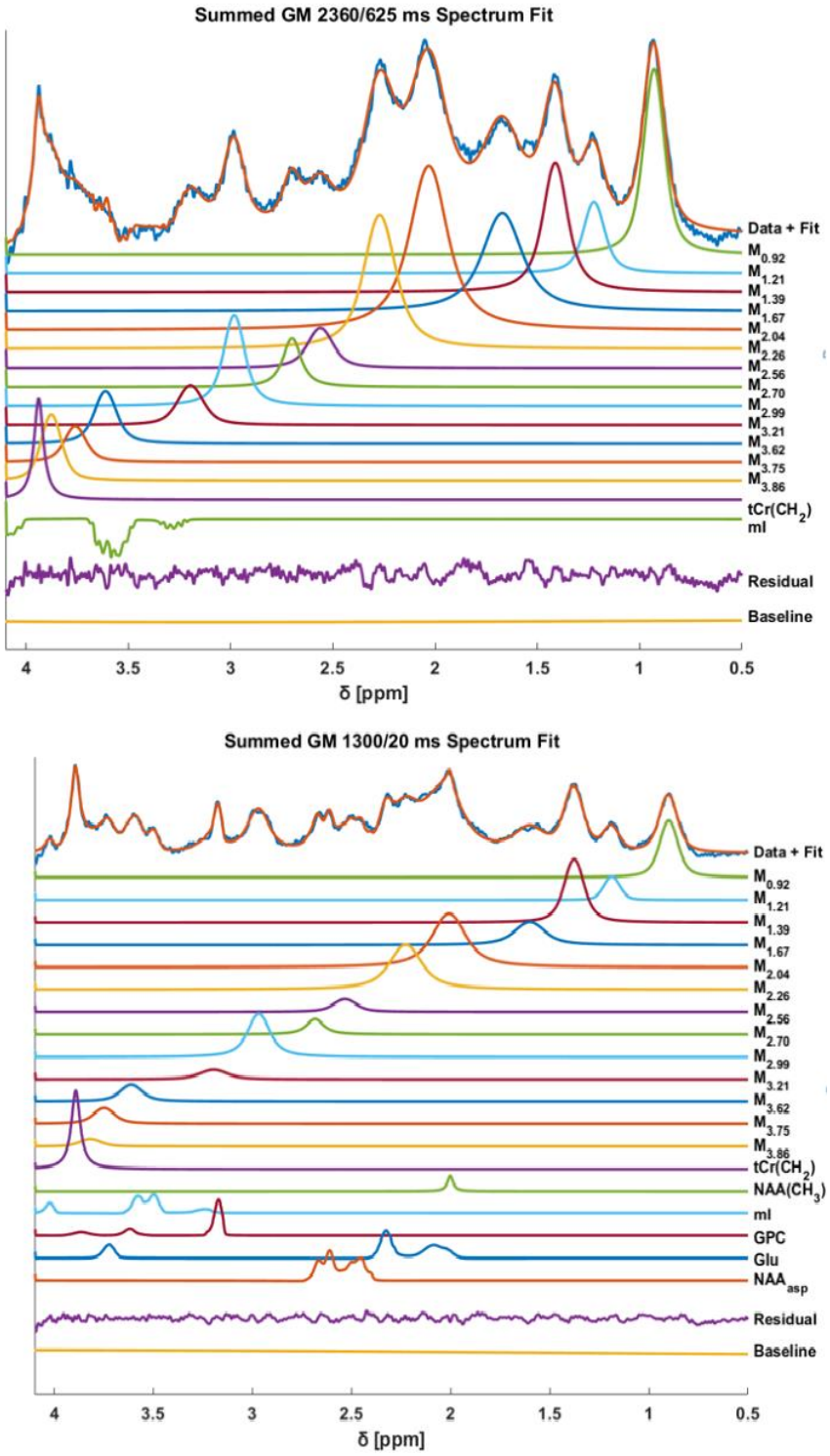

Figure 13: *Spectral fitting of MM peaks in LCModel for DIR MM spectra (summed across all the healthy volunteers) with TI_1/TI2: 2360/625 and 1300/20 ms. The figure is adapted from Publication 2.*

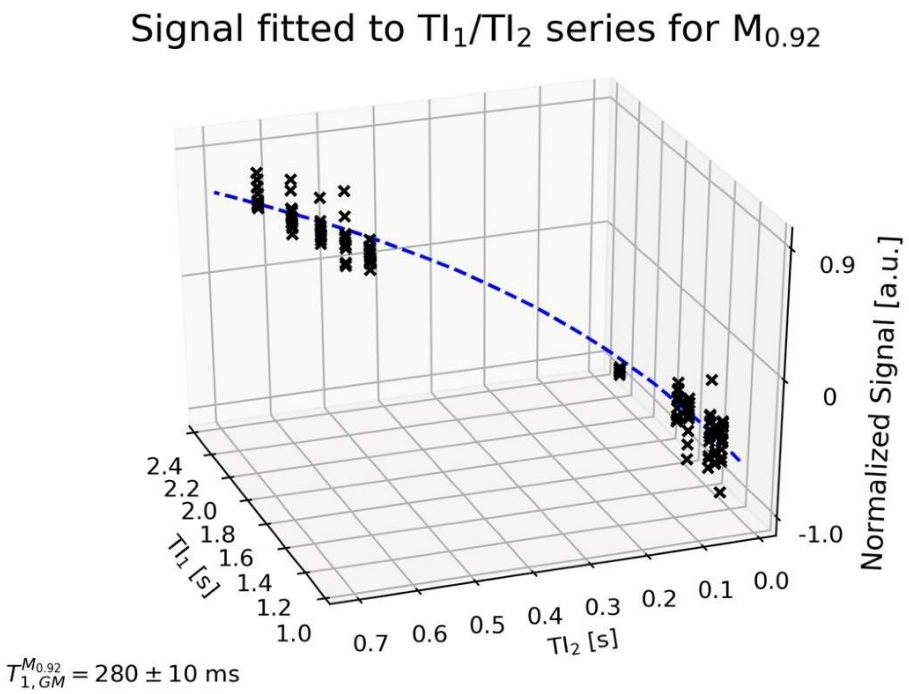

Figure 14: *A DIR series signal scatter plot for the $M_{0.92}$ peak from a GM-rich voxel. Black crosses represent data points from eleven healthy volunteers and the dark blue dashed line is the fitted solution to DIR signal Equation 29. No data points were excluded for this T_1 curve fit. The figure is adapted from Publication 2.*

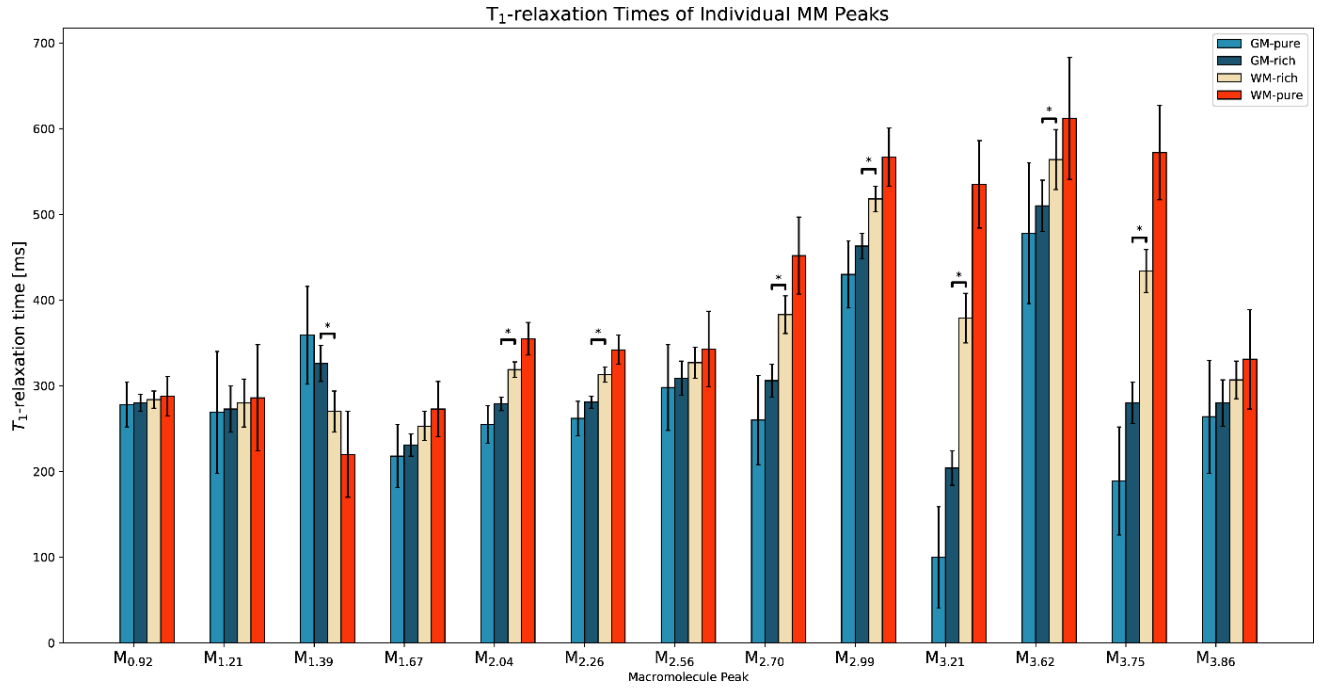

Figure 15: *The bar plots show calculated T_1 relaxation times for 13 individual MM peaks in GM-pure, GM-rich, WM-rich, and WM-pure voxels. T_1 relaxation times for MM peaks that have significant differences (P<0.0038) between GM- and WM-rich voxels from Welch's t-test and Bonferroni corrections are indicated with an asterisk *. The figure is adapted from Publication 2.*

Discussion

Although it is possible to estimate T_1 relaxation times of the MM peaks using a single inversion recovery technique by simultaneously fitting metabolites, this approach may lead to wrong estimation in the concentration of MM peaks that are overlapped by the metabolite peaks. In contrast, the proposed DIR technique reduced metabolite residuals to a large extent at the expense of T_1-weighting.

Out of the eleven TI_1/TI_2 combinations chosen, five of them had negative M_Z/M_0 ranging from -0.82 to -0.58, and five of them had positive M_Z/M_0 ranging from 0.42 to 0.53 when assuming a T_1 relaxation time of the whole MM spectrum of 420 ms as reported by Xin et al[75] at 7 T. The range of magnetizations chosen was limited by the additional need to

suppress the metabolite signal. However, the chosen range appeared to be sufficient since the R^2 of the T_1 curve and low standard deviations in the T_1 relaxation times of the MM peaks represented good confidence. The negative M_Z/M_0 points of $M_{2.99}$, $M_{3.62}$, and $M_{3.75}$ had a higher signal amplitude which skewed the 3D signal fits thereby resulting in longer T_1 relaxation times of these peaks. This might be due to lower weight metabolites contributing to MM resonance at these chemical shifts, which may have led to an overestimation of the respective T_1 relaxation times.

T_1 relaxation times of MM peaks strongly increase with increasing field strength, which is in agreement with BPP theory[57]. Table 2 shows T_1 relaxation times of MM peaks reported so far across various field strengths.

The broad range of T_1 relaxation times of MM peaks suggests that approximating these values as a single value for the entire MM spectrum may neither be ideal for quantifying the concentrations of MM peaks with high accuracy nor to consider MM contributions to metabolite spectra correctly. A linear relationship between T_1 relaxation times and tissue type was assumed and the values for pure GM and WM voxels were calculated. Pure GM and WM T_1 relaxation times can in a next step be utilized for correct modeling of MM contributions in voxels with arbitrary tissue composition which is especially useful in sequences with strong T_1-weighting such as the FID-MRSI.

Conclusion

The demonstrated novel method to determine T_1 relaxation times of MM peaks at 9.4 T is extendible to all field strengths. T_1 relaxation times of 13 MM peaks in GM- and WM-rich voxels in the human brain at 9.4 T are reported for the first time. The calculated T_1 relaxation times were used in the quantification of MM peaks (section 1.2.3) and were a key in the development of the relaxation-corrected sequence-specific MM simulation model[60].

T_1 relaxation times of macromolecular peaks in the human brain [ms]						
Study	**Murali-Manohar (2020) Publication 2**		**Xin (2013)[75]**	**Hoefemann (2020)[72]**	**Behar (1994)[67]**	**Kreis (2005)[76]**
B0 (T)	9.4		7	3	2.1	1.5
Sequence	DIR-MC-semiLASER		IR-SPECIAL	2DJ-IR MC-PRESS	IR-3D ISIS	IR-PRESS
Echo Time (ms)	24		12	20 - 95	17	20
Repetition Time (ms)	8000		7500	3000 - 4000	4450	400-9000
Region of Interest	Occipital lobe		Occipital lobe (GM rich)	Occipital lobe (GM rich)	Occipital lobe (mixed)	mixed voxel
	GM rich	WM rich				
M0.94	280 ± 10	284 ± 10	420 ± 20	290	250 ± 36	220 ± 60
M1.22	273 ± 27	280 ± 28		309		200 ± 50
M1.43	326 ± 21	270 ± 24				
M1.70	231 ±13	253 ± 17		225		
M1.81				247		
M1.90						
M2.05	279 ± 8	319 ± 9				
M2.07						
M2.17						
M2.27	281 ± 7	313 ± 9		263		
M2.36						
M2.47						
M2.57	309 ± 20	327 ± 18				
M2.74	306 ± 19	383 ± 22		[400]		
M2.97	463 ± 15	518 ± 15		[400]		
M3.00						
M3.09				[400]		
M3.21	204 ± 20	379 ± 29				
M3.26-3.28				[400]		
M3.4-3.6	510 ± 30	564 ± 35		[400]		
M3.71	280 ± 24	434 ± 25				
M3.79						
M3.87	280 ± 27	307 ± 22		347		
M3.97						
M4.20						

Table 2: *T_1 relaxation times of macromolecular peaks in the human brain from Publication 2 and other studies performed at different field strengths. The values in brackets reached the maximum limits set in the FitAid software. The table is adapted from the MM consensus article[57] (co-author publication).*

1.2.3 Quantification of macromolecules

Introduction

Several clinical biomarkers exist based on the changes in metabolite concentrations for neurological pathologies. Calculating MM concentrations reliably and to be able to compare them across different vendors and sites will open a completely new possibility of establishing potential biomarkers for various diseases. For example, changes in concentrations of MMs have been reported previously in multiple sclerosis[79], brain tumors[80], and stroke[81].

Since inversion recovery techniques used to acquire MM spectra introduce a severe T_1-weighting, it is essential to correct for the relaxation effects when estimating tissue concentrations of MM. Previous works have reported concentrations for some or all MM peaks without correcting for T_1 or T_2 relaxation times. Here in this section, the concentrations of MM peaks are reported for the first time after correcting for both spin-lattice and spin-spin relaxation effects using T_1 relaxation times from Publication 2 and T_2^{eff} relaxation times from Publication 1.

Study design

MP2RAGE images were acquired by using the home-built coil[68] in volume mode and driving power to all 8 transmit channels. The high-resolution anatomical images were then segmented into GM, WM, and CSF tissue content with SPM12[50].

GM- and WM-rich voxels (2×2×2 cm^3) were chosen in the occipital lobe and occipital-parietal transition respectively. Spectra were acquired using a DIR MC semiLASER sequence (TE/TR: 24/8000 ms) with TI_1/TI_2 = 2360/625 ms (Publication 2) since it corresponded to maximal MM signal retention and minimal metabolite residuals. Water reference spectra (TE/TR: 24/8000 ms) were acquired without MC. The acquired water spectra were used as internal reference. Spectral fitting was performed as described in section 1.2.2 using LCModel[30] using simulated Voigt peaks for 13 MM peaks.

The LCModel MM concentrations were then corrected for tissue fractions and relaxation effects of both MM peaks and water as described in section 1.1.8. Using the calculated T_1 relaxation times from Publication 2 (section 1.2.2) and T_2^{eff} relaxation times of MM peaks from Publication 1 (section 1.2.1), MM concentrations were quantified in protons mmol/kg[48] in both GM- and WM-rich voxels using internal water reference. Wilcoxon rank-sum tests (α = 0.05) were performed to assess for different concentrations for all MM peaks between tissue types.

Results

The average tissue content in the voxels were calculated to be GM/WM/CSF = 72 ± 2 / 22 ± 3 / 6 ± 4% and 35 ± 6 / 62 ± 7 / 3 ± 3% respectively. The concentrations of 13 MM peaks after correcting for tissue type specific water content and water and MM relaxation effects are reported in Figure 16 in protons per mmol/kg. $M_{2.04}$ has the highest concentration with 78.4 ± 10.7 and 76.6 ± 10.9 protons per mmol/kg in GM- and WM-rich voxels respectively.

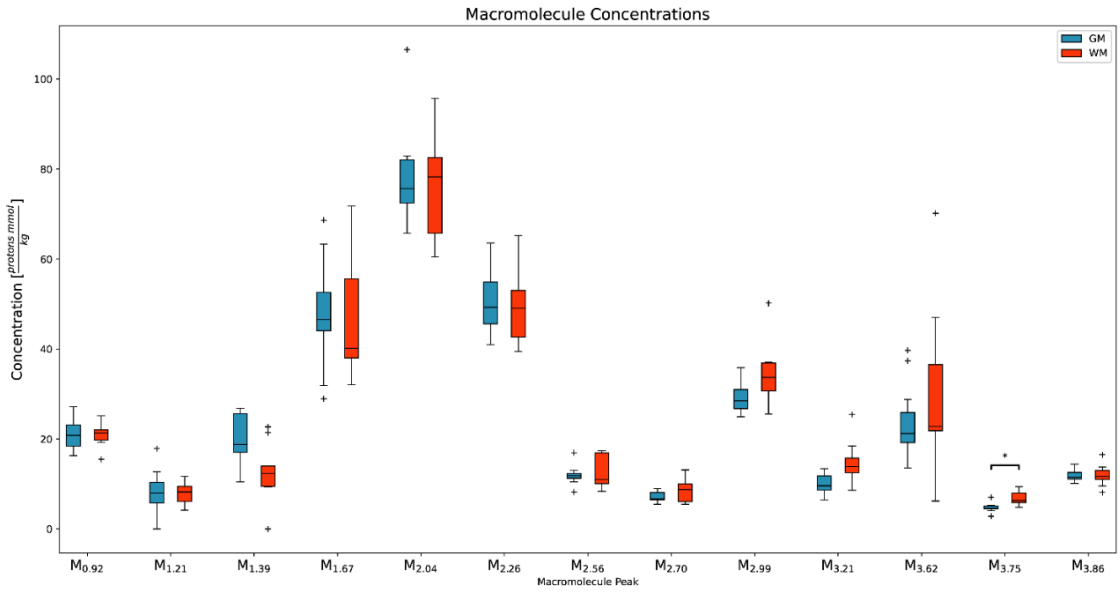

Figure 16: *Concentrations of MM peaks in GM- and WM-rich voxels are reported in protons mmol/kg. Black plus signs represent data points that were not within the 95% confidence interval when assuming a Gaussian distribution. The figure is adapted from Publication 2.*

Concentration of macromolecular peaks in the human brain [protons mmol/kg]							
Study	**Murali-Manohar (2020) Publication 2**		**Landheer [73](2020)**	**Giapitzakis[82] (2018)**		**Snoussi[83] (2015)**	**Snoussi[83] (2015)**
B0 (T)	9.4		3	9.4		3	7
Sequence	DIR MC semiLASER		DIR semiLASER	DIR MC semiLASER		IR-semiLASER	IR-semiLASER
Echo Time (ms)	24		20.1	24		31	31
Repetition Time (ms)	8000		2000	10000		1559	3000
Inversion Time(s) [ms]	2360/625		920/330	2360/625		600	900
T_1 correction	Yes		No	No		No	No
T_2 correction	Yes		Yes	No		No	No
Tissue fraction correction	Yes		Yes	Yes		Yes	Yes
Region of Interest	Occipital lobe		Occipital and frontal lobe	Occipital lobe (GM rich)	Left parietal lobe (WM rich)	Centrum semiovale and anterior cingulate cortex	Centrum semiovale and anterior cingulate cortex
	GM rich	WM rich					
M0.92	21.1 ± 3.3	21.0 ± 2.6	33.0 ± 4.1	8.31	7.05	~ 16	~ 15
M1.21	8.2 ± 4.6	7.9 ± 2.2	6.8 ± 1.7	1.82	2.63	~ 4	~ 5
M1.39	20.4 ± 5.3	12.6 ± 6.4	39.1 ± 15.1	5.48	5.97	~ 15	~ 14
M1.67	48.0 ± 11.2	46.7 ± 12.6	63.5 ± 15.1	8.63	5.34	~ 7	~ 6
M2.04	78.4 ± 10.7	76.6 ± 10.9	122.1 ± 33.1	11.31	11.56	~ 18	~ 19
M2.26	50.4 ± 6.8	49.0 ± 7.9	43.5 ± 13.7	9.54	9.42	~ 6	~ 5
M2.56	11.9 ± 2.0	13.0 ± 3.7	-	0.96	1.93	~ 5	~ 8
M2.70	7.1 ± 1.1	8.6 ± 2.6		1.84	2.14	-	-
M2.99	29.1 ± 3.0	34.7 ± 6.5	28.0 ± 6.1	3.97	3.89		
M3.21	10.0 ± 2.1	14.9 ± 4.6	17.2 ± 8.9	2.62	3.03		
M3.62	23.5 ± 8.1	23.5 ± 8.1	57.0 ± 7.1	1.10	1.23		
M3.75	4.8 ± 1.0	4.8 ± 1.0		3.34	3.66		
M3.86	11.8 ± 1.3	11.9 ± 2.3		0.83	1.36		
M3.87	-	-	-	7.59	7.00		
M4.20				1.83	1.70		

Table 3: *Concentration of macromolecular peaks [mmol/kg] reported from previous studies[73,82,83] is compared with the concentrations reported from Publication 2. Publication 2 has corrected for relaxation effects of the individual MM peaks whereas the other studies have not performed this correction. This leads to varying values of concentrations across different studies since the respective MM spectra have accumulated different T_1- and T_2-weightings based on the acquisition parameters used.*

Discussion

Since MM peaks are not yet assigned to specific proteins, peptides or amino acids, the number of protons contributing to each peak is unknown and hence not accountable. Therefore, the concentrations are reported with respect to each MM peak in protons per mmol/kg. Significant differences in concentration of $M_{3.75}$ peak was found between GM- and WM-rich voxels. Nevertheless, future work with a larger number of datasets is required to claim statistical differences with higher certainty.

Previous publications[73,82,83] have reported the concentrations for some or all MM peaks without correcting either for T_1 or T_2 relaxation times or both. Since inversion recovery techniques used to measure the MM peaks introduce some T_1-weighting of the MM spectrum and MM T_2 relaxation times are short in comparison to TEs of the utilized sequences, not correcting for relaxation effects would result in differences in MM concentration estimates across sites. Therefore, they might not be directly comparable. The concentration values reported by Landheer et al[73] appear to be somewhat in agreement with values from Publication 2; however, since Landheer et al[73] did not correct for T_1-weighting, there could be some discrepancy between the results. A comparison between the concentrations of MM peaks in the human brain reported from previous studies[73,82,83] and this study is presented in Table 3.

Conclusion

The concentrations of 13 individual MM peaks in both GM- and WM-rich voxels are reported. The values are reported in protons × mmol/kg using internal water referencing after correcting for tissue type specific water and MM T_1 and T_2^{eff} relaxation times. This is the first study to report the concentrations of MM peaks in the human brain after correcting for both T_1 and T_2^{eff} relaxation times of the MM peaks. The importance of performing such a correction is illustrated as it enables easier comparison across sites, sequences, field strengths and vendors.

1.3 Quantification of metabolites

MRS at UHF benefits from improved SNR, increase in frequency dispersion and more simplified spectral patterns from strong J-coupled systems[13]. This allows better detection of metabolites at UHF. Methodologies at UHF have underwent significant development in order to overcome the challenges that are posed by UHF such as B_0 inhomogeneity, inhomogeneous B_1^+ and B_1^- (transmit and receive respectively) fields, shorter T_2 relaxation times and so on.

Even though in NMR it is common to use both one-dimensional (1D) and two-dimensional (2D) spectroscopy techniques, the most commonly utilized method for in vivo ^{1}H MRS is one-dimensional spectroscopy. This is because of the fact that the 2D MRS techniques, especially in vivo, have longer scan durations and they require more advanced post-processing and dedicated spectral fitting routines. On the other hand, 2D MRS techniques may hold advantages in terms of quantifying low concentration and J-coupled metabolites more reliably.

This section of the thesis primarily aims at quantification of metabolite concentrations in the human brain at 9.4 T using both 1D (1.3.2) and 2D (1.3.3) MRS techniques and compare both approaches with each other. In addition, T_2 relaxation times of metabolites are calculated in section 1.3.1 in order to facilitate correction for T_2 relaxation times of metabolites in sections 1.3.2 and 1.3.3.

1.3.1 T_2 relaxation times of metabolites

Introduction

As discussed in section 1.1.8, concentrations of metabolites are comparable across different field strengths, vendors or localization schemes after correcting for tissue fraction composition and for T_1 and T_2 relaxation effects of both water and metabolites. Therefore, in order to quantify metabolite concentrations at 9.4 T, the knowledge of T_1 and T_2 relaxation times is essential. For this, T_1 and T_2 relaxation times of water in GM, WM and CSF at 9.4 T were considered from Hagberg et al[49]. T_1 relaxation times of metabolites at

9.4 T were taken from Wright et al[60,61] (co-author paper not a part of this thesis). T_2 relaxation times of metabolites at a given field strength, as mentioned in section 1.1.5, are not only tissue- and sequence-specific, but also specific to the brain region from where the values were measured[11]. Other than as a correction factor in the quantification of metabolites, the knowledge of T_2 relaxation estimates are also helpful in optimizing the acquisition parameters for 2D MRS (section 1.3.3). Moreover, T_2 relaxation times of metabolites have been observed to undergo changes in pathologies such as Alzheimer's disease[84]. This section of the thesis focuses on calculating T_2 relaxation times of metabolites in a GM-rich voxel in the occipital lobe from an echo-time series experiment using MC-semiLASER. The contribution of MM signal to the metabolite TE series was accounted for using the corresponding TE series of MM acquired in section 1.2.1.

Study Design

Eleven healthy volunteers participated in the study after providing written informed consent before the examination. The measurements were performed on a 9.4 T Magnetom whole-body MRI scanner using a home-built proton coil with 8 transmit and 16 receive channels[68]. For the spectroscopy experiments, the coil was driven in surface mode with the three bottom channels using an unbalanced three-way Wilkinson splitter as described in Giapitzakis et al[24]. The metabolite-cycled semiLASER[24] localization scheme was employed to acquire the 1D MRS data from a GM-rich voxel in the occipital lobe. For the calculation of the T_2 relaxation times of metabolites, an echo time series of MC-semiLASER[24] spectra (TE: 24, 32, 40, 52, and 60 ms; TR: 6000 ms; averages: 96; excitation frequency: 7.0 ppm) were acquired.

Raw data were preprocessed with an in-house written software in MATLAB. The preprocessing steps are described in detail in Publication 1. Metabolite basis sets were simulated using Vespa[33,85] (version 0.9.3) for the semiLASER sequence for real pulses. The following metabolites were included in the basis set: NAA, NAAG, GABA, Asp, Cr, Glu, Gln, GSH, GPC, Glyc, mI, Scy, Lac, PCr, PCho, PE, and Tau. The abbreviations of these metabolites are given in section 1.1.7. Also TE-specific MM spectrum (section 1.2.1) were included in the corresponding basis sets. Finally, the data were fitted in

LCModel[30] with the simulated basis set. The relative concentrations of metabolites obtained from LCModel for the TE series were fit to a mono-exponential decay.

T_2 relaxation times of metabolites were derived from the exponential decay curves. The mean coefficient of determination (R^2) was calculated for the exponential fit. T_2 relaxation times estimated from exponential fits that had $R^2 < 0.5$ were discarded. Therefore, T_2 relaxation times for Lac, Tau, and Scy were not reported.

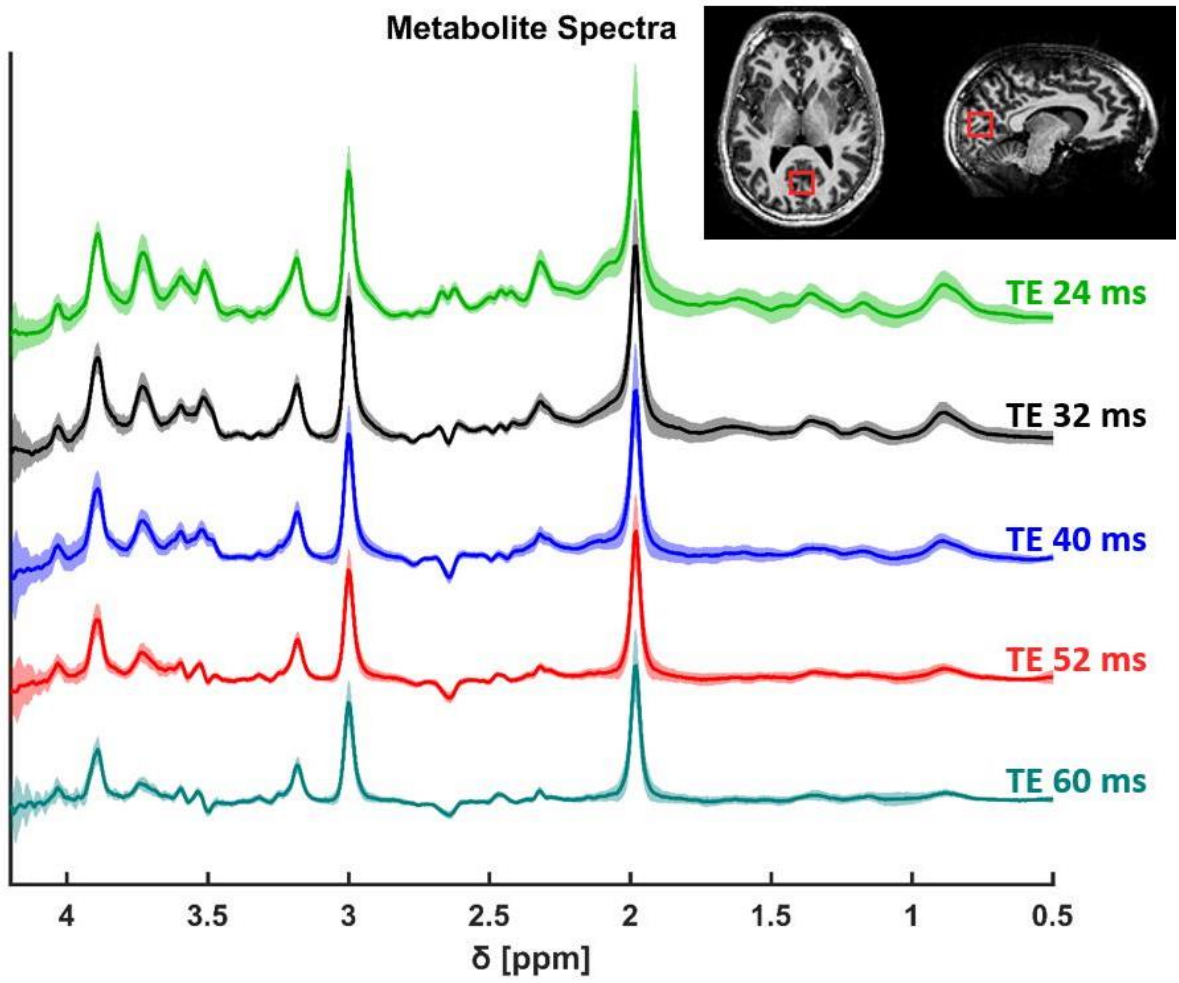

Figure 17: *Echo time series spectra of metabolites (TE: 24, 32, 40, 52, and 60 ms) obtained using MC-semiLASER localization for determining T_2 relaxation times of human brain metabolites at 9.4T. The figure is adapted from Publication 1.*

Results

Figure 17 shows the TE series of metabolite spectra from the GM-rich voxel in the occipital lobe. For TE = 32, 40, 52 and 60 ms, the J-evolution of Asp, Glu, mI, NAA(CH_2), and Tau can be observed. Spectral fitting for TE = 24 ms is shown in Figure 18.

The T_2 relaxation times calculated from both individual data and summed data (across 11 healthy volunteers) are shown as box plots in Figure 19. The T_2 relaxation times are reported along with respective R^2 values in Publication 1. The values range from 55 to 105 ms, except for NAAG with ~40 ms. R^2 values for all the reported metabolites were above 0.7 except for Asp and Glyc.

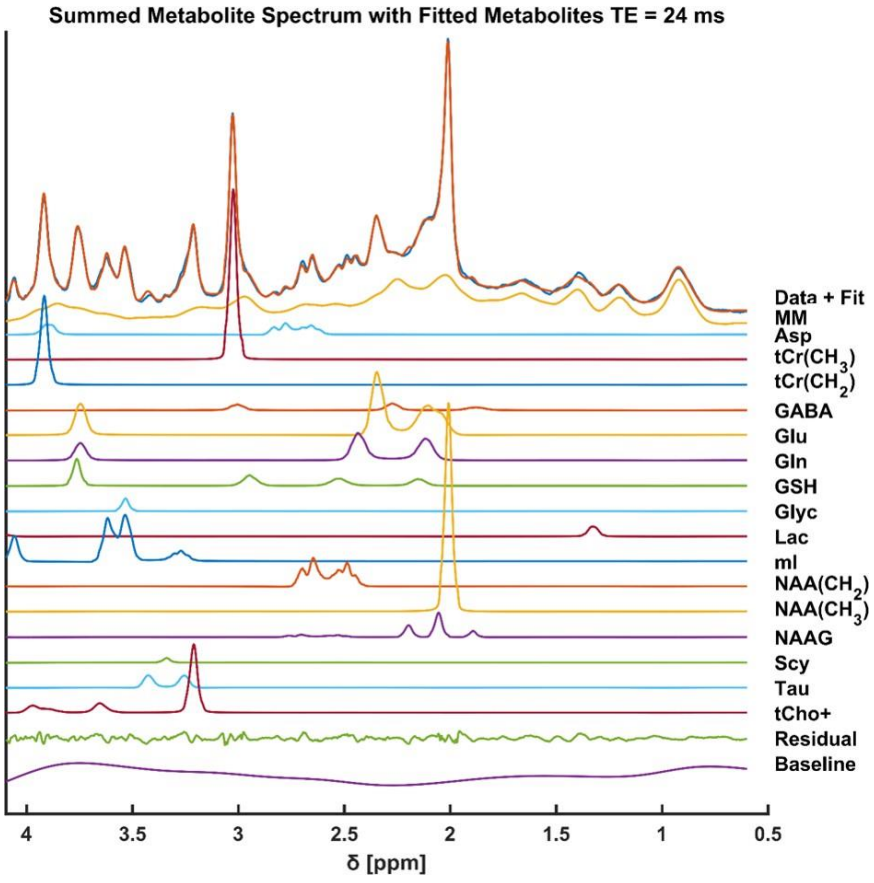

Figure 18: *LCModel spectral fit of metabolite basis vectors simulated using Vespa to subject-wise summed TE = 24 ms data. The figure is adapted from Publication 1.*

Discussion

This study reported the T_2 relaxation times of J-coupled metabolites at 9.4 T for the first time. The values of the T_2 relaxation times of singlet resonances from a previous study at 9.4 T[8] are lower compared to the values reported in this study. The higher values in this work may be attributed to TE specific MM spectra included in the basis set for spectral fitting. It is known that the underlying MM spectra are faster decaying components whose presence could have caused shorter T_2 relaxation values reported in the previous study at 9.4 T[8].

The T_2 relaxation times of metabolites reported in this study followed the same trend compared to previous literature[63,86–88] in terms of singlets such as NAA(CH_3), tCho and tCr(CH_3) having longer T_2 relaxation times than tCr(CH_2). NAAG has shorter T_2 relaxation times compared to NAA moieties[86]. All the reported T_2 relaxation times in this study followed the field strength trend, values decreasing with increasing field strength. T_2 relaxation time of Glu is higher than that of Gln[86]. However, the difference between the values was unexpected given that they have a similar distribution[89] in the human brain and that they have similar molecular weight. Therefore, most likely the T_2 relaxation time of Gln was underestimated in this study.

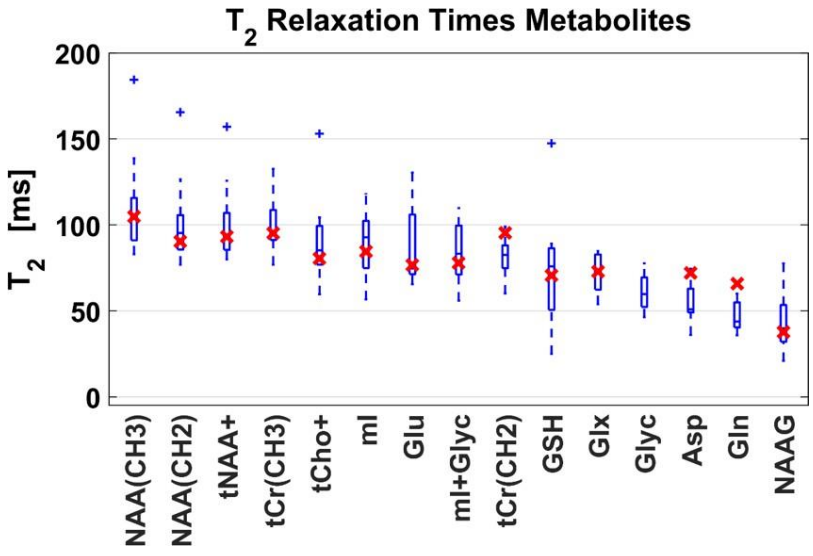

Figure 19: *T_2 relaxation times of metabolites are reported in ms for metabolites in box plots in descending order. The figure is adapted from Publication 1.*

Conclusion

T_2 relaxation times of 12 metabolites and metabolite moieties are reported for a GM-rich voxel in the occipital lobe at 9.4 T. The T_2 relaxation times ranged from 40 to 110 ms and are in line with the prediction of a decrease in T_2 relaxation times with increasing field strength. These values were further used in the correction factor for quantification of metabolite concentrations in sections 1.3.2 and 1.3.3.

1.3.2 One-dimensional spectroscopy (MC-semiLASER)

Introduction

Quantitative investigation of metabolite profiles in the human brain using ^{1}H MRS techniques have shown to aid clinical management of several brain pathologies[90]. Utilizing the advantages of UHF, non-invasive detection of up to 20 metabolites is possible using robust MRS acquisition methods[13]. Therefore, measuring the neurochemical profile of the human brain at UHF may help the neuroscientific and clinical research communities understand the disease mechanisms. This section focuses on the quantification of metabolite concentrations in the human brain using 1D MRS acquisition technique (MC-semiLASER) at 9.4T.

Study design

The experimental set up for this study was similar to the study design in section 1.3.1. For the quantification of metabolite concentrations, metabolite spectra were acquired with TE/TR: 24/6000 ms using MC-semiLASER[24] localization (averages: 32; excitation frequency: 2.4 ppm). In addition, unsuppressed water spectra (averages: 16; excitation frequency: 4.7 ppm) were acquired in order to quantify metabolite concentrations based on internal water signal.

Spectral fitting was performed in LCModel using a simulated basis set from Vespa. Same metabolites that were listed in section 1.3.1 were included here.

The high-resolution MP2RAGE[91] images (resolution: 0.6 mm^3) were segmented using SPM12[50] and the tissue compositions of the GM-rich voxels were calculated as GM:

32.9% ± 9.3%, WM: 64.7% ± 11.1%, and CSF: 2.4% ± 3.7%. The concentrations of the metabolites were then calculated using the formula given by Gasparovic et al[48] (section 1.1.8) including the relaxation time corrections for both water[91] and metabolites. For the quantification of metabolite concentrations, knowledge of relaxation times are necessary in order to correct for the T_1 and T_2 weighting in the MRS spectrum. T_1 relaxation times of metabolites were used from Wright et al[61] and T_2 relaxation times calculated in section 1.3.1 were utilized.

Results

Good spectral quality was achieved for all data and therefore, no data sets were excluded from further analysis.

The calculated concentrations of metabolites with and without T_2 correction are shown in Figure 20 for a fair comparison between this work and other studies, since some of those studies did not include a T_2 correction. Additionally, a consolidated comparison of concentrations of metabolites in mmol/kg was presented in a table in Publication 1.

Discussion

Corresponding MM spectra were included for each subject to account for the MM contribution in the metabolite spectrum. The residual tCr(CH_2) metabolite peak at 3.925 ppm was subtracted from the MM spectra before including the MM spectra in the basis set.

Previous metabolite quantification study[24] at 9.4 T using MC- semiLASER reported concentrations for 18 metabolites. However, the basis set was simulated assuming a a simple spin-echo sequence with TE: 6.5 ms due to the complex nature of the adiabatic pulses and their spin-locking effect[10]. This study included real adiabatic RF pulse shapes while simulating the basis set. The J-evolution pattern in the spectral data was mimicked well by the basis set both in this study and for the TE series basis sets that were simulated in section 1.3.1.

Mean T_2 relaxation times from all metabolites were used for correcting the concentrations of GABA, PE, and Scy as $R^2 < 0.5$ for the T_2 exponential curve fits in the previous section

1.3.1.NAA, Cr, tCho, PE, Tau, GABA, and mI concentrations with T_2 correction agree with previous literature[77,87,92–94]. However, Asp, Gln, Glyc, and Glu concentrations were significantly higher with T_2 correction. When considered without T_2 correction, the concentration values match with prvious literature for these metabolites. These discrepancies could have aroused because of the underestimated T_2 relaxation times of these metabolites. Particularly, the spline baseline behavior near the Gln chemical shift was negative, and this could not be compensated even when the stiffness factor DKNTMN in LCModel was set to 0.25. Therefore, there is a possibility of higher estimation of Gn concentrations. In addition, the T_1-weighting acquired in the DIR MM spectra (section 1.2.2) could also have influenced the concentration differences in some of these metabolites. The consolidated concentration comparison table provided in Publication 1 also described the relaxation corrections included in the previous literature, the sequence and the acquisition parameters considered[77,87,92–94].

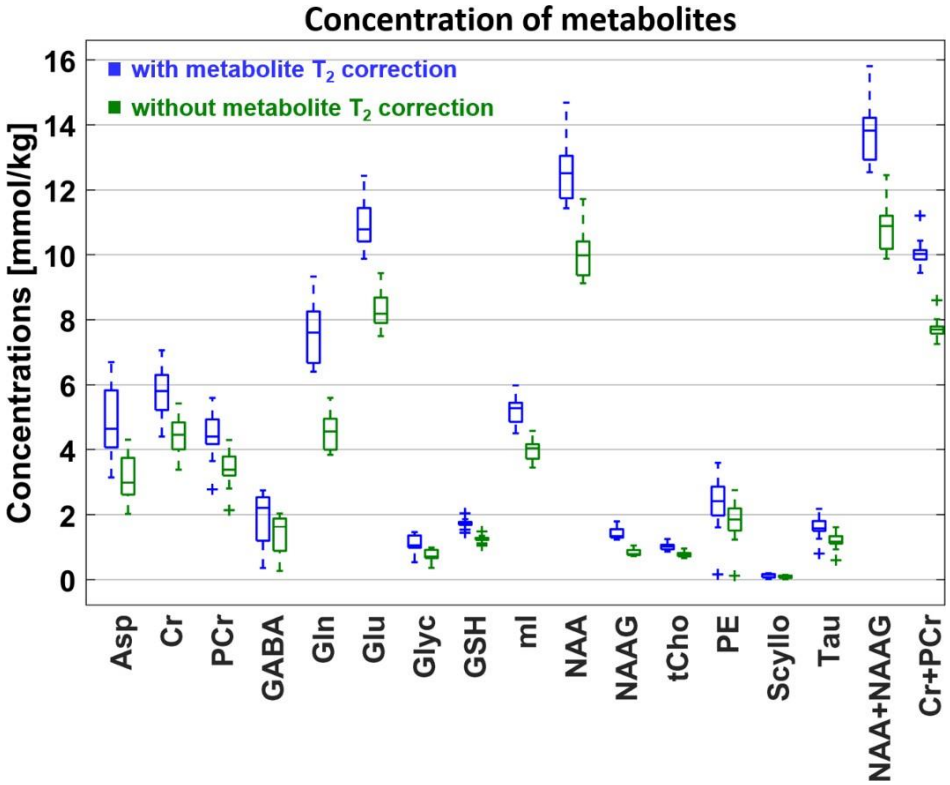

Figure 20: *Metabolite concentration box plots are shown here in mmol/kg with and without metabolite T_2 correction. The figure is adapted from Publication 1.*

Conclusion

The concentration values of metabolites measured in a GM-rich voxel in the occipital lobe are reported in mmol/kg both with and without T_2 correction. Most of the metabolite concentrations matched with previous literature with T_2 correction while some of the metabolite concentrations (Asp, Gln, Glyc and Glu) were higher compared to previous literature while including T_2 correction.

1.3.3 Two-dimensional spectroscopy (J-resolved MC-semiLASER)

Introduction

The NMR community has used the technique of multi-dimensional spectroscopy in order to reduce spectral overlap of peaks. Homonuclear two-dimensional techniques are also utilized in vivo and show promising results in detection and quantification of low SNR and J-coupled metabolite concentrations. Spectral acquisitions using correlation spectroscopy and J-resolved spectroscopy were shown to be feasible in vivo in humans at 1.5, 3 and 7 T[36–38]. The 2D techniques in vivo have longer scan durations and require sophisticated pre-processing and spectral fitting routines.

The detection capabilities are enhanced in 2D J-resolved spectroscopy[7] by spreading the spectral information into two dimensions by adding a step-wise increasing J-evolution delay during acquisition. In order to further improve the detection sensitivity, maximum echo sampling [7,95,96] is used where the data acquisition begins right after the final crusher gradients. This adds a tilt to the peak tails thereby further reducing spectral overlap[7].

This study shows the implementation of a 2D J-resolved MC-semiLASER sequence with a maximum echo sampling scheme at 9.4 T for human brain application and quantifies metabolite concentrations using ProFit v2.0[97], a dedicated 2D spectral fitting tool. In addition, respective quantification results are compared to previous 1D MRS studies.

Study design

Initially phantom measurements were performed in order to test the implementation of the 2D J-resolved MC-semiLASER sequence (Figure 21) and to optimize the sequence parameters.

2D metabolite spectra were then acquired from eleven healthy volunteers. Five healthy volunteers returned for the acquisition of 2D MM spectra. J-resolved MC-semiLASER with maximum echo sampling scheme (TR: 6000 ms, n: 85, Δt: 2ms, averages per TE: 8, transmit reference frequency: 2.4 ppm) acquisition was performed after second-order B_0 shimming[69] and voxel-based power calibration[70,78]. The encoding of the J-evolution in the second (indirect) dimension was created by inserting an incrementally increasing time delay of Δt/2 between the last pair of AFP pulses. TEs ranged from 24 to 194 ms incremented in steps of 2 ms. The MC pulse was turned off for the acquisition of 2D water reference spectra (average per TE:1) with transmit reference frequency set to 4.7 ppm.

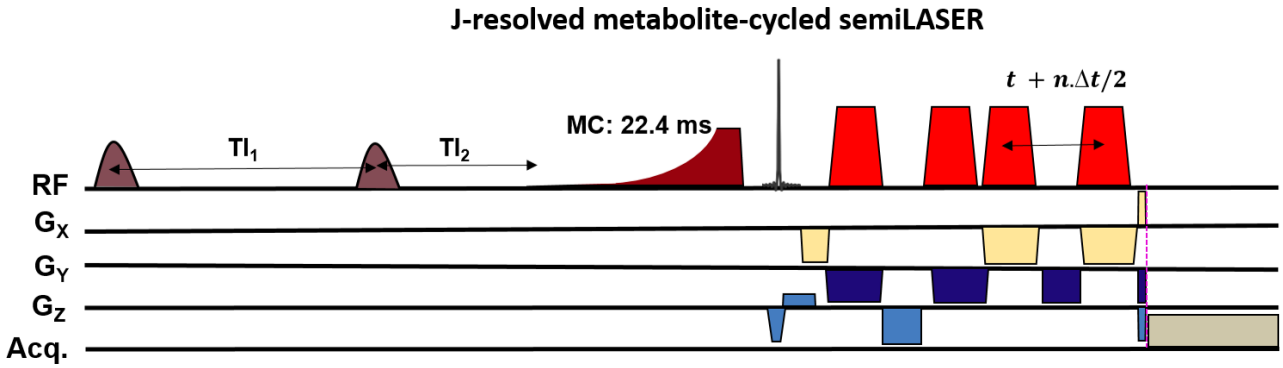

Figure 21: *Sequence diagram of J-resolved MC-semiLASER sequence is shown. The first two RF pulses are turned on for double inversion recovery in order to acquire a MM spectrum with two inversion times TI_1/TI_2 set as 2360/625 ms. They are turned off when acquiring the metabolite spectrum. The increasing J-evolution delay which corresponds to a progressively longer TE time is introduced between the last two AFP pulses in the sequence. Maximum echo sampling is implemented by beginning data acquisition right after the final set of crusher gradients after the last AFP pulse. The figure is adapted from Publication 3.*

MM spectra were acquired with DIR[59] (TI_1/TI_2: 2360/625 ms) J-resolved MC semiLASER sequence with all acquisition parameters set identical to metabolite spectra except TR set to 8000 ms.

Raw data were pre-processed as described in Publication 3 using an in-house MATLAB tool and J-resolved spectroscopy pre-processing tool which is a part of ProFit software[97,98] package. MP2RAGE[91] images were segmented into GM, WM and CSF tissue fractions using SPM12[50] in order to calculate the tissue composition specific tissue water content and metabolite and water relaxation correction factors during quantification of metabolite concentrations using internal water referencing (see section 1.1.8.).

Metabolite basis vectors (NAA, NAAG, GABA, Asp, Cr, Glu, Gln, Glc, GSH, GPC, Glyc, mI, Scyllo, Lac, PCr, PCho, PE and Tau) corresponding to 85 TE steps were simulated using Vespa[33] for the semiLASER sequence including real pulse shapes and sequence timings. All the 85 1D MRS basis sets were combined to form a 2D J-resolved MRS basis set. In addition, the summed MM spectrum from five healthy volunteers was also included in the 2D basis set.

As a next step, the 2D basis set were fitted to each of the metabolite spectra using ProFit 2.0[97]. Finally, metabolite concentrations were quantified in mmol/kg after the peak amplitudes obtained from the fitting software were referenced against the internal water were corrected for relaxation effects of both metabolites and water as well as tissue fractions[48].

Results

Figure 22 shows a metabolite spectrum acquired from a phantom with brain metabolites. There are no prominent artifacts due to truncation or t_1 noise in the indirect dimension. Also no visible J-refocused[38,99] peaks are seen. A representative 2D metabolite spectrum from a GM-rich voxel in the human occipital lobe (average content: GM/WM/CSF: 67 ± 8/ 29 ± 9/ 4 ± 1 % respectively) is shown in Figure 23.

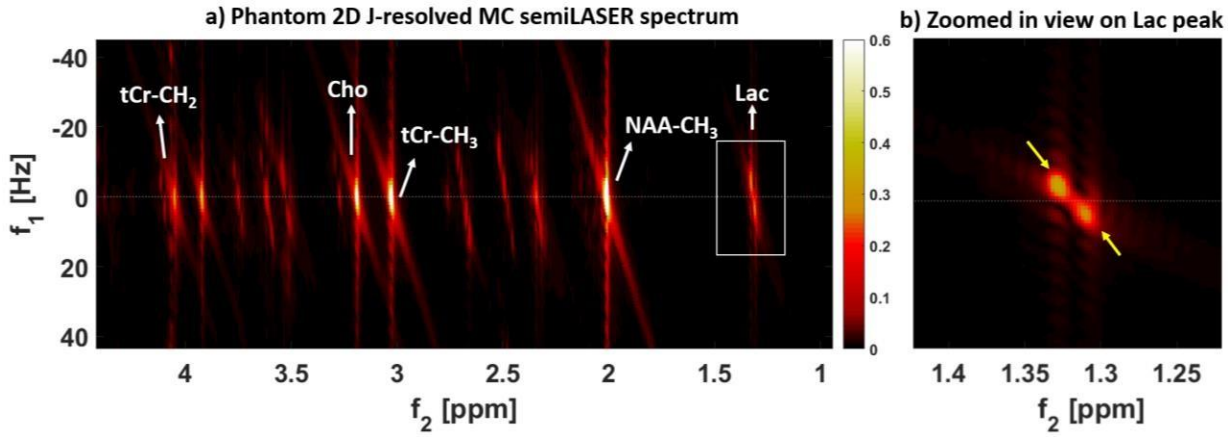

Figure 22: *Phantom spectrum acquired using the developed 2D J-resolved MC semiLASER sequence. To the right, zoomed in view of the lactate doublet present at 1.3 ppm is shown. The yellow arrows indicate the J-resolved peaks. The figure is adapted from Publication 3.*

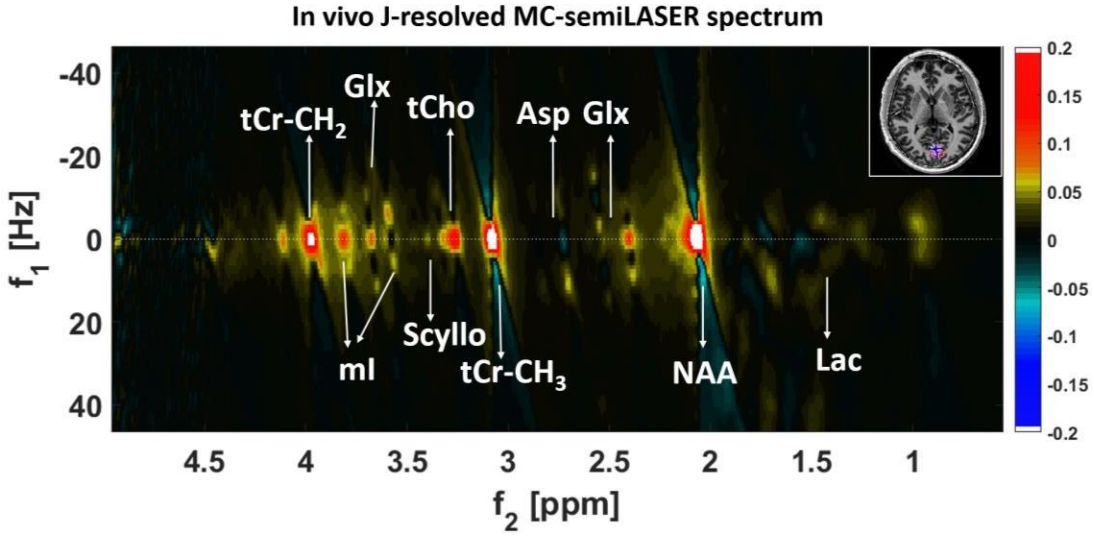

Figure 23: *2D J-resolved MC-semiLASER spectrum from a representative volunteer is shown with labeled metabolite peaks. The direct f_2 dimension has the chemical shift information and the indirect f_1 dimension has the J-coupling information. The figure inlay shows an anatomical MP2RAGE image with a gray matter rich voxel of interest in the occipital lobe. The figure is adapted from Publication 3.*

Spectral fitting of the 2D metabolite spectrum using ProFit 2.0[97] (Figure 24) yielded a minimum residual and demonstrate good agreement between model and experimental data. Finally, the metabolite concentration values after correcting for relaxation effects and tissue composition[48] are shown in bar plots in Figure 25. The bar plots aim at comparing the concentrations from this study and other recent 1D MRS studies at UHF[8,60,61,87,100,101].

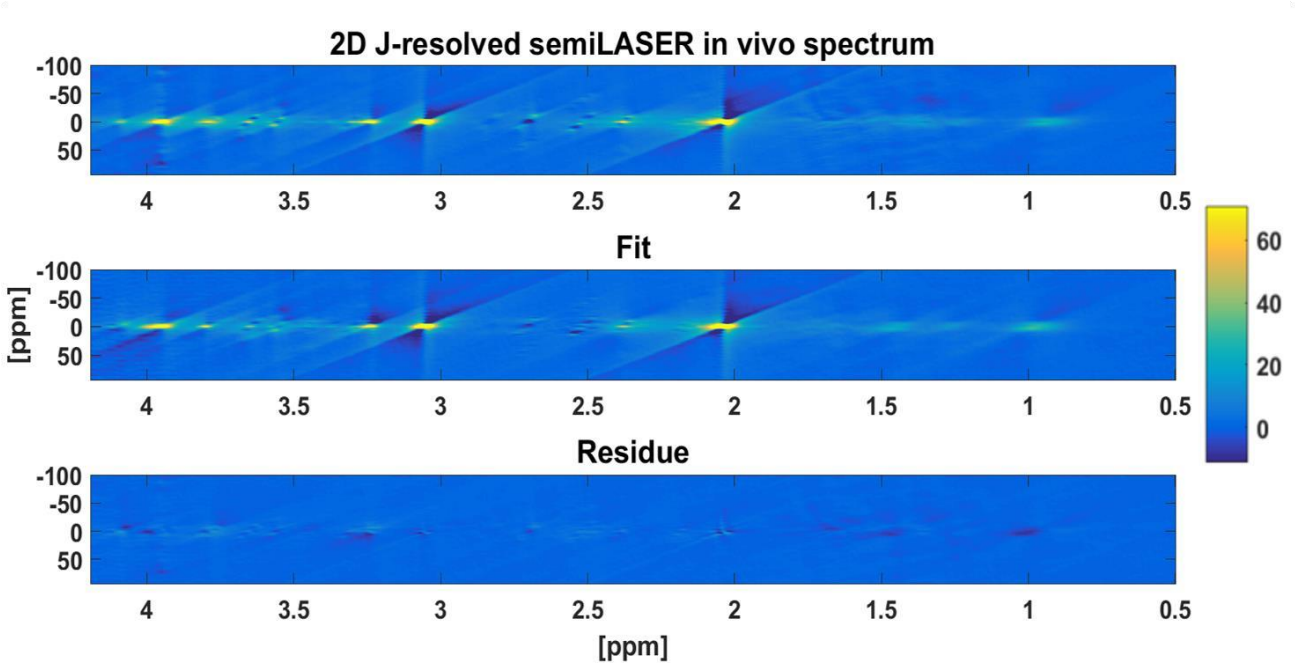

Figure 24: *Spectral fitting result for a representative in vivo 2D spectrum using ProFit 2.0. Top to bottom 2D MRS data, spectral fit and residue are shown. Minimum residual without any structured noise is achieved indicating that the tailored 2D basis set (simulated for 16 metabolites on Vespa including real pulses, sequence timings and experimentally acquired MM) fits the data well. The figure is adapted from Publication 3.*

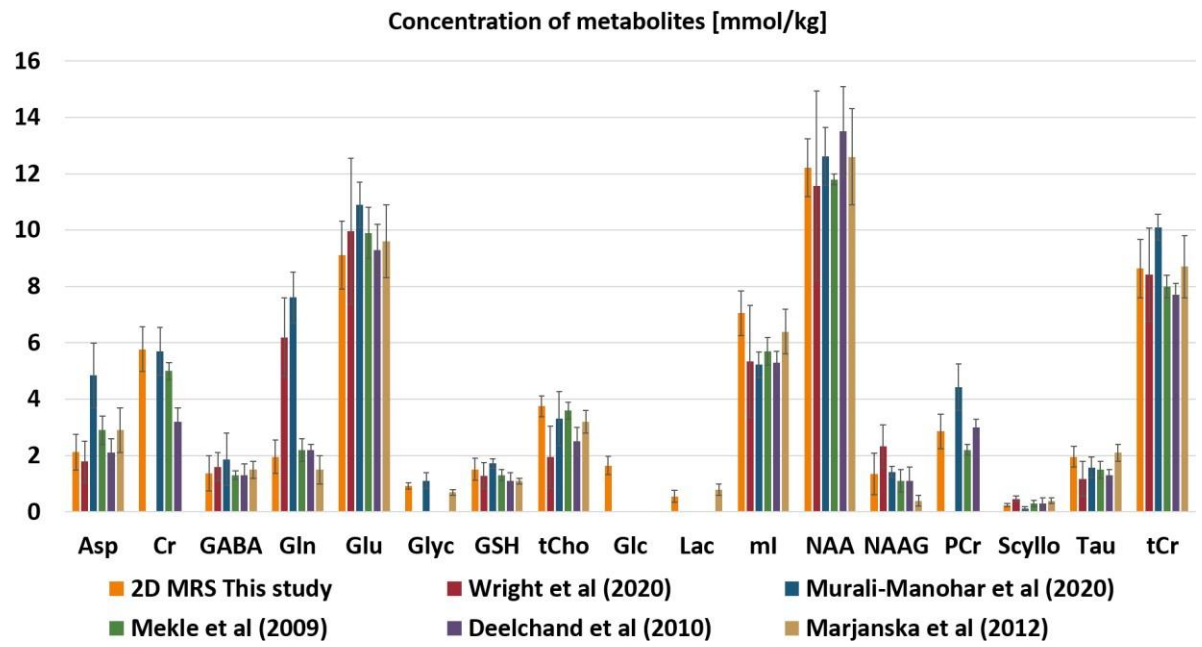

Figure 25: *Bar plots showing concentration of metabolites from this study and other recent 1D MRS studies*[8,60,61,87,100,101] *at UHF from a similar voxel location in the occipital lobe. The concentration values shown here are the mean and standard deviation of the metabolite concentrations reported by the respective studies. The figure is adapted from Publication 3.*

Discussion

Edden et al[99] showed that the chemical shift displacement effect causes spatially dependent differences in J-evolution of coupled spin systems for JPRESS spectra using both simulation and experimental methods at 3 and 7 T. This in turn can result in additional J-refocused peaks along the $f_1 = 0$ axis. The appearance of these unwanted additional peaks cause a loss of intensity in J-resolved peaks and more spectral overlap. Later Lin et al[38] demonstrated that the use of higher bandwidth pulses reduced the intensity of the J-refocused peaks by a factor of

$$(1 - \frac{\Delta\delta . B_0}{BW})$$

where $\Delta\delta$ is the chemical shift difference in ppm of the spins A and X in an AX spin system, B_0 is the frequency of the static magnetic field in MHz and BW is the bandwidth of the refocusing pulse. For the most separated lactate coupled peaks in upfield, the reduction in the intensity of the J-refocused peaks calculated is 86%. Therefore, it can be seen from Figure 22 that there are barely any J-refocused peaks present in the 2D spectrum.

Furthermore, this study reports the concentration of 16 metabolites in mmol/kg after correcting for relaxation effects and tissue content. Figure 25 compares the reported concentration from this study to concentration values from previous 1D MRS studies[8,60,61,87,100,101] at UHF for similarly located voxels in the occipital lobe. It can be observed from the figure that all the concentration values reported in this study lie within the range of values that were reported in previous studies except mI. The higher concentration of mI could possibly be due to a possible oppositely phased residual mI in the MM spectra as shown in a previous study (Publication 2). While removal of metabolite residuals is easier in 1D MRS, it is more complicated in 2D MRS especially with maximum echo sampling. Therefore, removal of metabolite residuals in the experimentally acquired 2D MM spectra or avoiding metabolite residuals using a relaxation-corrected sequence-specific MM simulation model[60] is necessary in the future for accurate estimation of mI concentration. For Asp, GABA, and Gln, the concentration values from this study are closer to previous literature[8,87,101] compared to values from 1D MRS studies[60,61,100] at 9.4 T. In addition, Glc and Lac are quantifiable with 2D MRS at 9.4T, while quantification of concentrations of these metabolites remains challenging with 1D MRS even at 9.4 T[60,61,100]. Statistical analysis was also performed to compare the 1D and 2D MRS acquisition techniques (Publication 3).

Not only the 2D metabolite spectrum show J-resolved peaks, but also the 2D MM spectrum and the 2D downfield spectrum show some well-resolved peaks. Given the efforts to assign MM and DF resonances to amino acids and metabolites, the 2D J-resolved acquisition technique may prove useful in assigning these peaks. Therefore, despite the longer scan durations of 2D MRS acquisition techniques at UHF, this may still be a good option to answer some open basic science questions in the field of MRS and brain metabolism. Open research questions include assigning unlabeled peaks in the DF

part of the spectrum, understanding the J-coupling behavior of MM peaks and aid assignment to amino acids, or in quantifying lower SNR J-coupled metabolite concentrations that are of importance in the brain energy metabolism in the healthy brain or in pathologies.

Conclusion

A two-dimensional J-resolved MC-semiLASER acquisition sequence with maximum echo sampling was implemented at 9.4 T. The concentration values of 16 metabolites in a GM-rich voxel in the occipital lobe are reported. Quantification of lower SNR and J-coupled metabolite concentrations such as Asp, GABA, Gln, Glc, and Lac was possible. The 2D MRS acquisition may prove beneficial to assign so far unlabeled downfield peaks between ~5.5 to 10.0 ppm, to understand the J-coupling behavior and the overlap of MM peaks, and for detection and quantification of lower SNR J-coupled metabolite concentrations such as Glc, and Glyc which are otherwise hard to assess.

1.4 Summary and Outlook

Extensive information about the neurochemical profile in the human brain can be obtained using in vivo ^{1}H MRS acquisition techniques. Therefore, MRS has steadily made its way as a key tool in the fields of neuroscience research and clinical diagnostics of brain disorders. In this thesis, characterization and quantification of concentrations and relaxation times of macromolecules and metabolites in the human brain using single voxel ^{1}H MRS at 9.4 T is presented.

There is very limited knowledge about the broad macromolecular resonances and several of their properties are yet to be thoroughly investigated. In view of this, a recent consensus article[57] on MRS visible macromolecules stressed the importance of studying the relaxation properties of the individual macromolecular peaks at various field strengths. As a first step towards this suggestion, this thesis achieved characterizing T_1 and T_2 relaxation times of individual macromolecular peaks at 9.4 T. In fact, the novel method proposed to determine the T_1 relaxation times of macromolecular peaks is extendible to all field strengths. The calculated T_1 and T_2 relaxation times of MM peaks were also discussed in the context of other studies performed at different field strengths.

The quantitative linewidth analysis of the MM peaks aided better understanding of the contribution to the residual linewidths of the MM peaks. Unlike the metabolite singlets whose linewidths were explainable by T_2 relaxation contribution and B_0 effects, the broader linewidths of the MM peaks were not explainable by T_2 relaxation contribution and B_0 effects alone. Therefore, it was concluded that the residual linewidth originated either from J-evolution effects or from spectral overlap of MM resonances that could originate from amino acids of the cytosolic protein. Depending on the large protein structure amino acids belong to, they can have different chemical shifts. However, these chemical shifts are distributed around a main resonance frequency for the bulk of proteins. This motivated fitting of macromolecular spectra to histograms of amino acids given in the Biological Magnetic Resonance Bank BMRB[102] (co-author abstract not a part of this thesis)[74]. The preliminary fits showed promising results with amino acids fitting model representing the MM spectra. Further development of a better spectral fitting model

of amino acids to MM peaks may allow characterization and quantification of amino acids from the MM spectra. This might also potentially help assign some of the unlabeled peaks in the downfield part of the proton spectrum to amino acids[74,102] and characterize the downfield peaks better[103] (co-author paper not a part of this thesis). Furthermore, the measured T_1 and T_2 relaxation times of macromolecules enabled T_1- and T_2-weighting corrections during quantification of these peaks. This, in turn, makes the concentration of the macromolecular peaks comparable across field strengths, vendors or sites opening a new possibility for potential clinical biomarkers for neurological diseases.

All the more, utilizing the T_1 and T_2 relaxation times of MM peaks as prior knowledge, a relaxation-corrected sequence-specific MM simulation model[60] (co-author paper not a part of this thesis) was constructed. This MM simulation model helps tackle some of the major challenges regarding the acquisition of MM spectra such as saving scan time in clinical applications or enable correct handling of MM in presence of short TR and TE magnetic resonance spectroscopic imaging[89,104] acquisitions.

Quantification of metabolite concentrations in mmol/kg was performed using one-dimensional MC-semiLASER acquisition at 9.4 T. T_2 relaxation times of metabolites were also reported which enabled T_2-weighting correction for quantification of metabolite concentrations.

Two-dimensional J-resolved MC-semiLASER acquisition method with maximum echo sampling was introduced and optimized at 9.4 T. It is seen as a good candidate for studies that aim at understanding the J-coupling and overlap in the macromolecular spectrum, assigning unlabeled downfield resonances or reliably quantifying J-coupled and lower SNR metabolite concentrations to understand changes in the energy metabolism in the healthy brain and in brain pathologies. The two-dimensional J-resolved semiLASER sequence was also optimized for 3 T[105] (own conference abstract) and is currently used in a clinical psychiatry study involving major depression disorder patients for a collaboration project during the course of my PhD. This also shows a potential clinical application for the developed 2D J-resolved semiLASER and its feasibility in a clinical environment.

1.5 References

1. de Graaf RA. *In Vivo NMR Spectroscopy*. John Wiley & Sons Ltd; 2007.
2. Keeler J. *Understanding NMR Spectroscopy*. John Wiley & Sons Ltd; 2006.
3. Levitt MH. *Spin Dynamics : Basics of Nuclear Magnetic Resonance*. 2nd editio. John Wiley & Sons Ltd; 2008.
4. Applications M resonance spectroscopy: tools for neuroscience research and emerging clinical. *No Title*. (STAGG CJ, ROTHMAN DL, eds.). Elsevier Inc.; 2014.
5. Kotitschke K, Jung H, Nekolla S, Haase A, Bauer A, Bogdahn U. High-resolution one-and two-dimensional 1H MRS of human brain tumor and normal glial cells. *NMR Biomed*. 1994;7(3):111-120. doi:10.1002/nbm.1940070303
6. Nagarajan R, Ramadan S, Thomas MA. Detection of Amide and Aromatic Proton Resonances of Human Brain Metabolites Using Localized Correlated Spectroscopy Combined with Two Different Water Suppression Schemes. *Magn Reson Insights*. 2010;4:MRI.S4739. doi:10.4137/MRI.S4739
7. Schulte RF, Lange T, Beck J, Meier D, Boesiger P. Improved two-dimensionalJ-resolved spectroscopy. *NMR Biomed*. 2006;19(2):264-270. doi:10.1002/nbm.1027
8. Deelchand DK, Moortele P-F Van de, Adriany G, et al. In vivo 1H NMR spectroscopy of the human brain at 9.4 T: Initial results. *J Magn Reson*. 2010;206(1):74-80. doi:10.1016/J.JMR.2010.06.006
9. Bloembergen N, Purcell EM, Pound R V. Nuclear magnetic relaxation. *Nature*. 1947;160(4066):475-476. doi:10.1038/160475a0
10. Allerhand A, Thiele E. Analysis of carr-purcell spin-echo NMR experiments on multiple-spin systems. II. The effect of chemical exchange. *J Chem Phys*. 1966;45(3):902-916. doi:10.1063/1.1727703
11. Hasan KM, Walimuni IS, Kramer LA, Narayana PA. Human brain iron mapping using atlas-based T_2 relaxometry. *Magn Reson Med*. 2012;67(3):731-739.

doi:10.1002/mrm.23054

12. Bloch F. Nuclear induction. *Phys Rev*. 1946;70(7-8):460-474. doi:10.1103/PhysRev.70.460

13. Henning A. Proton and multinuclear magnetic resonance spectroscopy in the human brain at ultra-high field strength: A review. *Neuroimage*. 2018;168:181-198. doi:10.1016/j.neuroimage.2017.07.017

14. Oz G, Alger JR, Barker PB, et al. The MRS Consensus Group. Clinical proton MR spectroscopy in central nervous system disorders. *Radiology*. 2014;270(3):658-679. doi:10.1148/radiol.13130531

15. Bottomley PA. *Spatial Localization in NMR Spectroscopy in Vivo*. http://www.mri.jhmi.edu/div_mri_res/PAB.PRESS.AnnalNYAcSci.1987.pdf. Accessed April 24, 2021.

16. Frahm J, Merboldt K, (1969) WH-J of MR, 1987 undefined. Localized proton spectroscopy using stimulated echoes. *Elsevier*. https://www.sciencedirect.com/science/article/pii/0022236487901545. Accessed April 24, 2021.

17. Scheenen TWJ, Klomp DWJ, Wijnen JP, Heerschap A. Short echo time1H-MRSI of the human brain at 3T with minimal chemical shift displacement errors using adiabatic refocusing pulses. *Magn Reson Med*. 2008;59(1):1-6. doi:10.1002/mrm.21302

18. Scheenen TWJ, Heerschap A, Dennis ·, et al. Towards 1 H-MRSI of the human brain at 7T with slice-selective adiabatic refocusing pulses. *Magn Reson Mater Phy*. 2008;21:95-101. doi:10.1007/s10334-007-0094-y

19. Garwood M, Delabarre L. The Return of the Frequency Sweep: Designing Adiabatic Pulses for Contemporary NMR. *J Magn Reson*. 2001;153:155-177. doi:10.1006/jmre.2001.2340

20. Mlynárik V, Gambarota G, Frenkel H, Gruetter R. Localized Short-Echo-Time

Proton MR Spectroscopy With Full Signal-Intensity Acquisition. *Wiley Online Libr*. 2006;56(5):965-970. doi:10.1002/mrm.21043

21. Öz G, Deelchand DK, Wijnen JP, et al. Advanced single voxel ^{1}H magnetic resonance spectroscopy techniques in humans: Experts' consensus recommendations. *NMR Biomed*. 2021;34(5):e4236. doi:10.1002/nbm.4236

22. Landheer K, Schulte RF, Treacy MS, Swanberg KM, Juchem C. Theoretical description of modern 1H in Vivo magnetic resonance spectroscopic pulse sequences. *J Magn Reson Imaging*. 2020;51(4):1008-1029. doi:10.1002/jmri.26846

23. Vaughan T, DelaBarre L, Snyder C, et al. 9.4T human MRI: Preliminary results. *Magn Reson Med*. 2006;56(6):1274-1282. doi:10.1002/mrm.21073

24. Giapitzakis I-A, Shao T, Avdievich N, Mekle R, Kreis R, Henning A. Metabolite-cycled STEAM and semi-LASER localization for MR spectroscopy of the human brain at 9.4T. *Magn Reson Med*. 2018;79(4):1841-1850. doi:10.1002/mrm.26873

25. Haase A, Frahm J, Hanicke W, Matthaei D. 1H NMR chemical shift selective (CHESS) imaging. *Phys Med Biol*. 1985;30(4):341-344. doi:10.1088/0031-9155/30/4/008

26. Tkáč I, Starčuk Z, Choi I-Y, Gruetter R. *In Vivo 1 H NMR Spectroscopy of Rat Brain at 1 Ms Echo Time*. Vol 41.; 1999. doi:10.1002/(SICI)1522-2594(199904)41:4

27. Dreher W, Leibfritz D. New method for the simultaneous detection of metabolites and water in localized in vivo1H nuclear magnetic resonance spectroscopy. *Magn Reson Med*. 2005;54(1):190-195. doi:10.1002/mrm.20549

28. Fichtner ND, Giapitzakis IA, Avdievich N, et al. In vivo characterization of the downfield part of 1H MR spectra of human brain at 9.4 T: Magnetization exchange with water and relation to conventionally determined metabolite content. *Magn Reson Med*. 2018;79(6):2863-2873. doi:10.1002/mrm.26968

29. Near J, Harris AD, Juchem C, et al. Preprocessing, analysis and quantification in

single-voxel magnetic resonance spectroscopy: experts' consensus recommendations. *NMR Biomed*. 2021;34(5):e4257. doi:10.1002/nbm.4257

30. Provencher SW. Automatic quantitation of localized in vivo 1H spectra with LCModel. *NMR Biomed*. 2001;14(4):260-264.

31. Chong DGQ, Kreis R, Bolliger CS, Boesch C, Slotboom J. Two-dimensional linear-combination model fitting of magnetic resonance spectra to define the macromolecule baseline using FiTAID, a Fitting Tool for Arrays of Interrelated Datasets. *Magn Reson Mater Physics, Biol Med*. 2011;24(3):147-164. doi:10.1007/s10334-011-0246-y

32. Stefan D, Cesare F Di, Andrasescu A, et al. Quantitation of magnetic resonance spectroscopy signals: The jMRUI software package. *Meas Sci Technol*. 2009;20(10):104035. doi:10.1088/0957-0233/20/10/104035

33. Soher B, Semanchuk P, Todd D, Steinberg J, Young K. VeSPA: integrated applications for RF pulse design, spectral simulation and MRS data analysis. *19th Meet ISMRM, Montr*. 2011.

34. Aue WP, Bartholdi E, Ernst RR. Two-dimensional spectroscopy. Application to nuclear magnetic resonance. *J Chem Phys*. 1976;64(5):2229-2246. doi:10.1063/1.432450

35. Macura S, Ernst RR. Elucidation of cross relaxation in liquids by two-dimensional N.M.R. spectroscopy. *Mol Phys*. 1980;41(1):95-117. doi:10.1080/00268978000102601

36. Ryner LN, Sorenson JA, Thomas MA. Localized 2D J-resolved 1H MR spectroscopy: Strong coupling effects in vitro and in vivo. *Magn Reson Imaging*. 1995;13(6):853-869. doi:10.1016/0730-725X(95)00031-B

37. Thomas MA, Hattori N, Umeda M, Sawada T, Naruse S. Evaluation of two-dimensional L-COSY and JPRESS using a 3?T MRI scanner: from phantoms to human brainin vivo. *NMR Biomed*. 2003;16(5):245-251. doi:10.1002/nbm.825

38. Lin M, Kumar A, Yang S. Two-dimensional J-resolved LASER and semi-LASER spectroscopy of human brain. *Magn Reson Med*. 2014;71(3):911-920. doi:10.1002/mrm.24732

39. Barker PB, Soher BJ, Blackband SJ, Chatham JC, Mathews VP, Bryan RN. Quantitation of proton NMR spectra of the human brain using tissue water as an internal concentration reference. *NMR Biomed*. 1993;6(1):89-94. doi:10.1002/nbm.1940060114

40. Thulborn KR, Ackerman JJH. Absolute molar concentrations by NMR in inhomogeneous B1. A scheme for analysis of in vivo metabolites. *J Magn Reson*. 1983;55(3):357-371. doi:10.1016/0022-2364(83)90118-X

41. Kreis R, Ernst T, Ross BD. Absolute Quantitation of Water and Metabolites in the Human Brain. II. Metabolite Concentrations. *J Magn Reson Ser B*. 1993;102(1):9-19. doi:10.1006/jmrb.1993.1056

42. Hennig J, Pfister H, Ernst T, Ott D. Direct absolute quantification of metabolites in the human brain with in vivo localized proton spectroscopy. *NMR Biomed*. 1992;5(4):193-199. doi:10.1002/nbm.1940050406

43. Narayana PA, Fotedar LK, Jackson EF, Bohan TP, Butler IJ, Wolinsky JS. Regional in vivo proton magnetic resonance spectroscopy of brain. *J Magn Reson*. 1989;83(1):44-52. doi:10.1016/0022-2364(89)90290-4

44. Buchli R, Boesiger P. Comparison of methods for the determination of absolute metabolite concentrations in human muscles by 31P MRS. *Magn Reson Med*. 1993;30(5):552-558. doi:10.1002/mrm.1910300505

45. Duc CO, Weber OM, Trabesinger AH, Meier D, Boesiger P. Quantitative 1H MRS of the human brain in vivo based on the simulation phantom calibration strategy. *Magn Reson Med*. 1998;39(3):491-496. doi:10.1002/mrm.1910390320

46. Akoka S, Barantin L, Trierweiler M. Concentration measurement by proton NMR using the ERETIC method. *Anal Chem*. 1999;71(13):2554-2557. doi:10.1021/ac981422i

47. Heinzer-Schweizer S, De Zanche N, Pavan M, et al. In-vivo assessment of tissue metabolite levels using 1H MRS and the Electric REference to access in vivo concentrations (ERETIC) method. *NMR Biomed*. 2010;23(4):406-413. doi:10.1002/nbm.1476

48. Gasparovic C, Song T, Devier D, et al. Use of tissue water as a concentration reference for proton spectroscopic imaging. *Magn Reson Med*. 2006;55(6):1219-1226. doi:10.1002/mrm.20901

49. Hagberg GE, Bause J, Ethofer T, et al. Whole brain MP2RAGE-based mapping of the longitudinal relaxation time at 9.4T. *Neuroimage*. 2017;144:203-216. doi:10.1016/j.neuroimage.2016.09.047

50. Ashburner J, Barnes G, Chen C, et al. *SPM12 Manual*. Wellcome Trust Centre for Neuroimaging, London, UK; 2014.

51. Behar KL, Rothman DL, Spencer DD, Petroff OAC. Analysis of macromolecule resonances in1H NMR spectra of human brain. *Magn Reson Med*. 1994;32(3):294-302. doi:10.1002/mrm.1910320304

52. Marjańska M, Deelchand DK, Hodges JS, et al. Altered macromolecular pattern and content in the aging human brain. *NMR Biomed*. 2018;31(2):1-8. doi:10.1002/nbm.3865

53. Louis MS, Alosco M, Rowland B, et al. Using Machine Learning techniques for identification of Chronic Traumatic Encephalopathy related Spectroscopic Biomarkers. *2017 IEEE Appl Imag Pattern Recognit Work*. 2017:1-5. doi:10.1109/AIPR.2017.8457949

54. Mader I, Karitzky J, Klose U, et al. Proton MRS in Kennedy disease: Absolute metabolite and macromolecular concentrations. *J Magn Reson Imaging*. 2002;16(2):160-167. doi:10.1002/jmri.10141

55. Mader I, Seeger U, Karitzky J, Erb M, Schick F, Klose U. Proton magnetic resonance spectroscopy with metabolite nulling reveals regional differences of macromolecules in normal human brain. *J Magn Reson Imaging*. 2002;16(5):538-

546. doi:10.1002/jmri.10190

56. Mlynárik V, Cudalbu C, Clément V, Marino D, Radovanovic I, Gruetter R. In vivo metabolic profiling of glioma-initiating cells using proton magnetic resonance spectroscopy at 14.1 Tesla. *NMR Biomed*. 2012;25(4):506-513. doi:10.1002/nbm.1763

57. Cudalbu C, Behar KL, Bhattacharyya PK, et al. Contribution of macromolecules to brain ^{1}H MR spectra: Experts' consensus recommendations. *NMR Biomed*. 2021;34(5):e4393. doi:10.1002/nbm.4393

58. Cudalbu C, Mlynárik V, Gruetter R. Handling Macromolecule Signals in the Quantification of the Neurochemical Profile. Mandal PK, ed. *J Alzheimer's Dis*. 2012;31(s3):S101-S115. doi:10.3233/JAD-2012-120100

59. Giapitzakis IA, Avdievich N, Henning A. Characterization of macromolecular baseline of human brain using metabolite cycled semi-LASER at 9.4T. *Magn Reson Med*. 2018;80(2):462-473. doi:10.1002/mrm.27070

60. Wright AM, Murali-Manohar S, Henning A. Relaxation corrected and Sequence-dependent Macromolecule Baseline Model. In: *ISMRM*. ; 2019:2247.

61. Wright A, Murali-Manohar S, Borbath T, Henning A. Longitudinal Relaxation Times of Metabolites in vivo at 9.4T. In: *27th Annu Meet Exhib Int Soc Magn Reson Med (ISMRM 2019)*. Montréal, QC, Canada; 2019.

62. Mader I, Seeger U, Weissert R, et al. Proton MR spectroscopy with metabolite-nulling reveals elevated macromolecules in acute multiple sclerosis. *Brain*. 2001;124(5):953-961. doi:10.1093/brain/124.5.953

63. Lopez-Kolkovsky AL, Mériaux S, Boumezbeur F. Metabolite and macromolecule T 1 and T 2 relaxation times in the rat brain in vivo at 17.2T. *Magn Reson Med*. 2016;75(2):503-514. doi:10.1002/mrm.25602

64. Pfeuffer J, Tkac I, Provencher SW, Gruetter R. Towards an In Vivo Neurochemical Profile: Quantification of 18 Metabolites in Short-Echo-Time 1H NMR Spectra of

the Rat Brain. *J Magn Reson*. 1999;141:104-120.

65. Graaf RA de, Brown PB, Mcintyre S, Nixon TW, Behar KL, Rothman DL. High Magnetic Field Water and Metabolite Proton T 1 and T 2 Relaxation in Rat Brain In Vivo. *Magn Reson Med*. 2006;56(2):386-394. doi:10.1002/mrm.20946

66. Xin L, Gambarota G, Mlynárik V, Gruetter R. Proton T2 relaxation time of J-coupled cerebral metabolites in rat brain at 9.4T. *NMR Biomed*. 2008;21(4):396-401. doi:10.1002/nbm.1205

67. Behar KL, Rothman DL, Spencer DD, Petroff OAC. Analysis of Macromolecule Resonances in 1 H NMR Spectra of Human Brain Preparation of Brain Tissue. *Isis*. 1994:294-302.

68. Avdievich NI, Giapitzakis I-A, Pfrommer A, Henning A. Decoupling of a tight-fit transceiver phased array for human brain imaging at 9.4T: Loop overlapping rediscovered. *Magn Reson Med*. 2018;79(2):1200-1211. doi:10.1002/mrm.26754

69. Gruetter R, Tkáč I. Field mapping without reference scan using asymmetric echo-planar techniques. *Magn Reson Med*. 2000;43(2):319-323. doi:10.1002/(SICI)1522-2594(200002)43:2<319::AID-MRM22>3.0.CO;2-1

70. Mekle R, Mlynárik V, Gambarota G, Hergt M, Krueger G, Gruetter R. MR spectroscopy of the human brain with enhanced signal intensity at ultrashort echo times on a clinical platform at 3T and 7T. *Magn Reson Med*. 2009;61(6):1279-1285. doi:10.1002/mrm.21961

71. Versluis MJ, Kan HE, van Buchem MA, Webb AG. Improved signal to noise in proton spectroscopy of the human calf muscle at 7 T using localized B_1 calibration. *Magn Reson Med*. 2010;63(1):207-211. doi:10.1002/mrm.22195

72. Hoefemann M, Bolliger CS, Chong DGQ, Veen JW, Kreis R. Parameterization of metabolite and macromolecule contributions in interrelated MR spectra of human brain using multidimensional modeling. *NMR Biomed*. June 2020. doi:10.1002/nbm.4328

73. Landheer K, Gajdošík M, Treacy M, Juchem C. Concentration and effective T $_2$ relaxation times of macromolecules at 3T. *Magn Reson Med*. May 2020:mrm.28282. doi:10.1002/mrm.28282

74. Borbáth T, Murali-Manohar S, Henning A. Towards a Fitting Model of Macromolecular Spectra: Amino Acids. In: *ISMRM*. ; 2019:1068.

75. Xin L, Schaller B, Mlynarik V, Lu H, Gruetter R. Proton *T* $_1$ relaxation times of metabolites in human occipital white and gray matter at 7 T. *Magn Reson Med*. 2013;69(4):931-936. doi:10.1002/mrm.24352

76. Kreis R, Slotboom J, Hofmann L, Boesch C. Integrated data acquisition and processing to determine metabolite contents, relaxation times, and macromolecule baseline in single examinations of individual subjects. *Magn Reson Med*. 2005. doi:10.1002/mrm.20673

77. Deelchand DK, Moortele PF Van De, Adriany G, et al. In vivo1H NMR spectroscopy of the human brain at 9.4 T: Initial results. *J Magn Reson*. 2010;206(1):74-80. doi:10.1016/j.jmr.2010.06.006

78. Versluis MJ, Kan HE, Van Buchem MA, Webb AG. Improved signal to noise in proton spectroscopy of the human calf muscle at 7 T using localized B1 calibration. *Magn Reson Med*. 2010;63(1):207-211. doi:10.1002/mrm.22195

79. Mader I. Proton MR spectroscopy with metabolite-nulling reveals elevated macromolecules in acute multiple sclerosis. *Brain*. 2001;124(5):953-961. doi:10.1093/brain/124.5.953

80. Mlynárik V, Cudalbu C, Clément V, Marino D, Radovanovic I, Gruetter R. In vivo metabolic profiling of glioma-initiating cells using proton magnetic resonance spectroscopy at 14.1 Tesla. *NMR Biomed*. 2012;25(4):506-513. doi:10.1002/nbm.1763

81. Petroff OAC, Graham GD, Blamire AM, et al. Spectroscopic imaging of stroke in humans: Histopathology correlates of spectral changes. *Neurology*. 1992;42(7):1349-1354. doi:10.1212/wnl.42.7.1349

82. Giapitzakis I-A, Avdievich N, Henning A. Characterization of macromolecular baseline of human brain using metabolite cycled semi-LASER at 9.4T. *Magn Reson Med*. 2018;80(2):462-473. doi:10.1002/mrm.27070

83. Snoussi K, Gillen JS, Horska A, et al. Comparison of brain gray and white matter macromolecule resonances at 3 and 7 Tesla. *Magn Reson Med*. 2015;74(3):607-613. doi:10.1002/mrm.25468

84. Wang H, Yuan H, Shu L, Xie J, Zhang D. Prolongation of T2 relaxation times of hippocampus and amygdala in Alzheimer's disease. *Neurosci Lett*. 2004;363(2):150-153. doi:10.1016/j.neulet.2004.03.061

85. Soher B. Versatile Simulation Pulses and Analysis. User Code Contributions – semi-LASER.

86. Wyss PO, Bianchini C, Scheidegger M, et al. In vivo estimation of transverse relaxation time constant (T2) of 17 human brain metabolites at 3T. *Magn Reson Med*. 2018;80(2):452-461. doi:10.1002/mrm.27067

87. Marjańska M, Auerbach EJ, Valabrègue R, Van de Moortele P-F, Adriany G, Garwood M. Localized ^{1}H NMR spectroscopy in different regions of human brain *in vivo* at 7T: T_2 relaxation times and concentrations of cerebral metabolites. *NMR Biomed*. 2012;25(2):332-339. doi:10.1002/nbm.1754

88. Kreis R, Slotboom J, Hofmann L, Boesch C. Integrated data acquisition and processing to determine metabolite contents, relaxation times, and macromolecule baseline in single examinations of individual subjects. *Magn Reson Med*. 2005;54(4):761-768. doi:10.1002/mrm.20673

89. Nassirpour S, Chang P, Henning A. High and ultra-high resolution metabolite mapping of the human brain using 1H FID MRSI at 9.4T. *Neuroimage*. 2018;168:211-221. doi:10.1016/j.neuroimage.2016.12.065

90. Wilson M, Andronesi O, Barker PB, et al. Methodological consensus on clinical proton MRS of the brain: Review and recommendations. *Magn Reson Med*. 2019;82(2):527-550. doi:10.1002/mrm.27742

91. Hagberg GE, Bause J, Ethofer T, et al. Whole brain MP2RAGE-based mapping of the longitudinal relaxation time at 9.4T. *Neuroimage*. 2017;144:203-216. doi:10.1016/j.neuroimage.2016.09.047

92. Mekle R, Mlynárik V, Gambarota G, Hergt M, Krueger G, Gruetter R. MR spectroscopy of the human brain with enhanced signal intensity at ultrashort echo times on a clinical platform at 3T and 7T. *Magn Reson Med*. 2009;61(6):1279-1285. doi:10.1002/mrm.21961

93. Terpstra M, Ugurbil K, Tkac I. Noninvasive quantification of human brain ascorbate concentration using ^{1}H NMR spectroscopy at 7T. *NMR Biomed*. 2010;23(3):227-232. doi:10.1002/nbm.1423

94. Penner J, Bartha R. Semi-LASER 1H MR spectroscopy at 7 Tesla in human brain: Metabolite quantification incorporating subject-specific macromolecule removal. *Magn Reson Med*. 2015;74(1):4-12. doi:10.1002/mrm.25380

95. Macura S, Brown LR. Improved sensitivity and resolution in two-dimensional homonuclear J-resolved NMR spectroscopy of macromolecules. *J Magn Reson*. 1983;53(3):529-535. doi:10.1016/0022-2364(83)90227-5

96. Kühn B, Dreher W, Leibfritz D, Heller M. Homonuclear uncoupled 1H-spectroscopy of the human brain using weighted accumulation schemes. *Magn Reson Imaging*. 1999;17(8):1193-1201. doi:10.1016/S0730-725X(99)00027-2

97. Fuchs A, Boesiger P, Schulte RF, Henning A. ProFit revisited. *Magn Reson Med*. 2014;71(2):458-468. doi:10.1002/mrm.24703

98. Schulte RF, Boesiger P. ProFit: Two-dimentional prior-knowledge fitting of J-resolved spectra. *NMR Biomed*. 2006;19(2):255-263. doi:10.1002/nbm.1026

99. Edden RAE, Barker PB. If J doesn't evolve, it won't J-resolve: J-PRESS with bandwidth-limited refocusing pulses. *Magn Reson Med*. 2011;65(6):1509-1514. doi:10.1002/mrm.22747

100. Murali-Manohar S, Borbath T, Wright AM, Soher B, Mekle R, Henning A. T_2

relaxation times of macromolecules and metabolites in the human brain at 9.4 T. *Magn Reson Med*. 2020;84(2):542-558. doi:10.1002/mrm.28174

101. Mekle R, Mlynárik V, Gambarota G, Hergt M, Krueger G, Gruetter R. MR spectroscopy of the human brain with enhanced signal intensity at ultrashort echo times on a clinical platform at 3T and 7T. *Magn Reson Med*. 2009;61(6):1279-1285. doi:10.1002/mrm.21961

102. Ulrich EL, Akutsu H, Doreleijers JF, et al. BioMagResBank. *Nucleic Acids Res*. 2007;36(Database):D402-D408. doi:10.1093/nar/gkm957

103. Borbath T, Murali-Manohar S, Wright AM, Henning A. In vivo characterization of downfield peaks at 9.4 T: T_2 relaxation times, quantification, pH estimation, and assignments. *Magn Reson Med*. 2021;85(2):587-600. doi:10.1002/mrm.28442

104. Chang P, Nassirpour S, Avdievitch N, Henning A. Non-water-suppressed 1H FID-MRSI at 3T and 9.4T. *Magn Reson Med*. 2018;80(2):442-451. doi:10.1002/mrm.27049

105. Murali-Manohar S, Giapitzakis I, Borbath T, Gaertner M, Henning A. Qualitative Comparison between In Vivo J-Resolved Semi-LASER at 3 T and 9.4 T. *25th Annu Meet Exhib Int Soc Magn Reson Med*. 2017.

2 Curriculum vitae

Saipavitra V Murali Manohar

PERSONAL INFORMATION

Address:

Mobile:

E-Mail:

Date of birth:

Nationality:

EDUCATION

02/2016 – now **PhD Student,** *Eberhard Karls Universität Tübingen, Max Planck Institute for Biological Cybernetics* (Physics)
Thesis: “Quantitative Magnetic Resonance Spectroscopy of Brain Metabolites and Macromolecules at Ultra-High Field”

06/2013 – 08/2015 **Master of Science in Physics,** *National Institute of Technology, Tiruchirappalli, Tamil Nadu, India*
Cumulative Grade: 9.7/10

06/2010 – 04/2013 **Bachelor of Science (Honors) in Physics,** *Sri Sathya Sai Institute of Higher Learning, Puttaparti, Andhra Pradesh, India*
Cumulative Grade: 4.97/5

WORK EXPERIENCE

02/2016 – now **MR Physicist PhD Student (Quantitative Magnetic Resonance Spectroscopy of Brain Metabolites and Macromolecules at Ultra-High Field)**

High Field Magnetic Resonance Center, Max Planck Institute of Biological Cybernetics, Tuebingen, Germany

06/2014 – 06/2015 **Postgraduate project (Effect of Annealing and Cu Doping on Structural and Optical Properties of ZnO Nanoparticles)**

Department of Physics, National Institute of Technology, Tiruchirappalli, India

05/2014 – 07/2014 **Internship (Coherence and Quantum States of Radiation)**

Department of Physics, Indian Institute of Technology - Madras, Chennai, India

06/2012 – 03/2013 **Undergraduate project (Study of Gamma Spectrum of ^{75}Se Decaying into ^{75}As)**

Department of Physics, Sri Sathya Sai Institute of Higher Learning, Andhra Pradesh, India

PROGRAMMING SKILLS

- C/C++
- Python
- Pulse Sequencing in IDEA (MRI scanner)
- R programming
- MATLAB
- LabView

LANGUAGE SKILLS

- English - Native
- German - Intermediate
- Hindi - Advanced
- Tamil - Mother tongue

ACHIEVMENTS

- **Summa Cum Laude award** from International Society for Magnetic Resonance in Medicine 2021
- **Institute Day Prize Winner** in M.Sc. Physics for first rank in III and IV semesters during 2014-2015
- **Institute Gold Medal** for securing highest CGPA in M.Sc. Physics
- **Outstanding student** in M.Sc. Physics 2014-2015 Award
- **Academic proficiency prize** for first rank in I and II semesters during 2013-2014.
- **Dr.T. Balasubramanian Endowment Award** for first rank in I and II semesters of M.Sc. Physics
- **Srimati.Parvathamma Gold medal** for being the topper of the university in B.Sc. (Hons.) Physics
- **Top Academic Performance Award** for excellent grades in academics in 1st year and 2nd year of B.Sc. (Hons.) Physics
- Participated in a free food & cloth distribution program across 150+ villages for 5 years by Sri Sathya Sai Organization recognized by UN ECOSOC

3 List of Publications

3.1 Appended Publications (3)

Journal Articles (3)

1. **Murali-Manohar S***, Borbath T*, Wright AM, Soher B, Mekle R, Henning A. "T2 relaxation times of macromolecules and metabolites in the human brain at 9.4 T." Magnetic resonance in medicine, 2020; 84:542–558. DOI: mrm.28174

2. **Murali-Manohar S*,** Wright AM*, Borbath T, Avdievich NI, Henning A. "A novel method to measure T1-relaxation times of macromolecules and quantification of the macromolecular resonances." Magnetic Resonance in Medicine, 2020. DOI: mrm.28484

3. **Murali-Manohar S**, Borbath T, Wright AM, Avdievich NI, Henning A. "Quantitative Two dimensional J-resolved semiLASER at 9.4 T in the human brain". (Submitted)

3.2 Other Recent publications

3.2.1 Journal Articles (6)

1. Giapitzakis IA*, Borbath T*, **Murali-Manohar S**, Avdievich N, Henning A. “Investigation of the influence of macromolecules and spline baseline in the fitting model of human brain spectra at 9.4 T”. Magnetic resonance in medicine, 2019;81(2):746-758. DOI: mrm.2746

2. Borbath T*, **Murali-Manohar S***, Wright AM, Henning A. “In vivo characterization of downfield peaks at 9.4 T: T2 relaxation times, quantification, pH estimation, and assignments.” Magnetic resonance in medicine, 2020. DOI: mrm.28442

3. Cudalbu C, Behar K, Bhattacharyya P, Bogner W, Borbath T, de Graaf R, Gruetter R, Henning A, Juchem C, Kreis R, Lee P, Lei H, Marjańska M, Mekle R, **Murali-Manohar S**, Považan M, Rackayová V, Simicic D, Slotboom J, Soher B, Starcuk Z, Starcukova J, Tkáč I, Williams S, Wilson M, Wright AM, Xin L, Mlynárik V. "Contribution of

macromolecules to brain 1H MR spectra: Experts' consensus recommendations.", NMR in Biomedicine, 2020 DOI: nbm.4393

4. Wright AM*, **Murali-Manohar S***, Borbath T, Avdievich NI, Henning A. "Relaxation corrected macromolecular model enables accurate determination of 1H longitudinal T1-relaxation times and concentrations of human brain metabolites at 9.4 T." Magnetic Resonance in Medicine. (Under review)

5. Borbath T, Dorst J, **Murali-Manohar S**, Wright AM, Henning A. “ProFit – v3: A single voxel fitting tool with adaptive baseline control.” Magnetic Resonance in Medicine. (Under review)

6. Borbath T, **Murali-Manohar S**, Henning A. “Human brain downfield peak assignments – a review from 9.4 T measurements perspective.” (In preparation)

***Equal contributions to the publication**

3.2.2 Talks (9)

First author contributions: 3

1. **Murali-Manohar S**, Borbath T, Wright A, Henning A. “Quantification of human brain metabolites using two-dimensional J-resolved metabolite-cycled semiLASER at 9.4 T” ISMRM & SMRT Virtual Conference & Exhibition, 2021.

2. **Murali-Manohar S**, Borbath T, Henning A. "Estimation of T2 Relaxation Times and Absolute Quantification of Metabolites in the Human Brain at 9.4 T." Proc. of the 36th Annual Meeting of the European Society for Magnetic Resonance in Medicine and Biology, 2019, Rotterdam, Netherlands.

3. **Murali Manohar S**, Wright A, Henning A. "T1 Relaxation Times of Macromolecular Resonances for Grey and White Matter Voxels in Human Brain at 9.4 T." Proc. of the 36th Annual Meeting of the European Society for Magnetic Resonance in Medicine and Biology, 2019, Rotterdam, Netherlands.

4. Wright A, **Murali-Manohar S**, Henning A. "Post-Acquisition Correction of Macromolecules using a Relaxation- and Sequence-dependent Simulation Model." Proc. of the 36th Annual Meeting of the European Society for Magnetic Resonance in Medicine and Biology, 2019, Rotterdam, Netherlands.

5. Borbath T, **Murali-Manohar S**, Henning A. “Towards a Fitting Model of Macromolecular Spectra: Amino Acids.” Proc. of the 27th Annual Meeting of the International Society for Magnetic Resonance in Medicine, 2019, Montréal, QC, Canada.

6. Wright A, **Murali-Manohar S**, Borbath T, Henning A. "Longitudinal Relaxation Times of Metabolites in vivo at 9.4 T." Proc. of the 27th Annual Meeting and Exhibition of the International Society for Magnetic Resonance in Medicine (ISMRM 2019), Montréal, QC, Canada.

7. Giapitzakis I-A, Fichtner N, Zaldivar D, Avdievich N, **Murali-Manohar S**, Kreis R, Henning A. "Simultaneous detection of water and metabolites alternations under visual stimulation in human visual cortex utilizing metabolite cycled semi-LASER at 9.4T: preliminary results." Proc. of the 34th Annual Scientific Meeting of the European Society for Magnetic Resonance in Medicine and Biology (ESMRMB 2017), Barcelona, Spain.

8. Borbath T, Giapitzakis IA, **Murali Manohar S**, Henning A. "Do macromolecular and spline baselines affect the metabolite quantification at 9.4T?" Proc. of the 34th Annual Scientific Meeting of the European Society for Magnetic Resonance in Medicine and Biology (ESMRMB 2017), Barcelona, Spain.

9. Giapitzakis IA, Avdievitch N, **Murali-Manohar S**, Fichtner N, Kreis R, Henning A. "Functional Magnetic Resonance Spectroscopy (fMRS) using metabolite cycled semi-LASER at 9.4T: a pilot study." Proc. of the 25th Annual Meeting and Exhibition of the International Society for Magnetic Resonance in Medicine (ISMRM 2017), Honolulu, HI, USA.

3.2.3 Posters (14)

First author contributions: 5

1. Wright A, **Murali-Manohar S**, Henning A. “Relaxation corrected simulated MM model for improved fitting and quantification of 1H FID MRSI data”. ISMRM & SMRT Virtual Conference & Exhibition (2021).

2. Borbath T, **Murali-Manohar S**, Dorst J, Henning A. “ProFit-v3: accuracy and precision evaluation of a new spectral fitting software”. ISMRM & SMRT Virtual Conference & Exhibition (2021).

3. Wright A, **Murali Manohar S**, Henning A. "Quantitative Metabolite Mapping of the Human Brain at 9.4 T." ISMRM & SMRT Virtual Conference & Exhibition (2020).

4. Borbath T, **Murali Manohar S**, Wright A, Henning A. "T2 Relaxation Times of Macromolecules in Human Brain Spectra at 9.4 T." Proc. of the 27th Annual Meeting and Exhibition of the International Society for Magnetic Resonance in Medicine (ISMRM 2019), Montréal, QC, Canada.

5. Geldschläger O, **Murali-Manohar S**, Wright A, Avdievitch N, Henning A. "First MRI of the human spinal cord at 9.4T." Proc. of the 27th Annual Meeting and Exhibition of the International Society for Magnetic Resonance in Medicine (ISMRM 2019), Montréal, QC, Canada.

6. **Murali-Manohar S**, Borbath T, Wright AM, Henning A. "Characterization of Downfield Resonances and their T2 Relaxation times in Human Brain at 9.4 T." Proc. of the 27th Annual Meeting and Exhibition of the International Society for Magnetic Resonance in Medicine (ISMRM 2019), Montréal, QC, Canada.

7. **Murali-Manohar S**, Wright AM, Borbath T, Henning A. "Longitudinal Relaxation times of Macromolecular Resonances at 9.4 T in Human Brain." Proc. of the 27th Annual Meeting and Exhibition of the International Society for Magnetic Resonance in Medicine (ISMRM 2019), Montréal, QC, Canada.

8. Wright AM, **Murali-Manohar S**, Henning A. "Relaxation corrected and Sequence-dependent Macromolecule Baseline Model." Proc. of the 27th Annual Meeting and Exhibition of the International Society for Magnetic Resonance in Medicine (ISMRM 2019), Montréal, QC, Canada.

9. Borbath T, **Murali-Manohar S**, Henning A. "Estimation of Tp2 Relaxation Times of Macromolecules in Human Brain Spectra at 9.4 T." MRS Workshop 2018 Metabolic Imaging, Utrecht, The Netherlands.

10. **Murali-Manohar S**, Wright AM, Henning A. "Challenges in estimating T1 Relaxation Times of Macromolecules in the Human Brain at 9.4T." MRS Workshop 2018 Metabolic Imaging, Utrecht, The Netherlands.

11. Wright AM, **Murali-Manohar S**, Henning A. "Longitudinal Relaxation Times of 5 Metabolites in vivo at 9.4T: preliminary results." MRS Workshop 2018 Metabolic Imaging, Utrecht, The Netherlands.

12. **Murali-Manohar S**, Borbath T, Fichtner N, Giapitzakis IA, Zaldivar D, Kreis R, Henning A. "Estimation of T2 Relaxation Times of Downfield Peaks in Human Brain at 9.4 T." Proc. of the Joint Annual Meeting ISMRM-ESMRMB 2018, Paris, France.

13. Borbath T, Giapitzakis I, **Murali-Manohar S**, Henning A. "Fitting comparison for 9.4T 1D semi-LASER and 2D-J-resolved semi-LASER data." Proc. of the 25th Annual Meeting and Exhibition of the International Society for Magnetic Resonance in Medicine (ISMRM 2017), Honolulu, HI, USA.

14. **Murali-Manohar S**, Giapitzakis IA, Borbath T, Gaertner M, Henning A. "Qualitative Comparison between In Vivo J-Resolved Semi-LASER at 3 T and 9.4 T." Proc. of the 25th Annual Meeting and Exhibition of the International Society for Magnetic Resonance in Medicine (ISMRM 2017), Honolulu, HI, USA.

4 Statement of Contributions

4.1 T_2 relaxation times of macromolecules and metabolites in the human brain at 9.4 T

T_2 relaxation times of individual macromolecular peaks at 9.4 T are reported for GM- and WM-rich voxels. Furthermore, the contribution of T_2 relaxation times and B_0 components to the linewidth of the macromolecular peaks are quantitatively analyzed in this work. Metabolite T_2 relaxation times are estimated in a GM-rich voxel in the occipital lobe. The obtained T_2 relaxation times were used as a correction factor, and fitted concentration values were corrected for tissue content and relaxation effects of both metabolites and water. The concentration of the metabolites are reported in mmol/kg.

- **S. Murali-Manohar** – Had the scientific idea to calculate T_2 relaxation times of macromolecules and metabolites. Set up the experiment, recruited volunteers and acquired in vivo data. Contributed in data analysis and data interpretation. Wrote majority of the manuscript.
- **T. Borbath** – Had the scientific idea of quantitatively analyzing the linewidth contributions to the macromolecular peaks. Simulated basis sets, and performed spectral fitting and quantification. Wrote parts of the manuscript.
- **A.M. Wright** – Reconstructed the anatomical images and performed tissue segmentation. Proofread the manuscript.
- **B. Soher** – Provided simulation code for semiLASER in VesPA software.
- **R. Mekle** – Provided the code for voxel-based power optimization. Proofread the manuscript.
- **A. Henning** – Supervised the project. Advised on the manuscript and proofread it.

4.2 A novel method to measure T_1-relaxation times of macromolecules and quantification of the macromolecular resonances

A novel double inversion recovery method is proposed to determine the T_1 relaxation times of 13 individual macromolecular peaks. Bloch simulations were performed to optimize inversion times for the double inversion recovery series. The fitted

concentrations of the individual macromolecule peaks from the double inversion series data were used to calculate the T_1 relaxation times. T_1 relaxation times are reported for both GM- and WM-rich voxels at 9.4 T. The proposed method is extendible to all field strengths. In addition, macromolecular concentrations in protons×mmol/kg are reported after correcting for relaxation effects and tissue content.

- **S. Murali-Manohar** – Wrote Bloch simulation script for double inversion recovery. Performed Bloch simulations and optimized sequence parameters. Acquired in vivo data at 9.4 T. Pre-processed the acquired data. Set up the spectral fitting pipeline and fit the MM data. Wrote parts of the manuscript.
- **A.M. Wright** – Performed Bloch simulations and optimized sequence parameters. Collected in vivo data at 9.4 T. Reconstructed the anatomical images and performed tissue segmentation. Wrote scripts to calculate T_1 relaxation times and quantification. Wrote parts of the manuscript.
- **T. Borbath** – Provided ideas for fitting. Proofread the manuscript.
- **N. Avdievich** – Provided the RF coil for 9.4 T.
- **A. Henning** – Provided ideas for the methodology and supervised the project. Advised on the manuscript and proofread it.

4.3 Quantitative two-dimensional J-resolved metabolite-cycled semiLASER at 9.4 T in the human brain

Two-dimensional J-resolved MC semiLASER pulse sequence is implemented for the first time at 9.4 T. The metabolite concentration values in gray matter rich voxel in the occipital lobe were reported in mmol/kg after correction for tissue content and relaxation effects. Quantification of 2D MRS data was performed and the values were compared against previous quantification results from 1D data.

- **S. Murali-Manohar** – Developed the pulse sequence and implemented it on the 9.4 T MRI scanner. Tested the sequence with phantom experiments and optimized the sequence parameters. Acquired single voxel MRS data in vivo. Pre-processed the acquired MRS data. Simulated basis sets for fitting and established the post-

processing pipeline for 2D proton spectra. Performed spectral fitting of the 2D data. Analyzed the data. Wrote the manuscript.

- **T. Borbath** – Provided ideas for 2D spectral fitting.
- **A.M. Wright** – Reconstructed the anatomical images and performed tissue segmentation.
- **N. Avdievich** – Provided the RF coil for 9.4 T.
- **A. Henning** – Supervised the project and provided ideas for fitting and comparison of the 1D vs. 2D data sets. Advised on the manuscript and proofread it.

5 Appended Publications

Publication 1

"T_2 relaxation times of macromolecules and metabolites in the human brain at 9.4 T"

S Murali-Manohar*, T Borbath*, A M Wright, B Soher, R Mekle, A Henning

Magnetic Resonance in Medicine, 2019, DOI: 10.1002/mrm.28174

Received: 30 July 2019 | Revised: 6 December 2019 | Accepted: 27 December 2019

DOI: 10.1002/mrm.28174

FULL PAPER

Magnetic Resonance in Medicine

T_2 relaxation times of macromolecules and metabolites in the human brain at 9.4 T

Saipavitra Murali-Manohar[1,2] | **Tamas Borbath**[1,2] | **Andrew Martin Wright**[1,3] | **Brian Soher**[4] | **Ralf Mekle**[5] | **Anke Henning**[1,6]

[1]High-Field Magnetic Resonance, Max Planck Institute for Biological Cybernetics, Tübingen, Germany

[2]Faculty of Science, University of Tübingen, Tübingen, Germany

[3]IMPRS for Cognitive & Systems Neuroscience, Tübingen, Germany

[4]Radiology, Duke University Medical Center, Durham, North Carolina

[5]Center for Stroke Research Berlin (CSB), Charité - Universitätsmedizin Berlin, Berlin, Germany

[6]Advanced Imaging Research Center, UT Southwestern Medical Center, Dallas, Texas

Correspondence
Saipavitra Murali-Manohar, High-Field Magnetic Resonance, Max Planck Institute for Biological Cybernetics, Max-Planck-Ring 11, 72076 Tübingen, Germany.
Email: saipavitra.murali.manohar@tuebingen.mpg.de

Funding information
Horizon 2020/CDS-QUAMRI (Grant No. 634541 to A.H., T.B., and S.M-M.), SYNAPLAST (Grant No. 679927 to A.H. and A.M.W.) and Cancer Prevention and Research Institute of Texas (CPRIT) (Grant No. RR180056 to A.H.)

Purpose: Relaxation times can contribute to spectral assignment. In this study, effective T_2 relaxation times (T_2^{eff}) of macromolecules are reported for gray and white matter–rich voxels in the human brain at 9.4 T. The T_2^{eff} of macromolecules are helpful to understand their behavior and the effect they have on metabolite quantification. Additionally, for absolute quantification of metabolites with magnetic resonance spectroscopy, appropriate T_2 values of metabolites must be considered. The T_2 relaxation times of metabolites are calculated after accounting for TE/sequence-specific macromolecular baselines.

Methods: Macromolecular and metabolite spectra for a series of TEs were acquired at 9.4 T using double inversion–recovery metabolite-cycled semi-LASER and metabolite-cycled semi-LASER, respectively. The T_2 relaxation times were calculated by fitting the LCModel relative amplitudes of macromolecular peaks and metabolites to a mono-exponential decay across the TE series. Furthermore, absolute concentrations of metabolites were calculated using the estimated relaxation times and internal water as reference.

Results: The T_2^{eff} of macromolecules are reported, which range from 13 ms to 40 ms, whereas, for metabolites, they range from 40 ms to 110 ms. Both macromolecular and metabolite T_2 relaxation times are observed to follow the decreasing trend, with increasing B_0. The linewidths of metabolite singlets can be fully attributed to T_2 and B_0 components. However, in addition to these components, macromolecule linewidths have contributions from J-coupling and overlapping resonances.

Saipavitra Murali-Manohar and Tamas Borbath contributed equally to this work.

[Correction added after online publication 22 February, 2020. Due to a publisher's error, the authors have corrected "alpha-fetoprotein pulse" on page 3, Section 2.2 to "Adiabatic Full Passage pulse".]

Conclusion: The T_2 relaxation times of all macromolecular and metabolite peaks at 9.4 T in vivo are reported for the first time. Metabolite relaxation times were used to calculate the absolute metabolite concentrations.

KEYWORDS

absolute quantification, macromolecules, MR spectroscopy, T_2 relaxation time, ultrahigh magnetic field

1 | INTRODUCTION

Single-voxel proton MRS, a noninvasive technique, has complemented MRI by providing a means to detect and quantify concentrations of metabolites in the human brain. This has proven clinically useful, as shown in the review paper by Öz et al,[1] in establishing biomarkers for pathologies in the brain.

Advantages of MRS using ultrahigh-field scanners (≥7 T) include higher SNR and increased spectral resolution.[2] Hence, the macromolecular background signal (MMB) lying underneath the metabolites has to be characterized more precisely. Especially for short TE sequences, reliable metabolite quantification is more challenging without accounting for the MMB. Therefore, a measured macromolecular (MM) spectrum should be included in the fitting model.[3] In addition, understanding macromolecules may help to identify valuable biomarkers for pathologies and several diseases of clinical relevance.[3-6] The T_2 relaxation times of MM peaks have been reported in previous studies in rat brain[7-10] and for the $M_{0.92}$ peak in human brain at 2.1 T by Behar et al.[11] However, T_2 relaxation times of multiple individual MM peaks in human brain have not been reported to the best of our knowledge. Estimating the T_2 relaxation times of individual macromolecules at 9.4 T could help in understanding and modeling their behavior.[12]

To derive absolute concentrations of metabolites in MRS, several different approaches exist.[13-15] In one method, the unsuppressed internal water signal is used as a reference.[16] However, the calculation of absolute concentrations from the apparent concentrations output by a quantification software requires a correction factor, which includes the T_2 relaxation times of the metabolites of interest.[16] In addition, to record 2D-MRS data, it is useful to have a rough estimate of T_2 relaxation times to optimize TE range, such that one obtains the highest possible SNR.[17,18] Additionally, altered T_2 relaxation times might provide information about evolving pathological or physiological states.[19]

Several studies have reported the T_2 relaxation time for metabolites in different regions of the human brain for a range of magnetic field strengths.[20-22] The T_2 relaxation times were measured at 9.4 T for singlets, but not for J-coupled metabolites by Deelchand et al[23]; however, this study did not consider the influence of T_2-dependent MM spectra, which affects the T_2 relaxation estimation of the singlets.

The primary goal of this study was to measure the effective T_2 relaxation times (T_2^{eff}) of MM peaks, which includes both relaxation and J-evolution effects, in a gray matter (GM)-rich and a white matter (WM)-rich voxel at 9.4 T in human brain. In addition, T_2 relaxation times of singlets and J-coupled metabolites in the GM-rich voxel were calculated after correcting for TE-specific MMBs. Furthermore, absolute concentrations of metabolites are reported after correcting for the corresponding T_2 and T_1 relaxation times.[24] The FWHM ($\Delta\nu_{1/2}$) of MM peaks and metabolites were analyzed quantitatively with respect to T_2 relaxation times, in addition to microsusceptibility and macrosusceptibility effects.

2 | METHODS

2.1 | Technical description and subjects

All measurements were performed on a 9.4 T Magnetom whole-body MRI scanner (Siemens Healthineers, Erlangen, Germany) using a home-built proton coil with 8 transmit and 16 receive channels.[25] For single-voxel spectroscopy experiments, 3 channels at the bottom of the coil were driven using an unbalanced three-way Wilkinson splitter as previously described.[26] Eleven healthy volunteers (8 males, 3 females, age: 26.3 ± 2.8 years) participated in this study for data acquisition in the GM-rich voxel. Data for the WM-rich voxels was acquired from 5 healthy volunteers (3 males, 2 females, age: 27.8 ± 1.9 years). The study was approved by the local ethics board, and written informed consent was given by all subjects before the examination.

2.2 | Data acquisition

Gradient-echo images were acquired using a 2D-FLASH sequence (in-plane resolution: 0.7 × 0.7 mm^2, 3.5-mm slice thickness, flip angle: 25º) along axial and sagittal orientations to facilitate placement of the spectroscopy voxel. A GM-rich voxel with the dimensions of 2 × 2 × 2 cm^3 was chosen in the occipital lobe for T_2 measurement of metabolites, whereas in addition to the GM-rich voxel, a WM-rich voxel of the same size was chosen in the occipital–parietal transition for T_2 measurement of MM peaks. First-order and second-order

TABLE 1 Chemical shifts of the modeled MM peaks

Macromolecule name	This work δ (ppm)	This work $\Delta\nu_{1/2}$ (Hz)		Lopez-Kolkovsky et al 2016[7] δ (ppm)	Pfeuffer et al 1999[8] δ (ppm)	Giapitzakis et al 2018[30] δ (ppm)
		Gray matter	White matter			
$M_{0.92}$	0.916	39.03 ± 4.70	41.87 ± 4.09	0.87	0.916	0.94
				0.94		
$M_{1.21}$	1.21	40.59 ± 5.53	38.67 ± 6.24	1.20	1.21	1.22
$M_{1.39}$	1.39	43.75 ± 6.23	42.92 ± 5.67	1.39	1.39	1.43
$M_{1.67}$	1.67	58.33 ± 8.10	58.33 ± 8.19	1.67	1.67	1.69
				1.81		
$M_{2.04}$	2.04	59.28 ± 7.42	58.04 ± 7.30	1.91	2.04	2.04
				1.93		
				2.04		
				2.13		
$M_{2.26}$	2.26	62.73 ± 5.59	59.89 ± 5.04	2.26	2.26	2.27
—	—			2.36		
—	—			2.46		
—	—			2.51		
$M_{2.56}$	2.56	49.09 ± 2.93	47.46 ± 1.98	2.56		2.57
$M_{2.70}$	2.70	32.07 ± 2.37	31.80 ± 1.96	2.68		2.74
				2.74		
$M_{2.99}$	2.99	49.70 ± 1.53	49.28 ± 1.44	2.97	2.99	3.01
				3.02		
$M_{3.21}$	3.21	71.81 ± 0.83	71.76 ± 0.84	3.09		
				3.22	3.21	3.21
				3.28		
—	—	—	—	3.54		
$M_{3.62}$	3.62	44.52 ± 0.65	44.21 ± 0.68	3.62		3.71
$M_{3.75}$	3.75	35.40 ± 0.49	35.20 ± 0.56	3.75	3.77	3.79
$M_{3.86}$	3.86	35.08 ± 2.05	34.79 ± 1.17	3.86		3.85
$M_{4.03}$	4.03	37.90 ± 0.90	37.53 ± 0.64	3.95		3.87
				4.05		
—	—	—	—	4.17		4.20
				4.26	4.29	
				4.33		—
				4.42		

Note: The chemical shifts (in parts per million) of MM peaks modeled with Voigt lines from this work compared with studies on rat brain at 17.2 T,[7] rat brain at 9. 4 T,[8] and human brain at 9.4 T.[30] The measured FWHM ($\Delta\nu_{1/2}$) of the MM peaks from this work is also reported.

B_0 shimming was performed using FAST(EST)MAP,[27] and then voxel-based power calibration[28,29] was executed.

Double inversion recovery (DIR) metabolite-cycled semi-LASER[30] and metabolite-cycled (MC) semi-LASER[26] spectra were acquired in the same 11 healthy volunteers. The TR was set to 10 seconds in the case of DIR-MC semi-LASER, and to 6 seconds for the MC semi-LASER, respectively, to ensure complete T_1 recovery of MM resonances and metabolites.[31] A 16-step phase-cycling scheme[32] was implemented for both spectroscopy sequences.

A series of DIR-MC semi-LASER spectra at different non-linearly spaced TEs (TE = 24 ms, 32 ms, 40 ms, 52 ms, and 60 ms; TI_1/TI_2 = 2360/625 ms; number of excitations = 32; transmit reference frequency ($_{ref}$) = 2.4 ppm) was acquired to estimate the T_2^{eff} of macromolecules. Setting $_{ref}$ to 2.4 ppm led to maximum chemical shift displacement effects of −11.5% for water and +2% for the acetyl moiety of NAA(CH_3) due to the large bandwidths of the corresponding RF pulses (excitation pulse and Adiabatic Full Passage pulse bandwidth of 8 kHz, creating a chemical-shift displacement effect of 5% per ppm).

To calculate the T_2 relaxation times of metabolites, a series of MC semi-LASER spectra at different nonlinearly spaced TEs (TE = 24 ms, 32 ms, 40 ms, 52 ms, and 60 ms; number of excitations = 96; $_{ref}$ = 7.0 ppm) was acquired, originally measured to characterize the T_2 relaxation times of downfield metabolites/resonances in the same healthy volunteers.[33] Setting $_{ref}$ to 7.0 ppm led to maximum chemical-shift displacement effects of +11.5% for water and +25% for NAA(CH_3).

In this study, for absolute quantification of metabolites, MC semi-LASER spectra (TE/TR: 24/6000 ms; number of excitations = 32) were acquired, with $_{ref}$ set to 2.4 ppm to minimize the chemical-shift displacement effect. To avoid any influence of MC pulses on quantification based on water, water-reference signals (number of excitations = 16) were acquired with semi-LASER (TE = 24 ms; $_{ref}$ = 4.7 ppm) without metabolite cycling.

Finally, magnetization-prepared two rapid gradient-echo[34] images were acquired using the same coil with RF transmission via all eight channels to calculate tissue-volume fractions for absolute quantification.

2.3 | Data preprocessing

Raw data were analyzed with in-house-written software in *MATLAB* (version 2016a; MathWorks, Natick, MA). The metabolite and MM MRS data were processed as described previously.[26,30] The following steps were used in processing the raw data: (1) truncation of FIDs at 250 ms for both metabolite and MM data; (2) frequency and phase alignment; (3) MC subtraction; (4) averaging; (5) zero-order phase and eddy current correction using the phase information from the MC water signal; (6) coil channel combination using a singular value decomposition method; (7) peak alignment in the frequency domain to 3.028 ppm and 3.925 ppm for the metabolite spectra and MM data, respectively; (8) residual water removal using a Hankel singular value decomposition method; and (9) truncation of FIDs at 150 ms for the MM data.

2.4 | Macromolecule fitting

An MM basis set was created in LCModel V6.3-1L[35] using simulated Voigt peaks, which is the best possible approximation used in literature[7,8,30,36] and does not account for J-evolution of these MM peaks. The chemical shifts of the Voigt lines were varied systematically based on previously reported values,[7,8,30] in which the ones reported by Pfeuffer et al[8] were found to be the best; therefore, the reported chemical shifts were chosen for the MM peaks from 0.9 to 2.3 ppm and from 2.9 to 3.5 ppm. The values of $M_{2.56}$ and $M_{2.70}$ were first reported in a human brain study at 9.4 T.[30] The chemical shifts of these two peaks were adapted to fit the shifts reported by the 17.2 T rat study.[7] The chemical shifts for MM peaks between 3.5 ppm and 4.2 ppm were chosen based on a previously mentioned study,[7] as the peaks were resolved more clearly in Lopez et al[7] compared with the other two studies.[8,30] All of these chemical shifts are summarized in Table 1.

The simulated basis set consisted of the following MM peaks: $M_{0.92}$ (0.916 ppm), $M_{1.21}$ (1.21 ppm), $M_{1.39}$ (1.39 ppm), $M_{1.67}$ (1.67 ppm), $M_{2.04}$ (2.04 ppm), $M_{2.26}$ (2.26 ppm), $M_{2.56}$ (2.56 ppm), $M_{2.70}$ (2.7 ppm), $M_{2.99}$ (2.99 ppm), $M_{3.21}$ (3.21 ppm), $M_{3.62}$ (3.62 ppm), $M_{3.75}$ (3.75 ppm), $M_{3.86}$ (3.86 ppm), $M_{4.03}$ (4.03 ppm), and $M_{4.17}$ (4.17 ppm). The same basis set was used throughout the TE series, with the $M_{2.70}$ peak being simulated with a negative amplitude for TE = 52 and 60 ms, as this peak was observed to be fully inverted due to J-evolution. A much narrower Voigt line was added to fit the residual creatine at 3.925 ppm. The chemical shifts, $\Delta\nu_{1/2}$s, and amplitudes were constrained in the LCModel as described in Supporting Information Annex B.

Each individual MM data set and the sum of all data sets were fitted to the simulated MM basis set while enforcing a flat baseline by setting the LCModel parameter DKNTMN to 99.

2.5 | Metabolite fitting

The metabolite basis set was simulated in *Vespa* (ver. 0.9.3)[37] using full quantum mechanical density matrix calculations for the semi-LASER sequence,[38] including the actual complex excitation and adiabatic RF pulse shapes for all TEs specified in section 2.2. The following 17 metabolites were simulated: NAA, NAA glutamate (NAAG), γ-aminobutyric acid (GABA), aspartate (Asp), creatine (Cr), glutamate (Glu), glutamine (Gln), glutathione, glycerophosphocholine, glycine (Glyc), myo-inositol (mI), scyllo-inositol (Scy), lactate (Lac), phosphocreatine (PCr), phosphocholine (PCho), phosphoethanolamine (PE), and taurine (Tau). Their chemical shifts and coupling constants were taken from Govindaraju et al,[39,40] except for the coupling constant of GABA, for which the values from Near et al[41] were chosen.

Selected metabolites were split into moieties for fitting the TE series to calculate the metabolites' T_2 times. As previous studies have shown, different moieties of the same metabolite have different relaxation times[7,20,21,23]: NAA was split into an NAA–acetyl moiety [NAA(CH_3)] and an NAA–aspartyl moiety [NAA(CH_2)], whereas instead of Cr and PCr metabolites, the singlets at 3.925 ppm total creatine [tCr(CH_2)] and at 3.028 ppm [tCr(CH_3)] were included in the basis set. The metabolites were used in their entirety to calculate absolute concentrations.

Because of the strong overlap and ill-posed problem of fitting PCho and glycerophosphocholine separately, these were combined to a total choline metabolite (tCho) with corresponding volume fractions of 0.6 mM PCho and 1 mM

glycerophosphocholine based on the mean concentration values from de Graaf.[42] Similarly, PCho, glycerophosphocholine, and PE were combined with tCho+ (corresponding to volume fractions of 0.6 mM PCho, 1.0 mM glycerophosphocholine, and 1.5 mM PE[42]), to obtain a robust metabolite fit for the T_2 calculations across the TE series.

Then, all individual metabolite spectra were fitted using the LCModel with the simulated basis set, including the respective MMB summed across subjects for each TE. The metabolite spectra summed across subjects were fitted similarly. Because the summed MMB spectra were included in the fit, DKNTMN was set to 0.25, resulting in a stiffer LCModel baseline compared with the default LCModel value of 0.15.[43]

To further improve the fitting procedure, two soft constraints were introduced into the echo series fit, namely, $NAA(CH_3)/NAA(CH_2) = 1.2 \pm 0.02$ (to account for possible faster decay of $NAA(CH_2)$ and mI/Glyc = 5 ± 0.5 (value extracted from the TE = 24 ms fit) (Supporting Information Annex B). No soft constraints were used for GABA or other metabolites.

2.6 | T_2 relaxation calculations

The concentrations of MM peaks and metabolite peaks from the individual data and the summed spectra were fit to a mono-exponential decay across the TE series to yield T_2 relaxation-time estimates. The mean coefficient of determination (R^2) value was calculated for the exponential fit across the individual subject data and was used to evaluate the quality of the exponential fits. Relaxation times with a mean R^2 smaller than 0.5 were discarded. The T_2 times for Lac, Tau, and Scy are not reported, as they did not satisfy the R^2 criterion.

2.7 | Linewidth calculations

After quantification and extracting the fitted lineshapes of MM peaks and metabolite singlets from the .coord files of LCModel quantification, the $\Delta\nu_{1/2}$ were measured. The contribution of T_2 relaxation to $\Delta\nu_{1/2}$ was calculated according to $\pi T_2^{eff\ -1}$, using the calculated T_2 values.

The residual linewidth was defined as

$$\Delta\nu_{residual} = \Delta\nu_{1/2} - \pi T_2^{eff\ -1} - \Delta\nu_{singlet}$$

The B_0 components were calculated from $NAA(CH_3)$ and $tCr(CH_2)$ as

$$\Delta\nu_{singlet} = \Delta\nu_{1/2} - \pi T_2^{eff\ -1} \approx \Delta\nu_{micro} + \Delta\nu_{macro}$$

respectively. The values of $\Delta\nu_{micro}$, $\Delta\nu_{macro}$ represent the microsusceptibility and macrosusceptibility, respectively.

2.8 | Absolute quantification

Using *Statistical Parametric Mapping 12* software (Wellcome Trust Centre for Neuroimaging, London, United Kingdom), the acquired magnetization-prepared two rapid gradient-echo images were segmented into the following tissues: WM, GM, and CSF. Final tissue compositions were calculated using an in-house written *Python* (ver. 3.7) method and were used for absolute quantification of metabolites. Obtained tissue compositions for the GM-rich voxels were GM: 69.2% ± 3.9%, WM: 25.8% ± 5.0%, and CSF: 4.9% ± 3.0%, and the WM-rich voxels were GM: 32.9% ± 9.3%, WM: 64.7% ± 11.1%, and CSF: 2.4% ± 3.7%.

The unsuppressed water-reference signal from the voxel was used as the internal concentration reference for absolute quantification calculated in millimolal values (millimoles per kilogram of solvent [mmol/kg]). The concentrations of the metabolites were absolutely quantified using the formula (Supporting Information Annex A) given by Gasparovic et al[16] for TE = 24 ms, including corrections for the T_1 and T_2 relaxation times of water in different compartments and the metabolite relaxation times. More specifically, the T_1 and T_2 relaxation times of water at 9.4 T in GM (T_1^{GM} = 2120 ms; T_2^{GM} = 37 ms) and WM (T_1^{WM} = 1400 ms; T_2^{WM} = 30 ms) were taken from Hagberg et al.[34] Relaxation times for CSF were calculated based on data from the same work (T_1^{CSF} = 4800 ms; T_2^{CSF} = 181 ms). The T_1 relaxation times of metabolites were taken from Wright et al.[24] The T_2 relaxation times of the metabolite peaks calculated in this study were used. For the metabolites, for which T_2 relaxation times could not be estimated, the mean T_2 relaxation time of all other metabolites was used.

3 | RESULTS

Spectra without major artifacts were obtained for all subjects: The $NAA(CH_3)$ SNR ranged from 526 ± 130 to 334 ± 82 for TE = 24-60 ms, respectively. However, between 0.9 and 1.8 ppm, some spectra, especially MM spectra from WM voxels (Figure 1 and Supporting Information Figure S1), presented outer-volume lipid impurities for some subjects, as lipid suppression techniques such as outer-volume saturation were not used. The value of $\Delta\nu_{1/2}$ of the unsuppressed water signal was 17.6 ± 1.3 Hz. The TE series of MM and metabolite spectra from the GM-rich voxel are shown in Figure 1, where the shaded area depicts the SD, illustrating the reproducibility of the data quality. Supporting Information Figure S1 shows the TE series of WM-MM spectra. No data sets were excluded.

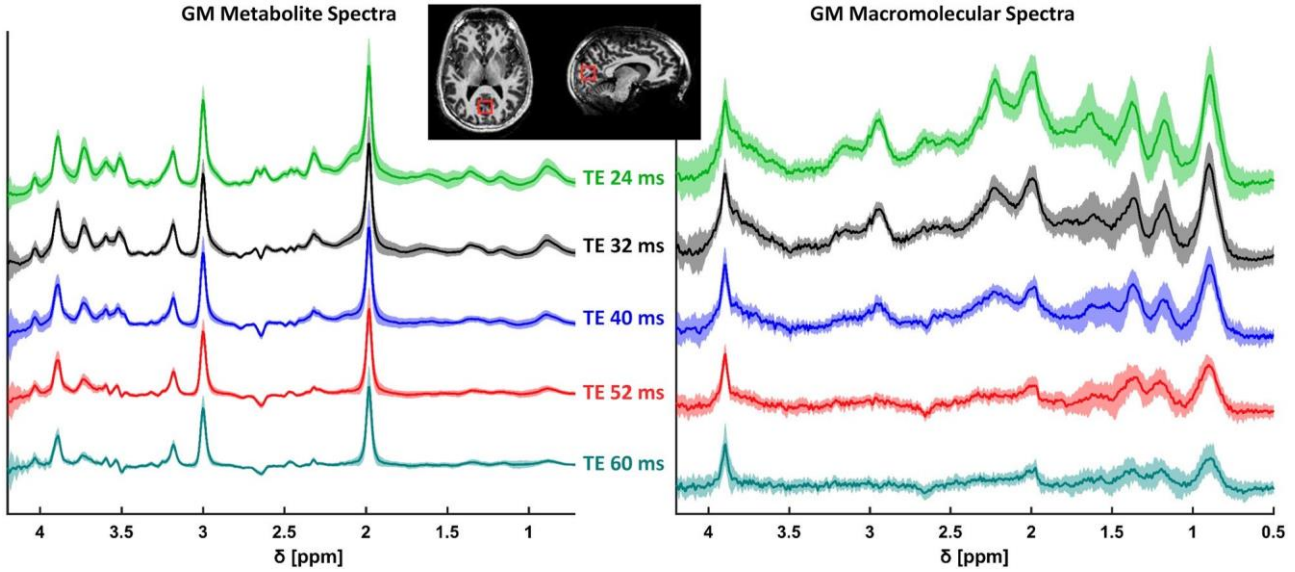

FIGURE 1 Echo time series (TE = 24, 32, 40, 52, and 60 ms) for metabolite spectra (left) and macromolecular spectra (right) from gray matter (GM), with solid lines showing the mean spectra and the shaded area indicating the SD across subjects. The inset shows the voxel placement on axial and sagittal magnetization-prepared two rapid gradient-echo images

FIGURE 2 Gray matter macromolecular (MM) spectrum summed across subjects ($_{subjects}$ ***GM MM Spectrum***) (TE = 24 ms) is shown with the fit using simulated Voigt lines. The residual total creatine 3.9 singlet [tCr(CH_2)] peak in the spectra is modeled with a significantly narrower linewidth

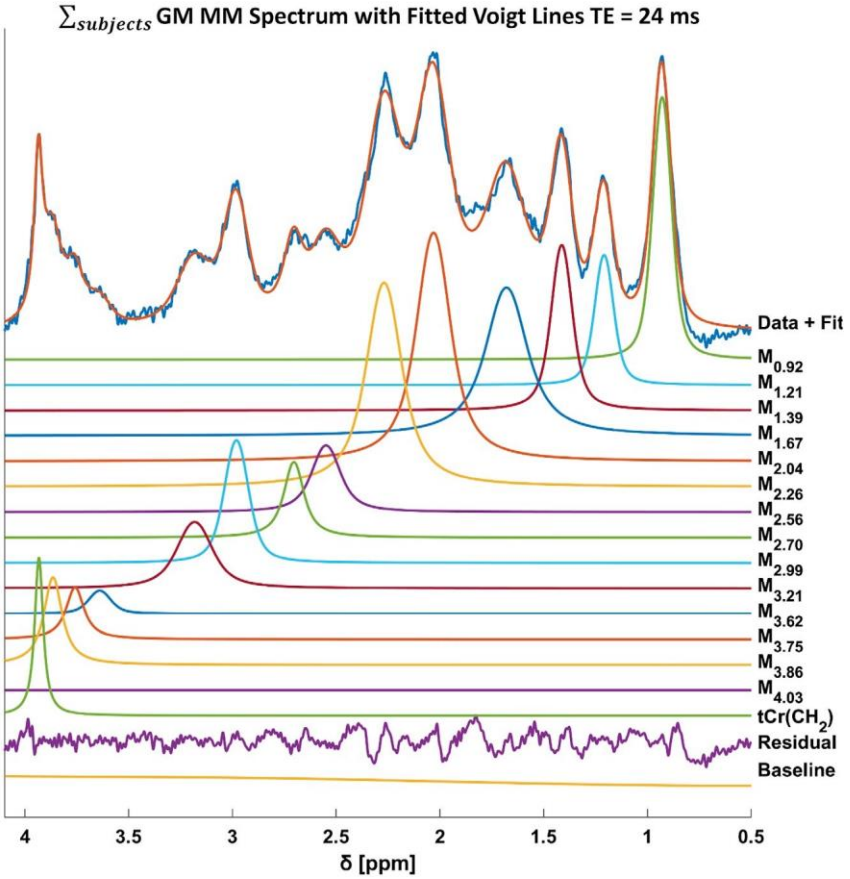

3.1 | Macromolecule fitting

The spectrum from the GM-rich voxel summed across subjects, together with all the fitted Voigt lines for the MM peaks, is shown in Figure 2 for TE = 24 ms and in Supporting Information Figure S2 for the other TEs. Supporting Information Figures S3 and S4 show the fit of the WM-TE series spectra summed across subjects. The fit residual is minimum without structured noise, indicating a high fit quality. Similar fit quality was achieved for all data sets across all TEs. The $M_{2.70}$ peak is observed to undergo a full inversion due to J-evolution over the TE steps. More precisely, the full-inversion $M_{2.70}$ occurred

between TE = 52 and TE = 60 ms, and was simulated as a negative peak. The signal of the MM and the metabolite peaks decreased with increasing TE, as expected.

The residual CH_2 resonance of total creatine [tCr(CH_2)] was modeled by fitting a sharper Voigt line at 3.925 ppm with a measured $\Delta\nu_{1/2}$ of around 0.035 ppm (14 Hz) across subjects. Next, the residual Cr was extracted from the LCModel fit, and was subtracted from the MM spectra to yield a more appropriate MMB for the metabolite fits (Figure 3). The resulting MMB was included in the basis set to fit the metabolite spectra for T_2 relaxation-time calculations as well as for absolute quantification.

3.2 | Metabolite fitting

The fit of the metabolites to the summed metabolite spectra is shown in Figure 4. The fit residual is small, indicating a high fit quality. For TE = 32, 40, 52 and 60 ms, the basis set modeled the J-evolution of mI, NAA(CH_2), Asp, Glu, and Tau well (Supporting Information Figure S5).

Adding ascorbic acid or glucose to the simulated basis set did not improve the fit in terms of Cramer-Rao lower bounds, T_2-fit result confidences, and residual artifacts. These resonances were not found by LCModel in most cases. Hence, these metabolites were not included in the final basis set.

3.3 | T_2 results

The calculated T_2^{eff} and T_2 relaxation times (Figure 5) for MM peaks and metabolites, respectively, were overall in good agreement for the fits of individual subject data and the summed spectra. Box plots of the resulting T_2 relaxation times are shown in decreasing order for metabolites and MM peaks in Figure 5. The T_2 relaxation time of the residual tCr(CH_2) peak in the MM spectra was also in agreement with the relaxation time of the tCr(CH_2) peak in the metabolite spectra.

The T_2 relaxation times of metabolites and MM peaks from the summed spectra and individual data, together with the mean and SD of R^2 of the corresponding exponential fits, are listed in Table 2.

The T_2 relaxation times of metabolites were found to lie between 55 ms and 105 ms, except for NAAG with approximately 40 ms. In contrast, the values of T_2^{eff} for all MM resonances were between 13 ms and 40 ms in WM and between 13 ms and 37 ms in GM.

The R^2 for the metabolite exponential decay fits were all above 0.70, except for Asp and Glyc. The mean R^2 of the exponential decay fits was above 0.70 for all MM peaks as well, except for $M_{4.03}$, which was subjected to water residuals and noise at longer TEs, hence the lower R^2 value. Furthermore, the uncertainties in the T_2^{eff} relaxation times of the $M_{1.21}$ and $M_{1.39}$ were influenced by lipid contaminations.

3.4 | Linewidth calculations

The value of $\Delta\nu_{1/2}$ of the MM resonances was measured to vary between 35 Hz and 85 Hz across all TEs (Table 1), whereas $\pi T_2^{eff}{}^{-1}$ was calculated to be between 4 Hz and 30 Hz (Figure 6). In the case of metabolite resonances, and for the residual tCr(CH_2) in the MM spectra, a $\Delta\nu_{1/2}$ of 11 Hz to 20 Hz was found, whereas $\pi T_2^{eff}{}^{-1}$ ranged between 2 Hz

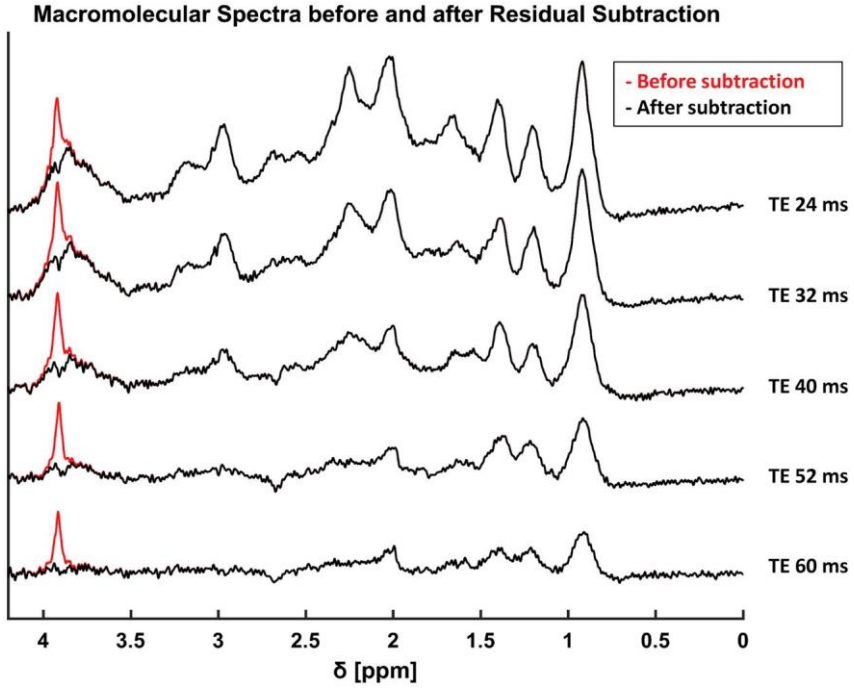

FIGURE 3 Echo time series of the GM-MM spectra summed across subjects with the tCr(CH_2) residual subtraction shown. The spectra after the residual tCr(CH_2) subtraction were used as the MM baseline in the basis set for the metabolite fitting. The red line shows the residual tCr(CH_2), and the black line shows the MM spectra after the residual subtraction. Residual tCr(CH_2) is extracted from the LCModel fit as shown in Figure 2

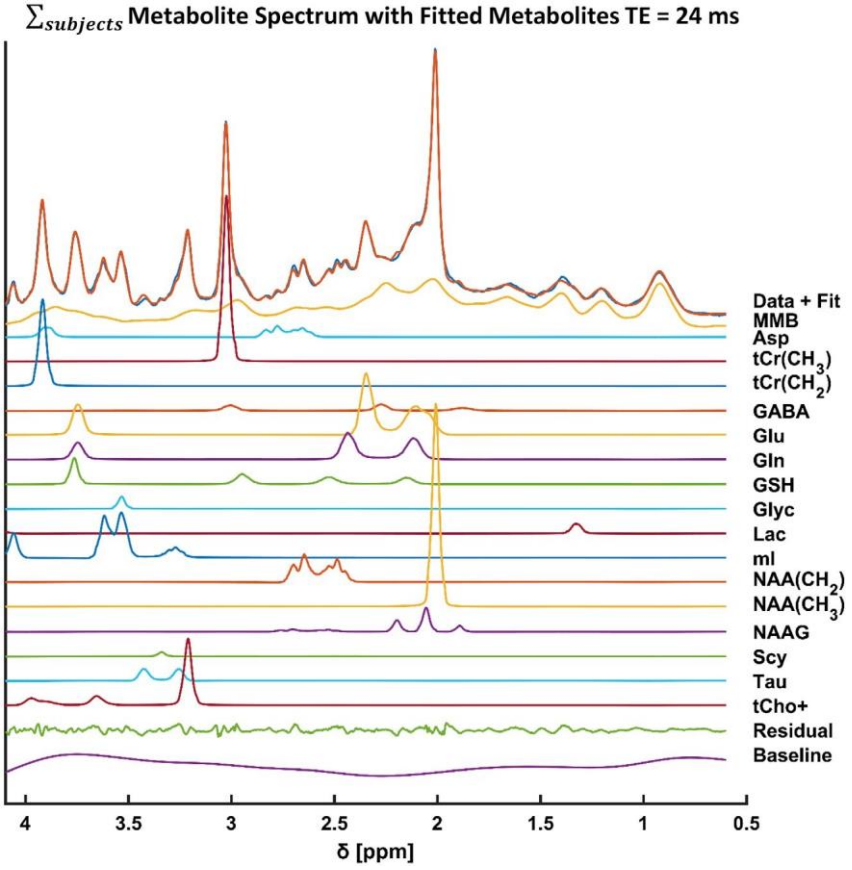

FIGURE 4 Summed metabolite spectrum ($\sum_{subjects}$ ***Metabolite Spectrum***) (TE = 24 ms) from GM with fitted metabolites and measured macromolecular background (MMB). The basis set configuration shown here was used to estimate the T_2 relaxation times and includes the tCr split into its moieties [tCr(CH_3) and tCr(CH_2)], NAA split into NAA(CH_2) and NAA(CH_3) moiety, and total choline (tCho) and phosphoethanolamine (PE) combined into tCho+. For each TE, a corresponding basis set was simulated with *Vespa*. For absolute quantification, the NAA moieties were combined, whereas creatine (Cr), phosphocreatine (PCr), tCho, and PE were fitted as independent metabolites. Abbreviations: Asp, aspartate; tCr(CH_2), GABA, γ-aminobutyric acid; Gln, glutamine; Glu, glutamate; Glyc, glycine; GSH, glutathione; Lac, lactate; mI, myo-inositol; NAA(CH_2), NAA–aspartyl moiety; NAA(CH_3), NAA–acetyl moiety; NAAG, NAA glutamate; Scy, scyllo-inositol; Tau, taurine; tCho+, combined phosphocholine, glycerophosphocholine, and phosphoethanolamine molecules; tCr(CH_2), total creatine 3.9 singlet; tCr(CH_3), total creatine 3.0 singlet

and 5 Hz. This led to a $\Delta\nu_{singlet}$ value of approximately 12 Hz for the metabolite singlets.

Supporting Information Figure S7 shows the $\Delta\nu_{residual}$ values of metabolites and MM peaks, which were calculated using the $\Delta\nu_{singlet}$ of NAA(CH_3) and tCr(CH_2) for the metabolite and MM spectra, respectively. The values of $\Delta\nu_{residual}$ of metabolites were around zero after applying the correction. In contrast, MM peaks had $\Delta\nu_{residual}$ values ranging between 10 Hz and 60 Hz.

3.5 | Concentrations

Absolute concentrations in millimoles per kilogram with and without T_2 correction are shown in Figure 7. The values for the metabolites are reported in Table 3 with and without the T_2 correction factor. In Supporting Information Figure S8 and Supporting Information Table S1, absolute concentrations are given in millimoles per tissue volume in a liter (mmol/L).

4 | DISCUSSION

In this study, transverse relaxation times of a wide range of MM peaks and metabolites at 9.4 T are reported. Additionally, in vivo absolute concentrations of metabolites for single-voxel MRS acquisitions from the occipital lobe are reported. The resulting T_2 values and absolute concentrations were largely in line with the literature.

4.1 | Spectral quality and fitting of MM spectra

The DIR technique sufficiently nulled all of the metabolites except tCr(CH_2) for the chosen TI_1 and TI_2, as the T_1 relaxation time of this resonance is the shortest among the singlets, as reported by Deelchand et al.[23] Indeed, the difference between the T_1 relaxation times of some of the MM peaks[44] and the CH_2 group of Cr is not large; thus, there is a residual peak present in the MM spectra. The residual tCr(CH_2) was subtracted using the fit of the Cr singlet fit from the LCModel. The resulting spectra (Figure 3) after the residual subtraction visually showed no leftover Cr.

For the fitting of the MM spectra, the chemical shifts and $\Delta\nu_{1/2}$ were systematically varied to achieve the lowest SD of the T_2 results among subjects, to maximize the R^2 values, and to minimize the mean Cramer-Rao lower bounds. These systematic variations supported that the values chosen by Lopez et al[7] were among the most suitable choices, and these values were also well justified by peak characteristics seen at 17.2 T.

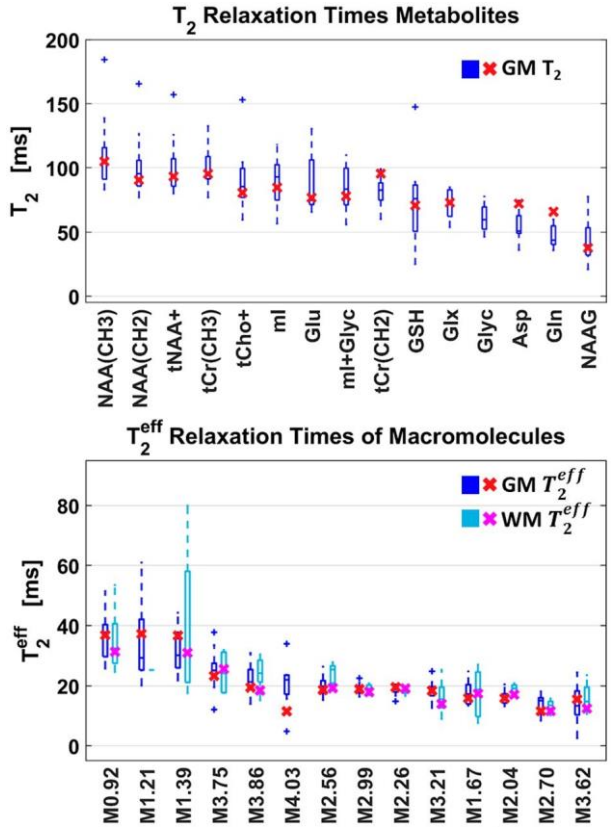

FIGURE 5 Calculated T_2 relaxation times for metabolites (top) and macromolecules (bottom) are shown in descending order. The red and pink crosses (X) indicate the calculations for the spectra summed across subjects ($T_2^{eff,sum}$), while the box plots show the per-subject fits. Horizontal lines inside the boxes indicate median values (50% quartile), whereas the bottom and top box boundaries illustrate 25% and 75% quartiles, respectively. Plus signs (+) show outliers. The summed and the individual fits are in good agreement. Abbreviations: Glx, total Glu and Gln; tNAA+, NAA(CH_3) and NAA(CH_2)

Hence, these values were chosen, with minor deviations as indicated in Table 1.

For the first time, the J-evolution of the $M_{2.7}$ resonance (Figures 1 and 3, Supporting Information Figure S1) was investigated in this study. This resonance was preliminarily assigned to β-methylene protons of aspartyl groups.[30] The Biological Magnetic Resonance Bank amino acid database[45] lists the following coupling constants for the β-methylene protons (δ2.7 ppm) of aspartate amino acids: approximately **5** and 8 Hz between α-methylene and β-methylene protons, and 17.5 Hz between β-methylene protons. These coupling constants are comparable to those of Asp and the aspartate moieties of NAA and NAAG,[40] which experience full inversion between TEs of 52 and 60 ms. All observations support the preliminary attribution of the $M_{2.7}$ resonance to the aspartyl groups. Nevertheless, the possibility cannot be excluded that the MM spectra also included NAA(CH_2) residuals, provided that this moiety has a short enough T_1 relaxation time. In particular, at longer TEs (52 and 60 ms), the contribution of NAA(CH_2) could be more significant, as metabolites have longer T_2 relaxation times than macromolecules.

4.2 | Metabolite fitting

Previous work at 9.4 T reported concentrations of 18 metabolites in the human brain using an MC semi-LASER sequence.[26] However, due to the complexity of the adiabatic pulses and their spin locking effect,[46] the simulated basis set was approximated using a spin-echo sequence with TE = 6.5 ms.[30] In this study, the basis set for MC-semi-LASER was simulated using actual adiabatic RF pulse shapes. In addition, the same TEs were used in the acquisition of both metabolite and MM spectra. This allowed to individually fit the metabolite spectra with the matching simulated basis set and the corresponding MMB for each TE. The fit results (Figure 4 and Supporting Information Figure S5) show that the simulated basis set represents the J-evolution patterns of the acquired spectra well.

4.3 | T_2 results

This study reports the T_2^{eff} of individual MM peaks as well as T_2 relaxation times of both singlets and J-coupled metabolites at 9.4 T in human brain. The values of T_2^{eff} of MM peaks are in agreement with previous work. Behar et al reporting 44-ms T_2 at 2.1 T for $M_{0.92}$ in human brain,[11] which is in agreement with a slow decay across field strengths, as shown in the rat brain studies.[7-10]

The T_2 of metabolite singlets, such as NAA(CH_3), tCr(CH_2), tCr(CH_3) and tCho, are higher than those previously reported at 9.4 T.[23] The higher values in this work can be attributed to the fact that a TE-specific experimentally measured MMB was included, which is a faster-decaying component. The reported T_2 relaxation times of the metabolites appear to follow the same trend compared with previous results,[7,20,21,47] with the longest relaxation times found for the singlets NAA(CH_3), tCho and tCr(CH_3) [the T_2 of tCr(CH_3) larger than for tCr(CH_2), difference decreasing with increasing field strength],[7,20,21,23,47] and significantly shorter T_2 for NAAG than for NAA moieties.[20] All reported T_2 relaxation times show the expected negative correlation with increasing field strength. Glutamate T_2 is higher than that of Gln, in agreement with previous studies.[7,20] However, the difference is unexpected, considering the similar molecular weight of the two metabolites and the similar distribution within the brain[48]; hence, most likely the T_2 of Gln is underestimated. Nevertheless, differences could arise from the presence in different compartments, or bindings to different transporters or enzymes.

The summed and individual fits are in good agreement for T_2 relaxation times for both MM resonances and metabolites

TABLE 2 T_2 relaxation times for metabolites and macromolecules

	Metabolite T_2			Macromolecule T_2^{eff}						
					Gray matter			White matter		
	T_2^{sum} (ms)	T_2 ± SD (ms)	R^2 ± SD		$T_2^{eff,sum}$ (ms)	T_2^{eff} ± SD (ms)	R^2 ± SD	$T_2^{eff,sum}$ (ms)	T_2^{eff} ± SD (ms)	R^2 ± SD
Asp	72	54.4 ± 11.5	0.72 ± 0.12	$M_{0.92}$	36.9	36.4 ± 7.0	0.91 ± 0.07	31.3	35.1 ± 10.0	0.86 ± 0.09
tCr(CH_3)	95.2	100.2 ± 16.0	0.90 ± 0.10	$M_{1.21}$	37.4	34.3 ± 13.1	0.79 ± 0.13	—	25.3 ± 0.0	0.98 ± 0.00
tCr(CH_2)	95.4	81.8 ± 10.8	0.83 ± 0.08	$M_{1.39}$	36.7	31.5 ± 7.4	0.83 ± 0.08	31	39.6 ± 24.2	0.75 ± 0.13
Glu	76.8	87.0 ± 23.3	0.73 ± 0.10	$M_{1.67}$	15.9	17.6 ± 3.6	0.92 ± 0.08	17.4	17.5 ± 7.5	0.89 ± 0.11
Gln	65.9	47.0 ± 8.6	0.81 ± 0.06	$M_{2.04}$	15.9	15.8 ± 2.1	0.98 ± 0.03	17.1	18.9 ± 1.5	0.98 ± 0.02
GSH	70.7	74.8 ± 34.2	0.73 ± 0.09	$M_{2.26}$	19.6	18.4 ± 1.5	0.96 ± 0.03	19.1	18.1 ± 1.0	0.96 ± 0.02
Glyc	—	60.9 ± 11.2	0.60 ± 0.07	$M_{2.56}$	18.7	20.1 ± 3.2	0.93 ± 0.04	19.3	23.9 ± 3.4	0.84 ± 0.10
mI	84.5	90.0 ± 18.0	0.70 ± 0.09	$M_{2.70}$	11.6	13.9 ± 2.9	0.93 ± 0.08	11.6	13.4 ± 1.9	0.94 ± 0.03
NAA(CH_2)	90.4	102.2 ± 23.8	0.92 ± 0.12	$M_{2.99}$	18.9	18.8 ± 1.6	0.94 ± 0.06	18	19.1 ± 1.3	0.93 ± 0.03
NAA(CH_3)	104.9	110.5 ± 27.7	0.93 ± 0.12	$M_{3.21}$	18.4	18.4 ± 3.2	0.93 ± 0.08	13.9	16.3 ± 5.4	0.91 ± 0.06
NAAG	37.7	45.0 ± 16.3	0.87 ± 0.09	$M_{3.62}$	15.5	13.9 ± 6.4	0.90 ± 0.07	12.4	15.9 ± 4.8	0.85 ± 0.06
tCho+	80.4	90.1 ± 23.5	0.92 ± 0.11	$M_{3.75}$	23.3	25.4 ± 6.8	0.91 ± 0.08	25.6	24.5 ± 6.8	0.82 ± 0.11
tNAA+	93.2	100.6 ± 21.8	0.93 ± 0.11	$M_{3.86}$	19.5	22.0 ± 5.3	0.91 ± 0.12	18.5	24.2 ± 5.2	0.84 ± 0.10
mI+Glyc	77.8	84.4 ± 16.8	0.77 ± 0.12	$M_{4.03}$	11.5	20.7 ± 8.2	0.71 ± 0.10	—	—	—
Glx	72.8	71.9 ± 10.5	0.76 ± 0.09	tCr(CH_2)	65.3	71.3 ± 7.9	0.75 ± 0.11	67.3	61.7 ± 3.1	0.84 ± 0.12

Note: Calculated T_2 relaxation times for metabolites (left), T_2^{eff} for MM gray matter (middle), and MM white matter (right) are shown for fitting the spectra summed across subjects (T_2^{sum} and $T_2^{eff,sum}$), the per-subject fits (mean and SD) with the confidence of the exponential fit (R^2). Some exponential decay fits are shown in Supporting Information Figure S6. The T_2 relaxation times of GABA, Lac, Scy, and PE are not included, as they did not satisfy the imposed $R^2 > 0.5$ criterion.

Abbreviation: GSH, glutathione.

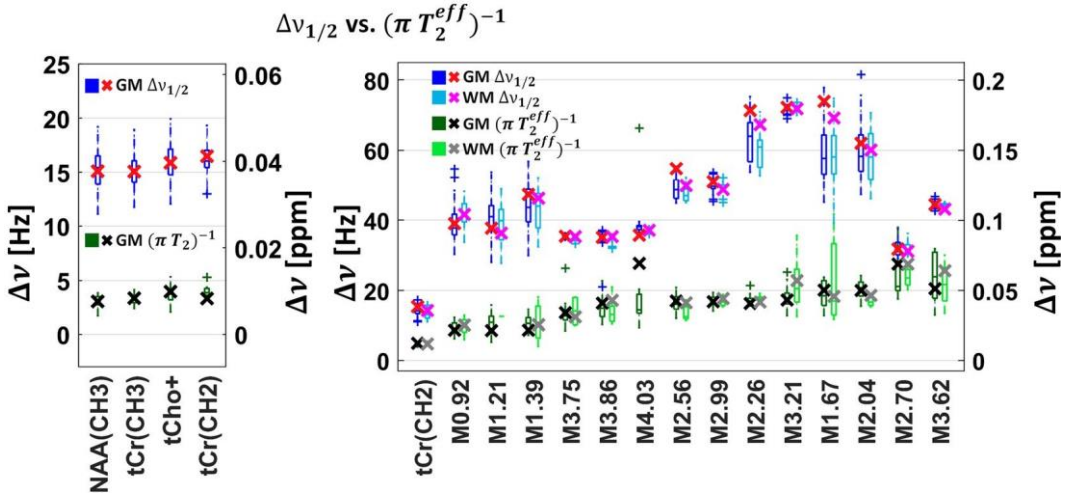

FIGURE 6 Calculated $\Delta\nu_{1/2}$ for the singlets of the metabolite spectra (left) and individual MM peaks and tCr(CH_2) peak of the MM spectra (right). The crosses (X) indicate the calculations for the spectra summed across subjects, whereas the box plots show the per-subject fits. Per-subject individual fits are shown in the blue box plots and red crosses (approximately 15 Hz for metabolite singlets and mostly between 40 Hz and 80 Hz for macromolecules). Values of $\nu T_2^{eff}{}^{-1}$ are shown in the green box plots and orange crosses (approximately 3.5 Hz for metabolite singlets and mostly between 5 Hz and 20 Hz for macromolecules). Horizontal lines inside the boxes indicate median values (50% quartile), whereas the bottom and top box boundaries illustrate 25% and 75% quartiles, respectively. Plus signs (+) show outliers. The value of $\Delta\nu_{residual}$ is displayed in Supporting Information Figure S7. Abbreviation: WM, white matter

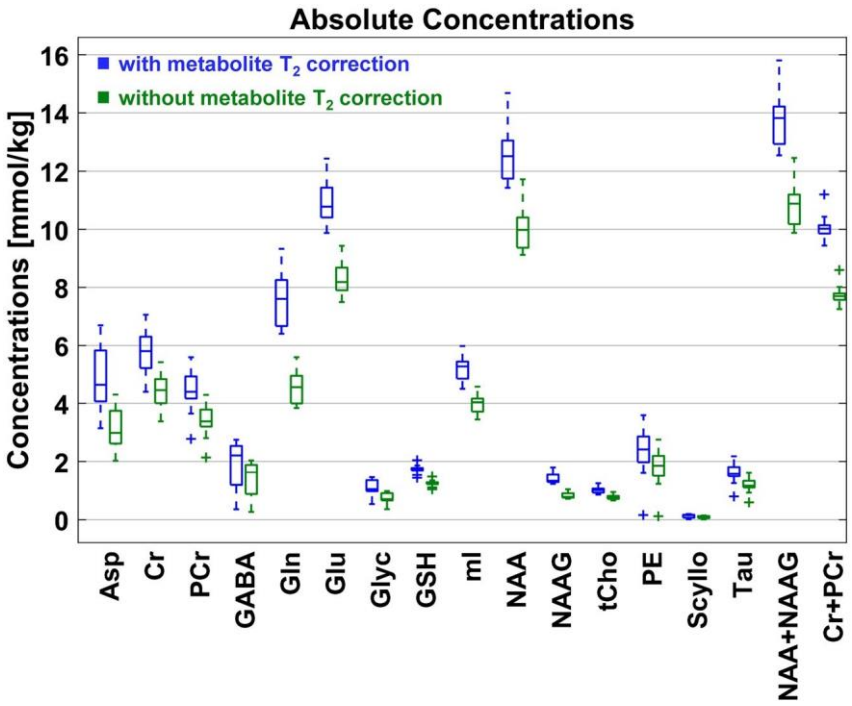

FIGURE 7 Calculated absolute concentrations for the metabolites in millimoles per kilogram for the different subjects. The blue box plots show the concentrations when metabolite T_2 correction is applied, whereas the green box plots show the concentrations without using this correction factor. Horizontal lines inside the boxes indicate median values (50% quartile), whereas the bottom and top box boundaries illustrate 25% and 75% quartiles, respectively. Plus signs (+) show outliers

(Table 2). It can also be noted that the relaxation time of the tCr(CH_2) in the metabolite spectra and the residual present in the MM spectra are in good agreement. The differences between T_2^{eff} relaxation times of MM peaks in WM-rich and GM-rich voxels were never investigated previously, nor were the relaxation times calculated for the peaks individually. Therefore, an attempt was made to calculate T_2^{eff} for both tissue compositions in this work. The T_2^{eff} relaxation times found in this study are comparable between these voxels.

However, it is known that the region of interest in the human brain is crucial when applying T_2 correction for absolute concentrations of metabolites.[20] Hence, no attempt was made to report the T_2 relaxation times of metabolites separately for GM and WM, as the selected voxel was neither

TABLE 3 Absolute concentrations (mmol/kg ± SD)

	Absolute concentrations (mmol/kg ± SD)							
	This work with T_2 correction	This work without T_2 correction	Terpstra et al 2009 7 T[51]	Mangia et al 2006 7 T[50]	Mekle et al 2009 3 T[29]	Mekle et al 2009 7 T[29]	Deelchand et al 2010 9.4 T[23]	Marjańska et al 2012 7 T[21]
	Occipital lobe GM-rich	Occipital lobe GM-rich	Occipital lobe	Occipital lobe	Occipital lobe GM-rich	Occipital lobe GM-rich	Occipital lobe	Occipital lobe mixed tissue
Asp	4.84 ± 1.15[b]	3.12 ± 0.74	2.0 ± 0.4	1 ± 0.26	3.1 ± 0.3	2.9 ± 0.5	2.1 ± 0.5	2.9 ± 0.8
Asc	—	—	1.1 ± 0.3	1.2 ± 0.21	—	—	—	0.4 ± 0.3
Cr	5.70 ± 0.85	4.38 ± 0.65	4.6 ± 0.3	5 ± 0.26	5.8 ± 0.2	5.0 ± 0.3	3.2 ± 0. 5	—
PCr	4.43 ± 0.83	3.40 ± 0.64	3.9 ± 0.5	3.4 ± 0.24	2.2 ± 0.19	3.0 ± 0.3	4.5 ± 0.4	—
GABA	1.87 ± 0.92[d]	1.39 ± 0.68	0.9 ± 0.1	1 ± 0.13	2.5 ± 0.4	1.3 ± 0.15	1.3 ± 0.4	1.5 ± 0.3
Glucose	—	—	—	1.1 ± 0.28	1.4 ± 0.3	—	—	w/Tau
Gln	7.61 ± 0.91[b]	4.56 ± 0.54	2.5 ± 0.2	2.9 ± 0.16	1.6 ± 0.4	2.2 ± 0.4	2.2 ± 0.2	1.5 ± 0.5
Glu	10.90 ± 0.80	8.27 ± 0.61	8.9 ± 0.3	11 ± 0.22	8.9 ± 0.9	9.9 ± 0.9	9.3 ± 0.9	9.6 ± 1.3
Glyc	1.11 ± 0.28[b]	0.75 ± 0.19	—	—	—	—	—	0.7 ± 0.1
GSH	1.72 ± 0.16	1.25 ± 0.12	0.7 ± 0.1	1 ± 0.1	1.4 ± 0.11	1.3 ± 0.2	1.1 ± 0.3	1.1 ± 0.1
Lac	—	—	0.7 ± 0.1	0.8 ± 0.1	—	0.7 ± 0.1	0.5 ± 0.1	0.8 ± 0.2
mI	5.22 ± 0.45	4.00 ± 0.34	—	—	5.3 ± 0.6	5.7 ± 0.5	5.3 ± 0.4	6.4 ± 0.8
NAA	12.61 ± 1.02	10.06 ± 0.81	12.4 ± 0.7	10.8 ± 0.14	11.2 ± 0.8	11.8 ± 0.2	13.5 ± 1.6	12.6 ± 1.7
NAAG	1.42 ± 0.19[a]	0.83 ± 0.11	1.2 ± 0.2	1.4 ± 0.11	1.0 ± 0.2	1.1 ± 0.4	1.1 ± 0.5	0.40 ± 0.2
tCho	1.03 ± 0.12	0.79 ± 0.09	1.0 ± 0.3	1.3 ± 0.05	1.1 ± 0.13	1.1 ± 0.05	0.9 ± 0.2	0.9 ± 0.1
PE	2.28 ± 0.95[d]	1.75 ± 0.73	2.1 ± 0.2	1.2 ± 0.19	2.2 ± 0.18	2.5 ± 0.3	1.6 ± 0.4	2.3 ± 0.4
Scy	0.13 ± 0.06[c,d]	0.09 ± 0.05[c]	0.3 ± 0.1	0.4 ± 0.05	0.4 ± 0.11	0.3 ± 0.12	0.3 ± 0.2	0.4 ± 0.1
Tau	1.58 ± 0.37	1.17 ± 0.27	1.7 ± 0.2	1.9 ± 0.18	1.4 ± 0.5	1.5 ± 0.3	1.3 ± 0.2	2.1 ± 0.3
NAA+NAAG	13.78 ± 1.01[a]	10.86 ± 0.79	—	—	12.3 ± 0.9	12.9 ± 0.4	—	—
mI+Glyc	6.34 ± 0.52	4.77 ± 0.39	6.3 ± 0.9	6.7 ± 0.2	6.2 ± 0.6	6.0 ± 0.4	—	—
Cr+PCr	10.10 ± 0.46[a]	7.76 ± 0.36	8.6 ± 1.2	—	8.0 ± 0.3	8.0 ± 0.4	7.7 ± 0.4	8.7 ± 1.1
Glu+Gln	17.96 ± 1.49[b]	12.86 ± 1.07	—	—	10.5 ± 1.2	12.1 ± 1.2	—	—

(Continues)

TABLE 3 (Continued)

	Absolute concentrations (mmol/kg ± SD)							
	This work with T_2 correction	**This work without T_2 correction**	**Terpstra et al 2009 7 T[51]**	**Mangia et al 2006 7 T[50]**	**Mekle et al 2009 3 T[29]**	**Mekle et al 2009 7 T[29]**	**Deelchand et al 2010 9.4 T[23]**	**Marjańska et al 2012 7 T[21]**
	Occipital lobe GM-rich	**Occipital lobe GM-rich**	**Occipital lobe**	**Occipital lobe**	**Occipital lobe GM-rich**	**Occipital lobe GM-rich**	**Occipital lobe**	**Occipital lobe mixed tissue**
Included MMB	measured	measured	measured	measured	From LCModel	measured	measured	measured
Metabolite T_2 correction	yes	no	no	no	no	no	no	yes
Tissue fraction, H_2O T_1, T_2 corrections	yes	yes	Assuming 80% water content	Assuming 80% water content	tCr set to 8 mmol/kg	tCr set to 8 mmol/kg	Not specified	yes
Sequence	semi-LASER	semi-LASER	STEAM	STEAM	SPECIAL	SPECIAL	STEAM	LASER
TE	24 ms	24 ms	6 ms	6 ms	6 ms	6 ms	8 ms	35 ms

Note: Absolute concentrations for the metabolites are shown (in mmol/kg). Concentrations for this work are reported with the correction of the metabolite T_2 values and without this correction. Both reported values use the T_1, T_2, and tissue-compartment corrections of the water signal. The concentrations without metabolite T_2 correction are all in good agreement with the millimolal concentrations reported in the literature at different field strengths from different studies (sequence and fitting configurations are also summarized). Absolute concentrations for the metabolites (in mmol/L) are found in Supporting Information Table S1 together with the literature comparison.

Abbreviation: Asc, ascorbic acid; GSH, glutathione.

[a]Concentrations that are higher than the literature values after metabolite T_2 correction (small changes).

[b]Concentrations that are higher than the literature values after metabolite T_2 correction (large changes).

[c]The Scy concentration is marked because it is possibly underestimated in this study. However, it is not clear whether the other literature used 1 or 6 proton resonances ($^{1\text{-}6}$CH) contributing to their Scy basis set simulation.

[d]Metabolites for which the mean T_2 relaxation time of all other metabolites was taken.

purely WM nor GM. This difference in T_2 relaxation times is highly influenced by the iron concentrations across the human brain, as shown by Hasan et al.[49] Hence, the T_2 relaxation times of metabolites reported in this work are specific to the region of the GM-rich occipital lobe.

The TE values of 24, 32, 40, 52, and 60 ms were chosen for the calculation of T_2 relaxation times, while keeping the shorter MM T_2^{eff} in mind. The MM signals were almost entirely decayed at TE = 60 ms. Having a corresponding MMB for the metabolite spectra improves the quantification of metabolite concentrations, hence the choice of identical TEs. The chosen TEs were sufficient to estimate the T_2 relaxation times of MM peaks and metabolites with shorter T_2 times. However, including some longer TE values would improve the accuracy of the T_2 relaxation times of metabolites with longer T_2s.

4.4 | Linewidth calculations

For any given voxel, B_0 inhomogeneities originate from a mixture of effects of $\Delta\nu_{micro}$, $\Delta\nu_{macro}$ as well as tissue compartment effects.[23] This B_0 effect experienced by spins is identical, whereas T_2 relaxation time is metabolite/resonance-specific. The $\Delta\nu_{1/2}$ of metabolite singlets, both in MC-semiLASER and tCr(CH_2) in DIR MC-semiLASER, clearly show the two components of the linewidth (Figure 6). The $\Delta\nu_{1/2}$ of tCr(CH_2) is in line with the ones previously reported.[23] The large differences between the $\Delta\nu_{1/2}$s of MM peaks and $\pi T_2^{eff}{}^{-1}$ (Figure 6, Table 1) indicate that these resonances are potentially composed of unresolved multiplets and/or different protons resonating at similar chemical shifts, which are strongly overlapping. Also, Supporting Information Figure S7 shows that the values of $\Delta\nu_{residual}$ for MM peaks are between 10 Hz and 60 Hz, whereas for metabolites they are closer to 0 Hz. The $\Delta\nu_{residual}$ value is consistent between GM and WM MM peaks, indicating that the magnitude of potential overlap and/or J-evolution[11] component for each MM peak is similar between different tissue types. These peaks could originate from amino acids[45] which, depending on the larger protein structure they belong to, can have different chemical shifts, but are distributed around a main resonance frequency for the bulk of protein peaks.

4.5 | Concentrations

Table 3 provides a consolidated comparison of absolute concentrations (millimoles per kilogram) of metabolites from literature[21,23,29,50,51] and this work.

Metabolite concentrations from this study are reported with and without T_2 correction for a fair comparison between the other studies and this work, as most of the other studies did not include T_2 correction due to the use of ultrashort TEs (<10 ms). The concentrations of NAA, NAAG, tCho, PE, Tau, Glu, GABA, and mI with T_2 correction are overall in good agreement with the literature.[21,23,29,50,51]

Concentrations of Asp, Gln, Glyc, and Glu are significantly higher after including the T_2 correction factor. However, their concentration values match those from the literature when considered without T_2 correction. Potential overestimations in this study could also arise due to an underestimation of the T_2 relaxation times of Gln, Glu and Asp, which exhibit strong J-evolution effects at TE = 52 ms and TE = 60 ms. In particular, the Gln concentration is likely overestimated, as the spline baseline exhibits negative behaviour in that area, which could not be compensated in the LCModel fits. Improved spectral resolution at ultrahigh field between Glu and Gln also influenced Gln concentrations in the current study. Furthermore, the loss of magnetization for individual MM components because of T_1 differences in DIR semi-LASER compared with semi-LASER could also influence our results. All referenced literature used single inversion recovery sequences to measure the MMB component. Similarly, Cr and PCr concentrations match the literature without T_2 correction, but are somewhat higher (~25%) when the T_2 correction is applied. This deviation could indicate that including the T_2 correction factor in the absolute quantification yields higher concentrations compared with the literature, as in most studies, no correction for the corresponding T_2 relaxation times of the metabolites was applied, or the Cr + PCr concentration was set to 8 mmol/kg. The shorter TEs used in the aforementioned studies, however, should not generally have a significant impact on metabolite concentrations.

Concentration of Scy, on the other hand, is lower in this study compared with other studies. However, it remains unclear whether care was taken to use all six carbon atoms, written as $^{1\text{-}6}$CH in Govindaraju et al,[40] each having a proton resonating at the same frequency, thus contributing to their Scy basis set simulation.

Absolute concentrations in millimoles per liter, given in Supporting Information Figure S8 and Supporting Information Table S1, are in excellent agreement with the concentrations that corrected for metabolite relaxations given by Penner et al[52] and with the literature comparison presented in the same article.

5 | CONCLUSIONS

In this study, for the first time, T_2 relaxation times of 14 individual macromolecule peaks ranging from 13 ms to 45 ms are measured in both GM-rich and WM-rich voxels.

In addition, in vivo transverse relaxation times of 12 metabolites and metabolite moieties in a GM-rich voxel in the occipital lobe at 9.4 T are reported. The T_2 relaxation values

ranged from 40 ms to 110 ms and were used as a correction factor for the absolute quantification of metabolites. The T_2^{eff} and T_2 values for MM peaks and metabolites, respectively, confirm the decreasing trend of transverse relaxation times with increasing static magnetic field. Finally, this work quantitatively shows the contribution of T_2 relaxation times and B_0 components to the linewidth of MM peaks. The residual linewidth includes not only components of J-coupling, but also chemical-shift distributions of amino acid proton groups.

ACKNOWLEDGMENTS

The authors acknowledge Gisela Hagberg for providing the recalculated relaxation times (T_2 and T_1) of water in brain CSF.

ORCID

Saipavitra Murali-Manohar
https://orcid.org/0000-0002-4978-0736

REFERENCES

1. Öz G, Alger JR, Barker PB, et al. Clinical proton MR spectroscopy in central nervous system disorders. *Radiology*. 2014;270:658–679.
2. Deelchand DK, Iltis I, Henry PG. Improved quantification precision of human brain short echo-time 1H magnetic resonance spectroscopy at high magnetic field: a simulation study. *Magn Reson Med*. 2014;72:20–25.
3. Cudalbu C, Mlynárik V, Gruetter R. Handling macromolecule signals in the quantification of the neurochemical profile. *J Alzheimers Dis*. 2012;31:S101–S115.
4. Louis MS, Alosco M, Rowland B, et al. Using machine learning techniques for identification of chronic traumatic encephalopathy related spectroscopic biomarkers. In: Proceedings of the 46th Annual IEEE Applied Imagery Pattern Recognition Workshop (AIPR), 2017, Washington DC. doi: https://doi.org/10.1109/AIPR.2017.8457949.
5. Mader I, Seeger U, Weissert R, et al. Proton MR spectroscopy with metabolite-nulling reveals elevated macromolecules in acute multiple sclerosis. *Brain*. 2001;124:953–961.
6. Mader I, Karitzky J, Klose U, et al. Proton MRS in Kennedy disease: absolute metabolite and macromolecular concentrations. *J Magn Reson Imaging*. 2002;16:160–167.
7. Lopez-Kolkovsky AL, Mériaux S, Boumezbeur F. Metabolite and macromolecule T1 and T2 relaxation times in the rat brain in vivo at 17.2 T. *Magn Reson Med*. 2016;75:503–514.
8. Pfeuffer J, Tkáč I, Provencher SW, Gruetter R. Toward an in vivo neurochemical profile: quantification of 18 metabolites in short-echo-time 1H NMR spectra of the rat brain. *J Magn Reson*. 1999;141:104–120.
9. de Graaf RA, Brown PB, McIntyre S, Nixon TW, Behar KL, Rothman DL. High magnetic field water and metabolite proton T1 and T2 relaxation in rat brain in vivo. *Magn Reson Med*. 2006;56:386–394.
10. Xin L, Gambarota G, Mlynárik V, Gruetter R. Proton T2 relaxation time of J-coupled cerebral metabolites in rat brain at 9.4 T. *NMR Biomed*. 2008;21:396–401.
11. Behar KL, Rothman DL, Spencer DD, Petroff OA. Analysis of macromolecule resonances in 1H NMR spectra of human brain. *Magn Reson Med*. 1994;32:294–302.
12. Wright A, Murali Manohar S, Henning A. Relaxation corrected and sequence-dependent macromolecule baseline model. In: Proceedings of the 27th Annual Meeting of ISMRM, 2019, Montréal, Canada. Abstract 2247.
13. Zoelch N, Hock A, Henning A. Quantitative magnetic resonance spectroscopy at 3T based on the principle of reciprocity. *NMR Biomed*. 2018;31:e3875.
14. Kreis R, Ernst T, Ross B. Absolute quantitation of water and metabolites in the human brain. II: Metabolite concentrations. *J Magn Reson Imaging B*. 1993;102:9–19.
15. Barker PB, Soher BJ, Blackband SJ, Chatham JC, Mathews VP, Bryan RN. Quantitation of proton NMR spectra of the human brain using tissue water as an internal concentration reference. *NMR Biomed*. 1993;6:89–94.
16. Gasparovic C, Song T, Devier D, et al. Use of tissue water as a concentration reference for proton spectroscopic imaging. *Magn Reson Med*. 2006;55:1219–1226.
17. Schulte RF, Lange T, Beck J, Meier D, Boesiger P. Improved two-dimensional J-resolved spectroscopy. *NMR Biomed*. 2006;19:264–270.
18. Murali Manohar S, Giapitzakis I, Borbáth T, Gaertner M, Henning A. Qualitative comparison between in vivo J-resolved semi-LASER at 3 T and 9.4 T. In: Proceedings of the 25th Annual Meeting of ISMRM, 2017, Honolulu, Hawaii. Abstract 3015.
19. Wang H, Yuan H, Shu L, Xie J, Zhang D. Prolongation of T2 relaxation times of hippocampus and amygdala in Alzheimer's disease. *Neurosci Lett*. 2004;363:150–153.
20. Wyss PO, Bianchini C, Scheidegger M, et al. In vivo estimation of transverse relaxation time constant (T2) of 17 human brain metabolites at 3T. *Magn Reson Med*. 2018;80:452–461.
21. Marjańska M, Auerbach EJ, Valabrègue R, Van de Moortele PF, Adriany G, Garwood M. Localized 1H NMR spectroscopy in different regions of human brain in vivo at 7 T: T2 relaxation times and concentrations of cerebral metabolites. *NMR Biomed*. 2012;25:332–339.
22. Mlynárik V, Gruber S, Moser E. Proton T 1 and T 2 relaxation times of human brain metabolites at 3 Tesla. *NMR Biomed*. 2001;14:325–331.
23. Deelchand DK, Van de Moortele P-F, Adriany G, et al. In vivo 1 H NMR spectroscopy of the human brain at 9.4 T: initial results. *J Magn Reson Imaging*. 2010;206:74–80.
24. Wright A, Murali Manohar S, Borbath T, Henning A. Longitudinal relaxation times of metabolites in vivo at 9.4 T. In: Proceedings of the 27th Annual Meeting of ISMRM, 2019, Montréal, Canada. Abstract 0514.
25. Avdievich NI, Giapitzakis IA, Pfrommer A, Henning A. Decoupling of a tight-fit transceiver phased array for human brain imaging at 9.4 T: loop overlapping rediscovered. *Magn Reson Med*. 2018;79:1200–1211.
26. Giapitzakis IA, Shao T, Avdievich N, Mekle R, Kreis R, Henning A. Metabolite-cycled STEAM and semi-LASER localization for MR spectroscopy of the human brain at 9.4 T. *Magn Reson Med*. 2018;79:1841–1850.
27. Gruetter R, Tkáč I. Field mapping without reference scan using asymmetric echo-planar techniques. *Magn Reson Med*. 2000;43:319–323.
28. Versluis MJ, Kan HE, van Buchem MA, Webb AG. Improved signal to noise in proton spectroscopy of the human calf muscle at 7 T using localized B1 calibration. *Magn Reson Med*. 2010;63:207–211.

29. Mekle R, Mlynárik V, Gambarota G, Hergt M, Krueger G, Gruetter R. MR spectroscopy of the human brain with enhanced signal intensity at ultrashort echo times on a clinical platform at 3T and 7T. *Magn Reson Med*. 2009;61:1279–1285.
30. Giapitzakis IA, Avdievich N, Henning A. Characterization of macromolecular baseline of human brain using metabolite cycled semi-LASER at 9.4 T. *Magn Reson Med*. 2018;80:462–473.
31. Fleysher R, Fleysher L, Kirov I, Hess DA, Liu S, Gonen O. Retrospective correction for T1-weighting bias in T2 values obtained with various spectroscopic spin-echo acquisition schemes. *Magn Reson Imaging*. 2009;27:1410–1419.
32. Boer V, van Lier A, Hoogduin J, Wijnen J, Luijten P, Klomp D. 7-T 1H MRS with adiabatic refocusing at short TE using radiofrequency focusing with a dual-channel volume transmit coil. *NMR Biomed*. 2011;24:1038–1046.
33. Murali Manohar S, Borbath T, Wright A, Henning A. Characterization of downfield resonances and their T2 relaxation times in human brain at 9.4 T. In: Proceedings of the 27th Annual Meeting of ISMRM, 2019, Montréal, Canada. Abstract 4248.
34. Hagberg GE, Bause J, Ethofer T, et al. Whole brain MP2RAGE-based mapping of the longitudinal relaxation time at 9.4 T. *NeuroImage*. 2017;144:203–216.
35. Provencher S. *LCModel & LCMgui User's Manual*. 2005.
36. Považan M, Strasser B, Hangel G, et al. Simultaneous mapping of metabolites and individual macromolecular components via ultra-short acquisition delay 1H MRSI in the brain at 7T. *Magn Reson Med*. 2018;79:1231–1240.
37. Soher B, Semanchuk P, Todd D, Steinberg J, Young K. VeSPA: integrated applications for RF pulse design, spectral simulation and MRS data analysis. In: Proceedings of the 19th Annual Meeting of ISMRM, 2011, Montréal, Canada. p 1410.
38. Soher B.Vespa: versatile simulation pulses and analysis. User code contributions—semi-LASER. https://scion.duhs.duke.edu/vespa/contr ib/wiki/1f03e57e-1d27-4d36-8b31-db9e5e2f73e82013. Accessed July 30, 2019.
39. Govind V, Young K, Maudsley AA. Corrigendum: proton NMR chemical shifts and coupling constants for brain metabolites. Govindaraju V, Young K, Maudsley AA. *NMR Biomed*. 2000;13:129–153. NMR Biomed. 2015;28:923–924.
40. Govindaraju V, Young K, Maudsley AA. Proton NMR chemical shifts and coupling constants for brain metabolites. *NMR Biomed*. 2000;13:129–153.
41. Near J, Evans CJ, Puts NA, Barker PB, Edden RA. J-difference editing of gamma-aminobutyric acid (GABA): simulated and experimental multiplet patterns. *Magn Reson Med*. 2013;70:1183–1191.
42. de Graaf RA. In vivo NMR Spectroscopy—static aspects. *In Vivo NMR Spectroscopy*. Hoboken, New Jersey: John Wiley & Sons; 2007:43–110.
43. Giapitzakis IA, Borbath T, Murali-Manohar S, Avdievich N, Henning A. Investigation of the influence of macromolecules and spline baseline in the fitting model of human brain spectra at 9.4 T. *Magn Reson Med*. 2019;81:746–758.
44. Murali Manohar S, Wright A, Borbath T, Henning A. Longitudinal relaxation times of macromolecular resonances at 9.4 T in human brain. In: Proceedings of the 27th Annual Meeting of ISMRM, 2019, Montréal, Canada. Abstract 2248.
45. Ulrich EL, Akutsu H, Doreleijers JF, et al. BioMagResBank. *Nucleic Acids Res*. 2007;36:D402–D408.
46. Allerhand A, Thiele E. Analysis of Carr-Purcell spin-echo NMR experiments on multiple-spin systems. II: The effect of chemical exchange. *J Chem Phys*. 1966;45:902–916.
47. Kreis R, Slotboom J, Hofmann L, Boesch C. Integrated data acquisition and processing to determine metabolite contents, relaxation times, and macromolecule baseline in single examinations of individual subjects. *Magn Reson Med*. 2005;54:761–768.
48. Nassirpour S, Chang P, Henning A. High and ultra-high resolution metabolite mapping of the human brain using 1H FID MRSI at 9.4 T. *NeuroImage*. 2018;168:211–221.
49. Hasan KM, Walimuni IS, Kramer LA, Narayana PA. Human brain iron mapping using atlas-based T2 relaxometry. *Magn Reson Med*. 2012;67:731–739.
50. Mangia S, Tkáč I, Gruetter R, et al. Sensitivity of single-voxel 1 H-MRS in investigating the metabolism of the activated human visual cortex at 7 T. *Magn Reson Imaging*. 2006;24:343–348.
51. Terpstra M, Ugurbil K, Tkac I. Noninvasive quantification of human brain ascorbate concentration using 1H NMR spectroscopy at 7 T. *NMR Biomed*. 2010;23:227–232.
52. Penner J, Bartha R. Semi-LASER 1H MR spectroscopy at 7 Tesla in human brain: metabolite quantification incorporating subject-specific macromolecule removal. *Magn Reson Med*. 2015;74:4–12.

SUPPORTING INFORMATION

Additional supporting information may be found online in the Supporting Information section.

FIGURE S1 Echo time series (TE = 24, 32, 40, 52, and 60 ms) for MM spectra (right) from WM, with solid lines showing the mean spectra and the shaded area indicating the SD across subjects

FIGURE S2 Gray Matter MM spectra summed across subjects (TE = 32, 40, 52 and 60 ms) are shown with the fitted macromolecules and tCr(CH_2) moiety. The basis set configuration shows the setup for inverting the $M_{2.70}$ peak at TE = 40, 52, and 60 ms

FIGURE S3 White matter MM spectrum summed across subjects (TE = 24 ms) is shown with the fit using simulated Voigt lines. The residual tCr(CH_2) peak in the spectra is modeled with a significantly narrower linewidth

FIGURE S4 White matter MM spectra summed across subjects (TE = 32, 40, 52, and 60 ms) are shown with the fitted macromolecules and tCr(CH_2) moiety. The basis set configuration shows the setup for inverting the $M_{2.70}$ peak at TE = 40, 52, and 60 ms

FIGURE S5 Metabolite spectra summed across subjects (TE = 32, 40, 52, and 60 ms) are shown with the fitted metabolites and measured MMB. The basis set configuration shown here with the tCr split to its moieties tCr(CH_3) and tCr(CH_2), NAA split to NAA(CH_2) and NAA(CH_3) moiety, and tCho and PE combined with tCho+ was used to estimate the T_2 relaxation times. For each TE, a corresponding basis set was simulated with *Vespa*

FIGURE S6 Exponential decay plots of $M_{0.92}$, $M_{2.04}$, $M_{2.26}$, and $M_{2.99}$ from summed GM and WM spectra. The lines show the fit, whereas the scatter shows the quantified data points. The y-axis is reported in arbitrary units, and no conclusions should be drawn between GM and WM concentration differences

FIGURE S7 The FWHMs for the singlets of the metabolite spectra (left) and individual MM peaks and tCr(CH_2) peak of the MM spectra (right) after correcting for the T_2 component of corresponding metabolite/macromolecule, and the B_0 components from NAA(CH_3) and tCr(CH_2), respectively. The metabolite FWHM of tCho+ and tCr(CH_2) reflects the multiple components contributing to the singlet peak. The crosses (X) indicate the calculations for the spectra summed across subjects, whereas the box plots show the per-subject fits. Horizontal lines inside the boxes indicate median values (50% quartile), whereas the bottom and top box boundaries illustrate 25% and 75% quartiles, respectively. Plus signs (+) show outliers

FIGURE S8 Calculated absolute concentrations for the metabolites for the different subjects (in mmol/L). The blue box plots show the concentrations when metabolite T_2 correction is applied, while the green box plots show the concentrations without applying this correction factor. Horizontal lines inside the boxes indicate median values (50% quartile), whereas the bottom and top box boundaries illustrate 25% and 75% quartiles, respectively. Plus signs (+) show outliers

TABLE S1 Absolute concentrations for the metabolites (in mmol/L)

Note: Concentrations for this work are reported with the correction of the metabolite T_2 values. The concentrations are all in good agreement with the millimolal concentrations reported by Penner et al (sequence and fitting configurations are also summarized).

[a]Concentrations that are higher than the literature values (small changes).

[b]Concentrations that are higher than the literature values (large changes).

[c]The Scy concentration is marked, because it is possibly underestimated in this study. However, it is not clear whether the other literature used 1 or 6 proton resonances (^{16}NH) contributing to their Scy basis set simulation.

[d]Metabolites for which the mean T_2 relaxation time of all other metabolites was taken.

How to cite this article: Murali-Manohar S, Borbath T, Wright AM, Soher B, Mekle R, Henning A. T_2 relaxation times of macromolecules and metabolites in the human brain at 9.4 T. *Magn Reson Med*. 2020;84:542–558. https://doi.org/10.1002/mrm.28174

SUPPORTING INFORMATION FIGURES

Supporting Information Figure S1: Echo time (TE) series (TE = 24, 32, 40, 52 and 60 ms) for macromolecular spectra (right) from white matter with solid lines showing the mean spectra and the shaded area indicating the standard deviation across subjects.

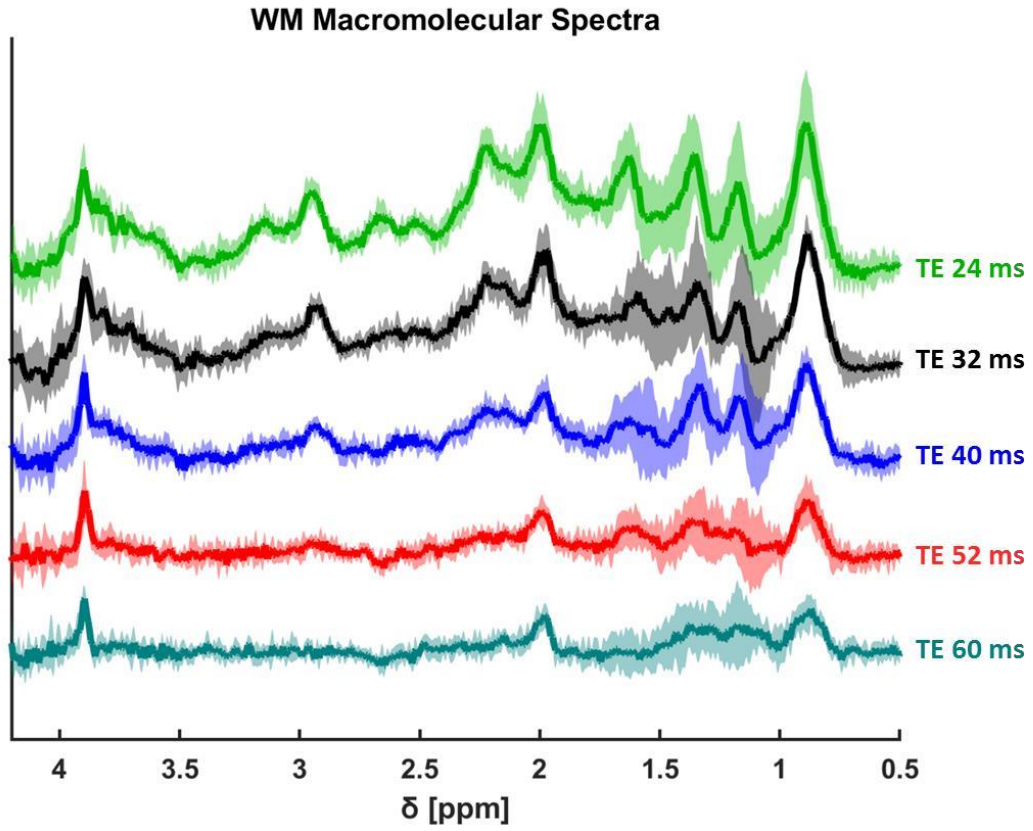

Supporting Information Figure S2: The gray matter across subjects summed macromolecular spectra (TE = 32, 40, 52 and 60 ms) are shown with the fitted macromolecules and tCr(CH_2) moiety. The basis set configuration shows the setup for inverting the $M_{2.70}$ peak at the TEs 40, 52 and 60 ms.

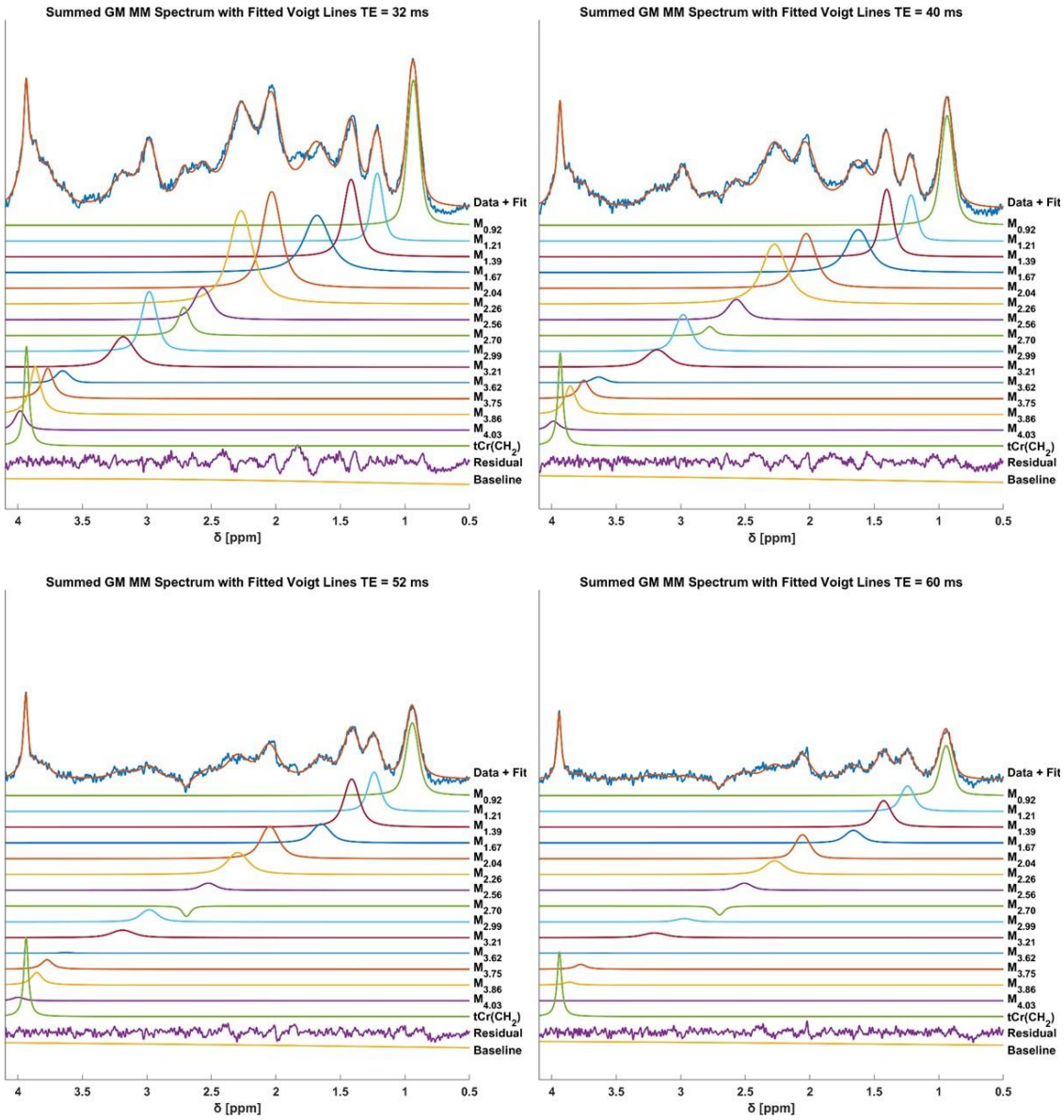

Supporting Information Figure S3: White matter macromolecular spectrum summed across subjects (TE = 24 ms) is shown with the fit using simulated Voigt lines. The residual total creatine – 3.9 singlet ($tCr(CH_2)$) peak in the spectra is modeled with a significantly narrower linewidth.

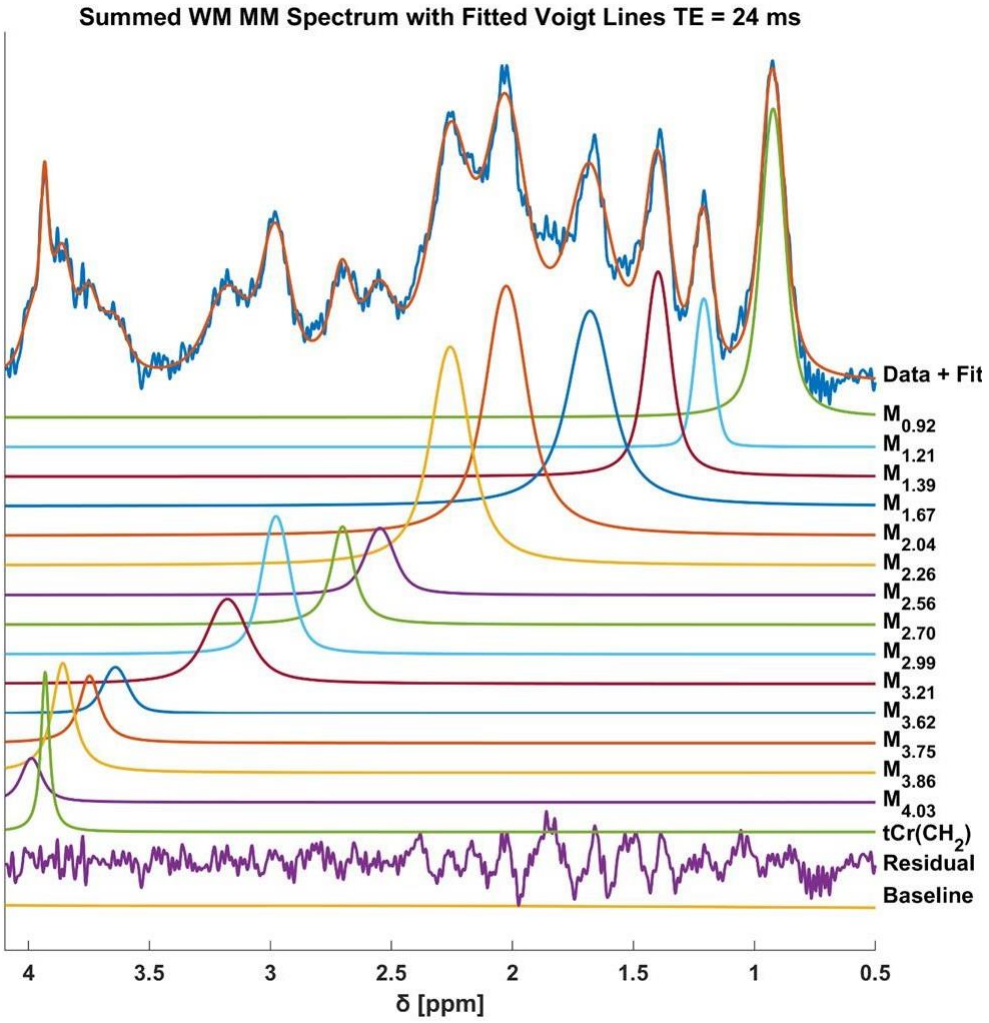

Supporting Information Figure S4: The white matter across subjects summed macromolecular spectra (TE = 32, 40, 52 and 60 ms) are shown with the fitted macromolecules and tCr(CH_2) moiety. The basis set configuration shows the setup for inverting the $M_{2.70}$ peak at the TEs 40, 52 and 60 ms.

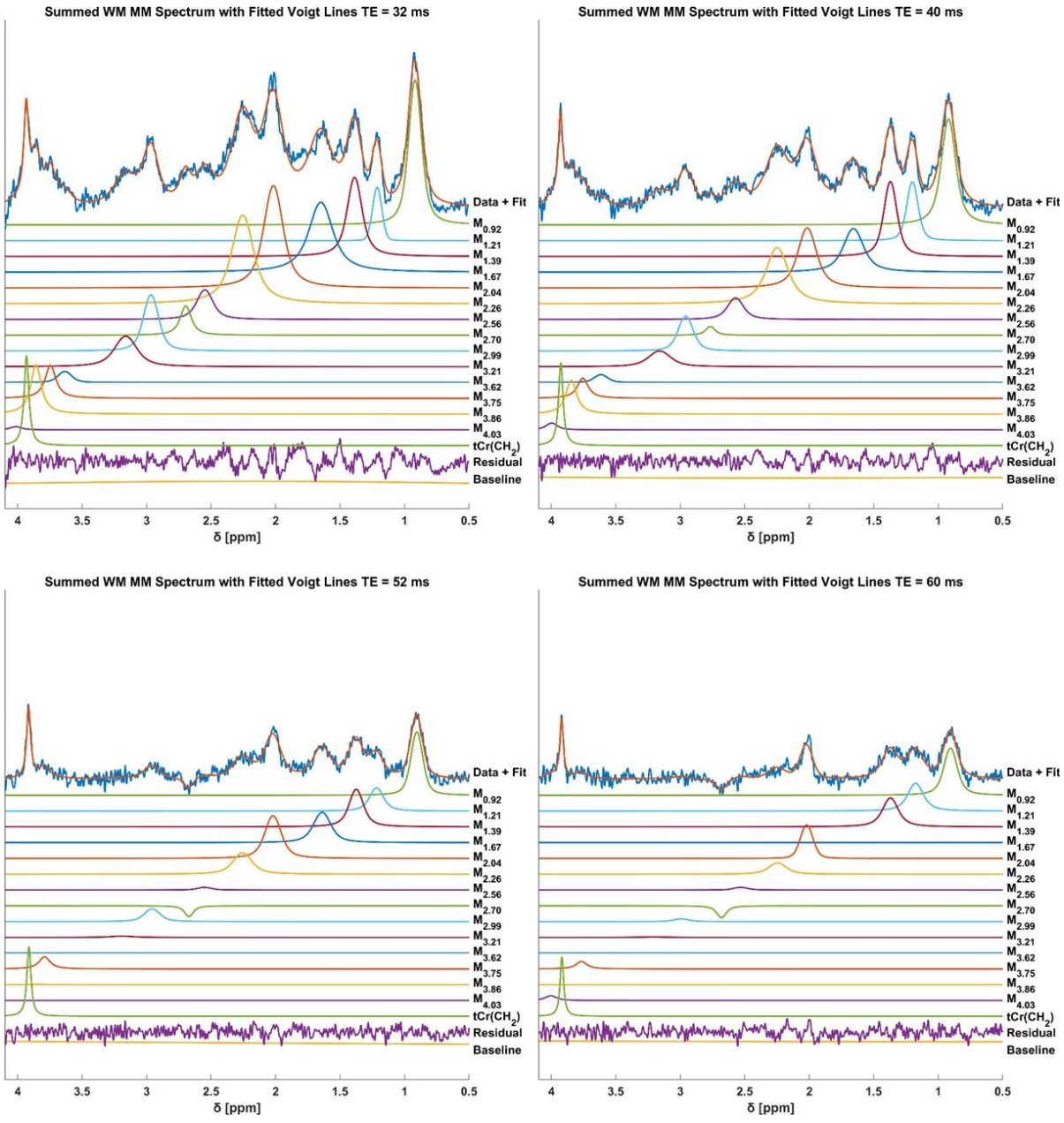

Supporting Information Figure S5: The across subjects summed metabolite spectra (TE = 32, 40, 52 and 60 ms) are shown with the fitted metabolites and measured MMB. The basis set configuration shown here with the tCr split to its moieties tCr(CH_3) and tCr(CH_2) , NAA split to NAA(CH_2) and NAA(CH_3) moiety, and tCho and PE combined to tCho+ was used to estimate the T_2 relaxation times. For each echo time a corresponding basis set was simulated with Vespa.

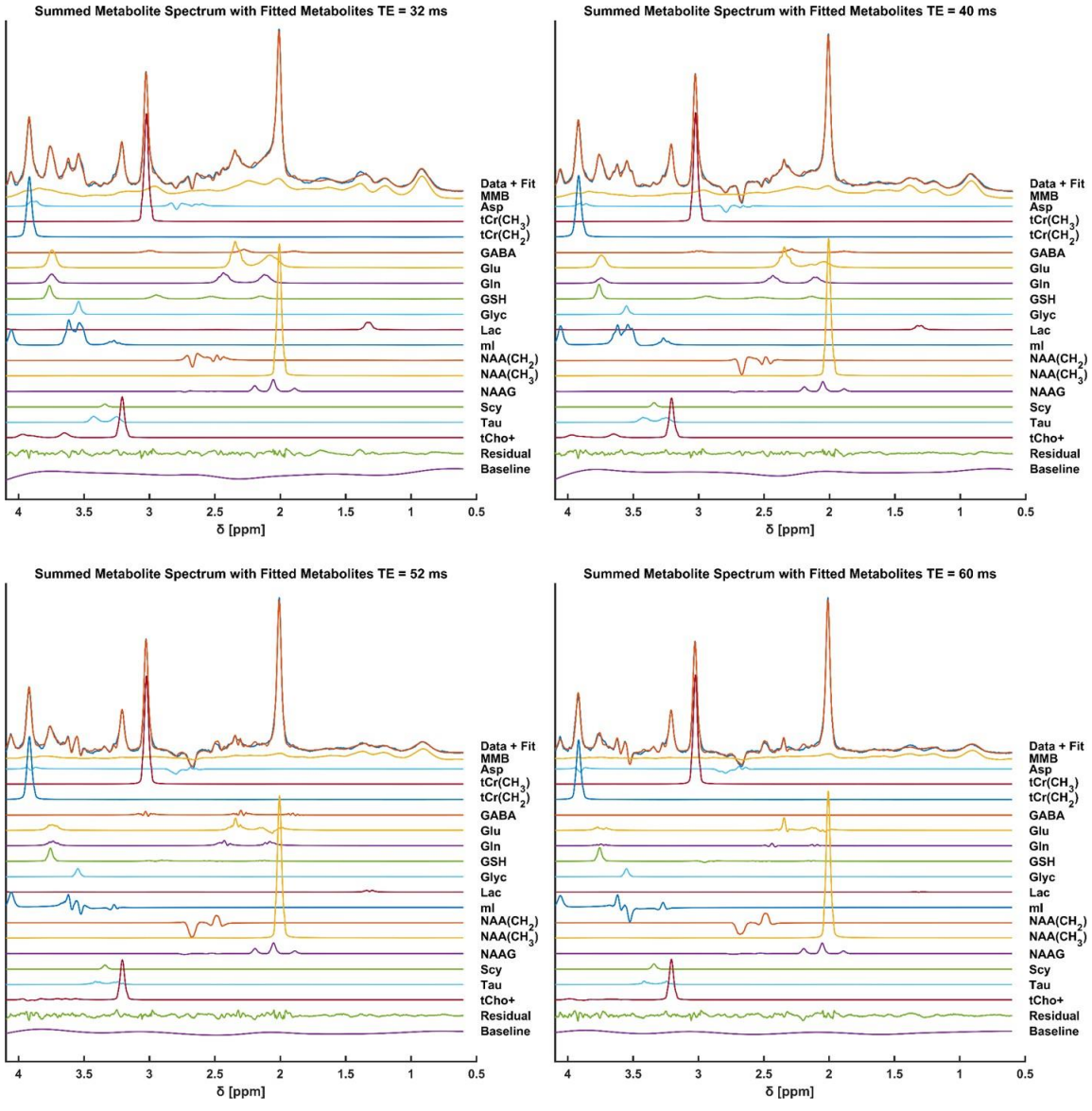

Supporting Information Figure S6: Exponential decay plots of $M_{0.92}$, $M_{2.04}$, $M_{2.26}$ and $M_{2.99}$ from summed GM and WM spectra. The lines show the fit while the scatter shows the quantified data points. The y-axis is reported in arbitrary units, and no conclusions should be drawn between GM and WM concentration differences.

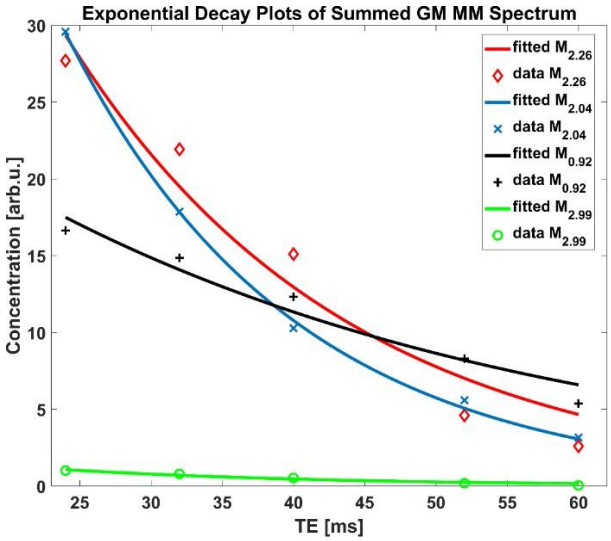

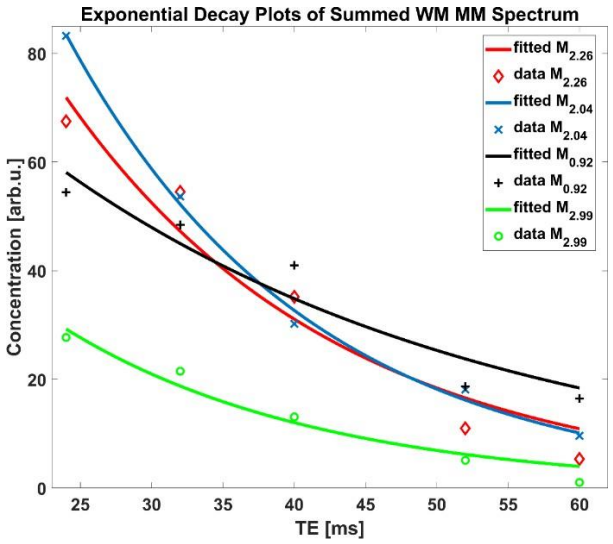

Supporting Information Figure S7: FWHMs for the singlets of the metabolite spectra (left) and individual MM peaks and tCr(CH_2) peak of the macromolecular spectra (right) after correcting for the T_2 component of corresponding metabolite/macromolecule, and the B_0 components from NAA(CH_3) and tCr(CH_2) respectively. The metabolite FWHM of tCho+ and tCr(CH_2) reflect the multiple components contributing to the singlet peak. The crosses (X) indicate the calculations for the spectra summed across subjects, while the box plots show the per subject fits. Horizontal lines inside the boxes indicate median values (50% quartile), whereas the bottom and top box boundaries illustrate 25% and 75% quartiles, respectively. Plus signs (+) show outliers.

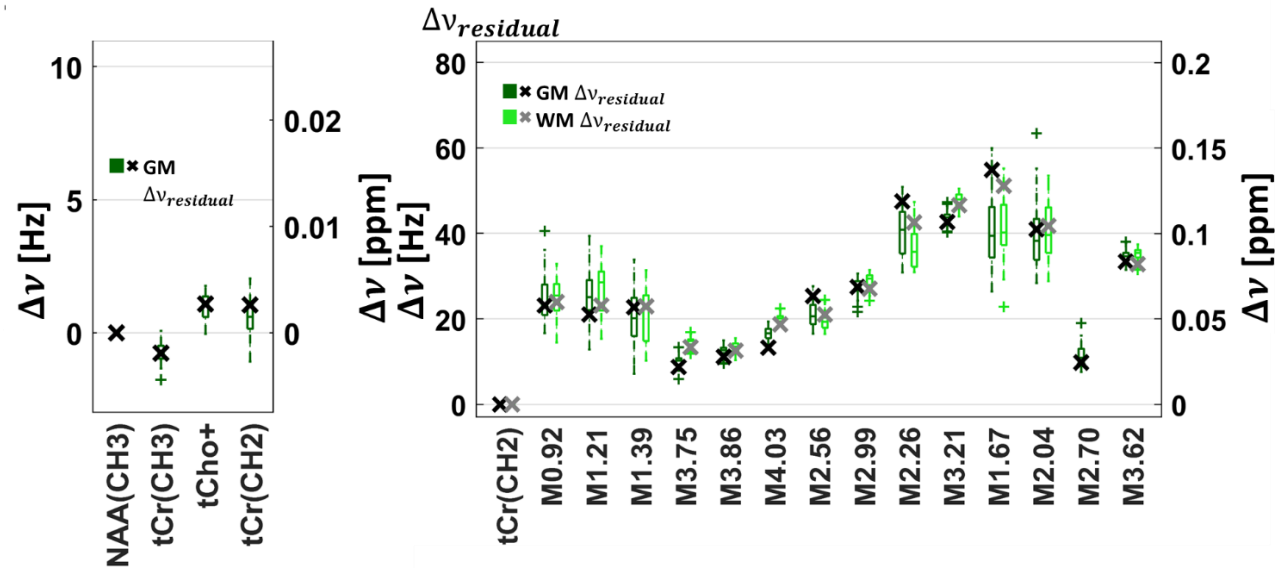

Supporting Information Figure S8: Calculated absolute concentrations for the metabolites in mmol/L for the different subjects. The blue box plots show the concentrations when metabolite T2 correction is applied, while the green box plots show the concentrations without applying this correction factor. Horizontal lines inside the boxes indicate median values (50% quartile), whereas the bottom and top box boundaries illustrate 25% and 75% quartiles, respectively. Plus signs (+) show outliers.

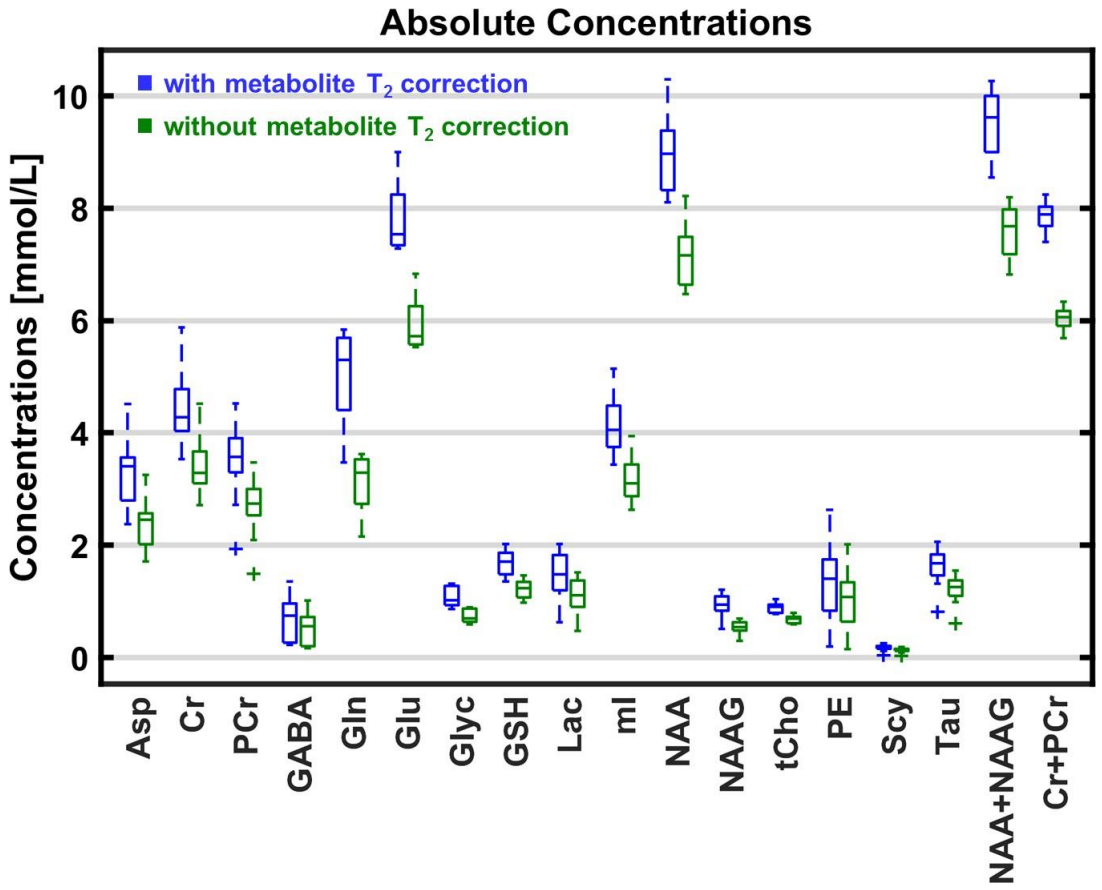

Supporting Information Table S1:

Absolute concentrations for the metabolites in mmol/L are shown. Concentrations for this work are reported with the correction of the metabolite T_2 values. The concentrations are all in good agreement with the mmolal concentrations reported by Penner et al., (sequence and fitting configurations are also summarized).

[a,b] Concentrations which are higher than the literature values are marked with [a] for small changes, and with [b] for large changes.
[c] The Scyllo concentration is marked with since it is possibly underestimated in this study. However, it is not clear, whether the other literature used one or six proton resonances ($^{1\text{-}6}$NH) contributing to their Scyllo basis set simulation.
[d] Metabolites for which the mean T_2 relaxation time of all the other metabolites was taken.

Absolute concentrations [mmol/L ± std]		
	This work with T_2 correction	Penner 2015 7T [10]
	Occipital lobe GM rich	Occipital lobe mixed tissue
Asp	3.19 ± 0.75	3.8 ± 1.3
Cr	4.21 ± 0.64	4.1 ± 0.6
PCr	3.27 ± 0.61	3.5 ± 0.9
GABA	1.37 ± 0.67 [d]	-
Gln	5.43 ± 0.67 [b]	2.2 ± 0.4
Glu	8.05 ± 0.63 [a]	10.7 ± 1.6
Glyc	0.81 ± 0.21	-
GSH	1.28 ± 0.12	1.6 ± 0.3
Lac	1.27 ± 0.58	-
mI	3.85 ± 0.33	-
NAA	9.31 ± 0.79	-
NAAG	1.07 ± 0.15	-
tCho	0.76 ± 0.09 [a]	1.8 ± 0.4
PE	1.68 ± 0.70 [d]	1.2 ± 0.5
Scy	0.09 ± 0.04 [c, d]	0.4 ± 0.1
Tau	1.15 ± 0.27	1.0 ± 0.5
NAA+NAAG	10.05 ± 0.78	11.8 ± 0.8
mI+Glyc	4.68 ± 0.39 [a]	5.9 ± 0.3
Cr+PCr	7.46 ± 0.33	7.6 ± 0.9
Glu+Gln	13.03 ± 1.15	12.9 ± 1.6
Included MMB	measured	measured
Metabolite T_2 correction	yes	yes
Tissue fraction corrections	yes	78% fractional water content of GM & WM, correction for CSF with water reference
Sequence	semiLASER	semiLASER
Echo time	24 ms	38 ms

ANNEX A - *Absolute Quantification*

Concentrations in mmolal

$$[\mathrm{M}]_{mmolal} = [\mathrm{M}]_{\mathrm{obs}} \times conc_{pure\_H2O} \times \frac{(\mathrm{f_{GM}} \times R_{H2O\_GM} + \mathrm{f_{WM}} \times R_{H2O\_WM} + \mathrm{f_{CSF}} \times R_{H2O\_CSF})}{(1 - \mathrm{f_{CSF}}) \times R_M} \times \frac{2}{1 + \mathrm{Fs}}$$

where $f_y = \frac{f_{y\_vol} \times a_y}{f_{GM\_vol} \times a_{GM} + f_{WM\_vol} \times a_{WM} + f_{CSF\_vol} \times a_{CSF}}$

where y corresponds to either GM, WM or CSF; f_{y_vol} is the fraction of the respective tissue type determined by segmentation; a_{GM}, a_{WM}, a_{CSF} (78%, 65%, 97% respectively) are the relative densities of MR-visible water for the given tissue type; The molal concentration of water in metabolite solution is 55510 mmoles/kg and is denoted by $conc_{pure\_H2O}$.

Concentrations in mmolar

$$[\mathrm{M}]_{mmolar} = [\mathrm{M}]_{\mathrm{obs}} \times conc_{pure\_H2O} \times \frac{2}{1 + \mathrm{Fs}} \times \frac{(\mathrm{f_{GM\_vol}} \times \alpha_{\mathrm{GM}} \times R_{H2O\_GM} + \mathrm{f_{WM\_vol}} \times \alpha_{\mathrm{WM}} \times R_{H2O\_WM} + \mathrm{f_{CSF\_vol}} \times \alpha_{\mathrm{CSF}} \times R_{H2O\_CSF})}{(1 - \mathrm{f_{CSF}}) \times R_M}$$

Where f_{y_vol} is the fraction of the respective tissue type determined by segmentation; a_{GM}, a_{WM}, a_{CSF} (78%, 65%, 97% respectively) are the relative densities of MR-visible water for the given tissue type; The molar concentration of water is 55126 mM and is denoted by $conc_{pure\_H2O}$.

For both cases, $R_{H2O\_y} = \exp[-\frac{TE}{T2_{H2O\_y}}][1 - \exp[-\frac{\mathrm{TR}}{T1_{H2O_y}}]]$ is the relaxation correction factor for each water compartment y. $T1_{H2O_y}$ and $T2_{H2O\_y}$ are the T_1 and T_2 relaxation times of water in the compartment y.. $R_M = \exp[-\frac{TE}{T2_{M\_ave}}][1 - \exp[-\frac{\mathrm{TR}}{T1_{M\_ave}}]]$ is the relaxation correction term for metabolites. The denominator $1 - f_{CSF}$ was implemented for partial-volume correction. The factor $\frac{2}{1+\mathrm{Fs}}$ was introduced to correct for the multiplication of even numbered acquisitions with the scaling factor (F_s). $[\mathrm{M}]_{\mathrm{obs}}$ is the concentration obtained from LCModel divided by the preset value (40873).

While quantifying NAA absolutely, the mean T_2 relaxation time of NAA(CH_3) and NAA(CH_2) was used; for Cr and PCr metabolites the mean T_2 relaxation time of tCr(CH_2) and tCr(CH_3) singlets was used. Calculating the mean value was numerically equivalent to fitting a T_2 exponential to the combined metabolite moiety concentrations across the TE series.

ANNEX B - ***Control files (.control) for LCModel quantification***

Sample LCModel .control files used for the quantification of the occipital lobe spectra for macromolecules and metabolite fitting.

Macromolecules fitting

Note: NAA_DF_basis.basis contains only the NAA 7.8 ppm peak, which seems relatively stable across TE series

```
$LCMODL
OWNER='Max Planck Institute biological Cybernetics'
TITLE= ‘Macromolecule_Fit_TE24
FILBAS='~/SampleConfigs/Basis_sets/ NAA_DF_basis.basis'
FILRAW='~/SampleConfigs/data/macromolecule_TE24.RAW'
FILH2O='~/SampleConfigs/data/water.RAW'
FILPS='~/SampleConfigs/Output/macromolecule_TE24.ps'
FILTAB='~/SampleConfigs/Output/macromolecule_TE24.table'
FILCSV='~/SampleConfigs/Output/macromolecule_TE24.csv'
FILCOO='~/SampleConfigs/Output/macromolecule_TE24.coord'
LTABLE=7
LCOORD=9
LCSV=11
atth2o= 1
deltat= 1.2500e-04
dkntmn= 0.25
doecc= F
dows=  T
hzpppm= 399.719
neach= 50
nunfil= 4096
ppmend= 0.2
ppmst= 8.2
ppmgap(1,1)= 7.6
ppmgap(2,1)= 4.1
sddegp= 0
sddegz= 0
wconc= 40873
shifmn(2) = -0.07
shifmx(2) = 0.07
nratio=0
nsimul= 15
chsimu(1)= 'MM09 @ 0.916 +- 0.01 FWHM= .08 < .11 +- .01 AMP= 1.'
chsimu(2)= 'MM12 @ 1.21 +- 0.01 FWHM= .08 < .11 +- .005 AMP= 1.'
chsimu(3)= 'MM14 @ 1.39 +- 0.01 FWHM= .08 < .11 +- .005 AMP= 1.'
chsimu(4)= 'MM17 @ 1.67 +- 0.01 FWHM= .10 < .13 +- .005 AMP= 1.'
```

```
chsimu(5)= 'MM20 @ 2.04 +- 0.01 FWHM= .10 < .13 +- .005 AMP= 1.'
chsimu(6)= 'MM22 @ 2.26 +- 0.005 FWHM= .10 < .13 +- .005 AMP= 1.'
chsimu(7)= 'MM26 @ 2.56 +- 0.01 FWHM= .09 < .11 +- .005 AMP= 1.'
chsimu(8)= 'MM27 @ 2.7 +- 0.05 FWHM= .04 < .08 +- .005 AMP= 1.'
chsimu(9)= 'MM30 @ 2.99 +- 0.01 FWHM= .10 < .12 +- .005 AMP= 1.'
chsimu(10)= 'MM32 @ 3.21 +- 0.02 FWHM= .12 < .18 +- .005 AMP= 1.'
chsimu(11)= 'MM36 @ 3.62 +- 0.02 FWHM= .09 < .11 +- .005 AMP= 1.'
chsimu(12)= 'MM37 @ 3.75 +- 0.02 FWHM= .02 < .10 +- .005 AMP= 1.'
chsimu(13)= 'MM38 @ 3.86 +- 0.01 FWHM= .02 < .10 +- .005 AMP= 1.'
chsimu(14)= 'MM40 @ 4.03 +- 0.01 FWHM= .05 < .10 +- .005 AMP= 1.'
chsimu(15)= 'Cre @ 3.925 +- 0.01 FWHM= .01 < .035 +- .003 AMP= 1.'
$END
```

Metabolite Fitting Absolute Quantification

```
$LCMODL
OWNER='Max Planck Institute biological Cybernetics'
TITLE= ‘Metabolite_Fit_TE24
FILBAS='~/SampleConfigs/Basis_sets/sLASER_2.4ppm_abs_quantif_met_TE24.basis'
FILRAW='~/SampleConfigs/data/metabolite_TE24.RAW'
FILH2O='~/SampleConfigs/data/water.RAW'
FILPS='~/SampleConfigs/Output/metabolite_TE24.ps'
FILTAB='~/SampleConfigs/Output/metabolite_TE24.table'
FILCSV='~/SampleConfigs/Output/metabolite_TE24.csv'
FILCOO='~/SampleConfigs/Output/metabolite_TE24.coord'
LTABLE=7
LCOORD=9
LCSV=11
atth2o= 1
deltat= 1.2500e-04
dkntmn= 0.25
doecc= F
dows=  T
hzpppm= 399.719
neach= 50
nunfil= 4096
ppmend= 0.6
ppmst= 4.1
sddegp= 1
sddegz= 1
wconc= 40873
nsimul = 0
nnot2= 0
nratio=0
$END
```

Metabolite Fitting Absolute Quantification

```
$LCMODL
OWNER='Max Planck Institute biological Cybernetics'
TITLE= ‘Metabolite_Fit_TE24
FILBAS='~/SampleConfigs/Basis_sets/sLASER_7ppm_moiety_met_TE24.basis'
FILRAW='~/SampleConfigs/data/metabolite_TE24.RAW'
```

```
FILH2O='~/SampleConfigs/data/water.RAW'
FILPS='~/SampleConfigs/Output/metabolite_TE24.ps'
FILTAB='~/SampleConfigs/Output/metabolite_TE24.table'
FILCSV='~/SampleConfigs/Output/metabolite_TE24.csv'
FILCOO='~/SampleConfigs/Output/metabolite_TE24.coord'
LTABLE=7
LCOORD=9
LCSV=11
atth2o= 1
deltat= 1.2500e-04
dkntmn= 0.25
doecc= F
dows=  T
hzpppm= 399.719
neach= 50
nunfil= 4096
ppmend= 0.6
ppmst= 4.1
sddegp= 1
sddegz= 1
wconc= 40873
nsimul = 0
nnot2= 0
nratio=2
chrato(1) = 'NAA_ac/NAA_as=1.2+-0.02'
chrato(2) = 'mI/Glyc=5+-0.5'
$END
```

Publication 2

“A novel method to measure T_1-relaxation times of macromolecules and quantification of the macromolecular resonances”

S Murali-Manohar*, A M Wright*, T Borbath, N I Avdievich, A Henning

Magnetic Resonance in Medicine, 2020, DOI: 10.1002/mrm.28484

Received: 8 January 2020 | Revised: 29 July 2020 | Accepted: 29 July 2020

DOI: 10.1002/mrm.28484

FULL PAPER

Magnetic Resonance in Medicine

A novel method to measure T_1-relaxation times of macromolecules and quantification of the macromolecular resonances

Saipavitra Murali-Manohar[1,2] | **Andrew Martin Wright**[1,3] | **Tamas Borbath**[1,2] | **Nikolai I. Avdievich**[1] | **Anke Henning**[1,4]

[1]High-Field Magnetic Resonance, Max Planck Institute for Biological Cybernetics, Tübingen, Germany

[2]Faculty of Science, University of Tübingen, Tübingen, Germany

[3]IMPRS for Cognitive & Systems Neuroscience, Tübingen, Germany

[4]Advanced Imaging Research Center, UT Southwestern Medical Center, Dallas, Texas, USA

Correspondence
Saipavitra Murali-Manohar, High-Field Magnetic Resonance, Max Planck Institute for Biological Cybernetics, Tübingen, Germany.
Email: saipavitra.murali.manohar@tuebingen.mpg.de

Funding information
This project was co-sponsored by the Horizon 2020/CDS-QUAMRI Grant number: 634541 (A. Henning, T. Borbath, and S. Murali-Manohar), SYNAPLAST Grant number: 679927 (A. Henning and A.M. Wright), and Cancer Prevention and Research Institute of Texas (CPRIT) Grant number: RR180056 (A. Henning)

Purpose: Macromolecular peaks underlying metabolite spectra influence the quantification of metabolites. Therefore, it is important to understand the extent of contribution from macromolecules (MMs) in metabolite quantification. However, to model MMs more accurately in spectral fitting, differences in T_1 relaxation times among individual MM peaks must be considered. Characterization of T_1-relaxation times for all individual MM peaks using a single inversion recovery technique is difficult due to eventual contributions from metabolites. On the contrary, a double inversion recovery (DIR) technique provided flexibility to acquire MM spectra spanning a range of longitudinal magnetizations with minimal metabolite influence. Thus, a novel method to determine T_1-relaxation times of individual MM peaks is reported in this work.

Methods: Extensive Bloch simulations were performed to determine inversion time combinations for a DIR technique that yielded adequate MM signal with varying longitudinal magnetizations while minimizing metabolite contributions. MM spectra were acquired using DIR-metabolite-cycled semi-LASER sequence. LCModel concentrations were fitted to the DIR signal equation to calculate T_1-relaxation times.

Results: T_1-relaxation times of MMs range from 204 to 510 ms and 253 to 564 ms in gray- and white-matter rich voxels respectively at 9.4T. Additionally, concentrations of 13 MM peaks are reported.

Conclusion: A novel DIR method is reported in this work to calculate T_1-relaxation times of MMs in the human brain. T_1-relaxation times and relaxation time corrected concentrations of individual MMs are reported in gray- and white-matter rich voxels for the first time at 9.4T.

Saipavitra Murali-Manohar and Andrew Martin Wright contributed equally to this work.

KEYWORDS
double inversion recovery, macromolecules, MR spectroscopy, quantification, semiLASER, T_1-relaxation times, ultra-high magnetic field

1 | INTRODUCTION

Broad macromolecular resonances underlie metabolite spectra in ^{1}H MR spectroscopy (MRS) at short echo times (TE). Macromolecules (MMs) between 0.5 and 4.5 ppm are attributed to mobile methyl, methylene, and methine groups of amino acids from cytosolic peptides and proteins.[1] Several studies at field strengths between 1.5 to 3 T have highlighted the clinical relevance of MMs in aging[2] and in pathologies such as traumatic encephalopathy,[3] Kennedy's disease,[4] acute multiple sclerosis,[5] and glioma.[6] To understand mechanisms better in the aforementioned pathologies, it is of interest to use advantages of higher field strengths. Due to increased spectral dispersion, signal-to-noise ratio (SNR), and resolution, more MM peaks are distinguishable at ultra-high field (UHF) ($B_0 \geq 7$ T); hence, it is possible to more accurately characterize the behavior of individual MM peaks.

On the other hand, the well-resolved underlying MM spectrum at UHF often distorts the metabolite spectrum. Therefore, characterizing MM peaks additionally improves accuracy in quantifying metabolites. Various techniques have been used to handle MM signals in metabolite spectra namely: (1) opting for longer TE while measuring the metabolite spectra,[7] (2) applying mathematical models such as a flexible spline baseline while fitting metabolite spectra,[8] and (3) using prior information from experimentally acquired MM spectra.[9]

The first two techniques (1, 2) do not prove to be the best solution at high field strengths (≥3 T). Using longer TEs (1) can lead to complications in quantifying metabolites due to decreased SNR and evolving J-coupling Therefore, short TEs are preferred in studies at UHF due to the generally faster transversal relaxation times of metabolites.[7] With a decrease in the amount of overlapping of MM peaks at UHF, a flexible spline baseline (2) may not hold to be a good solution to the problem of accounting for the MM spectrum accurately.[9] Work done previously at 14.1 T acquired the MM spectrum by nulling metabolite resonances, and reported that the use of a prior knowledge MM spectrum in spectral fitting leads to more accurate and more reliable metabolite quantification at UHF.[10] Hence, using prior information (3) from experimentally acquired MM spectra may prove to be a better solution.

Inversion recovery (IR) techniques are a reliable method for acquiring MM spectra due to the relatively fast T_1-relaxation times of MM peaks compared with those of metabolites.[11] However, IR techniques that are used to acquire MM spectra introduce T_1-weighting to the MM signals which depend on the chosen inversion time (TI) and repetition time (TR). It is likely that using T_1-weighted MM spectra when fitting metabolite spectra, that are acquired without inversion pulses and typically a shorter TR, will influence quantitative accuracy. Indeed, a better characterization of the behavior of the relaxation times of the MM spectrum will lead to improved spectral fitting and fitting reproducibility.

Previous studies have: characterized the T_1-relaxation times of MMs in the human brain for MM spectra as a whole[12-14]; or for non-overlapping MM peaks[1,15,16]; or for groups of MM peaks.[11,17] The T_1-relaxation times of individual MM peaks have yet to be reported for any field strength. Characterizing T_1-relaxation times for all individual MM peaks using a single inversion recovery technique is difficult due to eventual contributions from metabolites. More specifically, using a single-IR technique would have resulted in metabolites contaminating MM spectra at most TIs through an inversion series; consequently, making it challenging to estimate the T_1-relaxation times of most MM components with a sufficient range of longitudinal magnetization. Therefore, a double-IR (DIR) technique[18] was chosen for this study because it permitted flexibility for more consistent nulling of metabolites along with observing a range of magnetizations of MM peaks. The flexibility gained with a DIR approach comes from the freedom to change the TI for both of the inversion pulses. Moreover, when using adiabatic localization sequences such as semiLASER, a DIR technique[18] is more advantageous as this technique is shown to be insensitive to B_1^+ effects.[19]

Detection of 15 MM peaks between 0.8 and 4.2 ppm has been previously reported at 9.4 T by using DIR semiLASER with metabolite cycling (MC).[20] To measure an MM spectrum with minimal metabolite contribution an optimized combination of TIs (TI_1/TI_2 = 2360/625 ms) was required.[20] However, for the current study, more than a single TI_1/TI_2 combination was needed; consequently, several TI_1/TI_2 combinations that yielded a range from negative to positive longitudinal magnetizations of MMs and simultaneously suppressed the metabolite signal had to be determined.

Classically, characterizing T_1-relaxation times of metabolites requires either an inversion recovery series or a progressive saturation approach with a TR-series to induce a sweep from negative to positive longitudinal magnetizations of the resonances of interest. The goal of the current study was to calculate the T_1-relaxation times of 13 MM peaks between 0.8 and 4.0 ppm in the human brain. However, simultaneously minimizing metabolite contributions to detect MM peaks while also introducing a sufficiently broad range of

longitudinal magnetizations to determine T_1-relaxation times of the MM peaks required extensive optimization on combinations of TI_1/TI_2.

To determine suitable TI_1/TI_2 combinations, exhaustive Bloch simulations were performed for an optimized DIR technique. Ultimately, from all the Bloch simulation results, 11 TI_1/TI_2 combinations were chosen for this study. Hence, a novel DIR approach with 11 different combinations of two inversion delays is described to determine the T_1-relaxation times of individual MM resonances. Using this approach, T_1-relaxation times for all MM resonances between 0.8 and 4.0 ppm are reported for the first time in the human brain at 9.4 T in both gray matter (GM) and white matter (WM).

Furthermore, quantification using internal water as reference was performed for each MM peak reported in this work by using the knowledge gathered for the T_1-relaxation times of MM peaks and T_2-relaxation results from Murali-Manohar et al.[21]; thus, concentrations without correction for proton density are reported. This work is an extension of the preliminary results presented earlier as a conference abstract.[22]

2 | METHODS

2.1 | Study design

Eleven healthy volunteers (6 males, 5 females, age: 27.7 ± 2.3 years) were measured on a 9.4 T Siemens Magnetom whole-body MRI scanner (Siemens Healthineers, Erlangen, Germany) using a home-built 8Tx/16Rx coil.[23] The coil was driven in surface mode by a three-way splitter to drive power to the bottom three channel-elements as described in Giapitzakis et al.[20] A $2 \times 2 \times 2$ cm^3 voxel was placed spanning the longitudinal fissure of the occipital lobe for GM measurements, and a voxel was placed within the left occipital-parietal transition for WM measurements (Figure 1). All eleven volunteers completed participation for GM measurements; however, only nine volunteers (4 males, 5 females, age: 28.2 ± 2.2 years) finished the second acquisition for WM measurements. Studies were performed with approval of the local ethics committee, and volunteers provided written informed consent prior to measurements.

2.2 | Bloch Simulation

A range of longitudinal magnetization values for MM signals ranging from negative to positive M_Z are required to calculate T_1-relaxation times of MM resonances. To estimate individual MM peaks, the metabolite signals must be suppressed as much as possible. Hence, Bloch simulations were performed assuming a single proton spin to determine DIR schemes with suitable TIs TI_1 and TI_2. The magnetization vector (**M**(x, y, z)) was calculated for the actual inversion pulse shape implemented at the 9.4 T MRI scanner and the TIs (TI_1 and TI_2) as depicted in the DIR sequence scheme

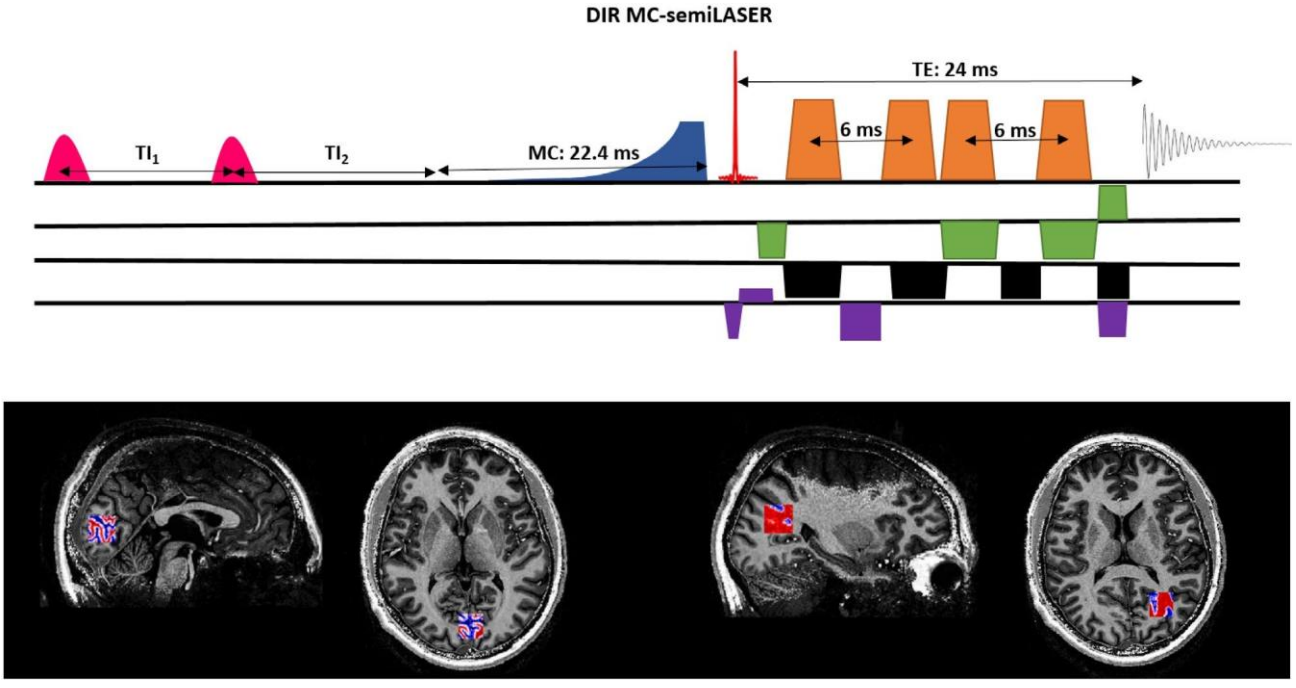

FIGURE 1 Top, MC semi-LASER sequence preceded by double inversion recovery scheme. TI_1 and TI_2 were changed as given in Table 1. Bottom, Voxels were placed into GM-rich (left) and WM-rich (right) regions to measure the inversion series. Red within the highlighted region represents WM; whereas, blue within the highlighted region represents GM. The average voxel content for GM-rich and WM-rich voxels were found to be GM/WM/CSF = 72 ± 2/22 ± 3/6 ± 4% and 35 ± 6/62 ± 7/3 ± 3%, respectively

in Figure 1; the inversion pulse profile is described in further detail by Giapitzakis et al.[19] The available longitudinal magnetization following a DIR block is given by the M_Z component, and the ratio of M_z to the initial magnetization (M_Z/M_0) was calculated for the inversion pulse profile[19] with a frequency offset range equal to the actual bandwidth of the pulse (−2000 to 2000 Hz, Supporting Information Figure S1, which is available online).[20]

Metabolite T_1-relaxation times were taken from previously acquired in vivo results at 9.4 T.[7] MM resonances were grouped as a single MM spectrum containing all resonances with a T_1-relaxation time measured in vivo at 7 T.[13] In addition to effects of T_1-relaxation, the transmit field strength B_1^+ and resonance offset effects were accounted for in the Bloch simulations. M_Z/M_0 for MM spectrum and metabolite peaks were systematically simulated in increments of 50 ms for the first pass sweeping a range from 800 to 2500 and from 10 to 800 ms for TI_1 and TI_2 respectively. Following the initial simulation, tighter increments were simulated for TI_1/TI_2 combinations to find optimal inversion delays. TI_1/TI_2 combinations were chosen such that spectra had minimal metabolite residual M_z while sweeping a range of M_z for MM signals as reported in the Results section. These resultant TI_1/TI_2 combinations were then further tested in vivo to ensure acquisition of clean MM spectra with minimal contribution from metabolites. For additional information, the script used for Bloch simulations has been provided in Supporting Information Material Annex A.

TABLE 1 Corresponding ratios of M_z to the initial magnetization (M_z/M_0) of MMs and a range for metabolite singlets (NAA(CH_3), tCr(CH_3), tCr(CH_2), and tCho) are reported from Bloch simulation results for each TI_1/TI_2 combination. Magnetization ratios are reported following simulation of the two inversion pulses and prior to any magnetization effects from localization pulses. Spin ensemble Bloch simulations used T_1-relaxation times from 9.4 T for metabolites[49] and from 7 T for the combined MM spectrum.[13] Ten of the TI_1/TI_2 combinations maintain minimal metabolite residuals; while one combination (1050/238 ms) was higher in metabolite contributions and used as an MM null point spectrum.

	M_Z/M_0	
TI_1/TI_2 [ms]	MMs	Metabolites
2360/625	0.5344	−0.0451 to 0.0200
2150/600	0.5079	−0.0020 to 0.0220
2000/575	0.4799	−0.0030 to 0.0225
1900/550	0.4501	0.0056 to 0.0362
1800/525	0.4191	0.0079 to 0.0521
1050/238	−0.0498	−0.0146 to 0.2195
1300/80	−0.5797	−0.3267 to 0.0080
1300/60	−0.6549	−0.3528 to −0.0033
1200/20	−0.7919	−0.3497 to 0.0290
1250/20	−0.8048	−0.3787 to 0.0011
1300/20	−0.8162	−0.4063 to −0.0261

2.3 | Data acquisition

High-resolution 2D FLASH images (in-plane resolution: 0.7 × 0.7 mm^2, slice thickness: 3.5 mm, 25 slices) were acquired in the sagittal and transversal planes to position spectroscopy voxels into GM- and WM-rich regions. Prior to spectroscopy measurements, localized FAST(EST)MAP[24] second-order shimming and power optimization[25,26] were performed to ensure that sufficient linewidths and adiabatic conditions would be fulfilled. The shim volume was set to be 150% of the volume of the voxel of interest.

A metabolite-cycled semi-LASER (MC semi-LASER) sequence[27] preceded by a novel DIR technique[20] (Figure 1) was used for spectroscopic acquisition (echo time [TE]/TR = 24/8000 ms; number of excitations [NEX] = 32) with 11 different combinations of TI_1 and TI_2 (Table 1). The TR used in all combinations of TI_1/TI_2 was given such that the following inversion pulse (TI_1) did not begin until 8000 ms after the position of the MC pulse (Figure 1). The transmit reference frequency was set at 2.4 ppm, and a 16-step phase cycling scheme was implemented. To avoid any influence of MC pulses on quantification based on internal water referencing, additional unsuppressed water reference signals (NEX: 16) were acquired with semi-LASER (TE: 24 ms) without MC.

MP2RAGE images[28] (resolution: 0.6 mm^3) were acquired with the same coil mentioned above by driving power to all eight channels. MP2RAGE data were used to calculate tissue volume fractions for each voxel to correct for the tissue composition dependence of T_1-relaxation as well as for MM quantification.

2.4 | Data preprocessing

The raw data were reconstructed with an in-house MATLAB (version 2016a, MathWorks, Natick, MA) tool and were processed with a similar method as described in Giapitzakis et al.[27]

Firstly, the FIDs were truncated to 250 ms so that data with better SNR were available for the following data preprocessing steps. Then they were frequency and phase-aligned in the time domain. This was followed by metabolite-cycling subtraction and the data were then averaged. After this, the data were zero-order phase and eddy current corrected using the phase information from the MC water signal. Signals from all 16 receive channels were then combined using an SVD method. The residual water in the spectra was removed using a HSVD method, and finally, the FIDs were truncated to 150 ms.

2.5 | Spectral fitting

Spectra were fitted with LCModel (v6.3-1L)[29] using simulated Voigt lines (CHSIMU) to fit 13 MM peaks. MM data were fit from 0.8 to 4.0 ppm. Initial fitting of MM spectra was performed using the subject-wise summed results for each TI_1/TI_2 combination. Metabolites predicted to contribute by Bloch simulations were initially included as characteristic spectral pattern in the basis sets, but only those metabolites which were fit in the initial trial (fitting subject-wise summed spectra) was kept in the final fit settings to avoid over-parameterization (Supporting Information Table S1). Complete basis vectors were not suitable for fitting metabolite residuals for the NAA(CH_3) singlet and tCr resonances at most TI_1/TI_2 combinations due to the minor contributions to spectra and different relaxation of different moieties of the same metabolites. Thus, the contributions from these metabolite signals were simulated using narrow Voigt line shapes. Following determination of metabolite contributions from summed spectra, optimized basis sets were defined for fitting of the individual data sets (Supporting Information Material Annex B).

The chosen combinations of simulated Voigt lines were used to represent residual singlets in the spectra: N-acetyl aspartate (NAA(CH_3) – 2.008 ppm), and creatine (tCr(CH_3) – 3.027 ppm and tCr(CH_2) – 3.925 ppm) across the inversion series to handle residual metabolite signals (Supporting Information Table S1). myo-Inositol (mI) was simulated in VesPA and was included in the basis set with negative a phase to fit spectra with TI_1/TI_2 = 2360/625, 2150/600, and 2000/575 ms (Supporting Information Table S2). Glycerophosphocholine (GPC), mI, glutamate (Glu), mI and aspartate moiety of NAA (NAA_{asp}) were simulated in VesPA,[30] and were included in the basis set only for TI_1/TI_2 combinations that had negative M_Z (i.e., inverted peaks with negative amplitudes). The chemical shifts of MM peaks were chosen from Murali-Manohar et al.[21] Fit settings files are given in Supporting Information Material Annex B.

To fit the MM null point data (TI_1/TI_2 = 1050/238 ms), a metabolite basis set including NAA(CH_3), tCr(CH_3), tCr(CH_2), GPC, glutamine (Gln), Glu, gamma-aminobutyricacid (GABA), glycine (Glycin), Aspartate (Asp), mI, NAA_{asp}, and taurine (Tau) were simulated using VeSPA.[30] Metabolite basis vectors were chosen to be given here because of the low MM signals and the strong metabolite contributions. The simulated basis set was created with a modified semiLASER protocol[31] with sequence parameters and pulses adjusted to match those in the present study.

Individual phases of metabolite residuals were adjusted in the LCModel basis sets as necessary depending on the magnetization achieved from a TI_1/TI_2 combination. Furthermore, the observed phase for DIR combinations was adjusted individually for GM- and WM-rich voxels to improve the accuracy of fits. DKNTMN parameter was set to 99 to keep the baseline stiff to allow for a more accurate fit of the MM data, and water scaling was performed to more accurately quantify the MM resonances.

LCModel water scaling was performed with respect to the downfield NAA amide resonance at 7.79 ppm (wsppm = 7.79, n1hmet = 1) rather than the LCModel default water scaling peak (tCr(CH_3) taking three protons contribution). In particular, there were no peaks in the upfield range of the spectrum that were not affected by the DIR scheme. Thus, the downfield NAA amide resonance was chosen as its amplitude was stable and was not affected by the DIR scheme. Water scaling with the stable NAA-NH resonance not only allowed shifting of the spectrum with respect to a known resonance frequency, but also was included to account for variations in coil loading across subjects. Automated LCModel phase correction was also constrained by the downfield NAA peak. This approach provided a stable reference for quality control of LCModel fitting results.

2.6 | Segmentation

MP2RAGE images were segmented into GM, WM, and CSF probability maps with SPM12.[32] 2D FLASH images used for voxel placement were co-registered to the MP2RAGE image using SPM12, which returned an affine transformation between the image spaces. The affine matrix relating the two images was used in a home-built Python (v3.7)[33,34] tool to determine the tissue fraction in spectroscopy voxels.

2.7 | T_1 calculation

Following spectral fitting in LCModel, all data were sorted by TI_1/TI_2 combination and fitted to the DIR signal equation[35]

$$S = \frac{a}{2}\left(1 - 2e^{-\frac{TI_2}{T_1}} + 2e^{-\frac{TI_1+TI_2}{T_1}}\right). \quad (1)$$

The optimization was done as a four-parameter bi-exponential model on the signal curve. In this model, TI_1 and TI_2 were both known parameters while a and T_1 were both unknown variables which were optimized on. Optimizing for T_1 from Equation (1) was performed in Python using the SciPy,[36] NumPy,[34] Matplotlib,[37] and Pandas[38] tool kits with a non-linear least squares, Levenberg-Marquardt algorithm; where a was assumed as a constant. Individual LCModel concentrations from all subjects were used in the curve fitting to calculate MM T_1-relaxation times.

T_1-relaxation has been shown to vary predominantly due to tissue type for water[28,39] in contrast to T_2-relaxation which also varies spatially depending on microscopic susceptibility differences.[40] Hence, an assumption to further estimate

the relaxation of theoretically pure GM and WM voxels, $T_{1,\,GM}^{\text{pure voxel}}$ and $T_{1,WM}^{\text{pure voxel}}$ respectively, was used. The following two linear equations were concurrently solved by assuming a linear relationship of relaxation time to the contribution of tissue type:

$$f_{GM\_vol} \cdot T_{1,GM}^{\text{pure voxel}} + f_{WM\_vol} \cdot T_{1,WM}^{\text{pure voxel}} = T_{1,GM}^{\text{rich voxel}} \cdot \left(1 - f_{CSF\_vol}\right) \quad (2)$$

$$f^{f}_{GM\_vol} \cdot T_{1,GM}^{\text{pure voxel}} + f^{f}_{WM\_vol} \cdot T_{1,WM}^{\text{pure voxel}} = T_{1,WM}^{\text{rich voxel}} \cdot \left(1 - f^{f}_{CSF\_vol}\right) \quad (3)$$

where f_{y_vol} represents the tissue fraction in measures from GM-rich voxels and $f^{f}_{y\_vol}$ represents the tissue fraction measures from WM-rich voxels. More specifically, by solving Equations (2) and (3) as a linear system, it allows us to then approximate the T_1-relaxation time of voxels with arbitrary ratios of GM and WM.

2.8 | Quantification of MM peaks

MM concentrations were quantified in protons mmol/kg by using spectra acquired with a TI_1/TI_2 combination of 2360/625 ms from all subjects in both GM- and WM-rich voxels. Spectra corresponding to TI_1/TI_2 combination of 2360/625 ms were chosen for quantification because it offered maximal MM signal retention as well as minimal metabolite residuals.

For internal water referencing, the concentrations resulting from LCModel fitting were corrected for tissue water fractions and relaxation times as follows[41]:

$$[M] = \frac{S_{MM} \times \left(f_{GM} \times R_{H20_{GM}} + f_{WM} \times R_{H20_{WM}} + f_{CSF} \times R_{H20_{CSF}}\right)}{S_{H20} \left(1 - f_{CSF}\right) \times R_{MM} \times \#H_{MM}} \times \frac{2}{1 + F_S} \times [H_2O]$$

where $f_y = \frac{f_{y\_vol} \times a_y}{f_{GM\_vol} \times a_{GM} + f_{WM\_vol} \times a_{WM} + f_{CSF\_vol} \times a_{CSF}}$.

Here y corresponds to either GM, WM, or CSF; f_{y_vol} is the fraction of the respective tissue type determined by segmentation; a_y are the relative densities of MR-visible water for the given tissue types (78%, 65%, 97% for GM, WM and CSF respectively[42]); these a_y remain uncorrected for the relative densities of GM and WM tissue (1.04 g/ml[43-45]) and were taken to be 1.0 g/ml. $\#H_{MM}$ is the number of protons that contribute to the signal of an MM peak, and was not accounted in this work. To arrive at proton mmol/kg concentrations, the concentration of water within a voxel, $[H_2O]$, was assumed to be that of pure water (55,510 mmol/kg). S_{MM} is the signal from an MM peak;

$$R_{H2O\_y} = \exp\left(-\frac{TE}{T2_{H2O_y}}\right)\left(1 - \exp\left(-\frac{TR}{T1_{H2O_y}}\right)\right)$$

is the relaxation correction factor for each water compartment y. $T1_{H2O_y}$ and $T2_{H2O_y}$ are the T_1- and T_2-relaxation times of water in the compartment y; in particular, the relaxation times of water in GM are $T1_{H20\_GM}$ = 2120 ms, $T2_{H20\_GM}$ = 37 ms; in WM are $T1_{H20\_WM}$ = 1400 ms, $T2_{H20\_WM}$ = 30 ms; and in CSF are $T1_{H20\_CSF}$ = 4800 ms, $T2_{H20\_CSF}$ = 181 ms at 9.4 T.[28]

$$R_{MM} = \left(1 - 2e^{\frac{TI_2}{T_1}} + 2e^{-\frac{TI_1 + TI_2}{T_1}}\right)\exp\left(-\frac{TE}{T2_{MM}}\right)\left(1 - \exp\left(-\frac{TR}{T_1}\right)\right)$$

is the relaxation correction term for macromolecules. $T2_{MM}$ were considered from Murali-Manohar et al[21] and $T1_{MM}$ determined from this work were taken. The denominator $1 - f_{CSF}$ was implemented for partial-volume correction arising from contributions of CSF to the voxel volume. The factor $\frac{2}{1+F_S}$ was introduced to correct for the multiplication of even numbered acquisitions with the scaling factor (F_s) from metabolite cycling.

3 | RESULTS

3.1 | Bloch simulations

Bloch simulation results for TI_1/TI_2 = 2000/575 and 2150/600 ms are shown in Supporting Information Figure S1. Simulations estimated similar metabolite nulling efficiency for the all chosen TIs retaining the MM signal at different observable magnetizations except for TI_1/TI_2 = 1050/238 ms. The MM null spectrum resulted in a maximum M_z/M_0 of 0.22 of metabolites and −0.05 of MM spectrum; this specific TI_1/TI_2 combination was optimized by confirming spectral quality in vivo from two healthy volunteers. Table 1 shows the chosen TIs and the corresponding M_z/M_0 for each MM spectrum. The M_z/M_0 for MM spectrum after DIR range block from −0.82 to 0.58 for the 11 chosen TI_1/TI_2 combinations.

3.2 | Inversion series of spectra and voxel content

Metabolite-nulled spectra were obtained with the 11 chosen TI_1/TI_2 combinations encompassing a range of magnetizations. Summed spectra from the inversion series for GM and WM MM spectra are displayed in Figure 2.

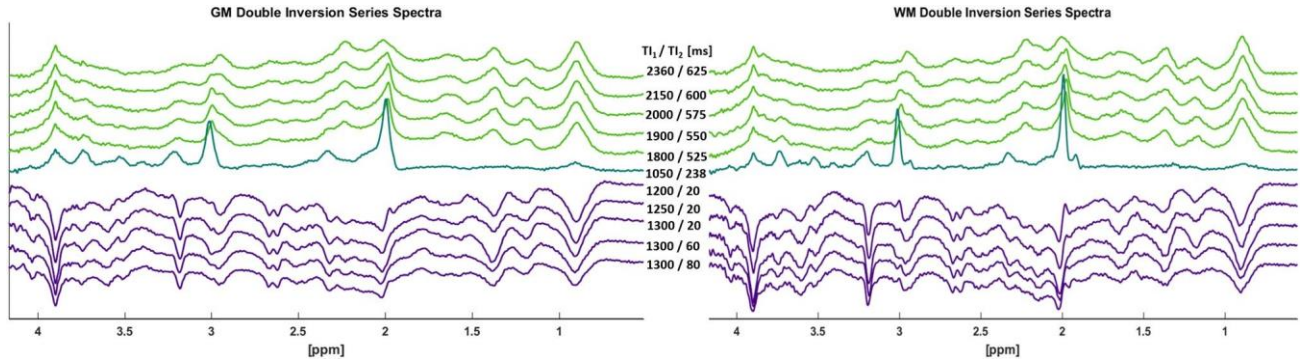

FIGURE 2 DIR series spectra from GM-rich (left) and WM-rich (right) voxels summed subject-wise. The same TI_1/TI_2 combinations were used to measure the T_1-relaxation times for GM- and WM-rich voxels. The DIR series shows a broad range of signal intensities measured for MM peaks while having simultaneously minimized metabolite peaks

The subject-wise summed spectra display good spectral quality with 13 resolved MM peaks across the 11 TI_1/TI_2 combinations. However, there was noticeable noise and sometimes slight lipid contamination in the individual, non-summed spectra. Nevertheless, 13 MM peaks could be observed in a majority of spectra in both GM-rich and WM-rich voxels. Therefore, all data sets were included in the analysis.

On average, the tissue content for GM-rich and WM-rich voxels were found to be GM/WM/CSF = 72 ± 2/22 ± 3/6 ± 4% and 35 ± 6/62 ± 7/3 ± 3% respectively. Indeed, residual metabolite signals were observed in several DIR spectra at various TI_1/TI_2 combinations, and the residual metabolite resonances corresponding to each TI_1/TI_2 combination is given in Supporting Information Table S1.

3.3 | Spectral fitting

Figure 3 shows fits and residues from LCModel for TI_1/TI_2 = 2360/625, 1300/20, and 1050/238 ms subject-wise summed spectra from GM-rich voxels. Fits corresponding to the same TI_1/TI_2 combinations from WM-rich voxels are given in Supporting Information Figure S2. Supporting Information Figure S3 shows fits for the remaining eight TI_1/TI_2 combinations for subject-wise summed spectra from GM-rich voxels. The tailored basis sets, for each TI_1/TI_2 combination and according to tissue type, fit the pre-processed data well. Furthermore, the residual for summed spectra fit from both GM-rich and WM-rich voxels showed minimized metabolite residuals. The fit residuals lacked structure in individual per subject fits (Figure 4). Metabolite residual fitting using basis vectors and fitted Voigt lines (Supporting Information Table S1) for residual peaks was sufficient for 10 TI_1/TI_2 combinations spectra; for the TI_1/TI_2 = 1050/238 ms combination yielding almost MM nulled spectra, a metabolite basis set was included, and it accurately accounted for metabolite contributions to spectra.

3.4 | T_1 relaxation times

Figure 5 and Supporting Information Figure S4 show all MM peak data fitted to Equation (1) to calculate the T_1-relaxation times of MM peaks in 3D signal plot diagrams. Black crosses represent individual data points from the TI_1/TI_2 series. The dashed, blue line represents the result from fitting the data to Equation (1) with a Levenberg-Marquardt algorithm. Resultant T_1-relaxation times of 13 MM peaks are reported for GM-rich and WM-rich voxels in Table 2 and shown in Figure 6. T_1-relaxation times of MM peaks range from 204 to 510 ms and 253 to 564 ms in GM-rich and WM-rich voxels respectively. $M_{3.62}$ had the longest T_1-relaxation time in both GM- and WM-rich voxels. The results from GM-rich and WM-rich voxels were used to solve for the T_1-relaxations of theoretically pure GM and WM voxels with a linear system of two equations and are reported in Table 2.

The goodness of fit for each MM T_1-relaxation time calculated was assessed by the coefficient of determination (R^2). The differences in T_1-relaxation times between GM- and WM-rich voxels were evaluated using Welch's t-test ($\alpha = 0.05$) for all MM peaks. Adjusted *P*-values were calculated using the Bonferroni correction $\frac{\alpha}{N^{tests}}$ to correct for multiple comparisons. Significant differences in T_1-relaxation times between GM- and WM-rich voxels are denoted in Figure 6 and Table 2 by an asterisk: $*P < .0038$. Results from Welch's t-test and *P* -values are reported in Supporting Information Table 3.

3.5 | Quantification of MM peaks

The TI_1/TI_2 combination of 2360/625 ms was chosen for quantification of MM peaks by means of internal water referencing. The unsuppressed water spectrum used for internal water referencing. The concentration results are thus reported in Figure 7 and Supporting Information Table S4. The concentration values were corrected for T_1-relaxation

times of MMs from this work and for T_2-relaxation times from Murali-Manohar et al,[21] with corrections as described in the Methods section. $M_{2.04}$ has the highest concentration in both GM- and WM-tissue types with 78.4 ± 10.7 and 76.6 ± 10.9 protons mmol/kg respectively. $M_{0.92}$ has similar concentrations in GM- and WM-voxels, 21.1 ± 3.3 and 21.0 ± 2.6 protons mmol/kg, respectively. Wilcoxon rank-sum tests ($\alpha = 0.05$) were performed to assess for differences in concentrations between tissue types for all MM peaks. After correcting for multiple comparisons, using a Bonferroni correction $\frac{\alpha}{N_{tests}} = 0.0038$, a significant difference for the concentration of $M_{3.75}$ ($P = .0009$) between GM and WM was found (Figure 7 and Supporting Information Table S4).

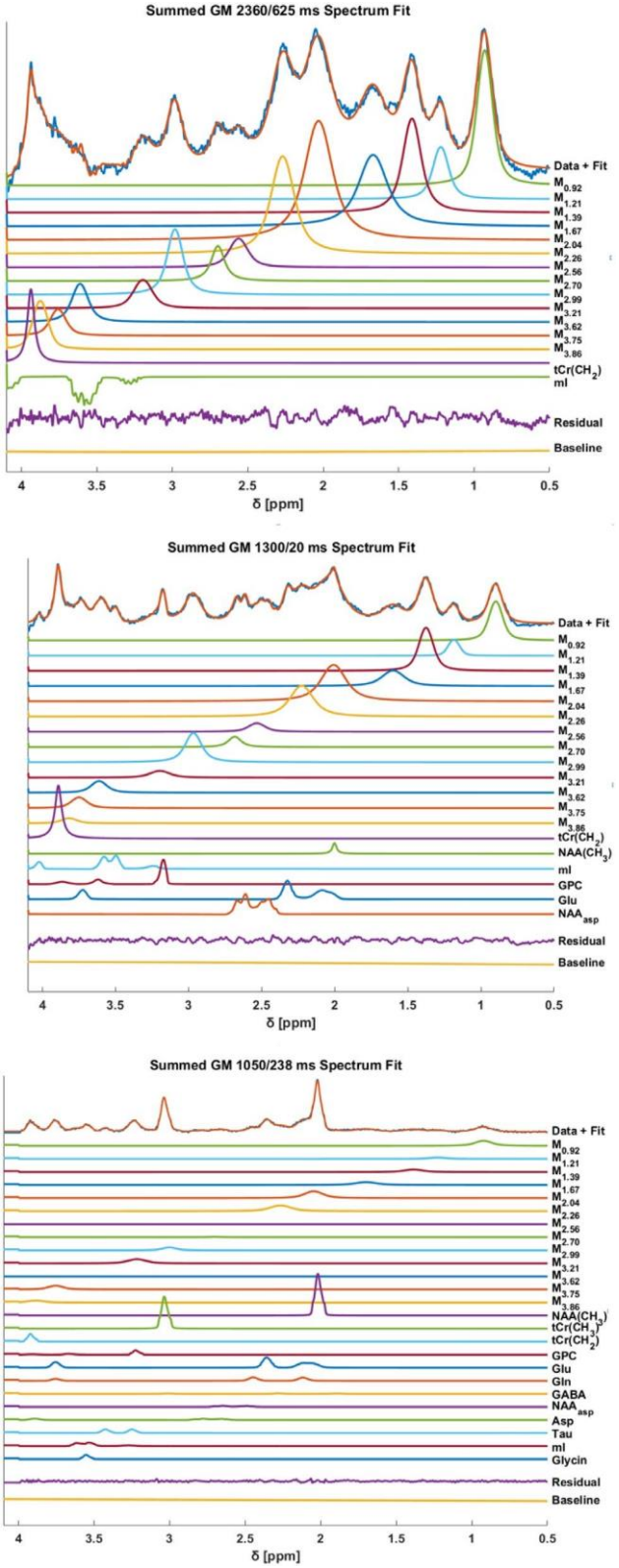

FIGURE 3 LCModel fits of summed spectra for 2360/625, 1200/20, and1050/238 ms for GM-rich voxel. Summed spectra were fitted using simulated Voigt lines for MM peaks. Metabolite contributions were accounted for using sharp Voigt lines to fit metabolite singlet residuals ($NAA(CH_3)$, $tCr(CH_2)$, and $tCr(CH_3)$) and basis vectors to fit other metabolite residuals. Fitting results from the subject-wise summed spectra were used to guide creation of basis sets for fitting of individual spectra. Corresponding subject-wise summed spectra for WM voxels are shown in Supporting Information Figure S2. The remaining inversion series fit for subject-wise summed spectra for GM voxels are displayed in Supporting Information Figure S3

4 | DISCUSSION

While it is possible to estimate T_1-relaxation time of the MM spectrum when using a single inversion recovery approach by simultaneously fitting metabolites, SIR techniques have been used to measure T_1-relaxation times of non-overlapping MM resonances as well as the whole MM spectrum. However, this could lead to misestimation of the MM peaks underlying metabolites and to ambiguities with respect to distinguishing metabolite and MM signals during spectral fitting.[46,47] Although there were also metabolite residuals present in the proposed DIR technique, this approach reduced metabolite residuals better at the expense of T_1-weighting. Bloch simulations were used to predict where metabolites would be contributing to the MM spectra. Supporting Information Table S1 shows in detail where metabolite vectors or singlets were included in the MM spectral fitting. Albeit, T_1-relaxation time estimates for individual MM peaks were possible.

Careful evaluation of Bloch simulation results helped determine valid sets of TI_1/TI_2 combinations. While there were many simulated TI_1/TI_2 combination results that maintained high M_Z of MMs, the contributions of metabolites in many of these cases led to heavy contamination in MM spectra or noisy MM spectra. While the chosen TI_1/TI_2 combinations provided good MM spectra there were still metabolite residuals that required fitting.

All 11 TI_1/TI_2 combinations were used in the calculation of T_1-relaxation times for MM peaks. The five TI_1/TI_2 combinations with negative M_z/M_0 covered a range from −0.82 to −0.58, and the five TI_1/TI_2 combinations with positive M_z/M_0 covered a range from 0.42 to 0.53 as can be seen from Table 1. Although the entire range of MMs M_Z/M_0 could not

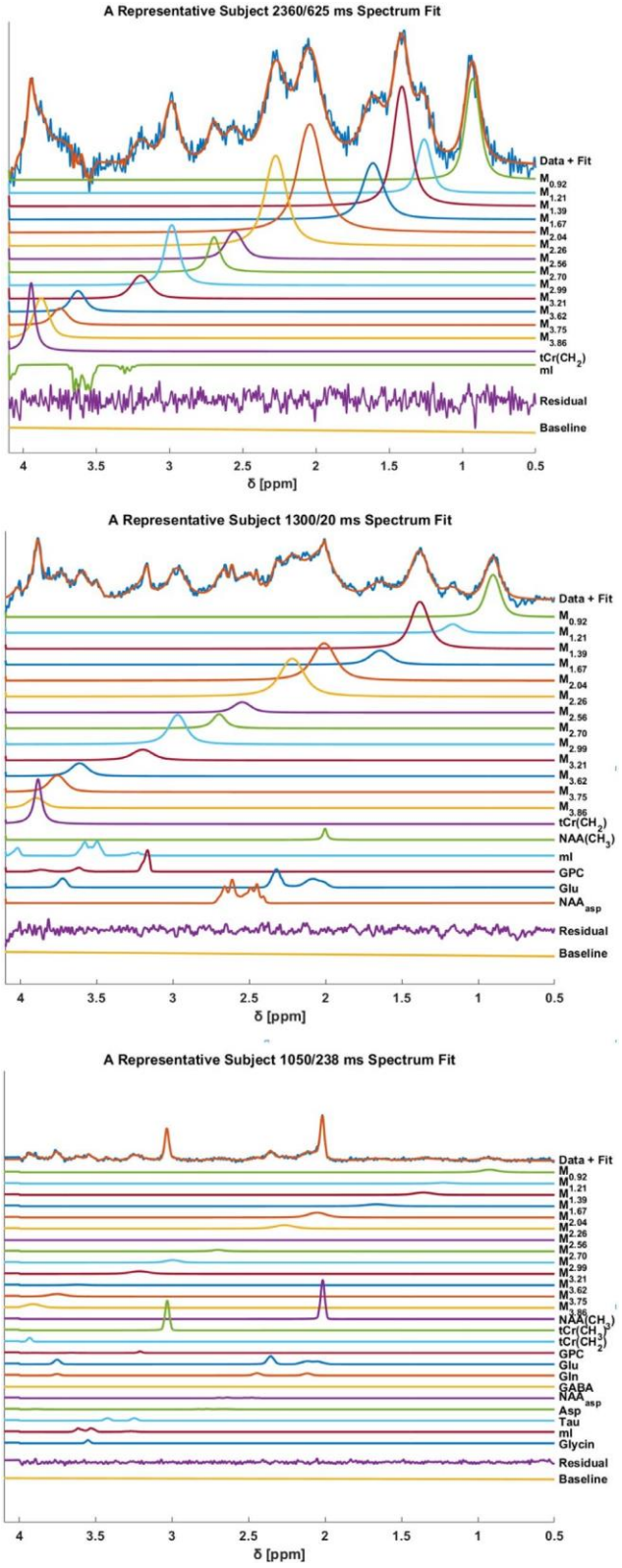

FIGURE 4 A representative subject fit for 2360/625, 1200/20, and1050/238 ms for GM-rich voxel. All three spectra are from the same subject. The peaks for metabolite residuals were modeled based on the summed spectra fit shown in Figure 3

be sampled due to the additional need to suppress metabolite signal, the chosen approach appears to be adequate for modeling the T_1-relaxation of MM peaks evidenced by the low standard deviation and R^2 of the curve fit for T_1-relaxation values which imply good confidence. Previous results[48] suggested a TR of 8000 ms to be the best bet for a comfortable scan duration and to stay within specific absorption rate limits.

It was expected that WM-rich voxels may be slightly noisier and lower in SNR. This arose from the fact that WM-rich voxels were typically further away from the transmit coil elements; thus, the achieved B_1 was lower for WM-rich voxels compared to GM-rich voxels. As was evidenced by the data in this study, WM data tended to be slightly noisier (Figure 2), but the metabolite residuals in MM spectra for GM-rich and WM-rich voxels were similar. However, MM peaks were T_1-weighted slightly differently in GM-rich and WM-rich voxels due to the differences in their T_1-relaxation times.

Reliable HSVD for residual metabolite suppression was not achievable for particular TI_1/TI_2 combinations potentially due to the broad linewidths encountered and low SNR. A detailed list of all the metabolite residuals present in the corresponding TI_1/TI_2 combination spectra that were fitted is given in Supporting Information Table S1. $M_{4.03}$ and $M_{4.20}$ were excluded from analysis due to water contamination in the spectra in multiple TI_1/TI_2 combinations.

NAA_{asp}, mI, Glu, and GPC were predicted to be metabolite residuals in the negative M_Z MM spectra due to their T_1-relaxation times,[49] and were furthermore visible when fitting spectra. To correct for the contribution these metabolites, they were simulated and added to all basis sets corresponding to TI_1/TI_2 combinations resulting in negative magnetization.

From Supporting Information Figure S4, it can be seen that the negative M_z points had larger amounts of signal for $M_{2.99}$, $M_{3.62}$, and $M_{3.75}$ which skewed the signal fit resulting in a longer calculated T_1-relaxation time. It could be that lower weight metabolites contributed to the resonances within these peaks, which led to the increased estimation of the T_1-relaxation time. Attempts to account for metabolite resonances at these peaks were performed by including metabolite basis vectors; however, it was not possible to reliably fit all potential contributions from lower weight metabolites with this scheme. The increased T_1-relaxation times for these peaks at 3T have been reported by Hoefemann et al[17]; in their study the observed T_1-relaxation times reached the "predefined borders of … 400 ms for T_1."

T_1-relaxation times of MM peaks in GM- and WM-rich voxels range from 204 to 510 ms and from 253 to 564 ms, respectively. For pure GM and WM voxels, T_1-relaxation times are between 189 and 478 ms, and between 220 and 612 ms respectively. Indeed, the linear relationship used to calculate T_1-relaxation times likely simplifies the complex nature of the MM spectrum. However, it could be useful in modelling MM spectra voxel-wise where T_1-weighting of MMs is present such as FID-MRSI.[50]

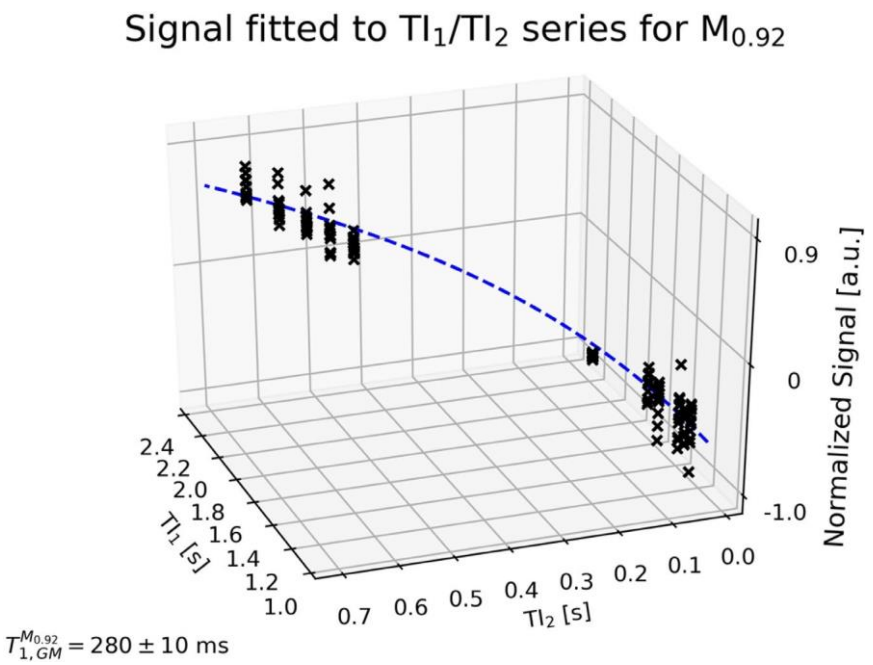

FIGURE 5 A signal scatter plot and fitted solution (blue dashed line) from the inversion series for $M_{0.92}$ fitted by Equation (1). Black crosses represent data points from the 11 volunteers acquired in GM-rich voxels, and the blue line is the fitted solution to Equation (1). T_1-relaxation calculation plots for the other MM peaks are reported in Supporting Information Figure S4. Points were excluded when the CRLB was equal to 999 because these points were not fitted in LCModel. In the present fit of $M_{0.92}$, no points are excluded

T_1 Relaxation times of Macromolecules

	GM-rich		WM-rich		Pure-GM	Pure-WM
MM	**T_1 [ms]**	**R^2**	**T_1 [ms]**	**R^2**	**T_1 [ms]**	**T_1 [ms]**
$M_{0.92}$	280 ± 10	0.959	284 ± 10	0.966	278 ± 26	288 ± 23
$M_{1.21}$	273 ± 27	0.752	280 ± 28	0.782	269 ± 71	286 ± 62
$M_{1.39}$*	326 ± 21	0.867	270 ± 24	0.828	358 ± 57	220 ± 50
$M_{1.67}$*	231 ±13	0.903	253 ± 17	0.894	218 ± 37	273 ± 32
M* 2.04	279 ± 8	0.971	319 ± 9	0.974	256 ± 22	355 ± 19
M*	281 ± 7	0.977	313 ± 9	0.972	263 ± 20	342 ± 17
$M_{2.56}$	309 ± 20	0.866	327 ± 18	0.915	299 ± 50	343 ± 44
M*	306 ± 19	0.879	383 ± 22	0.902	262 ± 52	452 ± 45
$M_{2.99}$*	463 ± 15	0.953	518 ± 15	0.966	431 ± 39	567 ± 34
M*	204 ± 20	0.785	379 ± 29	0.836	103 ± 59	535 ± 51
$M_{3.62}$*	510 ± 30	0.846	564 ± 35	0.853	479 ± 82	612 ± 71
M*	280 ± 24	0.805	434 ± 25	0.887	191 ± 63	571 ± 55
$M_{3.86}$	280 ± 27	0.764	307 ± 22	0.871	264 ± 66	331 ± 58

TABLE 2 T_1-relaxation times of 13 MM peaks in both GM-rich and WM-rich voxels at 9.4T are presented in the table with accompanying R^2 values for the fit of the data to Equation (1). Furthermore, T_1-relaxation times of pure GM and WM voxels for these peaks are also reported as solved by Equations (3) and (4). MM peaks that have significant differences between GM- and WM-rich voxels are indicated by an asterisk *$P < .0038$. Full statistical results are in Supporting Information Table S3

The broad range of MM peak T_1-relaxation times suggests that approximating the T_1-relaxation time of the MM spectrum as single value may not be ideal for quantifying MM peaks with high accuracy. Furthermore, when a measured IR MM spectrum is included to fit metabolites, T_1-weighting within the MM spectrum could lead to misestimates of metabolite concentrations. For example, the MM spectrum corresponding to TI_1/TI_2 = 2360/625 ms was used in fitting metabolites in previous works.[21,27] However, as seen from Table 3, T_1-weighting for MM peaks following this DIR scheme range from 42% to 87% in a GM-rich voxel and 35% to 83% in a WM-rich voxel. Hence, quantifying metabolites with this particular MM spectrum could lead to over- or under-fitting of metabolites amplitudes depending on the T_1-weighting of different MM peaks.

While comparing differences between GM- and WM-rich T_1-relaxation times, significant differences ($P < .0038$) between tissue types were found for all MM peaks except $M_{0.92}$, $M_{1.21}$, $M_{1.67}$, $M_{2.56}$, and $M_{3.86}$ as shown in Figure 6 and Supporting Information Table S3. Based on T_1-relaxation differences between GM and WM, tissue type specific MM models could be more appropriate than using averaged MM spectra to fit MM signals especially in metabolite spectra. The relaxation times of MM peaks do not follow a clear trend of increased T_1-relaxation time of resonances as field strength increase.[51] Behar et al[52] measured the T_1-relaxation

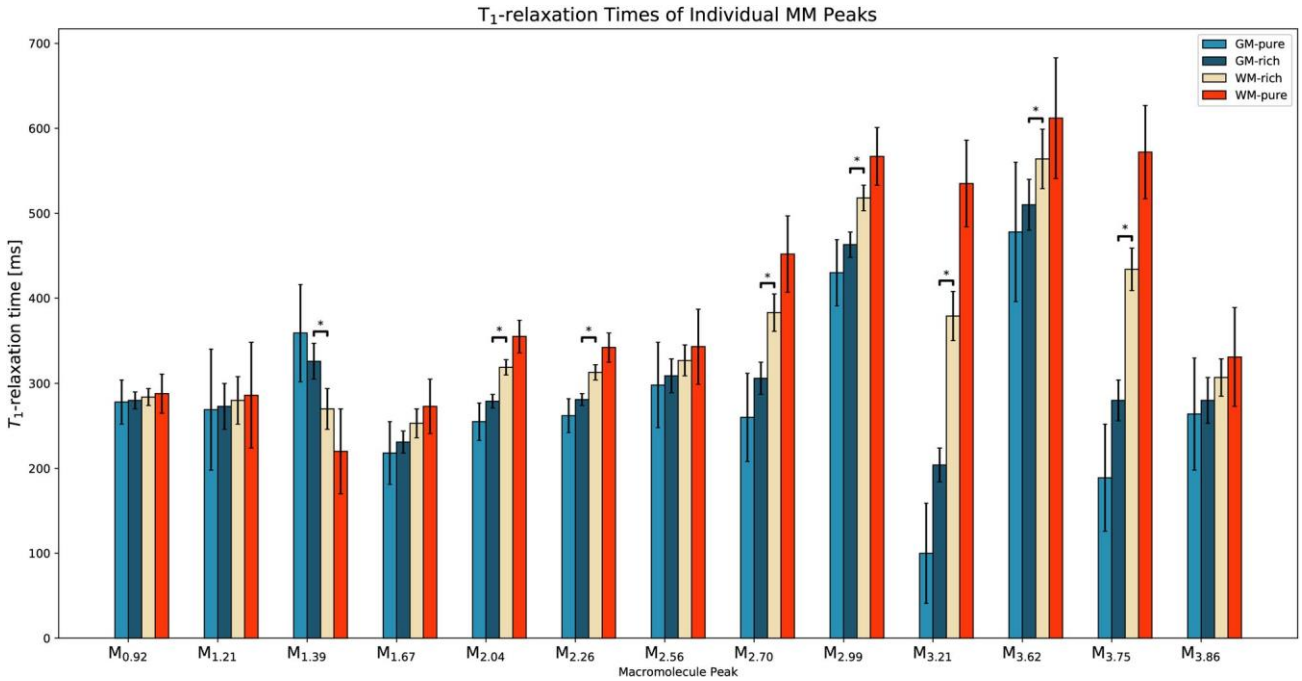

FIGURE 6 T_1-relaxation times for 13 MM peaks are reported. Results are shown for GM- and WM-rich voxels as well as for GM- and WM-pure voxels. The T_1-relaxation estimates for pure voxels were extrapolated by means of Equations (2) and (3). Additionally, these values are reported in Table 2. MM peaks that have significant differences following Welch's t-test and Bonferroni correction between GM- and WM-rich voxels are indicated by an asterisk $*P < .0038$. Full statistical results are in Supporting Information Table S3

TABLE 3 Calculated T_1-weighting in percent of MM peaks following DIR scheme (TI_1/TI_2 = 2360/625 ms; TR = 10 s) using T_1-relaxation times from measured GM- and WM-rich voxels in this work

T_1-weighting [%]													
	$M_{0.92}$	**$M_{1.21}$**	**$M_{1.39}$**	**$M_{1.67}$**	**$M_{2.04}$**	**$M_{2.26}$**	**$M_{2.56}$**	**$M_{2.70}$**	**$M_{2.99}$**	**$M_{3.21}$**	**$M_{3.62}$**	**$M_{3.75}$**	**$M_{3.86}$**
GM	78	80	71	87	79	78	74	74	48	91	42	79	79
WM	78	78	80	83	72	73	70	61	41	62	35	53	74

of the $M_{0.93}$ peak as 250 ms at 4.0T, which is slightly lower compared to the T_1-relaxation time measured in this work at 9.4 T confirming the field strength trend for this non-overlapping MM peak. However, recent work at 3 T found the T_1-relaxation time of $M_{0.92}$ to be about 290 ms.[17]

For the first time, concentrations of 13 MM peaks are reported (Supporting Information Table S4) for both GM- and WM-rich voxels after correcting for T_1- and T_2-relaxation times. Previous works[5,20,53,54] have reported concentrations for some or all peaks without correcting for T_1- or T_2-relaxation times. Inversion recovery preceding the localization scheme will lead to strong T_1- weighting of the MM spectrum, and not correcting for the relaxation times will result in discrepancies in concentrations across sites while using different inversion recovery techniques. Due to severe overlap of MM peaks, the number of protons contributing to each peak is not easily accountable; hence, the concentration values were not corrected for the number of contributing protons. The concentration of $M_{0.92}$ agrees with the values reported by Hofmann et al[55] and Snoussi et al,[53] and are slightly less than the recent results from Landheer et al.[54] However, concentrations for other MM peaks or groups of MM peaks vary among literature.[20,53-55] The results from Landheer et al[54] appear that they could be in agreement with the current work at 9.4 T; however, the uncorrected T_1-weighting could be a cause of discrepancy between results.

Statistical tests highlighted a significant difference for elevated concentration of $M_{3.75}$ ($P = .0009$) in WM. Furthermore, the results suggest that there could be slight variation between tissue types for $M_{1.39}$, $M_{2.99}$, and $M_{3.21}$; whereas the differences between GM and WM tissue signal for $M_{2.26}$ have been reported in MRSI results.[56] Figure 7 and Supporting Information Table S4 suggest that there are trends toward elevated concentrations of $M_{1.39}$ in GM and for $M_{2.99}$, and $M_{3.21}$ in WM; however, this study was not able to claim with certainty that these concentrations vary in a significant manner. Further work focusing on specific MM peaks is necessary to assess tissue concentration differences appropriately.

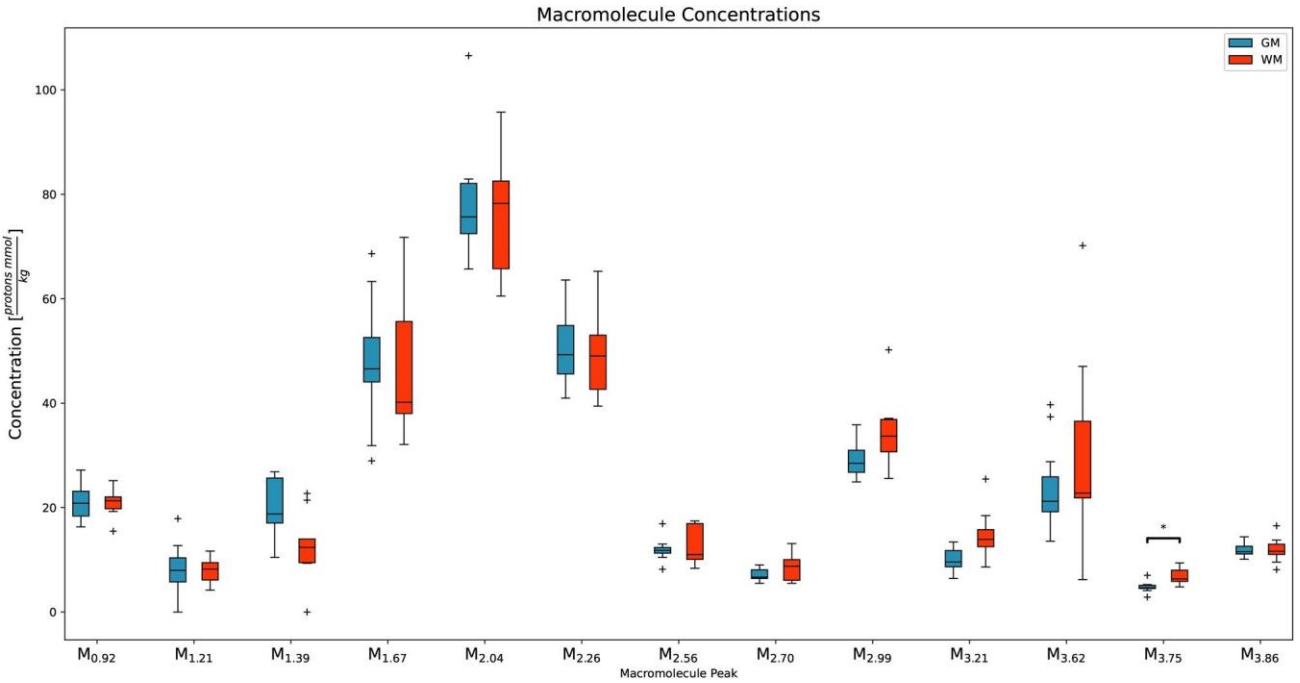

FIGURE 7 MM concentrations are reported in protons mmol/kg for each MM peak. Black crosses represent data points that were not within the 95% confidence interval (assuming a Gaussian distribution). Mann-Whitney U-tests ($\alpha = 0.05$), with Bonferroni adjustment $\frac{\alpha}{N_{tests}} = 0.0038$ for multiple comparisons were performed to test for statistical significance in differences between GM- and WM-rich voxels. Supporting Information Table S4 lists the results from Mann-Whitney U-tests

Finally, it has been previously reported by Giapitzakis et al[57] that significant differences arise in some of the metabolite concentrations while using MM spectrum from different brain region to account for MM contribution underlying the metabolite spectrum. Based on the differences in T_1-relaxation times of MM peaks in GM- and WM-rich voxels reported in this work, we believe that it could be beneficial to account for underlying MM spectra with tissue content considered in order to maintain quantitative accuracy in spectral fitting of metabolites.

5 | CONCLUSIONS

In this work, we report a novel DIR technique to measure T_1-relaxation times of individual macromolecular peaks. The study here is performed at 9.4 T; however, this technique is extendible to all field strengths. T_1-relaxation times for 13 MM resonances in vivo at 9.4 T are reported for the first time. The differences in the T_1-relaxation times between the MM resonances suggest that T_1-weighting from inversion pulses and short TRs should be considered while using experimentally acquired MM spectra in fitting metabolite spectra. Alternatively, simulation models which account for relaxation effects of MMs could also provide a solution for estimating MM contributions to metabolite spectra where overlapping peaks are difficult to distinguish. This will allow us to produce more accurate quantitative results by correcting for the influence of MMs in short TE spectra. Furthermore, concentrations of 13 MM peaks after correcting for both T_1- and T_2-weighting are reported.

ACKNOWLEDGMENTS

The authors thank Wolfgang Bogner, Cristina Cudalbu, Małgorzata Marjańska, Jim Murdoch, Kye Stachowski, and David Edmondson for the constructive discussions and valuable suggestions to this work. Open access funding enabled and organized by Projekt DEAL.

ORCID

Saipavitra Murali-Manohar https://orcid.org/0000-0002-4978-0736
Andrew Martin Wright https://orcid.org/0000-0002-7182-7270
Tamas Borbath https://orcid.org/0000-0003-3679-2380
Nikolai I. Avdievich https://orcid.org/0000-0001-7608-0869

REFERENCES

1. Behar KL, Rothman DL, Spencer DD, Petroff OAC. Analysis of macromolecule resonances in 1H NMR spectra of human brain. *Magn Reson Med*. 1994;32:294-302.
2. Marjańska M, Deelchand DK, Hodges JS, et al. Altered macromolecular pattern and content in the aging human brain. *NMR Biomed*. 2018;31:e3865.
3. Louis MS, Alosco M, Rowland B, et al. Using machine learning techniques for identification of chronic traumatic encephalopathy related spectroscopic biomarkers. In *IEEE Applied Imagery Pattern Recognition Workshop (AIPR)*, Washington, DC, 2017:1-5. https://doi.org/10.1109/AIPR.2017.8457949.
4. Mader I, Karitzky J, Klose U, et al. Proton MRS in Kennedy disease: Absolute metabolite and macromolecular concentrations. *J Magn Reson Imaging*. 2002;16:160-167.

5. Mader I, Seeger U, Weissert R, et al. Proton MR spectroscopy with metabolite-nulling reveals elevated macromolecules in acute multiple sclerosis. *Brain*. 2001;124:953-961.
6. Mlynárik V, Cudalbu C, Clément V, Marino D, Radovanovic I, Gruetter R. In vivo metabolic profiling of glioma-initiating cells using proton magnetic resonance spectroscopy at 14.1 Tesla. *NMR Biomed*. 2012;25:506-513.
7. Deelchand DK, Van De Moortele PF, Adriany G. et al. In vivo 1H NMR spectroscopy of the human brain at 9.4 T: Initial results. *J Magn Reson*. 2010;206:74-80.
8. Soher BJ, Young K, Maudsley AA. Representation of strong baseline contributions in 1H MR spectra. *Magn Reson Med*. 2001;45:966-972.
9. Cudalbu C, Mlynárik V, Gruetter R. Handling macromolecule signals in the quantification of the neurochemical profile. *J Alzheimer's Dis*. 2012;31(SUPPL. 3):S101-S115.
10. Cudalbu C, Mlynrik V, Xin L, Gruetter R. Quantification of in vivo short echo-time proton magnetic resonance spectra at 14.1 T using two different approaches of modelling the macromolecule spectrum. *Meas Sci Technol*. 2009;20:104034-104040.
11. Lopez-Kolkovsky AL, Mériaux S, Boumezbeur F. Metabolite and macromolecule T 1 and T 2 relaxation times in the rat brain in vivo at 17.2T. *Magn Reson Med*. 2016;75:503-514.
12. Cudalbu C, Mlynárik V, Xin L, Gruetter R. Comparison of T1 relaxation times of the neurochemical profile in rat brain at 9.4 Tesla and 14.1 Tesla. *Magn Reson Med*. 2009;62:862-867.
13. Xin L, Schaller B, Mlynarik V, Lu H, Gruetter R. Proton T1 relaxation times of metabolites in human occipital white and gray matter at 7 T. *Magn Reson Med*. 2013;69:931-936.
14. Pfeuffer J, Tkac I, Provencher SW, Gruetter R. Towards an in viva neurochemical profile: Quantification of 18 metabolites in 'H NMR spectra of rat brain at TE = 2 ms. *J Magn Reson*. 1999;120:55455.
15. De Graaf RA, Brown PB, McIntyre S, Nixon TW, Behar KL, Rothman DL. High magnetic field water and metabolite proton T1 and T 2 relaxation in rat brain in vivo. *Magn Reson Med*. 2006;56:386-394.
16. Kreis R, Slotboom J, Hofmann L, Boesch C. Integrated data acquisition and processing to determine metabolite contents, relaxation times, and macromolecule baseline in single examinations of individual subjects. *Magn Reson Med*. 2005;54:761-768.
17. Hoefemann M, Bolliger CS, Chong DGQ, Veen JW, Kreis R. Parameterization of metabolite and macromolecule contributions in interrelated MR spectra of human brain using multidimensional modeling. *NMR Biomed*. 2020;33:e4328–e4345.
18. Hwang J-H, Graham GD, Behar KL, Alger JR, Prichard JW, Rothman DL. Short echo time proton magnetic resonance spectroscopic imaging of macromolecule and metabolite signal intensities in the human brain. *Magn Reson Med*. 1996;35:633-639.
19. de Graaf RA, Brown PB, McIntyre S, Nixon TW, Behar KL, Rothman DL. High magnetic field water and metabolite proton T1 and T2 relaxation in rat brain in vivo. *Magn Reson Med*. 2006;56:386-394.
20. Giapitzakis I, Avdievich N, Henning A. Characterization of macromolecular baseline of human brain using metabolite cycled semi-LASER at 9.4T. *Magn Reson Med*. 2018;80:462-473.
21. Murali-Manohar S, Borbath T, Wright AM, Soher B, Mekle R, Henning A. T2 relaxation times of macromolecules and metabolites in the human brain at 9.4 T. *Magn Reson Med*. 2020;84:542-558.
22. Murali-Manohar S, Wright A, Borbath T, Henning A. Longitudinal Relaxation times of Macromolecular Resonances at 9.4 T in Human Brain. In: 27th Annu Meet Exhib Int Soc Magn Reson Med (ISMRM 2019). Montréal, QC, Canada; 2019.
23. Avdievich NI, Giapitzakis I-A, Pfrommer A, Henning A. Decoupling of a tight-fit transceiver phased array for human brain imaging at 9.4T: Loop overlapping rediscovered. *Magn Reson Med*. 2018;79:1200-1211.
24. Gruetter R, Tkáč I. Field mapping without reference scan using asymmetric echo-planar techniques. *Magn Reson Med*. 2000;43:319-323.
25. Versluis MJ, Kan HE, Van Buchem MA, Webb AG. Improved signal to noise in proton spectroscopy of the human calf muscle at 7 T using localized B1 calibration. *Magn Reson Med*. 2010;63:207-211.
26. Mekle R, Mlynárik V, Gambarota G, Hergt M, Krueger G, Gruetter R. MR spectroscopy of the human brain with enhanced signal intensity at ultrashort echo times on a clinical platform at 3T and 7T. *Magn Reson Med*. 2009;61:1279-1285.
27. Giapitzakis I-A, Shao T, Avdievich N, Mekle R, Kreis R, Henning A. Metabolite-cycled STEAM and semi-LASER localization for MR spectroscopy of the human brain at 9.4T. *Magn Reson Med*. 2018;79:1841-1850.
28. Hagberg GE, Bause J, Ethofer T, et al. Whole brain MP2RAGE-based mapping of the longitudinal relaxation time at 9.4T. *NeuroImage*. 2017;144:203-216.
29. Provencher SW. Automatic quantitation of localized in vivo 1H spectra with LCModel. *NMR Biomed*. 2001;14:260-264.
30. Soher B, Semanchuk P, Todd D, Steinberg J, Young K. VeSPA: Integrated applications for RF pulse design, spectral simulation and MRS data analysis. In *Proceedings of the ISMRM 19th Annual Meeting & Exhibition*, Montréal, Québec, Canada, 2011. p. 1410.
31. Soher B. *Versatile Simulation Pulses and Analysis. User Code Contributions – semi-LASER*. https://scion.duhs.duke.edu/vespa/contrib/wiki/1f03e57e-1d27-4d36-8b31-db9e5e2f73e82013
32. Ashburner J, Barnes G, Chen C, et al. *SPM12 Manual*. London, UK: Wellcome Trust Centre for Neuroimaging; 2014.
33. van Rossum G. *Python Tutorial, Technical Report CS-R9526*. Amsterdam: Centrum voor wiskunde en informatica (CWI); 1995.
34. Oliphant T. *A Guide to NumPy. Vol. 1*. Trelgol Publishing USA; 2006.
35. Redpath TW, Smith FW. Technical note: Use of a double inversion recovery pulse sequence to image selectively grey or white brain matter. *Br J Radiol*. 1994;67:1258-1263.
36. Jones E, Oliphant E, Peterson P, Al E. *SciPy: Open Source Scientific Tools for Python*. 2001.
37. Hunter JD. Matplotlib: A 2D graphics environment. *Comput Sci Eng*. 2007;9:90-95.
38. McKinney W. *pandas: A Foundational Python Library for Data Analysis and Statistics*. 2010.
39. Ethofer T, Mader I, Seeger U, et al. Comparison of longitudinal metabolite relaxation times in different regions of the human brain at 1.5 and 3 Tesla. *Magn Reson Med*. 2003;50:1296-1301.
40. Hasan KM, Walimuni IS, Kramer LA, Narayana PA. Human brain iron mapping using atlas-based T 2 relaxometry. *Magn Reson Med*. 2012;67:731-739.
41. Gasparovic C, Song T, Devier D, et al. Use of tissue water as a concentration reference for proton spectroscopic imaging. *Magn Reson Med*. 2006;55:1219-1226.
42. Ernst T, Kreis R, Ross B. Absolute quantitation of water and metabolites in the human brain. I. Compartments and water. *J Magn Reson Ser B*. 1993;102:1-8.

43. Rieth KG, Fujiwara K, Di Chiro G, et al. Serial measurements of CT attenuation and specific gravity in experimental cerebral edema. *Radiology*. 1980;135:343-348.
44. Torack RM, Alcala H, Gado M, Burton R. Correlative assay of computerized cranial tomography (CCT), water content and specific gravity in normal and pathological postmortem brain. *J Neuropathol Exp Neurol*. 1976;35:385-392.
45. Brooks R, Di Chiro G, Keller M. Explanation of cerebral white-gray contrast in computed tomography. *J Comput Assist Tomogr*. 1980;4:489-491.
46. Nassirpour S, Chang P, Henning A. High resolution maps of individual macromolecule components in the human brain at 9.4 T. In: The ISMRM 25th Annual Meeting and Exhibition. Honolulu, HI, USA; 2017. p. 619.
47. Heckova E, Považan M, Strasser B, et al. Effects of different macromolecular models on reproducibility of FID-MRSI at 7T. *Magn Reson Med*. 2020;83:12-21.
48. Murali-Manohar S, Wright A, Henning A. Challenges in estimating T1 Relaxation Times of Macromolecules in the Human Brain at 9.4 T. In: MRS Workshop 2018 Metabolic Imaging. Utrecht, Netherlands; 2018.
49. Wright A, Murali-Manohar S, Borbath T, Henning A. Longitudinal relaxation times of metabolites in vivo at 9.4 T. In: 27th Annu Meet Exhib Int Soc Magn Reson Med (ISMRM 2019).Montréal, QC, Canada; 2019. p. 0514.
50. Nassirpour S, Chang P, Henning A. High and ultra-high resolution metabolite mapping of the human brain using 1H FID MRSI at 9.4T. *NeuroImage*. 2016;(December):211-221.
51. Cudalbu C, Behar KL, Bhattacharyya PK, et al. Contribution of macromolecules to brain 1H MR spectra: Experts' consensus recommendations. *NMR Biomed.* 2020. https://doi.org/10.1002/nbm.4393.
52. Behar KL, Rothman DL, Spencer DD, Petroff OAC. Analysis of macromolecule resonances in 1H NMR spectra of human brain preparation of brain tissue. *Isis*. 1994;32:294-302.
53. Snoussi K, Gillen JS, Horska A, et al. Comparison of brain gray and white matter macromolecule resonances at 3 and 7 Tesla. *Magn Reson Med*. 2015;74:607-613.
54. Landheer K, Gajdošík M, Treacy M, Juchem C. Concentration and effective T2 relaxation times of macromolecules at 3T. *Magn Reson Med*. 2020.84:2327–2337.
55. Hofmann L, Slotboom J, Boesch C, Kreis R. Characterization of the macromolecule baseline in localized1H-MR spectra of human brain. *Magn Reson Med*. 2001;46:855-863.
56. Považan M, Strasser B, Hangel G, et al. Simultaneous mapping of metabolites and individual macromolecular components via ultra-short acquisition delay 1H MRSI in the brain at 7T. *Magn Reson Med*. 2017;79:1231-1240.
57. Giapitzakis IA, Borbath T, Murali-Manohar S, Avdievich N, Henning A. Investigation of the influence of macromolecules and spline baseline in the fitting model of human brain spectra at 9.4T. *Magn Reson Med*. 2019;81:746-758.

SUPPORTING INFORMATION

Additional Supporting Information may be found online in the Supporting Information section.

FIGURE S1 Bloch Simulation results for an inversion pulse profile[20] (pulse duration: 15 ms) after a DIR scheme with TIs (A) TI_1/TI_2 = 2000/575 ms and (B) TI_1/TI_2 = 2150/600. The resulting inversion bandwidth is represented by the frequency axis (x-axis); while the y-axis depicts the resulting M_Z/M_0 of MMs and metabolites at the end of the DIR sequence block. M_Z/M_0 of MM spectrum after DIR block are 0.48 and 0.51 in (A) and (B) respectively with almost nulled metabolites

FIGURE S2 Fit of WM subject-wise summed spectra of TI_1/TI_2 combinations 2360/625, 1300/20 and 1050/238 ms

FIGURE S3 Fits of subject-wise summed GM spectra of TI_1/TI_2 combinations 2150/600, 2000/575, 1900/550, 1800/525, 1300/60, 1300/80, 1200/20, and 1250/20 ms

FIGURE S4 Surface Curve fitted to TI_1/TI_2 series for $M_{1.21}$, $M_{1.39}$, $M_{1.67}$, $M_{2.04}$, $M_{2.26}$, $M_{2.56}$, $M_{2.70}$, $M_{2.99}$, $M_{3.21}$, $M_{3.62}$, $M_{3.75}$, and $M_{3.96}$ from GM-rich voxel to calculate T_1-relaxation times. For better visualization of the 3D plots a cine is provided as Supporting Information Video S1.

TABLE S1 Residual peaks present corresponding to each TI_1/TI_2 are given in the table. $tCr(CH_2)$, $tCr(CH_3)$, and $NAA(CH_3)$ residual peaks were added as singlets using simulated Voigt lines in LCModel for fitting spectra. NAA_{asp}, mI, GPC, and Glu were added to handle the residuals in negative M_z spectra. For TI_1/TI_2 = 1050/238 ms, a complete basis set was provided which was simulated for a semi-LASER sequence using VeSPA; specifically without singlets used in the basis set for any metabolite residuals

TABLE S2 Bloch simulation considering DIR scheme for mI has a negative contribution in TI_1/TI_2 = 2360/625, 2150/575, 2000/550 ms spectra (considering T_1-relaxation times from Wright et al.[46])

TABLE S3 Differences in T_1-relaxation times between GM- and WM-rich tissue types were analyzed using Welch's t-test with Bonferron i adjusted p-values to account for multiple comparisons $\frac{\alpha}{n} = 0.0038$. Significant differences are denoted by an aste^{n}risk, and p-values are given for all analyses

TABLE S4 Concentrations (protons mmol / kg) of 13 MM peaks are given in the table below after correcting for T_1 and T_2 relaxation times. Mann-Whitney U-tests were performed with multiple comparisons being accounted using Bonferroni corrections $\frac{\alpha}{n} = 0.0038$. A significant difference for $M_{3.75}$ being elevate^{n}d in WM was found when assessing MM concentrations

Video S1 The cine representation of Figure 5 shows a rotation of the 3D space of the T_1-relaxation time curve fitting for M0.92. TI_1 and TI_2 are given in the x- and y- axes respectively in seconds; z-axis represents the normalized signal [a.u.]. The black crosses are individual data points from eleven volunteers and the blue line is the projected fitting to equation 1.

How to cite this article: Murali-Manohar S, Wright AM, Borbath T, Avdievich NI, Henning A. A novel method to measure T_1-relaxation times of macromolecules and quantification of the macromolecular resonances. *Magn Reson Med*. 2021;85:601–614. https://doi.org/10.1002/mrm.28484

Supporting Information Figure S1: Bloch Simulation results for an inversion pulse profile[27] (pulse duration: 15 ms) after a DIR scheme with inversion times a) TI_1/TI_2 = 2000/575 ms and b) TI_1/TI_2 = 2150/600. The resulting inversion bandwidth is represented by the frequency axis (x-axis); while the y-axis depicts the resulting M_Z/M_0 of MM and metabolites at the end of the DIR sequence block. M_Z/M_0 of MM spectrum after DIR block are 0.48 and 0.51 in a) and b) respectively with almost nulled metabolites.

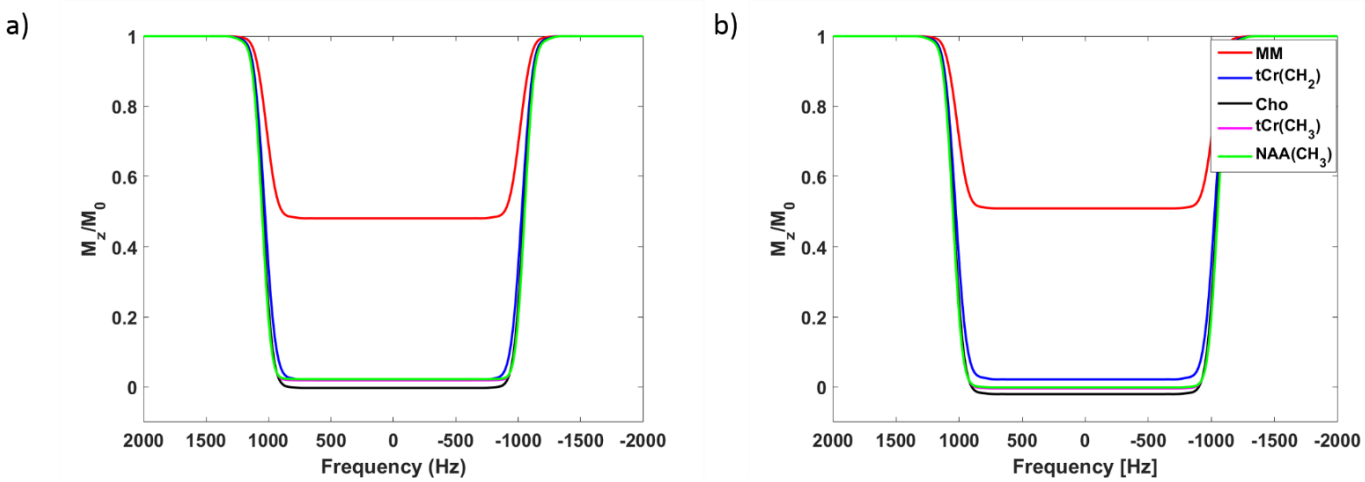

Supporting Information Figure S2: Fit of WM subject-wise summed spectra of TI_1/TI_2 combinations 2360/625, 1300/20 and 1050/238 ms

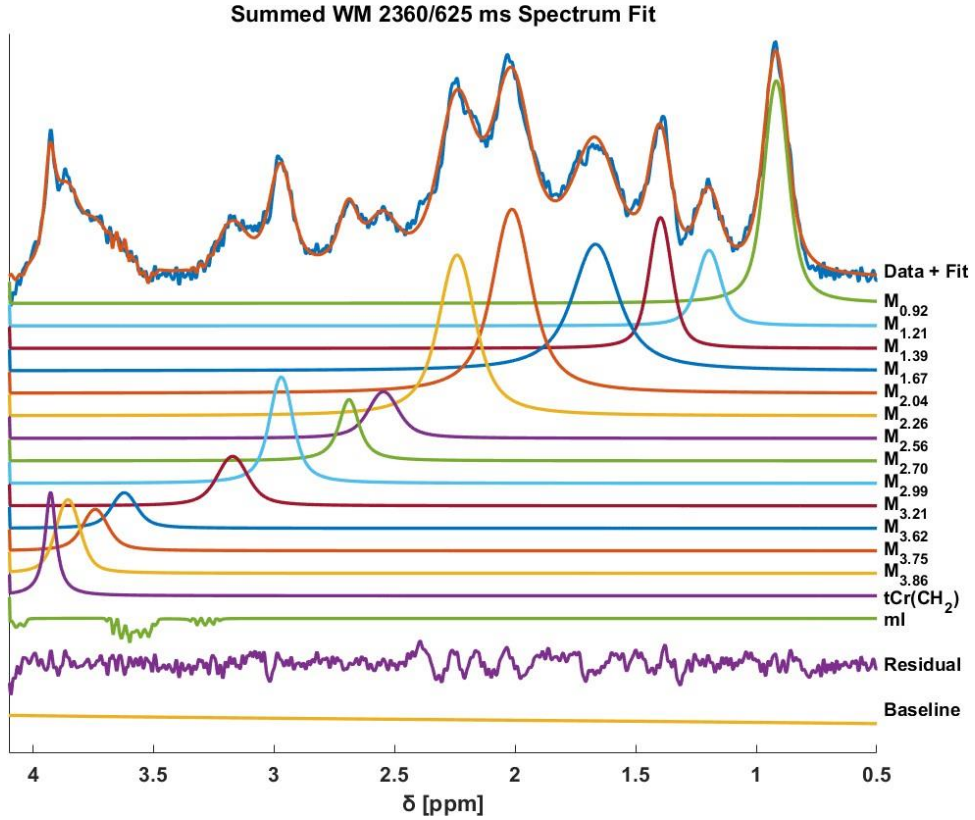

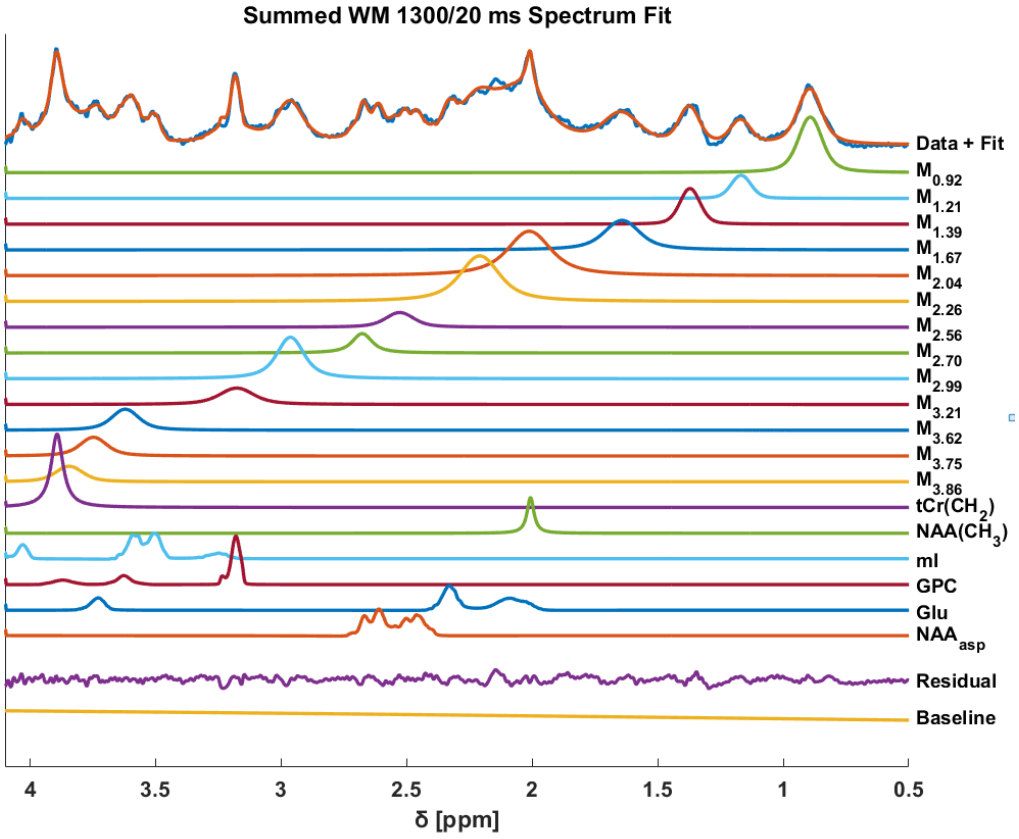
Summed WM 1300/20 ms Spectrum Fit
Data + Fit
M0.92
M1.21
M1.39
M1.67
M2.04
M2.26
M2.56
M2.70
M2.99
M3.21
M3.62
M3.75
M3.86
tCr(CH2)
NAA(CH3)
ml
GPC
Glu
NAAasp
Residual
Baseline
4
3.5
3
2.5
2
1.5
1
0.5
δ [ppm]

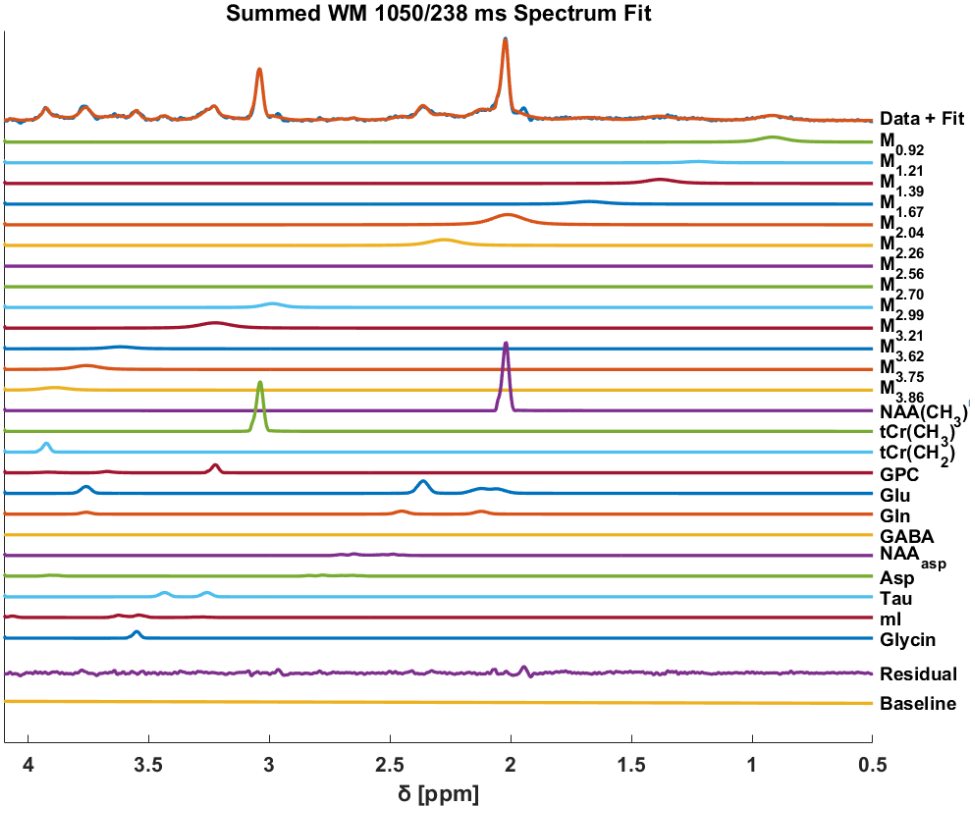
Summed WM 1050/238 ms Spectrum Fit
Data + Fit
M0.92
M1.21
M1.39
M1.67
M2.04
M2.26
M2.56
M2.70
M2.99
M3.21
M3.62
M3.75
M3.86
NAA(CH3)
tCr(CH3)
tCr(CH2)
GPC
Glu
Gln
GABA
NAAasp
Asp
Tau
ml
Glycin
Residual
Baseline
4
3.5
3
2.5
2
1.5
1
0.5
δ [ppm]

Supporting Information Figure S3: Fits of subject-wise summed GM spectra of TI_1/TI_2 combinations 2150/600, 2000/575, 1900/550, 1800/525, 1300/60, 1300/80, 1200/20, and 1250/20 ms

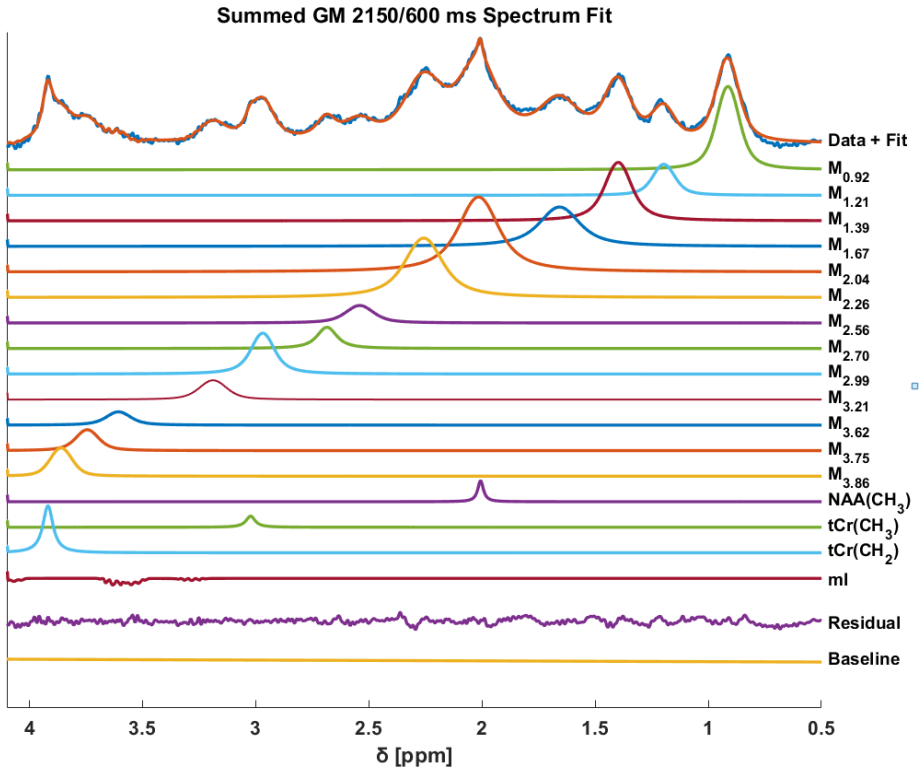

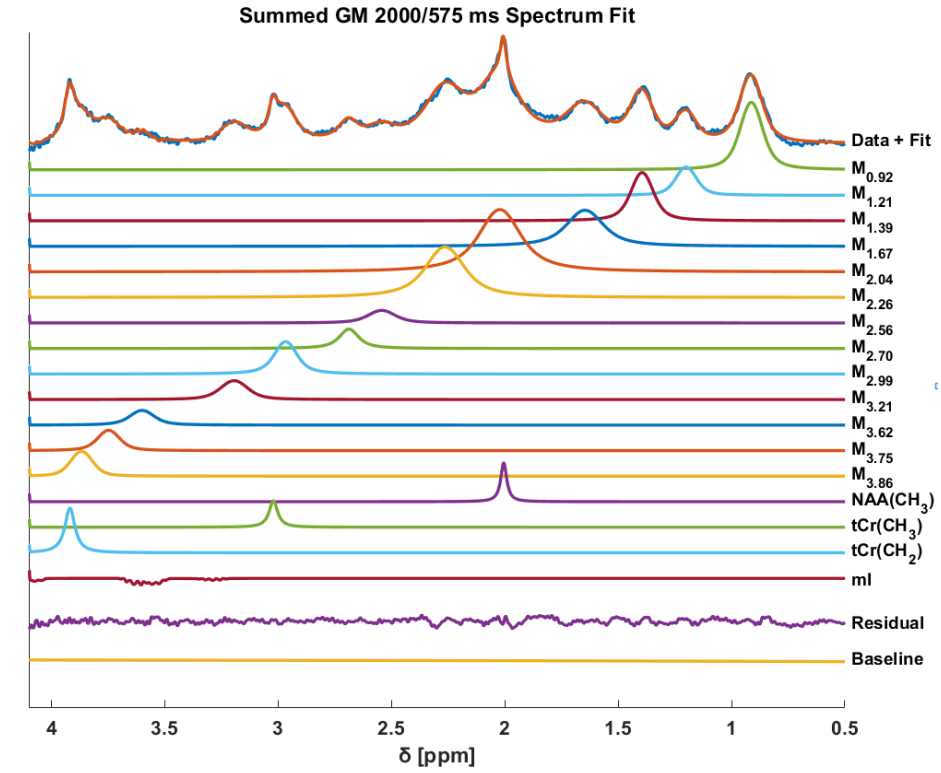
Summed GM 2000/575 ms Spectrum Fit
Data + Fit
M0.92
M1.21
M1.39
M1.67
M2.04
M2.26
M2.56
M2.70
M2.99
M3.21
M3.62
M3.75
M3.86
NAA(CH3)
tCr(CH3)
tCr(CH2)
ml
Residual
Baseline
4
3.5
3
2.5
2
1.5
1
0.5
δ [ppm]

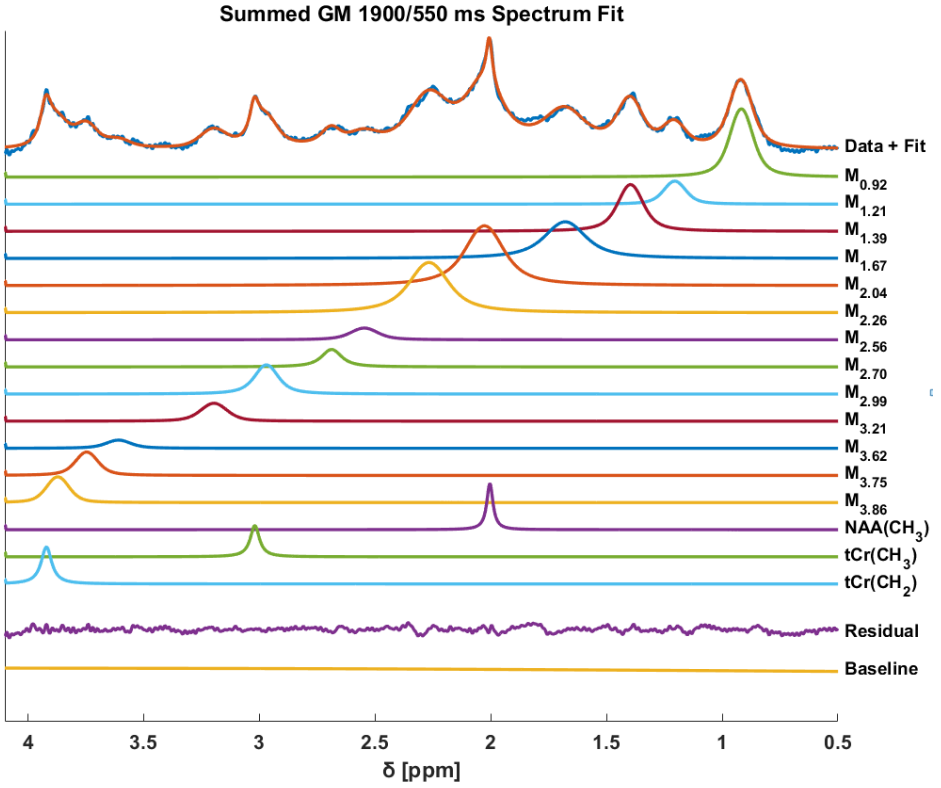
Summed GM 1900/550 ms Spectrum Fit
Data + Fit
M0.92
M1.21
M1.39
M1.67
M2.04
M2.26
M2.56
M2.70
M2.99
M3.21
M3.62
M3.75
M3.86
NAA(CH3)
tCr(CH3)
tCr(CH2)
Residual
Baseline
4
3.5
3
2.5
2
1.5
1
0.5
δ [ppm]

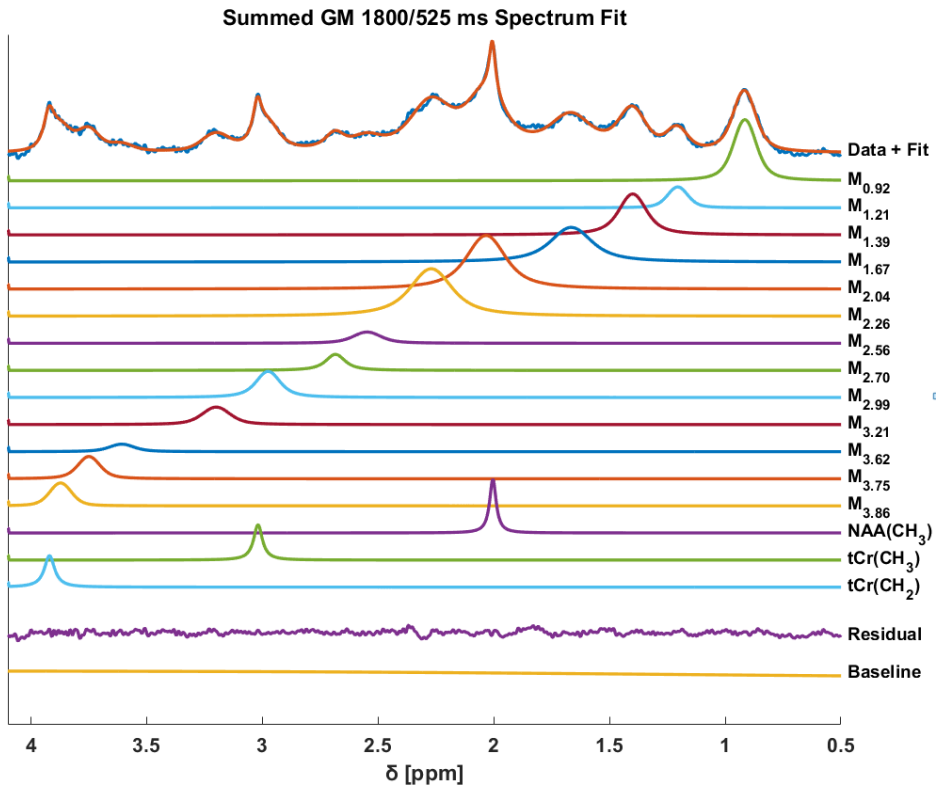
Summed GM 1800/525 ms Spectrum Fit
Data + Fit
M0.92
M1.21
M1.39
M1.67
M2.04
M2.26
M2.56
M2.70
M2.99
M3.21
M3.62
M3.75
M3.86
NAA(CH3)
tCr(CH3)
tCr(CH2)
Residual
Baseline
4
3.5
3
2.5
2
1.5
1
0.5
δ [ppm]

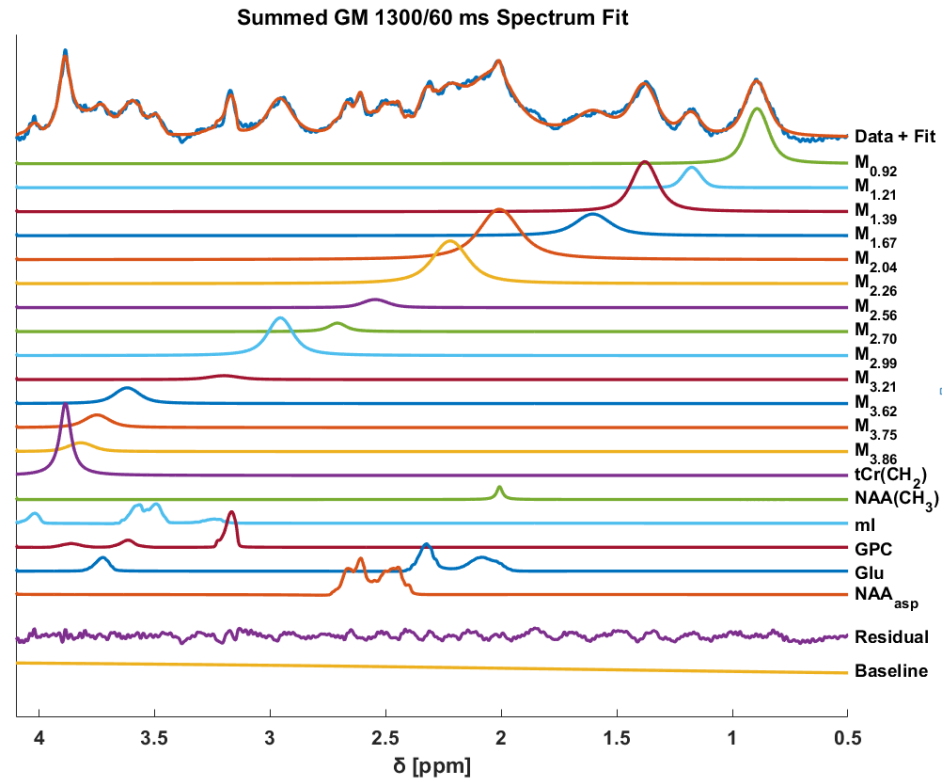
Summed GM 1300/60 ms Spectrum Fit
Data + Fit
M0.92
M1.21
M1.39
M1.67
M2.04
M2.26
M2.56
M2.70
M2.99
M3.21
M3.62
M3.75
M3.86
tCr(CH2)
NAA(CH3)
ml
GPC
Glu
NAAasp
Residual
Baseline
4
3.5
3
2.5
2
1.5
1
0.5
δ [ppm]

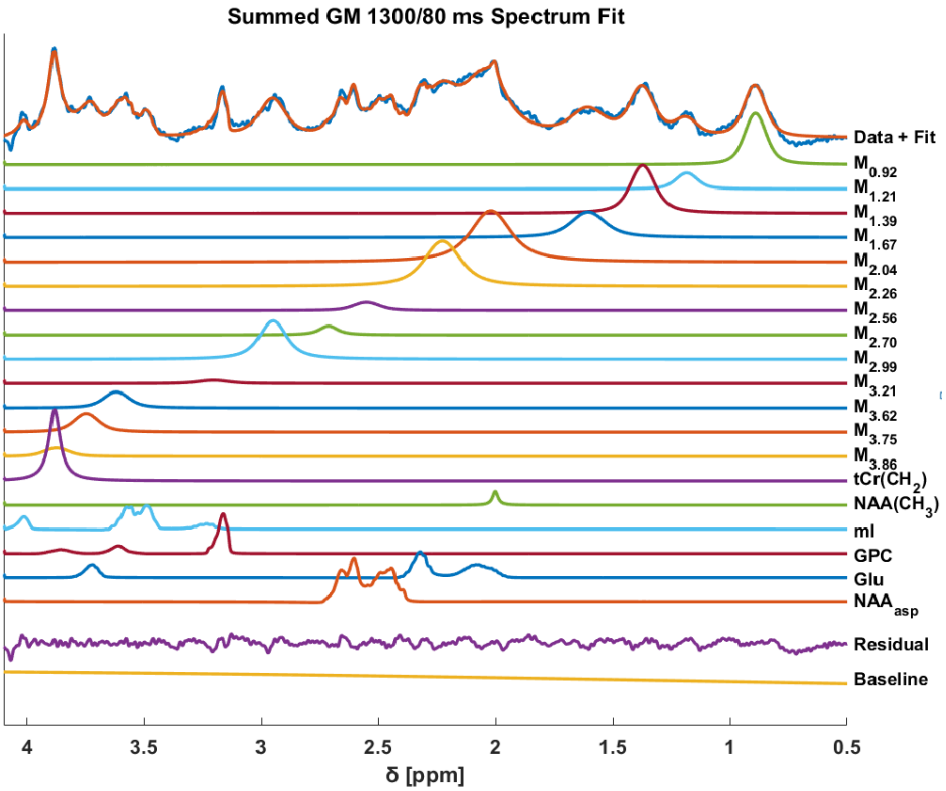
Summed GM 1300/80 ms Spectrum Fit
Data + Fit
M0.92
M1.21
M1.39
M1.67
M2.04
M2.26
M2.56
M2.70
M2.99
M3.21
M3.62
M3.75
M3.86
tCr(CH2)
NAA(CH3)
ml
GPC
Glu
NAAasp
Residual
Baseline
4
3.5
3
2.5
2
1.5
1
0.5
δ [ppm]

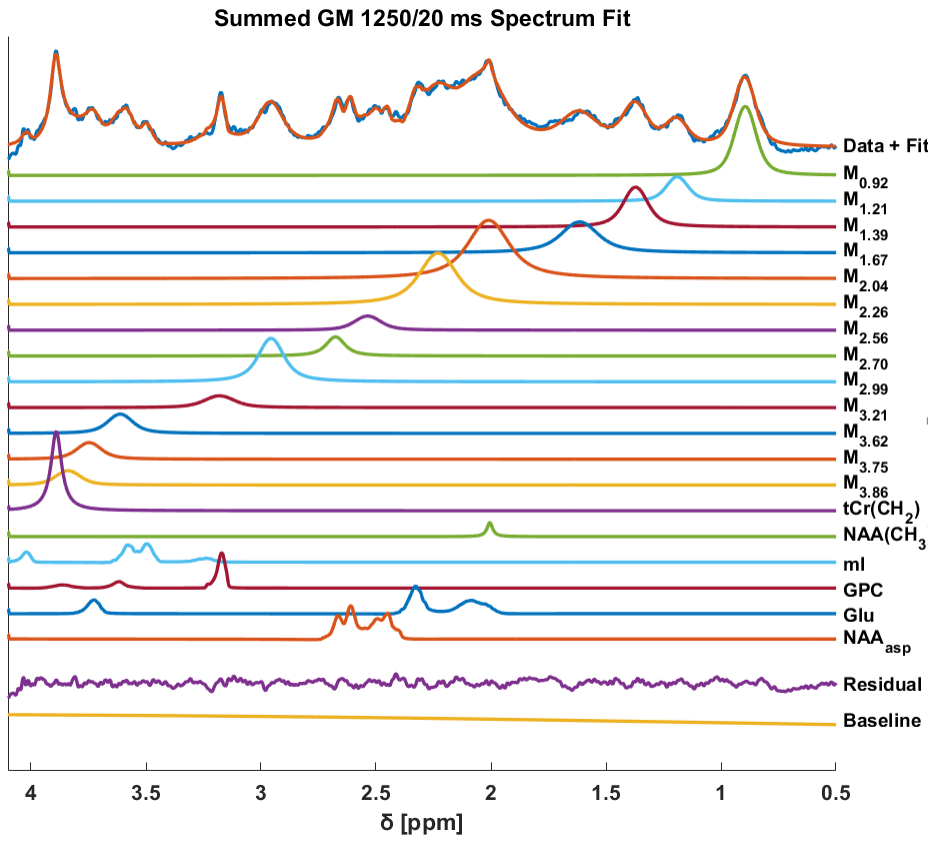
Summed GM 1250/20 ms Spectrum Fit
Data + Fit
M0.92
M1.21
M1.39
M1.67
M2.04
M2.26
M2.56
M2.70
M2.99
M3.21
M3.62
M3.75
M3.86
tCr(CH2)
NAA(CH3
mI
GPC
Glu
NAAasp
Residual
Baseline
4
3.5
3
2.5
2
1.5
1
0.5
δ [ppm]

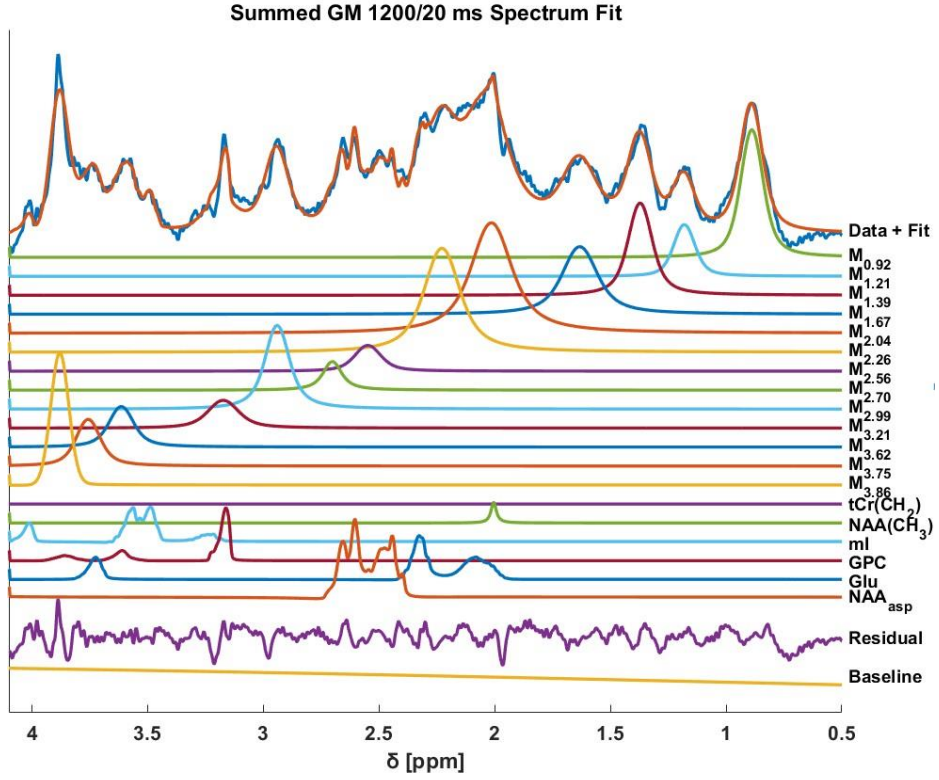
Summed GM 1200/20 ms Spectrum Fit
Data + Fit
M0.92
M1.21
M1.39
M1.67
M2.04
M2.26
M2.56
M2.70
M2.99
M3.21
M3.62
M3.75
M3.86
tCr(CH2)
NAA(CH3)
mI
GPC
Glu
NAAasp
Residual
Baseline
4
3.5
3
2.5
2
1.5
1
0.5
δ [ppm]

Supporting Information Figure S4: Surface Curve fitted to TI_1/TI_2 series for $M_{1.21}$, $M_{1.39}$, $M_{1.67}$, $M_{2.04}$, $M_{2.26}$, $M_{2.56}$, $M_{2.70}$, $M_{2.99}$, $M_{3.21}$, $M_{3.62}$, $M_{3.75}$, and $M_{3.96}$ from GM-rich voxel to calculate T_1-relaxation times. For better visualization of the 3D plots a cine is provided as Supporting Information Video S1.

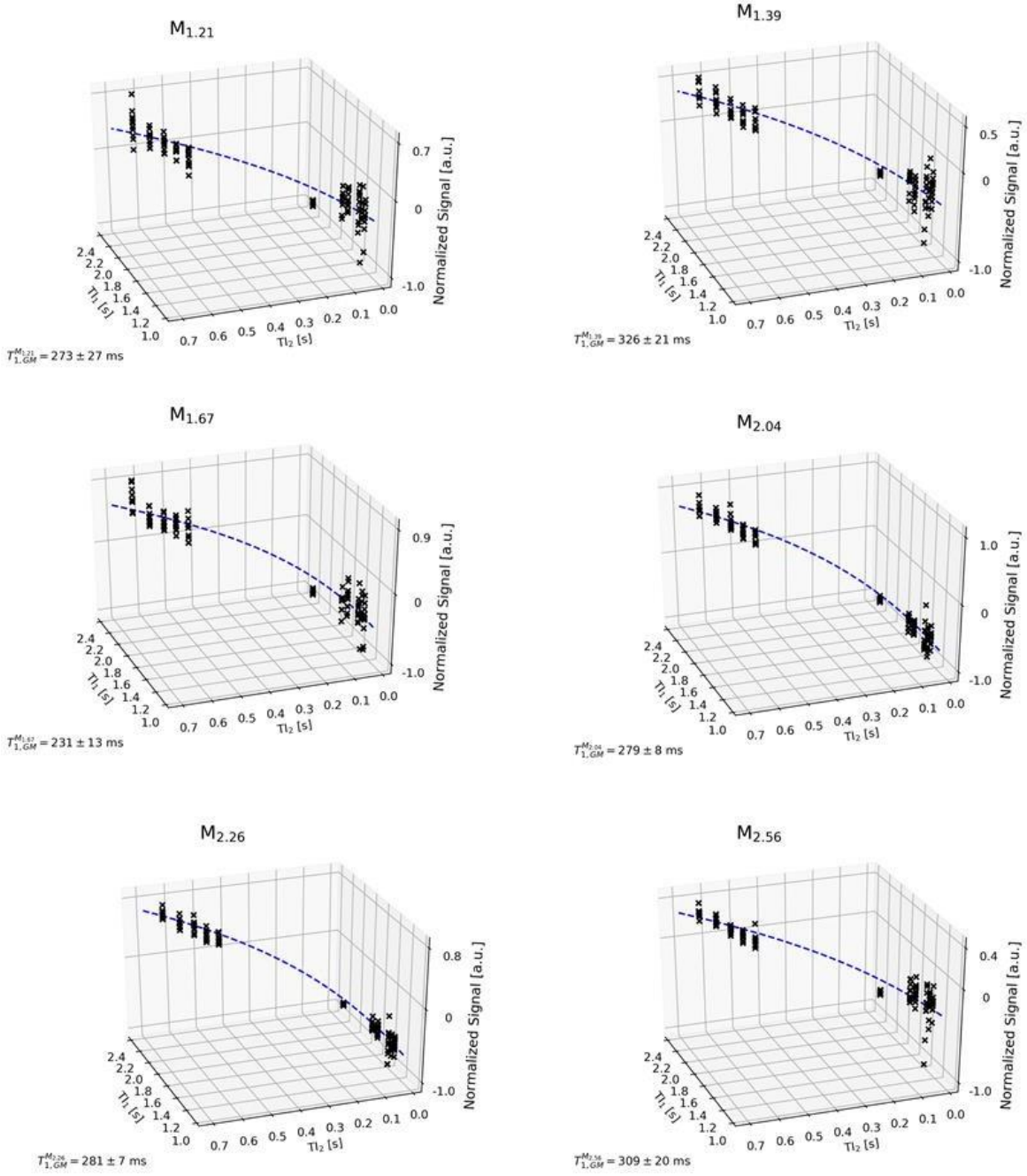

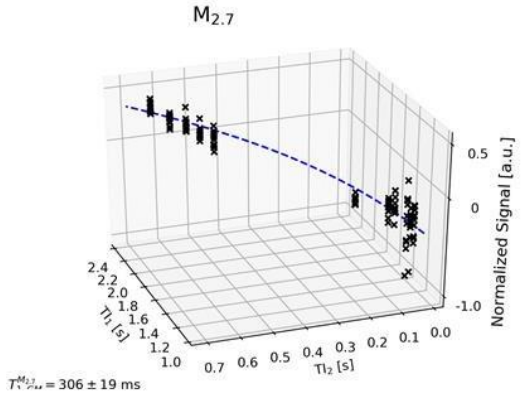
M2.7
Normalized Signal [a.u.]
TI1 [s]
TI2 [s]
$T_{1,GM}^{M_{2.7}} = 306 \pm 19$ ms

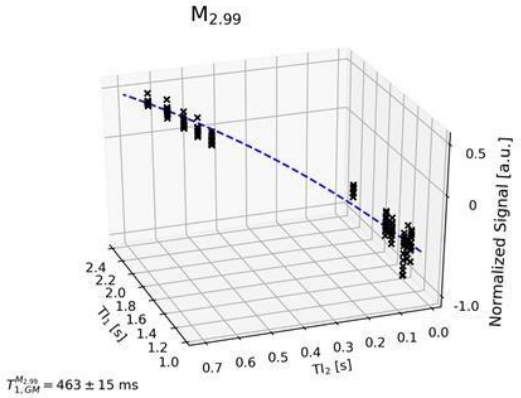
M2.99
Normalized Signal [a.u.]
TI1 [s]
TI2 [s]
$T_{1,GM}^{M_{2.99}} = 463 \pm 15$ ms

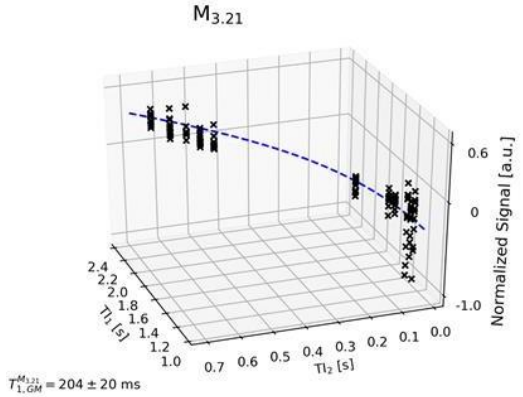
M3.21
Normalized Signal [a.u.]
TI1 [s]
TI2 [s]
$T_{1,GM}^{M_{3.21}} = 204 \pm 20$ ms

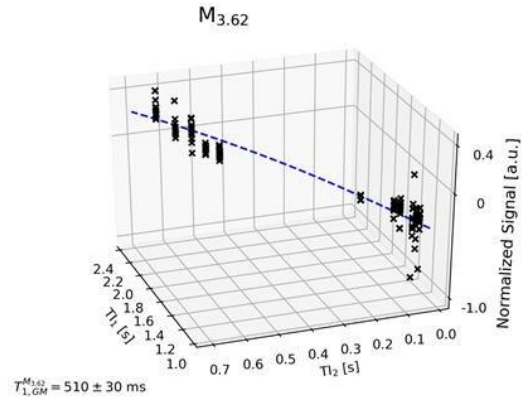
M3.62
Normalized Signal [a.u.]
TI1 [s]
TI2 [s]
$T_{1,GM}^{M_{3.62}} = 510 \pm 30$ ms

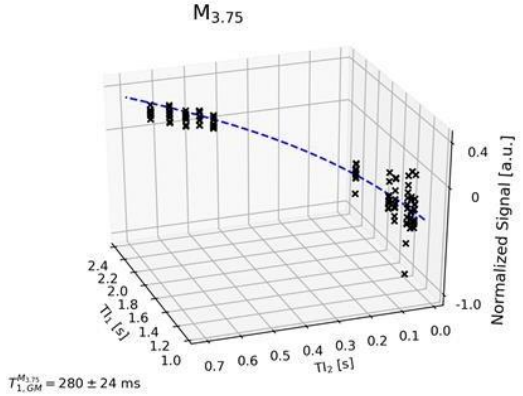
M3.75
Normalized Signal [a.u.]
TI1 [s]
TI2 [s]
$T_{1,GM}^{M_{3.75}} = 280 \pm 24$ ms

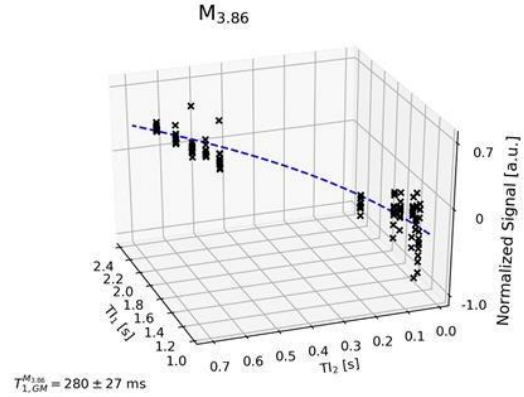
M3.86
Normalized Signal [a.u.]
TI1 [s]
TI2 [s]
$T_{1,GM}^{M_{3.86}} = 280 \pm 27$ ms

Supporting Information Table S1: Residual peaks present corresponding to each TI_1/TI_2 are given in the table. $tCr(CH_2)$, $tCr(CH_3)$, and $NAA(CH_3)$ residual peaks were added as singlets using simulated Voigt lines in LCModel for fitting spectra. NAA_{asp}, mI, GPC, and Glu were added to handle the residuals in negative M_z spectra. For TI_1/TI_2 = 1050/238 ms, a complete basis set was provided which was simulated for a semi-LASER sequence using VeSPA; specifically without singlets used in the basis set for any metabolite residuals.

TI_1/TI_2 [ms]	Residual peaks present
2360/625	$tCr(CH_2)$, mI*
2150/600	$tCr(CH_2)$, $tCr(CH_3)$, $NAA(CH_3)$, mI*
2000/575	$tCr(CH_2)$, $tCr(CH_3)$, $NAA(CH_3)$, mI*
1900/550	$tCr(CH_2)$, $tCr(CH_3)$, $NAA(CH_3)$
1800/525	$tCr(CH_2)$, $tCr(CH_3)$, $NAA(CH_3)$
1300/20	$tCr(CH_2)$, $NAA(CH_3)$, GPC, mI, Glu, NAA_{asp}
1300/60	$tCr(CH_2)$, $NAA(CH_3)$, GPC, mI, Glu, NAA_{asp}
1200/20	$tCr(CH_2)$, $NAA(CH_3)$, GPC, mI, Glu, NAA_{asp}
1250/20	$tCr(CH_2)$, $NAA(CH_3)$, GPC, mI, Glu, NAA_{asp}
1300/80	$tCr(CH_2)$, $NAA(CH_3)$, GPC, mI, Glu, NAA_{asp}
1050/238	$tCr(CH_2)$, $tCr(CH_3)$, $NAA(CH_3)$, GPC, GABA, Glu, Gln, Glycin, Tau, mI, Asp, NAA_{asp}

*mI was added with a negative phase

Supporting Information Table S2: Bloch simulation considering DIR scheme for mI has a negative contribution in TI_1/TI_2 = 2360/625, 2150/575, 2000/550 ms spectra (considering T_1-relaxation times from Wright et al.[46])

TI_1/TI_2 [ms]	mI: M_Z/M_0	
	GM (T_1 = 1470 ms)	WM (T_1 = 1423 ms)
2360/625	-0.0448	-0.0436
2150/600	-0.0217	-0.0224
2000/575	-0.0056	-0.0077

Supporting Information Table S3: Differences in T_1-relaxation times between GM- and WM-rich tissue types were analyzed using Welch's t-test with Bonferroni adjusted p-values to account for multiple comparisons ($\frac{\alpha}{n} = 0.0038$). Significant differences are denoted by an asterisk, and p-values are given for all analyses.

T_1-relaxation times	
MM peak	p-value
$M_{0.92}$	0.3858
$M_{1.21}$	0.5793
$M_{1.39}$*	< 0.0001
$M_{1.67}$	0.0056
$M_{2.04}$*	< 0.0001
$M_{2.26}$*	< 0.0001
$M_{2.56}$	0.0489
$M_{2.70}$*	< 0.0001
$M_{2.99}$*	< 0.0001
$M_{3.21}$*	< 0.0001
$M_{3.62}$*	0.0020
$M_{3.75}$*	< 0.0001
$M_{3.86}$	0.0242

Supporting Information Table S4: Concentrations (protons mmol / kg) of 13 MM peaks are given in the table below after correcting for T_1 and T_2 relaxation times. Mann-Whitney U-tests were performed with multiple comparisons being accounted using Bonferroni corrections $(\frac{\alpha}{n} = 0.0038)$. A significant difference for $M_{3.75}$ being elevated in WM was found when assessing MM concentrations.

Concentration [protons mmol/kg]			
	GM	WM	p-value
$M_{0.92}$	21.1 ± 3.3	21.0 ± 2.6	0.4697
$M_{1.21}$	8.2 ± 4.6	7.9 ± 2.2	0.5000
$M_{1.39}$	20.4 ± 5.3	12.6 ± 6.4	0.0061
$M_{1.67}$	48.0 ± 11.2	46.7 ± 12.6	0.4396
$M_{2.04}$	78.4 ± 10.7	76.6 ± 10.9	0.4099
$M_{2.26}$	50.4 ± 6.8	49.0 ± 7.9	0.2717
$M_{2.56}$	11.9 ± 2.0	13.0 ± 3.7	0.5000
$M_{2.70}$	7.1 ± 1.1	8.6 ± 2.6	0.1617
$M_{2.99}$	29.1 ± 3.0	34.7 ± 6.5	0.0138
$M_{3.21}$	10.0 ± 2.1	14.9 ± 4.6	0.0049
$M_{3.62}$	23.5 ± 8.1	30.3 ± 17.7	0.1437
$M_{3.75}^{*}$	4.8 ± 1.0	7.0 ± 1.5	0.0009
$M_{3.86}$	11.8 ± 1.3	11.9 ± 2.3	0.5000

ANNEX A – Matlab script for Bloch Simulation

```
%pulse profile
time       = 15*1e-3; %s
freqOffset = (-2000:10:2000);
nPoints    = 512;
timeAxis   =  linspace(0,time,nPoints)*1e+3;
x = linspace(-pi,pi,nPoints);
b = 1.904;
AM = sech(b*x);
FM = 1017*tanh(-x*1.89);
PM = (2*pi*cumsum(FM)*time/length(FM));

%Magnetization vectors
M0      = zeros(length(freqOffset),3);
M0(:,3) = 1;
M = applyRotation( alpha,beta, M0 );


ih = [0 1 2 -2 -1];
for i = 1:5
    Bampl      = (1+ih(i)*0.15)*15 *1e-6; %in T
    B  = Bampl*AM.*exp(1i*PM);

Bampl      = 24 *1e-6; %in T
B          = Bampl*AM.*exp(1i*PM);
TE = 24; %ms
TR = 8000; %ms
[alpha, beta] = fSLR( B', freqOffset, time/length(B),0);


T1 = [430 1030 1513 1746 1777]; % MM Cr-CH2 Cho Cr-CH3 NAA (Values for
metabolites are from Deelchand et al at 9.4 T and MM is from Xin et al at 7
T)

T2 = [23.88 81.82 90.11 100.21 110.49]; % (Values are from Murali-Manohar et
al at 9.4 T)

for TI1 = [2360]        % 2150 2000 1900 2360 1800 1050 1300 1300 1200 1250
1300
        for TI2 = [625]  % 600  575  550  625  525  238  80   60   20   20
20
            for i = 1:length(T1)
                M = applyRotation( alpha, beta, M0 );
                Mrelax = applyRelaxation( M,T1(i),T2(i),TI1);
                Mrelax = applyRotation( alpha,beta, Mrelax );
                Mrelax = applyRelaxation( Mrelax,T1(i),T2(i),TI2 );
                mag.Data{i} = min(Mrelax(:,3));

function [alpha, beta] = fSLR( B1, freqOffset, deltaT,rephasePoint)
%FSLR Summary of this function goes here
% B1 profile in T
% freqOffset in Hz
% deltaT     in secs

gammaHz   = 42.576 *1e+6; %Hz/T
```

```
gammaRads = gammaHz*2*pi; %rad/(s*T)
freqOffset = freqOffset.';
G         = freqOffset./gammaHz; %Tesla
a = zeros(length(freqOffset),2);
b = zeros(length(freqOffset),2);
a(:,1)      = ones(length(freqOffset),1);
flagRephase = true;
for i=1:length(B1)
      if flagRephase
        if (i == rephasePoint +1 )
           G= -G;
           flagRephase = false;
        end
      end

B1eff = B1(i).*ones(size(freqOffset));
phi = -gammaRads * deltaT * sqrt( abs(B1eff).^2 + G.^2 );
n0 = (gammaRads*deltaT./abs(phi));
n   = [real(B1eff).*n0, imag(B1eff).*n0, G.*n0];

av = cos(phi/2) -1i*n(:,3).*sin(phi/2);
bv = -1i*(n(:,1)+1i*n(:,2)).*sin(phi/2);

a(:,2) = av.*a(:,1) - conj(bv).*b(:,1);
b(:,2) = bv.*a(:,1) + conj(av).*b(:,1);

a(:,1) = a(:,2); b(:,1) = b(:,2);
end

alpha = a(:,2);  beta  = b(:,2);

function M = applyRotation( a,b, M0 )
M       =  zeros(length(M0),3);

M1tmp   =   conj(a).^2     .*M0(:,1)    - b.^2  .*M0(:,2)  +   2*conj(a).*b
.*M0(:,3);

M2tmp   =  -conj(b).^2     .*M0(:,1)    + a.^2  .*M0(:,2)  +   2*conj(b).*a
.*M0(:,3);

M3tmp   =  -conj(a.*b)     .*M0(:,1)    - a.*b .*M0(:,2) + (abs(a).^2-
abs(b).^2)    .*M0(:,3);

M(:,1)= M1tmp;  M(:,2)= M2tmp;  M(:,3)= M3tmp;
end


function M = applyRelaxation( M0,T1,T2,time )

M           =  zeros(length(M0),3);
M(:,1)      =   M0(:,1)*exp(-time/T2);
M(:,2)      =   M0(:,2)*exp(-time/T2);
M(:,3)      =  (M0(:,3)-1)*exp(-time/T1)+1;
end
```

ANNEX B – Example *Control files (.control) for LCModel quantification*
Control file to fit TI_1/TI_2 = 1050/238 ms DIR spectrum

The sample fit settings file is given to fit TI_1/TI_2 = 1050/238 ms DIR spectrum with a semiLASER basis set included. The basis set included NAA downfield peak, NAA(CH_3), tCr(CH_3), tCr(CH2), GPC, glutamine (Gln), glutamate (Glu), glycine (Glycin), GABA, NAA_{asp}, mI (myo-inositol) and taurine (Tau).

```
$LCMODL
OWNER='Max Planck Institute biological Cybernetics'
TITLE='ExampleFit'
FILBAS='/path/Basis_sets/semiLASER_basis.basis'
FILRAW='/path/Example.RAW'
FILH2O='/path/Example_water.RAW'
FILPS='/path/Output/ps'
FILTAB='/path/Output/table'
FILCSV='/path/Output/csv'
FILCOO='/path/Output/coord'
LTABLE=7
LPS = 8
LCOORD=9
LCSV=11
atth2o= 1
deltat= 1.2500e-04
dkntmn= 99
doecc= F
dows= T
hzpppm= 399.719
neach= 50
nunfil= 4096
ppmend= 0.2
ppmst= 8.2
ppmgap(1,1)= 7.6
ppmgap(2,1)= 4.0
sddegp= 0
sddegz= 0
shifmn(2) = -0.04
shifmx(2) = 0.04
rfwhm= 0.6
wsppm= 7.790
wsmet= 'Cr'
n1hmet= 1
wconc= 40873
nsimul= 14
chsimu(1)= 'MM09 @ 0.916 +- 0.02 FWHM= .08 < .11 +- .005 AMP= 1.'
chsimu(2)= 'MM12 @ 1.21 +- 0.01 FWHM= .08 < .11 +- .005 AMP= 1.'
chsimu(3)= 'MM14 @ 1.39 +- 0.01 FWHM= .08 < .11 +- .005 AMP= 1.'
```

```
chsimu(4)= 'MM17 @ 1.67 +- 0.01 FWHM= .10 < .13 +- .005 AMP= 1.'
chsimu(5)= 'MM20 @ 2.04 +- 0.01 FWHM= .10 < .13 +- .005 AMP= 1.'
chsimu(6)= 'MM22 @ 2.26 +- 0.005 FWHM= .10 < .13 +- .005 AMP= 1.'
chsimu(7)= 'MM26 @ 2.56 +- 0.005 FWHM= .09 < .11 +- .005 AMP= 1.'
chsimu(8)= 'MM27 @ 2.7 +- 0.01 FWHM= .04 < .08 +- .005 AMP= 1.'
chsimu(9)= 'MM30 @ 2.99 +- 0.005 FWHM= .07 < .09 +- .005 AMP= 1.'
chsimu(10)= 'MM32 @ 3.21 +- 0.005 FWHM= .10 < .13 +- .005 AMP= 1.'
chsimu(11)= 'MM36 @ 3.62 +- 0.005 FWHM= .08 < .11 +- .005 AMP= 1.'
chsimu(12)= 'MM37 @ 3.75 +- 0.005 FWHM= .08 < .11 +- .005 AMP= 1.'
chsimu(13)= 'MM38 @ 3.86 +- 0.02 FWHM= .09 < .11 +- .005 AMP= 1.'
chsimu(14)= 'MM39 @ 4.03 +- 0.01 FWHM= .10 < .14 +- .005 AMP= 1.'
$END
```

For the other TI_1/TI_2 combinations DIR spectra resulting in a positive MM magnetization, a basis set containing the NAA downfield peak was given. mI was included in the basis set with a negative phase for TI_1/TI_2 = 2360/625, 2150/600 and 2000/575 ms. Simulated Voigt lines (chsimu) were included to fit the residual singlets [tCr(CH_2), tCr(CH_3) and NAA(CH_3)] as specified in the Supporting Information Table S1.

Control file to fit TI_1/TI_2 = 2360/625 ms DIR spectrum

```
…
FILBAS='/home/smanohar/Desktop/MM_T1/GM/Basis_sets/NAA_DF_basis.basis'
…
nsimul= 15
chsimu(1)= 'MM09 @ 0.916 +- 0.02 FWHM= .08 < .11 +- .005 AMP= 1.'
chsimu(2)= 'MM12 @ 1.21 +- 0.01 FWHM= .08 < .11 +- .005 AMP= 1.'
chsimu(3)= 'MM14 @ 1.39 +- 0.01 FWHM= .08 < .11 +- .005 AMP= 1.'
chsimu(4)= 'MM17 @ 1.67 +- 0.01 FWHM= .10 < .13 +- .005 AMP= 1.'
chsimu(5)= 'MM20 @ 2.04 +- 0.01 FWHM= .10 < .13 +- .005 AMP= 1.'
chsimu(6)= 'MM22 @ 2.26 +- 0.005 FWHM= .10 < .13 +- .005 AMP= 1.'
chsimu(7)= 'MM26 @ 2.56 +- 0.005 FWHM= .09 < .11 +- .005 AMP= 1.'
chsimu(8)= 'MM27 @ 2.7 +- 0.01 FWHM= .04 < .08 +- .005 AMP= 1.'
chsimu(9)= 'MM30 @ 2.99 +- 0.005 FWHM= .07 < .09 +- .005 AMP= 1.'
chsimu(10)= 'MM32 @ 3.21 +- 0.005 FWHM= .10 < .13 +- .005 AMP= 1.'
chsimu(11)= 'MM36 @ 3.62 +- 0.005 FWHM= .08 < .11 +- .005 AMP= 1.'
chsimu(12)= 'MM37 @ 3.75 +- 0.005 FWHM= .08 < .11 +- .005 AMP= 1.'
chsimu(13)= 'MM38 @ 3.86 +- 0.02 FWHM= .09 < .11 +- .005 AMP= 1.'
chsimu(14)= 'MM39 @ 4.03 +- 0.01 FWHM= .10 < .14 +- .005 AMP= 1.'
chsimu(15)= 'Cr39 @ 3.925 +- 0.04 FWHM= .006 < .06 +- .003 AMP= 1.'
$END
```

Control file to fit TI_1/TI_2 = 2150/600 ms DIR spectrum

```
…
FILBAS='/home/smanohar/Desktop/MM_T1/GM/Basis_sets/NAA_DF_basis.basis'
…
nsimul= 17
chsimu(1)= 'MM09 @ 0.916 +- 0.02 FWHM= .08 < .11 +- .005 AMP= 1.'
chsimu(2)= 'MM12 @ 1.21 +- 0.01 FWHM= .08 < .11 +- .005 AMP= 1.'
chsimu(3)= 'MM14 @ 1.39 +- 0.01 FWHM= .08 < .11 +- .005 AMP= 1.'
chsimu(4)= 'MM17 @ 1.67 +- 0.01 FWHM= .10 < .13 +- .005 AMP= 1.'
chsimu(5)= 'MM20 @ 2.04 +- 0.01 FWHM= .10 < .13 +- .005 AMP= 1.'
chsimu(6)= 'MM22 @ 2.26 +- 0.005 FWHM= .10 < .13 +- .005 AMP= 1.'
chsimu(7)= 'MM26 @ 2.56 +- 0.01 FWHM= .09 < .11 +- .005 AMP= 1.'
chsimu(8)= 'MM27 @ 2.7 +- 0.05 FWHM= .04 < .08 +- .005 AMP= 1.'
chsimu(9)= 'MM30 @ 2.99 +- 0.01 FWHM= .10 < .12 +- .005 AMP= 1.'
chsimu(10)= 'MM32 @ 3.21 +- 0.02 FWHM= .12 < .18 +- .005 AMP= 1.'
chsimu(11)= 'MM36 @ 3.62 +- 0.02 FWHM= .09 < .11 +- .005 AMP= 1.'
chsimu(12)= 'MM37 @ 3.75 +- 0.02 FWHM= .09 < .11 +- .005 AMP= 1.'
chsimu(13)= 'MM38 @ 3.86 +- 0.02 FWHM= .09 < .11 +- .005 AMP= 1.'
chsimu(14)= 'MM39 @ 4.03 +- 0.01 FWHM= .10 < .14 +- .005 AMP= 1.'
chsimu(15)= 'Cr39 @ 3.925 +- 0.04 FWHM= .006 < .06 +- .003 AMP= 1.'
chsimu(16)= 'Cr30 @ 3.028 +- 0.01 FWHM= .002 < .05 +- .003 AMP= 1.'
chsimu(17)= 'NAA @ 2.008 +- 0.02 FWHM= .003 < .03 +- .003 AMP= 1.'
$END
```

Control file to fit TI_1/TI_2 = 2000/575 ms DIR spectrum

```
…
FILBAS='/home/smanohar/Desktop/MM_T1/GM/Basis_sets/NAA_DF_basis.basis'
…
nsimul= 17
chsimu(1)= 'MM09 @ 0.916 +- 0.02 FWHM= .08 < .11 +- .005 AMP= 1.'
chsimu(2)= 'MM12 @ 1.21 +- 0.01 FWHM= .08 < .11 +- .005 AMP= 1.'
chsimu(3)= 'MM14 @ 1.39 +- 0.01 FWHM= .08 < .11 +- .005 AMP= 1.'
chsimu(4)= 'MM17 @ 1.67 +- 0.01 FWHM= .10 < .13 +- .005 AMP= 1.'
chsimu(5)= 'MM20 @ 2.04 +- 0.01 FWHM= .10 < .13 +- .005 AMP= 1.'
chsimu(6)= 'MM22 @ 2.26 +- 0.005 FWHM= .10 < .13 +- .005 AMP= 1.'
chsimu(7)= 'MM26 @ 2.56 +- 0.01 FWHM= .09 < .11 +- .005 AMP= 1.'
chsimu(8)= 'MM27 @ 2.7 +- 0.05 FWHM= .04 < .08 +- .005 AMP= 1.'
chsimu(9)= 'MM30 @ 2.99 +- 0.01 FWHM= .10 < .12 +- .005 AMP= 1.'
chsimu(10)= 'MM32 @ 3.21 +- 0.02 FWHM= .12 < .18 +- .005 AMP= 1.'
chsimu(11)= 'MM36 @ 3.62 +- 0.02 FWHM= .09 < .11 +- .005 AMP= 1.'
chsimu(12)= 'MM37 @ 3.75 +- 0.02 FWHM= .09 < .11 +- .005 AMP= 1.'
chsimu(13)= 'MM38 @ 3.86 +- 0.02 FWHM= .09 < .11 +- .005 AMP= 1.'
chsimu(14)= 'MM39 @ 4.03 +- 0.01 FWHM= .10 < .14 +- .005 AMP= 1.'
chsimu(15)= 'Cr39 @ 3.925 +- 0.04 FWHM= .006 < .06 +- .003 AMP= 1.'
chsimu(16)= 'Cr30 @ 3.028 +- 0.01 FWHM= .002 < .05 +- .003 AMP= 1.'
chsimu(17)= 'NAA @ 2.008 +- 0.02 FWHM= .003 < .03 +- .003 AMP= 1.'
$END
```

Control file to fit TI_1/TI_2 = 1900/550 ms DIR spectrum

```
…
FILBAS='/home/smanohar/Desktop/MM_T1/GM/Basis_sets/NAA_DF_basis.basis'
…
nsimul= 17
chsimu(1)= 'MM09 @ 0.916 +- 0.02 FWHM= .08 < .11 +- .005 AMP= 1.'
chsimu(2)= 'MM12 @ 1.21 +- 0.01 FWHM= .08 < .11 +- .005 AMP= 1.'
chsimu(3)= 'MM14 @ 1.39 +- 0.01 FWHM= .08 < .11 +- .005 AMP= 1.'
chsimu(4)= 'MM17 @ 1.67 +- 0.01 FWHM= .10 < .13 +- .005 AMP= 1.'
chsimu(5)= 'MM20 @ 2.04 +- 0.01 FWHM= .10 < .13 +- .005 AMP= 1.'
chsimu(6)= 'MM22 @ 2.26 +- 0.005 FWHM= .10 < .13 +- .005 AMP= 1.'
chsimu(7)= 'MM26 @ 2.56 +- 0.005 FWHM= .09 < .11 +- .005 AMP= 1.'
chsimu(8)= 'MM27 @ 2.7 +- 0.01 FWHM= .04 < .08 +- .005 AMP= 1.'
chsimu(9)= 'MM30 @ 2.99 +- 0.005 FWHM= .07 < .09 +- .005 AMP= 1.'
chsimu(10)= 'MM32 @ 3.21 +- 0.005 FWHM= .12 < .18 +- .005 AMP= 1.'
chsimu(11)= 'MM36 @ 3.62 +- 0.005 FWHM= .08 < .11 +- .005 AMP= 1.'
chsimu(12)= 'MM37 @ 3.75 +- 0.005 FWHM= .08 < .11 +- .005 AMP= 1.'
chsimu(13)= 'MM38 @ 3.86 +- 0.02 FWHM= .09 < .11 +- .005 AMP= 1.'
chsimu(14)= 'MM39 @ 4.03 +- 0.01 FWHM= .10 < .14 +- .005 AMP= 1.'
chsimu(15)= 'Cr39 @ 3.925 +- 0.02 FWHM= .006 < .06 +- .003 AMP= 1.'
chsimu(16)= 'Cr30 @ 3.028 +- 0.01 FWHM= .002 < .05 +- .003 AMP= 1.'
chsimu(17)= 'NAA @ 2.008 +- 0.02 FWHM= .003 < .03 +- .003 AMP= 1.'
$END
```

Control file to fit TI_1/TI_2 = 1800/575 ms DIR spectrum

```
…
FILBAS='/home/smanohar/Desktop/MM_T1/GM/Basis_sets/NAA_DF_basis.basis'
…
nsimul= 17
chsimu(1)= 'MM09 @ 0.916 +- 0.02 FWHM= .08 < .11 +- .005 AMP= 1.'
chsimu(2)= 'MM12 @ 1.21 +- 0.01 FWHM= .08 < .11 +- .005 AMP= 1.'
chsimu(3)= 'MM14 @ 1.39 +- 0.01 FWHM= .08 < .11 +- .005 AMP= 1.'
chsimu(4)= 'MM17 @ 1.67 +- 0.01 FWHM= .10 < .13 +- .005 AMP= 1.'
chsimu(5)= 'MM20 @ 2.04 +- 0.01 FWHM= .10 < .13 +- .005 AMP= 1.'
chsimu(6)= 'MM22 @ 2.26 +- 0.005 FWHM= .10 < .13 +- .005 AMP= 1.'
chsimu(7)= 'MM26 @ 2.56 +- 0.005 FWHM= .09 < .11 +- .005 AMP= 1.'
chsimu(8)= 'MM27 @ 2.7 +- 0.01 FWHM= .04 < .08 +- .005 AMP= 1.'
chsimu(9)= 'MM30 @ 2.99 +- 0.005 FWHM= .07 < .09 +- .005 AMP= 1.'
chsimu(10)= 'MM32 @ 3.21 +- 0.005 FWHM= .10 < .13 +- .005 AMP= 1.'
chsimu(11)= 'MM36 @ 3.62 +- 0.005 FWHM= .08 < .11 +- .005 AMP= 1.'
chsimu(12)= 'MM37 @ 3.75 +- 0.005 FWHM= .08 < .11 +- .005 AMP= 1.'
chsimu(13)= 'MM38 @ 3.86 +- 0.02 FWHM= .09 < .11 +- .005 AMP= 1.'
chsimu(14)= 'MM39 @ 4.03 +- 0.01 FWHM= .10 < .14 +- .005 AMP= 1.'
chsimu(15)= 'Cr39 @ 3.925 +- 0.04 FWHM= .006 < .06 +- .003 AMP= 1.'
chsimu(16)= 'Cr30 @ 3.028 +- 0.01 FWHM= .002 < .05 +- .003 AMP= 1.'
chsimu(17)= 'NAA @ 2.008 +- 0.02 FWHM= .003 < .03 +- .003 AMP= 1.'
$END
```

For the ones resulting in a negative MM magnetization, GPC, mI, Glu, and NAA_{asp} were also given in the basis set in addition to the NAA downfield peak. Simulated Voigt lines (chsimu) were included to fit the residual singlets [tCr(CH_2), tCr(CH_3) and NAA(CH_3)] as specified in the Supporting Information Table S1.

Control file to fit TI_1/TI_2 = 1300/80 ms DIR spectrum

```
…
FILBAS='/home/smanohar/Desktop/MM_T1/GM/Basis_sets/NAADF_NAA_asp_basis.basis'
…
degzer = 180
…
nsimul= 16
chsimu(1)= 'MM09 @ 0.916 +- 0.02 FWHM= .08 < .11 +- .005 AMP= 1.'
chsimu(2)= 'MM12 @ 1.21 +- 0.01 FWHM= .08 < .11 +- .005 AMP= 1.'
chsimu(3)= 'MM14 @ 1.39 +- 0.01 FWHM= .08 < .11 +- .005 AMP= 1.'
chsimu(4)= 'MM17 @ 1.67 +- 0.01 FWHM= .10 < .13 +- .005 AMP= 1.'
chsimu(5)= 'MM20 @ 2.04 +- 0.01 FWHM= .10 < .13 +- .005 AMP= 1.'
chsimu(6)= 'MM22 @ 2.26 +- 0.005 FWHM= .10 < .13 +- .005 AMP= 1.'
chsimu(7)= 'MM26 @ 2.56 +- 0.005 FWHM= .09 < .11 +- .005 AMP= 1.'
chsimu(8)= 'MM27 @ 2.7 +- 0.01 FWHM= .04 < .08 +- .005 AMP= 1.'
chsimu(9)= 'MM30 @ 2.99 +- 0.005 FWHM= .07 < .09 +- .005 AMP= 1.'
chsimu(10)= 'MM32 @ 3.21 +- 0.005 FWHM= .10 < .13 +- .005 AMP= 1.'
chsimu(11)= 'MM36 @ 3.62 +- 0.005 FWHM= .08 < .11 +- .005 AMP= 1.'
chsimu(12)= 'MM37 @ 3.75 +- 0.005 FWHM= .08 < .11 +- .005 AMP= 1.'
chsimu(13)= 'MM38 @ 3.86 +- 0.02 FWHM= .09 < .11 +- .005 AMP= 1.'
chsimu(14)= 'MM39 @ 4.03 +- 0.01 FWHM= .10 < .14 +- .005 AMP= 1.'
chsimu(15)= 'Cr39 @ 3.925 +- 0.06 FWHM= .0008 < .06 +- .003 AMP= 1.'
chsimu(16)= 'NAA @ 2.008 +- 0.02 FWHM= .003 < .03 +- .003 AMP= 1.'
$END
```

Control file to fit TI_1/TI_2 = 1300/60 ms DIR spectrum

```
…
FILBAS='/home/smanohar/Desktop/MM_T1/GM/Basis_sets/NAADF_NAA_asp_basis.basis'
…
degzer = 180
…
nsimul= 16
chsimu(1)= 'MM09 @ 0.916 +- 0.02 FWHM= .08 < .11 +- .005 AMP= 1.'
chsimu(2)= 'MM12 @ 1.21 +- 0.01 FWHM= .08 < .11 +- .005 AMP= 1.'
chsimu(3)= 'MM14 @ 1.39 +- 0.01 FWHM= .08 < .11 +- .005 AMP= 1.'
chsimu(4)= 'MM17 @ 1.67 +- 0.01 FWHM= .10 < .13 +- .005 AMP= 1.'
chsimu(5)= 'MM20 @ 2.04 +- 0.01 FWHM= .10 < .13 +- .005 AMP= 1.'
chsimu(6)= 'MM22 @ 2.26 +- 0.005 FWHM= .10 < .13 +- .005 AMP= 1.'
chsimu(7)= 'MM26 @ 2.56 +- 0.005 FWHM= .09 < .11 +- .005 AMP= 1.'
chsimu(8)= 'MM27 @ 2.7 +- 0.01 FWHM= .04 < .08 +- .005 AMP= 1.'
chsimu(9)= 'MM30 @ 2.99 +- 0.005 FWHM= .07 < .09 +- .005 AMP= 1.'
chsimu(10)= 'MM32 @ 3.21 +- 0.005 FWHM= .10 < .13 +- .005 AMP= 1.'
chsimu(11)= 'MM36 @ 3.62 +- 0.005 FWHM= .08 < .11 +- .005 AMP= 1.'
chsimu(12)= 'MM37 @ 3.75 +- 0.005 FWHM= .08 < .11 +- .005 AMP= 1.'
```

```
chsimu(13)= 'MM38 @ 3.86 +- 0.02 FWHM= .09 < .11 +- .005 AMP= 1.'
chsimu(14)= 'MM39 @ 4.03 +- 0.01 FWHM= .10 < .14 +- .005 AMP= 1.'
chsimu(15)= 'Cr39 @ 3.925 +- 0.06 FWHM= .0008 < .06 +- .003 AMP= 1.'
chsimu(16)= 'NAA @ 2.008 +- 0.02 FWHM= .003 < .03 +- .003 AMP= 1.'
$END
```

Control file to fit TI_1/TI_2 = 1300/20 ms DIR spectrum

```
…
FILBAS='/home/smanohar/Desktop/MM_T1/GM/Basis_sets/NAADF_NAA_asp_basis.basis'
…
degzer = 180
…
nsimul= 16
chsimu(1)= 'MM09 @ 0.916 +- 0.02 FWHM= .08 < .11 +- .005 AMP= 1.'
chsimu(2)= 'MM12 @ 1.21 +- 0.01 FWHM= .08 < .11 +- .005 AMP= 1.'
chsimu(3)= 'MM14 @ 1.39 +- 0.01 FWHM= .08 < .11 +- .005 AMP= 1.'
chsimu(4)= 'MM17 @ 1.67 +- 0.01 FWHM= .10 < .13 +- .005 AMP= 1.'
chsimu(5)= 'MM20 @ 2.04 +- 0.01 FWHM= .10 < .13 +- .005 AMP= 1.'
chsimu(6)= 'MM22 @ 2.26 +- 0.005 FWHM= .10 < .13 +- .005 AMP= 1.'
chsimu(7)= 'MM26 @ 2.56 +- 0.005 FWHM= .09 < .11 +- .005 AMP= 1.'
chsimu(8)= 'MM27 @ 2.7 +- 0.01 FWHM= .04 < .08 +- .005 AMP= 1.'
chsimu(9)= 'MM30 @ 2.99 +- 0.005 FWHM= .07 < .09 +- .005 AMP= 1.'
chsimu(10)= 'MM32 @ 3.21 +- 0.005 FWHM= .10 < .13 +- .005 AMP= 1.'
chsimu(11)= 'MM36 @ 3.62 +- 0.005 FWHM= .08 < .11 +- .005 AMP= 1.'
chsimu(12)= 'MM37 @ 3.75 +- 0.005 FWHM= .08 < .11 +- .005 AMP= 1.'
chsimu(13)= 'MM38 @ 3.86 +- 0.02 FWHM= .09 < .11 +- .005 AMP= 1.'
chsimu(14)= 'MM39 @ 4.03 +- 0.01 FWHM= .10 < .14 +- .005 AMP= 1.'
chsimu(15)= 'Cr39 @ 3.925 +- 0.06 FWHM= .0008 < .06 +- .003 AMP= 1.'
chsimu(16)= 'NAA @ 2.008 +- 0.02 FWHM= .003 < .03 +- .003 AMP= 1.'
$END
```

Control file to fit TI_1/TI_2 = 1250/20 ms DIR spectrum

```
…
FILBAS='/home/smanohar/Desktop/MM_T1/GM/Basis_sets/NAADF_NAA_asp_basis.basis'
…
degzer = 180
…
nsimul= 16
chsimu(1)= 'MM09 @ 0.916 +- 0.02 FWHM= .08 < .11 +- .005 AMP= 1.'
chsimu(2)= 'MM12 @ 1.21 +- 0.01 FWHM= .08 < .11 +- .005 AMP= 1.'
chsimu(3)= 'MM14 @ 1.39 +- 0.01 FWHM= .08 < .11 +- .005 AMP= 1.'
chsimu(4)= 'MM17 @ 1.67 +- 0.01 FWHM= .10 < .13 +- .005 AMP= 1.'
chsimu(5)= 'MM20 @ 2.04 +- 0.01 FWHM= .10 < .13 +- .005 AMP= 1.'
chsimu(6)= 'MM22 @ 2.26 +- 0.005 FWHM= .10 < .13 +- .005 AMP= 1.'
chsimu(7)= 'MM26 @ 2.56 +- 0.005 FWHM= .09 < .11 +- .005 AMP= 1.'
chsimu(8)= 'MM27 @ 2.7 +- 0.01 FWHM= .04 < .08 +- .005 AMP= 1.'
chsimu(9)= 'MM30 @ 2.99 +- 0.005 FWHM= .07 < .09 +- .005 AMP= 1.'
chsimu(10)= 'MM32 @ 3.21 +- 0.005 FWHM= .10 < .13 +- .005 AMP= 1.'
```

```
chsimu(11)= 'MM36 @ 3.62 +- 0.005 FWHM= .08 < .11 +- .005 AMP= 1.'
chsimu(12)= 'MM37 @ 3.75 +- 0.005 FWHM= .08 < .11 +- .005 AMP= 1.'
chsimu(13)= 'MM38 @ 3.86 +- 0.02 FWHM= .09 < .11 +- .005 AMP= 1.'
chsimu(14)= 'MM39 @ 4.03 +- 0.01 FWHM= .10 < .14 +- .005 AMP= 1.'
chsimu(15)= 'Cr39 @ 3.925 +- 0.06 FWHM= .0008 < .06 +- .003 AMP= 1.'
chsimu(16)= 'NAA @ 2.008 +- 0.02 FWHM= .003 < .03 +- .003 AMP= 1.'
$END
```

Control file to fit TI_1/TI_2 = 1200/20 ms DIR spectrum

```
…
FILBAS='/home/smanohar/Desktop/MM_T1/GM/Basis_sets/NAADF_NAA_asp_basis.basis'
…
degzer = 180
…
nsimul= 16
chsimu(1)= 'MM09 @ 0.916 +- 0.02 FWHM= .08 < .11 +- .005 AMP= 1.'
chsimu(2)= 'MM12 @ 1.21 +- 0.01 FWHM= .08 < .11 +- .005 AMP= 1.'
chsimu(3)= 'MM14 @ 1.39 +- 0.01 FWHM= .08 < .11 +- .005 AMP= 1.'
chsimu(4)= 'MM17 @ 1.67 +- 0.01 FWHM= .10 < .13 +- .005 AMP= 1.'
chsimu(5)= 'MM20 @ 2.04 +- 0.01 FWHM= .10 < .13 +- .005 AMP= 1.'
chsimu(6)= 'MM22 @ 2.26 +- 0.005 FWHM= .10 < .13 +- .005 AMP= 1.'
chsimu(7)= 'MM26 @ 2.56 +- 0.005 FWHM= .09 < .11 +- .005 AMP= 1.'
chsimu(8)= 'MM27 @ 2.7 +- 0.01 FWHM= .04 < .08 +- .005 AMP= 1.'
chsimu(9)= 'MM30 @ 2.99 +- 0.005 FWHM= .07 < .09 +- .005 AMP= 1.'
chsimu(10)= 'MM32 @ 3.21 +- 0.005 FWHM= .10 < .13 +- .005 AMP= 1.'
chsimu(11)= 'MM36 @ 3.62 +- 0.005 FWHM= .08 < .11 +- .005 AMP= 1.'
chsimu(12)= 'MM37 @ 3.75 +- 0.005 FWHM= .08 < .11 +- .005 AMP= 1.'
chsimu(13)= 'MM38 @ 3.86 +- 0.02 FWHM= .09 < .11 +- .005 AMP= 1.'
chsimu(14)= 'MM39 @ 3.98 +- 0.01 FWHM= .10 < .14 +- .005 AMP= 1.'
chsimu(15)= 'Cr39 @ 3.925 +- 0.06 FWHM= .0008 < .06 +- .003 AMP= 1.'
chsimu(16)= 'NAA @ 2.008 +- 0.02 FWHM= .0001 < .03 +- .003 AMP= 1.'
$END
```

Publication 3

“Quantitative two-dimensional J-resolved metabolite-cycled semiLASER at 9.4 T”

S Murali-Manohar, T Borbath, A M Wright, N I Avdievich, A Henning

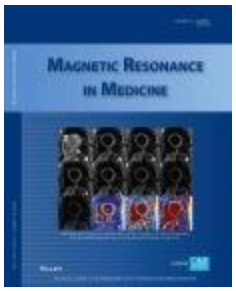

Quantitative two-dimensional J-resolved metabolite-cycled semiLASER at 9.4 T

Journal:	*Magnetic Resonance in Medicine*
Manuscript ID	MRM-21-22166
Wiley - Manuscript type:	Research Article
Research Type:	Spectroscopy/Spectroscopic Imaging < Technique Development, High field MR techniques < Technique Development
Research Focus:	Brain < Neurological

Quantitative two-dimensional J-resolved metabolite-cycled semiLASER at 9.4 T

Saipavitra Murali-Manohar[1,2*], Tamas Borbath[1,2], Andrew Martin Wright[1,3], Nikolai I. Avdievich[1], and Anke Henning[1,4]

[1] High-Field Magnetic Resonance, Max Planck Institute for Biological Cybernetics, Tübingen, Germany

[2] Faculty of Science, University of Tübingen, Tübingen, Germany

[3] IMPRS for Cognitive & Systems Neuroscience, Tübingen, Germany

[4] Advanced Imaging Research Center, UT Southwestern Medical Center, Dallas, Texas

Grant sponsors: This project was co-sponsored by the Horizon 2020/ CDS-QUAMRI Grant number: 634541 (A. Henning, T. Borbath, and S. Murali-Manohar), SYNAPLAST Grant number: 679927 (A. Henning, A.M. Wright, and S. Murali-Manohar), and Cancer Prevention and Research Institute of Texas (CPRIT) Grant number: RR180056 (A. Henning)

.

Words total: 5021

*Correspondence to Saipavitra Murali-Manohar M.Sc., High-Field Magnetic Resonance, Max Planck Institute for Biological Cybernetics, Tübingen, Germany. Telephone: +49 7071 601 1725.

E-mail: saipavitra.murali.manohar@tuebingen.mpg.de

Abstract

Purpose:

Several localization schemes and data processing techniques have been developed for better detection and accurate quantification of metabolites in the human brain. This study proposes a two-dimensional (2D) J-resolved metabolite-cycled (MC) semiLASER localization sequence at 9.4 T in the human brain.

Methods:

Initially, the J-resolved MC semiLASER localization sequence with maximum echo sampling (MES) scheme was optimized using phantom measurements. Then metabolite spectra were acquired using the developed sequence from a voxel in the occipital lobe at 9.4 T. In order to account for the underlying macromolecular (MM) spectrum, J-resolved MM spectra were acquired using a double inversion recovery (DIR) J-resolved MC semiLASER with MES scheme. Spectral fitting was performed with ProFit 2.0 using simulated basis set from VesPA. Metabolite concentrations were calculated using internal water referencing.

Results:

J-resolved MC semiLASER with optimized sequence parameters was developed at 9.4 T to quantify human brain metabolites. Quantification values for 16 metabolites in mmol/kg are reported after correcting for proton contribution, tissue content, and relaxation effects of both water and metabolites at 9.4 T. Bland-Altman plots were calculated in order to compare the differences in concentration values from this study versus values from a previous 1D MRS study.

Conclusion:

2D J-resolved MC semiLASER sequence was optimized for the first time at 9.4 T. The sensitivity in the detection of J-coupled metabolites such as glutamine, glucose, lactate etc., improved with the use of 2D MRS technique along with MES scheme.

Keywords: 2D J-resolved spectroscopy, Ultra-high field, Maximum echo sampling, ProFit 2.0, Quantification, J-semiLASER, Metabolite-cycling

1. Introduction

Single voxel proton magnetic resonance spectroscopy (^{1}H-MRS) is a popular non-invasive technique used to study the metabolism in the human brain. It enables detection and quantification of the neurochemical profile in a particular region of interest, thereby aids in setting appropriate biomarkers for various pathologies in the human brain[1]. However, complex spectral patterns and severe spectral overlap often pose a challenge in quantifying individual metabolite concentrations[2]. Therefore, enhancing the signal-to-noise ratio (SNR) and spectral resolution has always been one of the aims of the MRS community.

One technique used by the NMR community to reduce spectral overlap is multi-dimensional spectroscopy[3,4]. Homonuclear two-dimensional (2D) techniques such as correlation spectroscopy and J-resolved spectroscopy were shown to be feasible in vivo at 1.5, 3 and 7 T[5–7] and hold the promise to yield accurate quantification results for a large number of metabolites in clinical trials of neurological and psychiatric disorders[8–14]. Nevertheless, this technique owes to longer measurement durations and requires non-standard pre-processing, fitting and quantification routines.

In two-dimensional (2D) J-resolved spectroscopy[15], the spectral information is spread into two orthogonal axes by adding a step-wise increasing evolution delay in the pulse sequence. This helps improve specificity in the detection of J-coupled metabolites. To further improve detection sensitivity maximum echo sampling (MES)[16] was introduced for in vivo 2D 1H MRS[8,17]. In MES scheme, acquisition begins right after the final crusher gradient of the last refocusing pulse in the localization technique. Later Schulte et al[15] compared the sensitivity values of short-echo point-resolved spectroscopy (PRESS), JPRESS with traditional half echo sampling (where the acquisition begins at the echo top) and JPRESS with MES. JPRESS with MES had increased sensitivity in comparison to traditional half echo sampling. Yet another advantage of MES is that it adds a tilt to the peak tails in the spectrum[15] and thus largely reduces overlap of the water peak tail with the metabolites peaks of interest.

Another means to clearly distinguish more peaks is ultra-high field (UHF) (≥ 7 T) ^{1}H MRS[18,19]. It is well known that spectroscopy studies at UHF benefit from both increased spectral resolution and improved SNR in comparison to lower field strengths. However, at UHF B_1^+ inhomogeneity is one of the crucial challenges posed. Also with increasing static B_0 field strength, chemical shift displacement error between the metabolite peaks increases.

Using simulation and experimental methods at 3 T and 7 T Edden et al[20] showed that the chemical shift displacement effect causes spatially dependent differences in J-evolution of coupled spin systems in JPRESS spectra. Due to the larger spectral dispersion along with reduced peak transmit field strength B_1^+, the chemical shift displacement error is increasing with increasing field strength. The appearance of additional J-refocused peaks result in loss of intensity in the J-resolved peaks and more spectral overlap thereby leading to uncertain spectral quantification. However, Lin et al[6] compared the spectral quality of JPRESS, J-resolved semiLASER and J-resolved LASER sequences and demonstrated that the use of adiabatic pulses reduced the appearance of J-refocused peaks to a great extent due to their higher bandwidth. Adiabatic pulses in the localization schemes are also effective in reducing the effect of B_1^+ inhomogeneity at UHF[21]. Both the implications discussed above emphasize the need to use adiabatic localization when implementing J-resolved spectroscopy at UHF.

Therefore, in this work, we developed a 2D J-resolved metabolite-cycled (MC) semiLASER sequence at 9.4 T for the first time. Implementing MC[21,22] for J-resolved spectroscopy eliminates the need for acquiring an interleaved water reference for the sake of eddy current correction or frequency alignment. This in turn significantly reduces the scan duration when the aim is to calculate metabolite ratios, thereby tackling one of the problems of 2D spectroscopy in vivo.
Spectral fitting was performed using ProFit v2.0[23], a dedicated 2D fitting software, which incorporates the theory of LCModel[24] and VARPRO[25] in attaining a global minimum. The non-linear fitting routine iterates four times, each time with increasing degrees of freedom. Fuchs et al[26] enhanced the software by adding a spline baseline fit and a spline lineshape model using self-deconvolution. Additionally, in order to account for the MM contribution in the 2D metabolite spectra, an experimentally acquired 2D MM spectra was used during the fitting procedure.

Subsequently, quantification of metabolites was performed using the internal water referencing method taking into account the tissue composition in the voxel of interest, and water concentration. The concentration values were also further corrected for T_1 relaxation times of both metabolites[27] and water[28] at 9.4 T. Finally, quantification results obtained with 2D J-resolved spectroscopy and 1D MRS at 9.4 T were compared with each other and against concentrations published in previous literature. To the best of our knowledge, the effect of bringing together the two complementary approaches of UHF and 2D J-resolved spectroscopy to enhance spectral resolution and hence spectral quantification has not been evaluated yet. This work is an extension of the initial results reported earlier in a conference abstract[29].

2. Methods

2.1 Study Design

All measurements were performed on a 9.4 T Siemens Magnetom whole-body MRI scanner (Siemens Healthineers, Erlangen, Germany) using a home-built coil[30] with eight transmit and sixteen receive channels. Eleven healthy volunteers (6 male and 5 female, age: 28.0 ± 2.3 years) participated in this study. Five volunteers returned for a second visit for the acquisition of 2D MM signal. The study was approved by the local ethics board, and written informed consent was provided by the volunteers prior to the measurements.

2.2 MRS Sequence

Figure 1a shows the J-resolved metabolite-cycled (MC) semiLASER sequence diagram. The asymmetric adiabatic MC[31] pulse (duration: 22.4 ms) preceded the conventional semiLASER[31] block. A hamming filtered 90 degree-sinc pulse[31] (bandwidth: 8000 Hz) was used for excitation. This pulse was followed by two pairs of adiabatic full passage pulses (duration: 3.5 ms, bandwidth: 8000 Hz). The indirect dimension (t_1) was created by inserting an incrementally increasing time delay of $\Delta t/2$ between the last pair of adiabatic full passage pulses[31], which encodes the J-evolution. The acquisition of the signal began immediately after the final crusher gradient of the last adiabatic full passage pulse which is called maximum echo sampling (MES) scheme[15].

In order to optimize the number of TE steps n, knowledge of T_2 relaxation times of metabolites in vivo at 9.4 T was utilized from Murali-Manohar et al[32]. Additionally, phantom measurements (Figure 2) were performed with different time increment steps (Δt: 2, 3, and 4 ms) and different number of TE steps (n: 50, 85) to confirm the absence of J-refocused peaks and whether the peaks are distinctly J-resolved without noise and truncation artifacts in the indirect dimension.

A double inversion recovery (DIR) block preceding the J-resolved MC semiLASER sequence (Figure 1b) was used for the acquisition of macromolecular signal. The inversion pulse[33] duration was 15 ms and the inversion bandwidth was approximately 1650 Hz. The optimized inversion times[33,34] (TI_1/TI_2) combination of 2360 and 625 ms was used in the DIR block.

2.3 Data Acquisition

2.3.1 Anatomical Imaging

MP2RAGE[28] images (resolution: 0.6 × 0.6 × 0.6 mm^3) were acquired while using the coil in volume mode driving power to all the eight transmit coil elements. Following this, the volunteer was instructed to remain stationary on the patient table while the coil setup was changed to suit the spectroscopy measurements (see 2.3.2).

For the MM acquisition, only 2D FLASH images were acquired which then were co-registered to the previously acquired MP2RAGE images using rigid body transformation.

2.3.2 Spectroscopy Measurements

For the spectroscopy measurements, power was driven to the bottom three coil elements near the region of interest using unbalanced three-way Wilkinson splitter[31]. A localizer was reacquired to ensure there was no motion of the volunteer between the anatomical and the spectroscopy scan. This was followed by acquisition of high-resolution 2D FLASH images (in-plane resolution: 0.7 × 0.7 mm^2, slice thickness: 3.5 mm, 25 slices) in the sagittal and transversal orientations to position the spectroscopy voxel (2 × 2 × 2 cm^3) in the occipital lobe. Localized second-order shimming was performed using FAST(EST) MAP[35] setting the shim volume to be 150% of the volume of the voxel of interest. Then, voxel-based power optimization[36,37] was performed to ensure that the adiabatic conditions were fulfilled.

Two-dimensional metabolite spectra were acquired using the J-resolved MC semiLASER sequence (Figure 1a) (TR: 6000 ms, averages: 8 per TE step, four-step phase cycling) described above in the MRS Sequence section. TE ranged from 24 to 194 ms (n: 85) incremented in steps of Δt = 2ms. In addition, 2D water reference signals were acquired (average per TE: 1) to avoid any effect due to MC pulse. The transmit reference frequency for the water reference sequence was set to 4.7 ppm.

In order to account for the MM contribution in the 2D metabolite spectra, 2D MM spectra were acquired from five healthy volunteers using the DIR sequence (TI_1/TI_2 : 2360/625 ms) shown in Figure 1b. TE ranged from 24 to 144 ms (n: 60) since MM signal decays faster in comparison to metabolite signal[32]. All the other acquisition parameters were identical to the metabolite spectra except the TR which was set to 8000 ms.

2.4 Data Preprocessing

Spectroscopy raw data were preprocessed using an in-house MATLAB (version 2016a, MathWorks, Natick, MA) tool. Both metabolite and MM data were reconstructed as described in Giapitzakis et al[31]. Firstly, the data were frequency and phase-aligned based on the water signal in the time domain for 85 and 60 blocks for metabolite and MM data respectively. This was followed by metabolite-cycling subtraction and then the data were averaged within each TE block. Then Eddy current correction was performed using the phase information from the MC water signal. Signals from all 16 receive channels were then combined using the SVD method. The

metabolite and MM data were truncated at 250 and 150 ms respectively for better SNR. Automated zeroth- and first-order phase corrections were performed in the J-resolved spectroscopy preprocessing tool[15,38] which is a part of ProFit. The applied phase correction was visually verified for correctness as recommended by the recent consensus article[39]. Using the same ProFit preprocessing tool, residual water in both the dimensions in the spectra was removed using a HSVD method. The final 2D spectrum displayed is after applying Fourier transformation to the data in both the dimensions. SNR of the NAA(CH_3) peak at 2.008 ppm was calculated as the peak intensity from the real part of the spectrum with respect to the noise window from -4.0 to -1.0 ppm.

2.5 MP2RAGE Segmentation

The high-resolution MP2RAGE images were segmented into gray matter (GM), white matter (WM) and cerebrospinal fluid (CSF) fractions using SPM12[40]. 2D FLASH images acquired during the MM scan session were co-registered to the MP2RAGE images acquired during the first scan session for four volunteers. A home-built Python (v3.7) tool was used to determine the tissue fractions in the voxels of interest.

2.6 Spectral Fitting

Metabolite basis sets corresponding to 85 TE steps were simulated using VesPA considering full quantum mechanical density matrix calculations for the semiLASER sequence including the excitation and adiabatic full passage pulse shapes. The simulation also incorporated the sequence timings including the MES scheme. The following metabolites were simulated: n-acetyl aspartate (NAA), NAA glutamate (NAAG), γ-aminobutyric acid (GABA), aspartate (Asp), creatine (Cr), glutamate (Glu), glutamine (Gln), glucose (Glc), glutathione (GSH), glycerophosphocholine (GPC), glycine (Glyc), myo-inositol (mI), scyllo-inositol (Scy), lactate (Lac), phosphocreatine (PCr), phosphocholine (PCho), phosphoethanolamine (PE), and taurine (Tau). Their chemical shifts and coupling constants were chosen according to Govindaraju et al[41], except for the coupling constant of GABA, for which the values from Near et al[42] were chosen. Subsequently different metabolite peaks were scaled to correct for the number of proton contributions. GPC, PCho and PE combined together is denoted by tCho. Finally, all the 85 1D basis sets and the measured MM spectra were combined to form a complete 2D basis set using an in-house written MATLAB script.

All the metabolite spectra were fitted using ProFit 2.0[26] (2D PRiOr knowledge FITting). It takes the exponential decay of the metabolite signal and the scalar coupling constants into account and fits the J-resolved spectrum after 2D Fourier transform in both the direct and the indirect dimensions.

2.7 Quantification

Metabolite concentrations $[\mathrm{M}]$ were quantified in mmol/kg from the ProFit 2.0 concentration results after fitting the metabolite spectra acquired from all subjects.

For internal water referencing, the concentration values from fitting were corrected for tissue water fractions and relaxation times as follows:

$$[M] = \frac{S_{Met} \times (f_{GM} \times R_{H20_{GM}} + f_{WM} \times R_{H20_{WM}} + f_{CSF} \times R_{H20_{CSF}})}{S_{H20} (1 - f_{CSF}) \times R_{Met}} \times \frac{2}{(1 + F_S)} \times [H_2O]$$

where $f_y = \frac{f_{y\_vol} \times a_y}{f_{GM\_vol} \times a_{GM} + f_{WM\_vol} \times a_{WM} + f_{CSF\_vol} \times a_{CSF}}$

Here y corresponds to either GM, WM, or CSF; f_{y_vol} is the fraction of the respective tissue type determined by segmentation; a_y are the relative densities of MR-visible water for the given tissue types (78%, 65%, 97% for GM, WM and CSF respectively); these a_y values were further scaled for the relative densities of GM and WM tissue (1.04 g/ml)[43–46]. To arrive at mmol/kg units , the concentration of the MR-visible water [H_2O] within a voxel was considered in molal concentration and assumed to be that of pure water (55,510 mmol / kg)[47]. S_{Met} is the signal from the metabolite peak.

ProFit 2.0 accounts for the T_2 relaxation times of water and metabolites between the second TE and the last TE by including respective line shape models specific to each metabolite in the fitting algorithm . Therefore, T_2 correction was included only for the first TE = 24 ms.

$$R_{H2O\_y} = \left[1 - \exp\left[-\frac{TR}{T1_{H2O_y}}\right]\right] \exp\left[-\frac{TE}{T2_{H2O_y}}\right]$$

is the relaxation correction factor for each tissue type y. $T1_{H2O_y}$ is the T_1 relaxation time of water in the tissue type y; in particular, the T_1 relaxation times of water in GM are $T1_{H20\_GM}$ = 2120 ms; in WM are $T1_{H20\_WM}$= 1400 ms; and in CSF are $T1_{H20\_CSF}$ = 4800 ms at 9.4 T[28]. $T2_{H2O}$ is the T_2 relaxation time of water in the tissue type y; $T2_{H2O\_GM}$ = 37 ms, $T2_{H2O\_WM}$ = 30 ms, and $T2_{H2O\_CSF}$ = 181 ms.

$$R_{Met} = \left(1 - \exp\left[-\frac{TR}{T1_{Met}}\right]\right)\left[-\frac{TE}{T2_{Met}}\right]$$

is the relaxation correction term for metabolites. $T1_{Met}$ values from were taken Wright et al[27] and $T2_{Met}$ values were taken from Murali-Manohar et al[32]. The denominator $1 - f_{CSF}$ was implemented for partial-volume correction arising from contributions of CSF to the voxel volume. The factor $\frac{2}{1+Fs}$ was introduced to correct for the multiplication of even numbered acquisitions with the scaling factor (F_s) from metabolite cycling.

2.8. Statistics

The concentration values reported in this study are mean values from eleven healthy volunteers and the standard deviation between them. Recent 1D MRS studies[27,48–52] at ultra-high field reporting concentrations in mmol/kg from a similarly located voxel in the occipital lobe as chosen for this study were considered for comparison.

For a more thorough statistical comparison data from previous 1D MRS study[27,48] at 9.4 T was used. The study[27,48] used MC-semiLASER sequence with same sequence parameters (TE/TR: 24/6000 ms) as used in this study. Seven out of eleven healthy volunteers participated in both studies and hence paired values were considered for statistical analysis. Spectral fitting was performed in LCModel[53] and MM contribution was accounted for from experimentally measured MM spectra with DIR method (TI /TI : 2360/625 ms). Two-tailed nonparametric Wilcoxon signed

rank test was performed (α < 0.05) for matched data. Adjusted *p*-values were obtained using Holm-Bonferroni correction for multiple comparisons ($\frac{\alpha}{N} = 0.0038$).

Bland-Altman plots[54] were calculated to show the differences in the quantification values between this study (2D MRS) and the previous 1D MRS study[27,48]. The most updated concentration values from the 1D MRS study[27,48] were considered. Let i denote the subject and k the metabolite of interest; superscripts $2D$ and $1D$ represent the 2D and 1D MRS study respectively. Then, the Bland-Altman calculations for metabolite concentrations in mmol/kg is given by

$$c_{i,k} = \frac{\left(c_{i,k}^{2D} - c_{i,k}^{1D}\right)}{mean\left(c_{i,k}^{2D}, c_{i,k}^{1D}\right)}$$

3. Results

3.1 Voxel Content and Spectral Quality

The spectra from the phantom tests (n: 50, Δt: 2, 3, and 4 ms) showed stronger 't_1 ridges'[20] when TE_{max} was shorter (Figure 2). In other words, when TE_{max} = 124 ms, the 't_1 ridges'[20] were the strongest. t_1 noise was the least when TE_{max} = 224 ms. When TE_{max} was set to 100, 99, and 100 ms for Δt: 2 ms (n: 50), 3 ms (n: 33), and 4 ms (n: 25) respectively, the 't_1 ridges' were not seen to be impacted (Supporting information figure S1). However, Δt: 2 ms corresponded to higher SNR since it allows for more number of averages.

Figure 3 shows a phantom metabolite spectrum (n: 85, Δt: 2 ms, TE_{max}: 194 ms) in the absolute magnitude mode. There are no prominent J-refocused peaks appearing in the spectrum or there are no visible truncation artifacts or t_1 noise in the indirect dimension. Even though the t_1 noise seemed minimum for a TE_{max} = 224 ms, TE_{max} = 194 ms was chosen for in vivo studies as T_2 relaxation times are generally longer in phantom than in in vivo tissues. Δt was set to 2 ms since this allows for a higher number of averages within the given range of TE which is essential for a good SNR in vivo spectrum.

Figure 4 shows a representative single subject 2D MC J-resolved semiLASER metabolite spectrum (n: 85, Δt: 2 ms) with an inlay showing the voxel position. The average tissue content of the metabolite spectroscopy measurement voxel in the occipital lobe of eleven healthy volunteers was GM/WM/CSF = 67 ± 8/ 29 ± 9/ 4 ± 1 % respectively. The 2D metabolite spectra obtained from voxels in the occipital lobe showed uncoupled peaks lying on the f_1 = 0 Hz axis. This is because during t_1, only the coupling information is obtained. However, the J-coupled multiplets are resolved at an angle of 45° with respect to f_1 = 0 Hz since t_2 holds both chemical shift and coupling information. The SNR of the NAA(CH_3) peak was 906 ± 147 indicating that the spectra were of good quality. Also, the spectra did not show any major artifacts such as lipid contamination or water tails. Therefore, no data sets were excluded from further analysis.

The summed MM spectrum from five healthy volunteers is shown in Figure 5. $M_{0.92}$, $M_{1.21}$, $M_{1.39}$, $M_{1.67}$, $M_{2.04}$, $M_{2.26}$, $M_{2.56}$, $M_{2.70}$, $M_{2.99}$ and $M_{3.86}$ are clearly seen to have J-resolved peaks. On an average, the MM spectroscopy voxel (five healthy volunteers) had GM/WM/CSF = 61 ± 10/ 35 ± 8/ 4 ± 3 % respectively.

Figure 6a shows the summed downfield spectrum (5.1 to 9.5 ppm) from eleven healthy volunteers. The NAA (7.82 ppm) peak and $DF_{6.83}$ peaks are observed to split into doublets in the

spectrum. Also, the $DF_{5.97}$ peak begins to J-resolve into a doublet. In addition, the zoomed view of the downfield spectrum (Figure 6b) from 8.7 to 9.45 ppm shows the two low SNR NAD^+ multiplet peaks of nicotinamide moiety that are present at 8.83 and 9.33 ppm.

3.2 Spectral Fitting

A representative metabolite 2D spectral fit is shown in Figure 7. The minimum residual shows the good quality of fit indicating that the metabolites included in the basis set modeled the acquired data sufficiently well. The fit quality was similar for all the datasets.

3.3 Concentrations

Supporting information figure S2 shows a bar plot of concentrations of metabolites calculated in mmol/kg. Table 1 and Figure 8 compares the quantification results in mmol/kg from this study with previous literature[27,48–52].

Significant differences in concentrations obtained from 1D[27,48] and 2D MRS data ($p < 0.0038$) are denoted by an asterisk (*) in Table 1. Bland Altman plots are shown for 12 metabolites in Figure 9 comparing 2D MRS data and 1D MRS data[27,48]. The most updated concentration values from the 1D MRS study[27,48] are used here.

4. Discussion

4.1 Spectral Quality

The phantom tests performed to optimize the step size (Δt) along with the knowledge of T_2 relaxation times of metabolites in vivo at 9.4 T from Murali-Manohar et al.,[32] led to the choice of Δt = 2 ms and number of steps, n = 85 for acquisition in vivo. There was sufficient sampling (500 Hz) in the indirect dimension to cover the frequency range of interest in all cases. The final choice of the scan parameters was made since the appearance of 't_1-ridges'[20] due to t_1 noise and sinc character from t_1 truncation was diminished significantly by longer TE_{max} keeping in mind also comfortable scan durations. Furthermore, T_2-weighting signal loss was avoided largely by setting the first echo time TE_{min} to be 24 ms, as short as possible. According to Murali-Manohar et al[52], the T_2 relaxation times in the gray-matter rich voxel present in the occipital lobe ranged from ~45 to 110 ms. Thus, the chosen parameters swept a decent range of TEs from 24 to 194 ms.

Using the adiabatic J-resolved semiLASER localization sequence proposed herein resulted in a chemical shift displacement of 5% per ppm for each voxel dimension (bandwidth: 8000 Hz). Lin et al[6] showed that the intensity of the J-refocused peaks can be reduced by a factor of

$$(1 - \frac{\Delta\delta.B_0}{BW})$$

where $\Delta\delta$ is the chemical shift difference in ppm of the spins A and X in an AX spin system, B_0 is the frequency of the static magnetic field in MHz and BW is the bandwidth of the refocusing pulse. Considering lactate coupled peaks at 1.31 and 4.09 ppm, the resulting reduction in the intensity of the J-refocused peaks is 86%. Therefore, there were barely any J-refocused peaks (please see Figure 3) and no J-refocused peaks in Figure 4 that usually appear because of spatially dependent evolution (because of limited bandwidth refocusing pulses) of the J-coupled peaks[20]. Consequently, the J-resolved multiplet peaks retained maximum possible intensity.

Implementation of the MES scheme resulted in tilt of the peak tails and hence y avoids the overlap of phase-twisted line shapes when f_1 = 0 Hz. For each TE increment, when the time delay introduced is Δt, the acquisition starts $\Delta t/2$ earlier with respect to the echo top. Therefore, data corresponding to each TE had to be aligned with the corresponding echo tops by shifting them in the time domain as described in Schulte et al[15]. The tilt created in the time domain directly translates after a Fourier transform to the frequency domain where the peak tails along the direct dimension (f_2) are also tilted by 26.6°. This minimizes the overlap of the peak tails with the metabolite peaks, thus reducing contamination and allowing for better quantification of the metabolite signals especially of J-coupled spin systems.

The knowledge of T_2 relaxation times of MM (approximately ranging from 15 to 37 ms in GM-rich voxel) at 9.4 T from Murali-Manohar et al[32] was utilized in setting n = 60 (covering TE: 24 to 144 ms) for the acquisition of MM spectra using DIR MC J-resolved semiLASER. By TE_{max} = 144 ms, MM signal decayed completely. Therefore, for n = 61 to 85 no corresponding MM spectra were provided in the basis set for metabolite spectral fitting. This also reduced the acquisition duration making it feasible for in vivo investigations. $M_{0.92}$, $M_{1.21}$, $M_{1.39}$, $M_{1.67}$, $M_{1.75}$, $M_{2.04}$, $M_{2.26}$, $M_{2.56}$, $M_{2.70}$, $M_{2.99}$ and $M_{3.86}$ are observed to undergo J-evolution and they appear as multiplets in the 2D J-resolved spectrum shown in Figure 5 indicating that these peaks have J-coupled spin systems. This observation agrees with Behar et al[55] who reported the above-mentioned peaks (except $M_{2.56}$ and $M_{2.70}$) as J-coupled MM observed from COSY and J-resolved spectra of dialyzed human cerebral cytosol at 8.4 T. Giapitzakis et al[56] reported $M_{2.56}$ and $M_{2.70}$ peaks for the first time and assigned them to β-methylene protons of aspartyl groups which correspond to doublet-of-doublets. Figure 5 also shows $M_{1.75}$, $M_{1.91}$, $M_{1.95}$, $M_{2.32}$, $M_{2.36}$, $M_{3.02}$, $M_{3.09}$, $M_{3.17}$, and $M_{3.28}$ peaks which are observed here in 2D MRS, but not in 1D MRS[32–34] in the human brain at 9.4 T. These MM peaks other than $M_{1.75}$, $M_{2.32}$ and $M_{3.28}$ were previously only reported at 17.2 T in rat brain by Lopez et al[57].

All the downfield peaks reported by Borbath et al[58] at 9.4 T in vivo were present also in the 2D downfield spectra in this study (Figure 6). Since there was no water suppression scheme implemented it was also possible to detect some of the exchanging downfield peaks ($DF_{5.75}$, $DF_{6.83}$)[59] in 2D. It was unclear from the 1D spectra[58] whether the $DF_{6.83}$ peak could be assigned to Gln (a singlet) or Tyrosine (multiplets). However, it can be seen from Figure 6 that the $DF_{6.83}$ resonance splits into two peaks across f_1 = 0 axis. Nagarajan et al[60] reported that the four phenyl ring protons of tyrosine give rise to multiplets in their 2D L-COSY study in the human brain at 3 T[60]. Also, fitting of amino acid spectral models to the downfield spectra results in fitting Tyrosine multiplet to the $DF_{6.83}$ peak[61]. This leads to potentially assigning the peak detected at $DF_{6.83}$ to Tyrosine. A quadruplet splitting ($DF_{5.48}$) at around 5.48 ppm can also be observed from the 2D downfield spectrum. This peak has not been reported earlier and further investigation is necessary in order to confirm the peak presence. Since this study focused on the upfield metabolites, the transmit reference frequency was set to 2.4 ppm in the upfield part of the spectrum. However, a study focusing on the downfield part of the ^{1}H spectra in the human brain using 2D MRS with the transmit reference frequency set to 7.0 ppm could be of interest since it could lead to better characterization of some of the unassigned peaks.

2D MRS acquisition technique has longer scan durations, especially at UHF due to SAR constraints. In particular, 2D J-resolved MC-semiLASER and 2D J-resolved DIR MC-semiLASER sequences had an acquisition duration of 68 and 128 minutes respectively. This is a disadvantage compared to 1D MRS techniques at UHF, which typically have shorter scan duration in

comparison and are thus better suited for clinical applications. On the other hand, the 2D MRS technique at UHF looks promising to answer some basic research questions such as assigning unlabeled peaks in the downfield part of the spectrum or in understanding the overlap and J-coupling behavior of the MM peaks. It could also be utilized in quantifying lower SNR J-coupled metabolites in order to understand mechanisms of brain energy metabolism, neurotransmission, or antioxidants.

4.2 Spectral Fitting

Edden and Barker[20] suggested that it is important to include the bandwidth of the refocusing pulse while simulating the basis sets in order to also account for the J-refocused peaks if any. Therefore, the basis sets simulated to fit the 2D metabolite spectra using VesPA included real pulse shapes with exact durations, bandwidths and the MES scheme. Therefore, it can be seen from Figure 7 that the simulated 2D basis set fits the data very well.

Spectral fitting of 2D J-resolved data using Profit 2.0 can also be used to determine T_2 relaxation times of metabolites as shown by Wyss et al[62].

4.3 Metabolite Concentrations

This study quantifies and reports concentration values of 16 metabolites in mmol/kg using an adiabatic 2D J-resolved localization technique at 9.4T in the human brain for the first time. The calculated millimolal concentration values lie within the range of values that were reported in previous literature[27,48–52] for most of the metabolites. Mekle et al[50] and Deelchand et al[49] did not perform T_2 relaxation correction. However, these studies used shorter TE times; therefore, the contribution from T_2 weighting may have been insignificant. All the studies included experimentally acquired MM spectrum during the fitting procedure. Mekle et al[50] set tCr to 8 mmol/kg.

For metabolites with J-coupled spin systems, low peak amplitudes and/or overlap with larger singlets such as GABA, GSH, NAAG and Tau the concentrations measured from this study are in line with previous 1D MRS studies at 7T[51,63] and 9.4T[27,48]. Moreover, the 2D MRS technique could decently quantify Glc, Lac, and Glyc, which are otherwise challenging to quantify in 1D MRS studies even at 9.4 T. Separation of PCr and Cr was achieved in this study along with two previous 9.4T study[32] and two previous 7T studies[51,63]. The concentration of Asp measured in this study is in line with two out of three previous 9.4T[27,48,64] and two 7T human brain studies[51,63]. Gln concentrations from this study are closely matching those measured in two previous 7T studies[50,65] and one 9.4T study[49], but deviate from results of two other previous 1D MRS studies at 9.4T[27,48,52]. mI concentrations are higher in this study in comparison to all previous studies due to a possible oppositely phased residual mI peak in the experimental MM spectra[34].

Figure 9 shows Bland-Altman plots[54] for 12 metabolites indicating changes in metabolite concentrations of individual subjects while using 1D and 2D MRS at 9.4T (seven healthy volunteers were considered as paired datasets). The mean of the metabolite concentrations are plotted along the x-axis and the difference in the measured concentration of metabolites between 1D and 2D MRS along the y-axis. These Bland-Altman plots enable us to visually assess the differences in the concentrations measured using 1D versus 2D MRS. A statistical significant difference is found in the concentration of Gln between 1D and 2D MRS study. Gln concentration estimate from the 1D MRS study[27,48] is higher than expected. Tau also has a significant difference; however, the concentration of Tau varies across different studies and the concentration from 2D MRS data agrees with Marjanska et al[51]. Baeshen et al[66] performed a similar analysis to analyze

the test-retest reliability of measuring GABA and Glx with JPRESS, PRESS, and MEGA-PRESS at 3T. They concluded that MEGA-PRESS and JPRESS reliably detected GABA at 3T when compared to PRESS. However, Glx was measured reliably with PRESS, MEGA-PRESS and JPRESS[66].

5. Conclusion

The 2D J-resolved MC-semiLASER sequence implemented at 9.4 T quantified the lower SNR and J-coupled metabolites such as GABA, Gln, Lac, and Glc. Despite longer acquisition durations of 2D J-resolved MRS at UHF, it still seems beneficial to answer open questions in the field of MRS including assigning unlabeled peaks in the downfield part of the spectrum, understanding J-coupling behavior of the MM peaks (which are severely overlapped broad peaks in 1D MRS), and to quantify the lower SNR J-coupled metabolites with accuracy. The quantification results in mmol/kg are reported for 16 metabolites in the occipital lobe and they are compared with previous literature.

Acknowledgement

The authors would like to thank Brian Soher for providing the Vespa simulation code for semiLASER sequence.

References

1. Oz G, Alger JR, Barker PB, et al. The MRS Consensus Group. Clinical proton MR spectroscopy in central nervous system disorders. *Radiology*. 2014;270(3):658-679. doi:10.1148/radiol.13130531
2. Stanley JA, Pettegrew JW, Keshavan MS. Magnetic resonance spectroscopy in schizophrenia: Methodological issues and findings - Part I. *Biol Psychiatry*. 2000;48(5):357-368. doi:10.1016/S0006-3223(00)00949-5
3. Aue WP, Bartholdi E, Ernst RR. Two-dimensional spectroscopy. Application to nuclear magnetic resonance. *J Chem Phys*. 1976;64(5):2229-2246. doi:10.1063/1.432450
4. Macura S, Ernst RR. Elucidation of cross relaxation in liquids by two-dimensional N.M.R. spectroscopy. *Mol Phys*. 1980;41(1):95-117. doi:10.1080/00268978000102601
5. Ryner LN, Sorenson JA, Thomas MA. Localized 2D J-resolved 1H MR spectroscopy: Strong coupling effects in vitro and in vivo. *Magn Reson Imaging*. 1995;13(6):853-869. doi:10.1016/0730-725X(95)00031-B
6. Lin M, Kumar A, Yang S. Two-dimensional J-resolved LASER and semi-LASER spectroscopy of human brain. *Magn Reson Med*. 2014;71(3):911-920. doi:10.1002/mrm.24732
7. Thomas MA, Hattori N, Umeda M, Sawada T, Naruse S. Evaluation of two-dimensional L-COSY and JPRESS using a 3?T MRI scanner: from phantoms to human brainin vivo. *NMR Biomed*. 2003;16(5):245-251. doi:10.1002/nbm.825
8. Kotitschke K, Jung H, Nekolla S, Haase A, Bauer A, Bogdahn U. High-resolution one-and two-dimensional 1H MRS of human brain tumor and normal glial cells. *NMR Biomed*. 1994;7(3):111-120. doi:10.1002/nbm.1940070303
9. Ke Y, Cohen BM, Bang JY, Yang M, Renshaw PF. Assessment of GABA concentration in human brain using two-dimensional proton magnetic resonance spectroscopy. *Psychiatry Res* -

Neuroimaging. 2000;100(3):169-178. doi:10.1016/S0925-4927(00)00075-5

10. Rémy C, Grand S, Laï ES, et al. 1H mrs of human brain abscesses in vivo and in vitro. *Magn Reson Med*. 1995;34(4):508-514. doi:10.1002/mrm.1910340404

11. Jensen JE, de B. Frederick B, Renshaw PF. Grey and white matter GABA level differences in the human brain using two-dimensional, J-resolved spectroscopic imaging. *NMR Biomed*. 2005;18(8):570-576. doi:10.1002/nbm.994

12. Ramadan S, Lin A, Stanwell P. Glutamate and glutamine: A review of in vivo MRS in the human brain. *NMR Biomed*. 2013;26(12):1630-1646. doi:10.1002/nbm.3045

13. Walter M, Henning A, Grimm S, et al. The relationship between aberrant neuronal activation in the pregenual anterior cingulate, altered glutamatergic metabolism, and anhedonia in major depression. *Arch Gen Psychiatry*. 2009;66(5):478-486. doi:10.1001/archgenpsychiatry.2009.39

14. Soeiro-De-Souza MG, Pastorello BF, Da Costa Leite C, Henning A, Moreno RA, Otaduy MCG. Dorsal anterior cingulate lactate and glutathione levels in euthymic bipolar i disorder: 1H-MRS study. *Int J Neuropsychopharmacol*. 2016;19(8):1-8. doi:10.1093/ijnp/pyw032

15. Schulte RF, Lange T, Beck J, Meier D, Boesiger P. Improved two-dimensionalJ-resolved spectroscopy. *NMR Biomed*. 2006;19(2):264-270. doi:10.1002/nbm.1027

16. Macura S, Brown LR. Improved sensitivity and resolution in two-dimensional homonuclear J-resolved NMR spectroscopy of macromolecules. *J Magn Reson*. 1983;53(3):529-535. doi:10.1016/0022-2364(83)90227-5

17. Kühn B, Dreher W, Leibfritz D, Heller M. Homonuclear uncoupled 1H-spectroscopy of the human brain using weighted accumulation schemes. *Magn Reson Imaging*. 1999;17(8):1193-1201. doi:10.1016/S0730-725X(99)00027-2

18. Ladd ME, Bachert P, Meyerspeer M, et al. Pros and cons of ultra-high-field MRI/MRS for human application. *Prog Nucl Magn Reson Spectrosc*. 2018;109:1-50. doi:10.1016/j.pnmrs.2018.06.001

19. Henning A. Proton and multinuclear magnetic resonance spectroscopy in the human brain at ultra-high field strength: A review. *Neuroimage*. 2018. doi:10.1016/j.neuroimage.2017.07.017

20. Edden RAE, Barker PB. If J doesn't evolve, it won't J-resolve: J-PRESS with bandwidth-limited refocusing pulses. *Magn Reson Med*. 2011;65(6):1509-1514. doi:10.1002/mrm.22747

21. Giapitzakis I, Shao T, Avdievich N, Mekle R, Kreis R, Henning A. Metabolite-cycled STEAM and semi-LASER localization for MR spectroscopy of the human brain at 9.4T. *Magn Reson Med*. 2018;79(4):1841-1850. doi:10.1002/mrm.26873

22. Dreher W, Leibfritz D. New method for the simultaneous detection of metabolites and water in localized in vivo1H nuclear magnetic resonance spectroscopy. *Magn Reson Med*. 2005;54(1):190-195. doi:10.1002/mrm.20549

23. Fuchs A, Boesiger P, Schulte RF, Henning A. ProFit revisited. *Magn Reson Med*. 2014;71(2):458-468. doi:10.1002/mrm.24703

24. Provencher SW. Automatic quantitation of localized in vivo 1H spectra with LCModel. *NMR Biomed*. 2001;14(4):260-264.

25. van der Veen JWC, de Beer R, Luyten PR, van Ormondt D. Accurate quantification of in vivo 31P NMR signals using the variable projection method and prior knowledge. *Magn Reson Med*. 1988;6(1):92-98. doi:10.1002/mrm.1910060111

26. Fuchs A, Boesiger P, Schulte RF, Henning A. ProFit revisited. *Magn Reson Med*. 2014;71(2):458-468. doi:10.1002/mrm.24703

27. Wright A, Murali-Manohar S, Borbath T, Henning A. Longitudinal Relaxation Times of Metabolites in vivo at 9.4T. In: *27th Annu Meet Exhib Int Soc Magn Reson Med (ISMRM 2019)*. Montréal, QC, Canada; 2019.

28. Hagberg GE, Bause J, Ethofer T, et al. Whole brain MP2RAGE-based mapping of the longitudinal relaxation time at 9.4T. *Neuroimage*. 2017;144:203-216. doi:10.1016/j.neuroimage.2016.09.047

29. Murali-Manohar S, Borbath T, Wright AM, Henning A. Quantification of Human Brain Metabolites using Two-Dimensional J-Resolved Metabolite-Cycled semiLASER at 9.4 T. *Annu Proc Interantional Soc Magn Reson Med*. 2021;0284.

30. Avdievich NI, Giapitzakis I-A, Pfrommer A, Henning A. Decoupling of a tight-fit transceiver phased array for human brain imaging at 9.4T: Loop overlapping rediscovered. *Magn Reson Med*. 2018;79(2):1200-1211. doi:10.1002/mrm.26754

31. Giapitzakis I-A, Shao T, Avdievich N, Mekle R, Kreis R, Henning A. Metabolite-cycled STEAM and semi-LASER localization for MR spectroscopy of the human brain at 9.4T. *Magn Reson Med*. 2018;79(4):1841-1850. doi:10.1002/mrm.26873

32. Murali-Manohar S, Borbath T, Wright AM, Soher B, Mekle R, Henning A. T2 relaxation times of macromolecules and metabolites in the human brain at 9.4 T. *Magn Reson Med*. 2020. doi:10.1002/mrm.28174

33. Giapitzakis IA, Avdievich N, Henning A. Characterization of macromolecular baseline of human brain using metabolite cycled semi-LASER at 9.4T. *Magn Reson Med*. 2018;80(2):462-473. doi:10.1002/mrm.27070

34. Murali-Manohar S, Wright AM, Borbath T, Avdievich NI, Henning A. A novel method to measure T_1-relaxation times of macromolecules and quantification of the macromolecular resonances. *Magn Reson Med*. 2021;85(2):601-614. doi:10.1002/mrm.28484

35. Gruetter R, Tkáč I. Field mapping without reference scan using asymmetric echo-planar techniques. *Magn Reson Med*. 2000;43(2):319-323. doi:10.1002/(SICI)1522-2594(200002)43:2<319::AID-MRM22>3.0.CO;2-1

36. Mekle R, Mlynárik V, Gambarota G, Hergt M, Krueger G, Gruetter R. MR spectroscopy of the human brain with enhanced signal intensity at ultrashort echo times on a clinical platform at 3T and 7T. *Magn Reson Med*. 2009;61(6):1279-1285. doi:10.1002/mrm.21961

37. Versluis MJ, Kan HE, Van Buchem MA, Webb AG. Improved signal to noise in proton spectroscopy of the human calf muscle at 7 T using localized B1 calibration. *Magn Reson Med*. 2010;63(1):207-211. doi:10.1002/mrm.22195

38. Schulte RF, Boesiger P. ProFit: Two-dimentional prior-knowledge fitting of J-resolved spectra. *NMR Biomed*. 2006;19(2):255-263. doi:10.1002/nbm.1026

39. Near J, Harris AD, Juchem C, et al. Preprocessing, analysis and quantification in single-voxel magnetic resonance spectroscopy: experts' consensus recommendations. *NMR Biomed*. February 2020:e4257. doi:10.1002/nbm.4257

40. Ashburner J, Barnes G, Chen C, et al. *SPM12 Manual*. Wellcome Trust Centre for Neuroimaging, London, UK; 2014.

41. Govindaraju V, Young K, Maudsley AA. Proton NMR chemical shifts and coupling constants for brain metabolites. *NMR Biomed*. 2000;13(3):129-153. doi:10.1002/1099-1492(200005)13:3<129::AID-NBM619>3.0.CO;2-V

42. Near J, Evans CJ, Puts NAJ, Barker PB, Edden RAE. *J* -difference editing of gamma-aminobutyric acid (GABA): Simulated and experimental multiplet patterns. *Magn Reson Med*. 2013;70(5):1183-1191. doi:10.1002/mrm.24572

43. Ernst T, Kreis R, Ross B. Absolute Quantitation of Water and Metabolites in the Human Brain. I. Compartments and Water. *J Magn Reson Ser B*. 1993;102(1):1-8. doi:10.1006/jmrb.1993.1055

44. Rieth KG, Fujiwara K, Di Chiro G, et al. Serial measurements of CT attenuation and specific gravity in experimental cerebral edema. *Radiology*. 1980;135(2):343-348. doi:10.1148/radiology.135.2.6768102

45. Torack RM, Alcala H, Gado M, Burton R. Correlative Assay of Computerized Cranial Tomography (CCT), Water Content and Specific Gravity in Normal and Pathological Postmortem Brain. *J Neuropathol Exp Neurol*. 1976;35(4):385-392. doi:10.1097/00005072-197607000-00001

46. Brooks RA, Chiro G Di, Keller MR. Explanation of Cerebral White-Gray Contrast in Computed Tomography. *J Comput Assist Tomogr*. 1980;4(4):489-491. doi:10.1097/00004728-198008000-00016

47. Gasparovic C, Song T, Devier D, et al. Use of tissue water as a concentration reference for proton spectroscopic imaging. *Magn Reson Med*. 2006;55(6):1219-1226. doi:10.1002/mrm.20901

48. Wright AM, Murali-Manohar S, Henning A. Relaxation corrected and Sequence-dependent Macromolecule Baseline Model. In: *ISMRM*. ; 2019:2247.

49. Deelchand DK, Moortele P-F Van de, Adriany G, et al. In vivo 1H NMR spectroscopy of the human brain at 9.4 T: Initial results. *J Magn Reson*. 2010;206(1):74-80. doi:10.1016/J.JMR.2010.06.006

50. Mekle R, Mlynárik V, Gambarota G, Hergt M, Krueger G, Gruetter R. MR spectroscopy of the human brain with enhanced signal intensity at ultrashort echo times on a clinical platform at 3T and 7T. *Magn Reson Med*. 2009;61(6):1279-1285. doi:10.1002/mrm.21961

51. Marjańska M, Auerbach EJ, Valabrègue R, Van de Moortele P-F, Adriany G, Garwood M. Localized ^{1}H NMR spectroscopy in different regions of human brain *in vivo* at 7 T: T_2 relaxation times and concentrations of cerebral metabolites. *NMR Biomed*. 2012;25(2):332-339. doi:10.1002/nbm.1754

52. Murali-Manohar S, Borbath T, Wright AM, Soher B, Mekle R, Henning A. T_2 relaxation times of macromolecules and metabolites in the human brain at 9.4 T. *Magn Reson Med*. 2020;84(2):542-558. doi:10.1002/mrm.28174

53. Provencher SW. Automatic quantitation of localized in vivo 1H spectra with LCModel. *NMR*

Biomed. 2001;14(4):260-264. doi:10.1002/nbm.698

54. Martin Bland J, Altman DG. STATISTICAL METHODS FOR ASSESSING AGREEMENT BETWEEN TWO METHODS OF CLINICAL MEASUREMENT. *Lancet*. 1986;327(8476):307-310. doi:10.1016/S0140-6736(86)90837-8

55. Behar KL, Rothman DL, Spencer DD, Petroff OAC. Analysis of macromolecule resonances in1H NMR spectra of human brain. *Magn Reson Med*. 1994;32(3):294-302. doi:10.1002/mrm.1910320304

56. Giapitzakis I-A, Avdievich N, Henning A. Characterization of macromolecular baseline of human brain using metabolite cycled semi-LASER at 9.4T. *Magn Reson Med*. 2018;80(2):462-473. doi:10.1002/mrm.27070

57. Lopez-Kolkovsky AL, Mériaux S, Boumezbeur F. Metabolite and macromolecule T 1 and T 2 relaxation times in the rat brain in vivo at 17.2T. *Magn Reson Med*. 2016;75(2):503-514. doi:10.1002/mrm.25602

58. Borbath T, Murali-Manohar S, Wright AM, Henning A. In vivo characterization of downfield peaks at 9.4 T: T_2 relaxation times, quantification, pH estimation, and assignments. *Magn Reson Med*. 2021;85(2):587-600. doi:10.1002/mrm.28442

59. Fichtner ND, Giapitzakis IA, Avdievich N, et al. In vivo characterization of the downfield part of 1H MR spectra of human brain at 9.4 T: Magnetization exchange with water and relation to conventionally determined metabolite content. *Magn Reson Med*. 2018;79(6):2863-2873. doi:10.1002/mrm.26968

60. Nagarajan R, Ramadan S, Thomas MA. Detection of Amide and Aromatic Proton Resonances of Human Brain Metabolites Using Localized Correlated Spectroscopy Combined with Two Different Water Suppression Schemes. *Magn Reson Insights*. 2010;4:MRI.S4739. doi:10.4137/MRI.S4739

61. Borbáth T, Murali-Manohar S, Henning A. Towards a Fitting Model of Macromolecular Spectra: Amino Acids. In: *ISMRM*. ; 2019:1068.

62. Wyss PO, Bianchini C, Scheidegger M, et al. In vivo estimation of transverse relaxation time constant (T 2) of 17 human brain metabolites at 3T. *Magn Reson Med*. 2018;80(2):452-461. doi:10.1002/mrm.27067

63. Mekle R, Mlynárik V, Gambarota G, Hergt M, Krueger G, Gruetter R. MR spectroscopy of the human brain with enhanced signal intensity at ultrashort echo times on a clinical platform at 3T and 7T. *Magn Reson Med*. 2009;61(6):1279-1285. doi:10.1002/mrm.21961

64. Deelchand DK, Moortele PF Van De, Adriany G, et al. In vivo1H NMR spectroscopy of the human brain at 9.4 T: Initial results. *J Magn Reson*. 2010;206(1):74-80. doi:10.1016/j.jmr.2010.06.006

65. Marjańska M, Auerbach EJ, Valabrègue R, Van de Moortele PF, Adriany G, Garwood M. Localized 1H NMR spectroscopy in different regions of human brain in vivo at 7T: T 2 relaxation times and concentrations of cerebral metabolites. *NMR Biomed*. 2012;25(2):332-339. doi:10.1002/nbm.1754

66. Baeshen A, Wyss PO, Henning A, et al. Test–Retest Reliability of the Brain Metabolites GABA and Glx With JPRESS, PRESS, and MEGA-PRESS MRS Sequences in vivo at 3T. *J Magn Reson Imaging*. 2020;51(4):1181-1191. doi:10.1002/jmri.26921

List of Figures:

Figure 1: Pulse sequence diagram of J-resolved metabolite-cycled semiLASER localization scheme. The two inversion pulses were turned off when acquiring the metabolite spectra. For the acquisition of macromolecular spectra, double inversion recovery technique was used with TI_1/TI_2 set to 2360/625 ms. The indirect dimension is created by increasing the time interval between the last two AFP pulses by $\Delta t/2$. Both the sequences have maximum echo sampling scheme implemented i.e., acquisition begins right after the final crusher gradient of the last AFP.

Figure 2: (Top to bottom) 2D J-resolved MC semiLASER spectra from Braino phantom containing NAA, Cr, Cho, Glu and Lac with n = 50 and Δt = 2, 3 and 4 ms. White arrows indicate the t_1-ridges as a result of t_1 noise and truncation sinc artifacts in the indirect dimension. The ridges are strongly pronounced when TE_{max} = 124 ms and minimum when TE_{max} = 224 ms.

Figure 3: a) 2D metabolite spectrum from Braino phantom (n = 85, Δt = 2ms) in magnitude mode b) Zoomed in view of the lactate peak showing a J-resolved doublet but barely any J-refocused peaks. An 86% suppression (considering Lac peaks at 1.31 and 4.09 ppm since they have a maximum separation of values in the observable range of the spectrum) of the J-refocused peaks is expected when calculated as suggested by Lin et al[6] resulting in barely any visible J-refocused peaks. This in turn leads to maximum intensity of the J-resolved peaks.

Figure 4: 2D J-resolved MC semiLASER spectrum from a representative subject with n = 85 and Δt = 2 ms. The figure inlay shows the voxel positioning on the MP2RAGE image in transversal view. Additionally, the observed metabolites are labeled in the figure.

Figure 5: 2D DIR J-resolved MC semiLASER (TI_1/TI_2: 2360/625 ms, n = 60, Δt = 2 ms) summed spectrum from five healthy volunteers. The subscripts in the labelled MM peaks are the chemical shift in ppm at which the respective MM resonance occurs.

Figure 6: a) Subject-wise summed (eleven healthy volunteers) two-dimensional downfield (5.1 to 9.5 ppm) spectrum b) Low SNR NAD^+ peaks of nicotinamide moiety at 8.7 and 9.45 ppm detected in a zoomed view.

Figure 7: A representative fit of 2D J-resolved MC semiLASER data acquired at 9.4 T. The figure shows the data, the fit and the residual from top to bottom scaled similarly. The fitting was performed in ProFit 2.0 using a tailored 2D basis set created using VesPA.

Figure 8: The figure shows the metabolite concentration values in the occipital lobe of healthy volunteers at 9.4T measured using 2D J-resolved MC semiLASER localization technique. The concentration values obtained using 2D spectral fitting for Asp, Gln and GABA are in line with previous literature. However, the previous 1D MRS studies[27,48,52] using MC semiLASER reported elevated values of these metabolites in comparison to previous literature. In conclusion, 2D MRS may perform better for the quantification of overlapped and J-coupled resonances such as Gln and GABA, and additionally also allows for the quantification of Glc and Lac.

Table 1: Quantification results from this study in mmol/kg are reported for 16 metabolites after correcting for tissue content and water and metabolite relaxation times. T_1 and T_2 relaxation times at 9.4 T from Wright et al[27,48] and Murali-Manohar et al[52] were used to account for the T_1-weighting

of metabolites. Additionally, results from the previous 1D MRS studies[27,48–52] are also presented for comparison. The tissue content and water and metabolite relaxation times included for these studies are briefly given in the Discussion section.

Figure 9: Bland-Altman plots[54] for 12 metabolites comparing concentration values from this study with the 1D MRS study. The center line shows the mean value of the concentrations of respective metabolite between the measurements performed using 1D and 2D MRS. The lines at the top and the bottom represent mean + 1.96 SD and mean – 1.96 SD respectively.

Supporting information figure captions

Supporting information figure S1: (Top to bottom) Phantom spectrum with TE_{max} = 100, 99, and 100 ms for Δt: 2 ms (n: 50), 3 ms (n: 33), and 4 ms (n: 25) respectively. SNR is higher when Δt: 2 ms compared to 3 and 4 ms; t_1 ridges are not seen to be impacted.

Supporting information figure S2: Box plots of metabolite concentrations in mmol/kg measured using 2D J-resolved MC semiLASER spectra. Horizontal lines inside the box plots show median values (50% quartile). The bottom and the top boundaries of the boxes indicate 25% and 75% quartiles respectively. Plus signs (+) show outlier values.

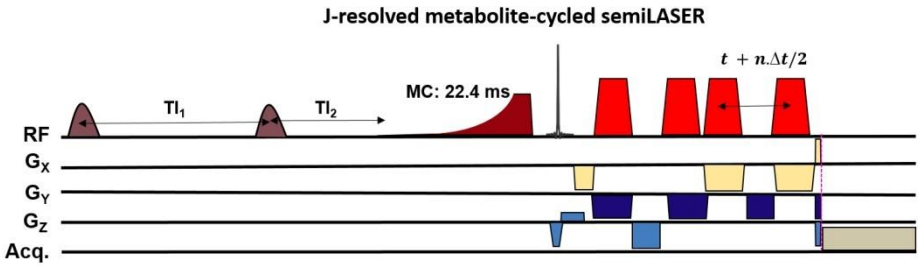

Figure 1: Pulse sequence diagram of J-resolved metabolite-cycled semiLASER localization scheme. The two inversion pulses were turned off when acquiring the metabolite spectra. For the acquisition of macromolecular spectra, double inversion recovery technique was used with TI_1/TI_2 set to 2360/625 ms. The indirect dimension is created by increasing the time interval between the last two AFP pulses by Δt/2. Both the sequences have maximum echo sampling scheme implemented i.e., acquisition begins right after the final crusher gradient of the last AFP.

274x100mm (150 x 150 DPI)

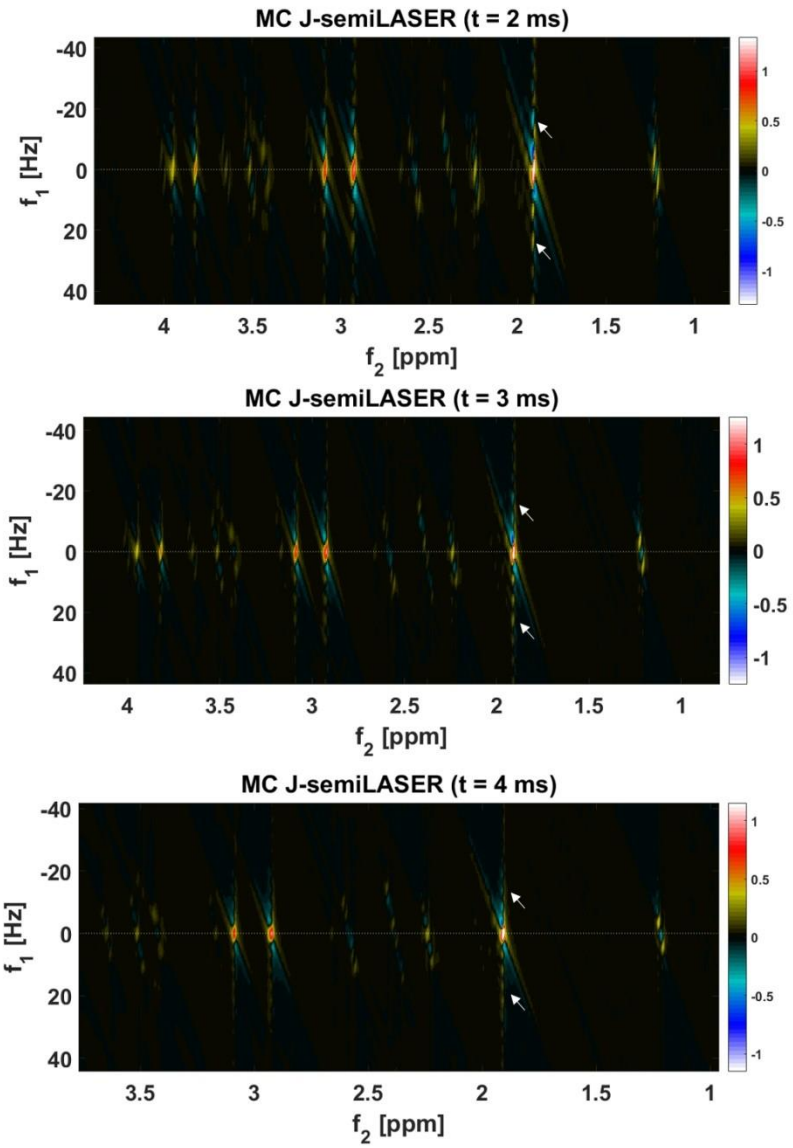

Figure 2: (Top to bottom) 2D J-resolved MC semiLASER spectra from Braino phantom containing NAA, Cr, Cho, Glu and Lac with n = 50 and Δt = 2, 3 and 4 ms. White arrows indicate the t_1-ridges as a result of t_1 noise and truncation sinc artifacts in the indirect dimension. The ridges are strongly pronounced when TE_{max} = 124 ms and minimum when TE_{max} = 224 ms.

204x263mm (150 x 150 DPI)

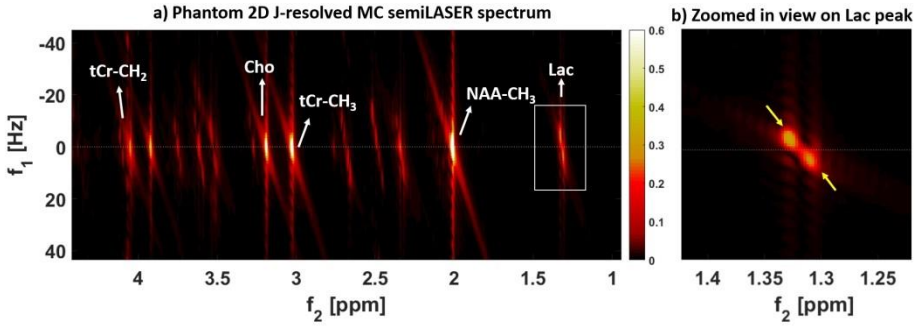

Figure 3: a) 2D metabolite spectrum from Braino phantom (n = 85, Δt = 2ms) in magnitude mode b) Zoomed in view of the lactate peak showing a J-resolved doublet but barely any J-refocused peaks. An 86% suppression (considering Lac peaks at 1.31 and 4.09 ppm since they have a maximum separation of values in the observable range of the spectrum) of the J-refocused peaks is expected when calculated as suggested by Lin et al[6] resulting in barely any visible J-refocused peaks. This in turn leads to maximum intensity of the J-resolved peaks.

373x134mm (150 x 150 DPI)

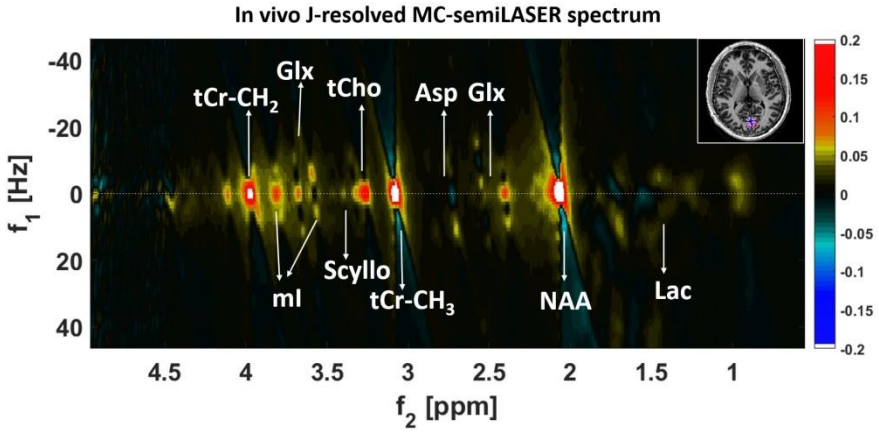

Figure 4: 2D J-resolved MC semiLASER spectrum from a representative subject with n = 85 and Δt = 2 ms. The figure inlay shows the voxel positioning on the MP2RAGE image in transversal view. Additionally, the observed metabolites are labeled in the figure.

352x169mm (150 x 150 DPI)

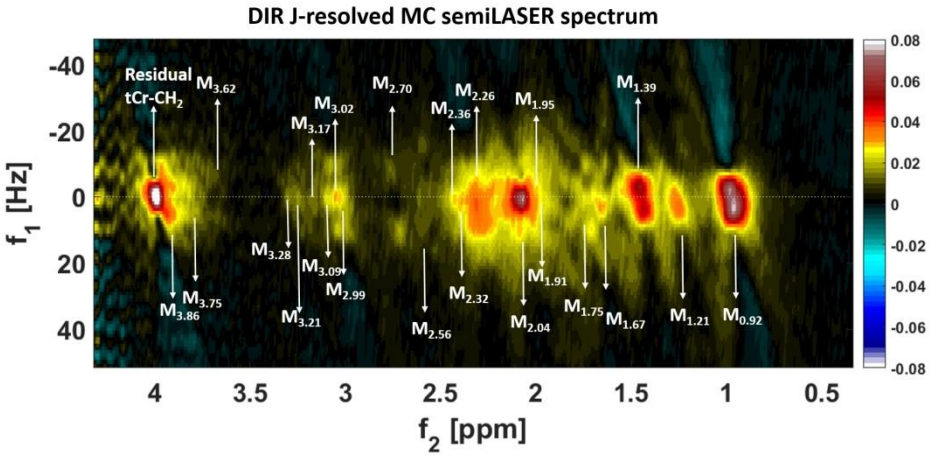

Figure 5: 2D DIR J-resolved MC semiLASER (TI_1/TI_2: 2360/625 ms, n = 60, Δt = 2 ms) summed spectrum from five healthy volunteers. The subscripts in the labelled MM peaks are the chemical shift in ppm at which the respective MM resonance occurs.

336x166mm (150 x 150 DPI)

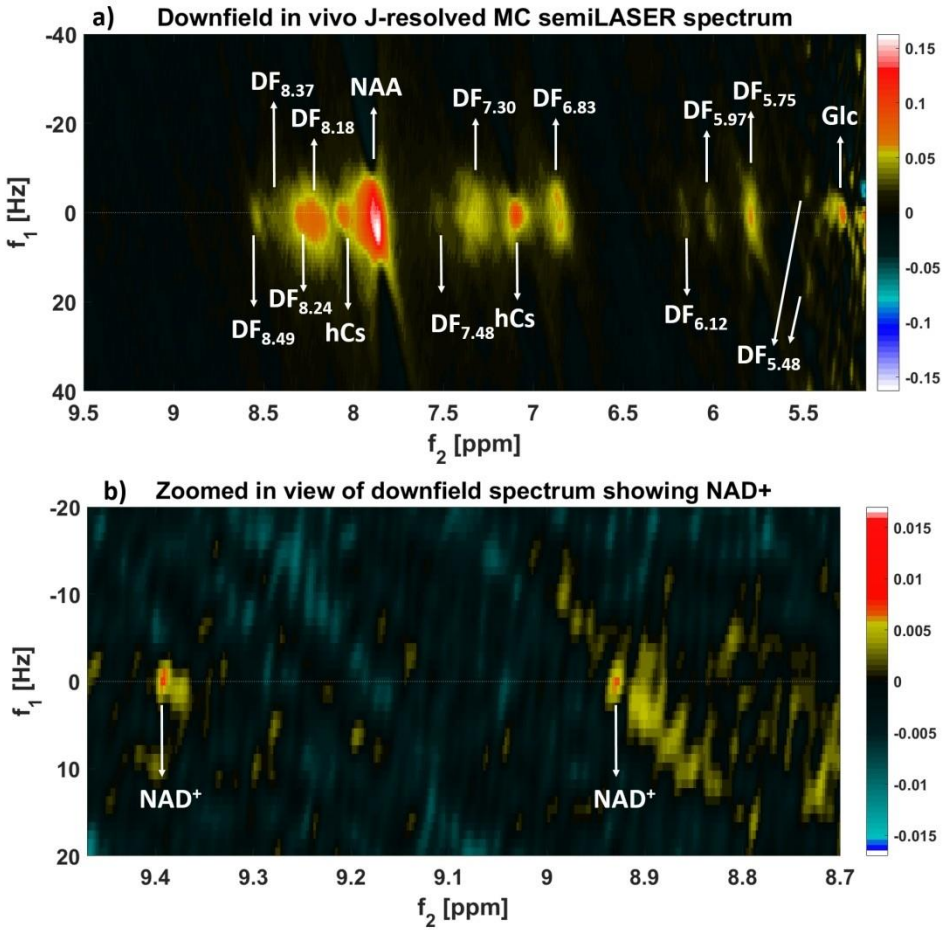

Figure 6: a) Subject-wise summed (eleven healthy volunteers) two-dimensional downfield (5.1 to 9.5 ppm) spectrum b) Low SNR NAD^+ peaks of nicotinamide moiety at 8.7 and 9.45 ppm detected in a zoomed view.
352x363mm (150 x 150 DPI)

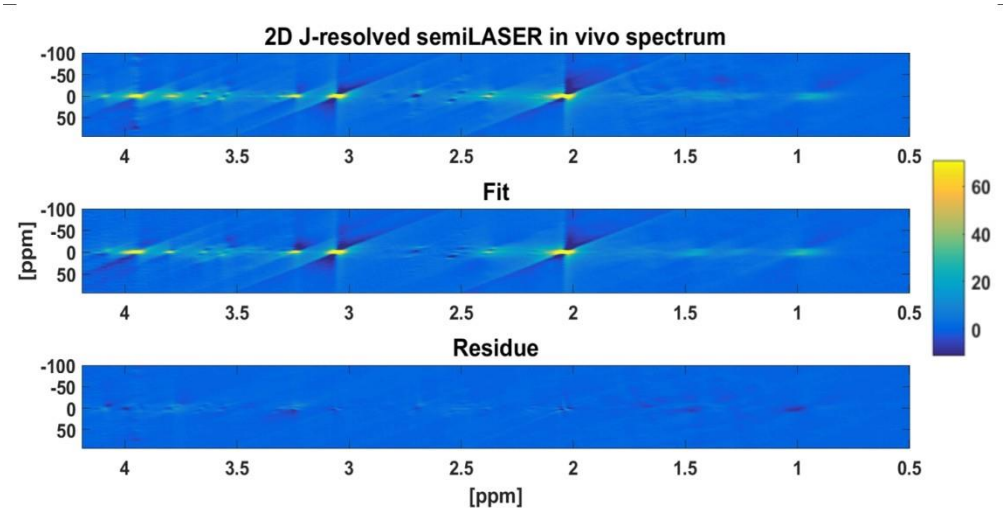

Figure 7: A representative fit of 2D J-resolved MC semiLASER data acquired at 9.4 T. The figure shows the data, the fit and the residual from top to bottom scaled similarly. The fitting was performed in ProFit 2.0 using a tailored 2D basis set created using VesPA.

252x139mm (150 x 150 DPI)

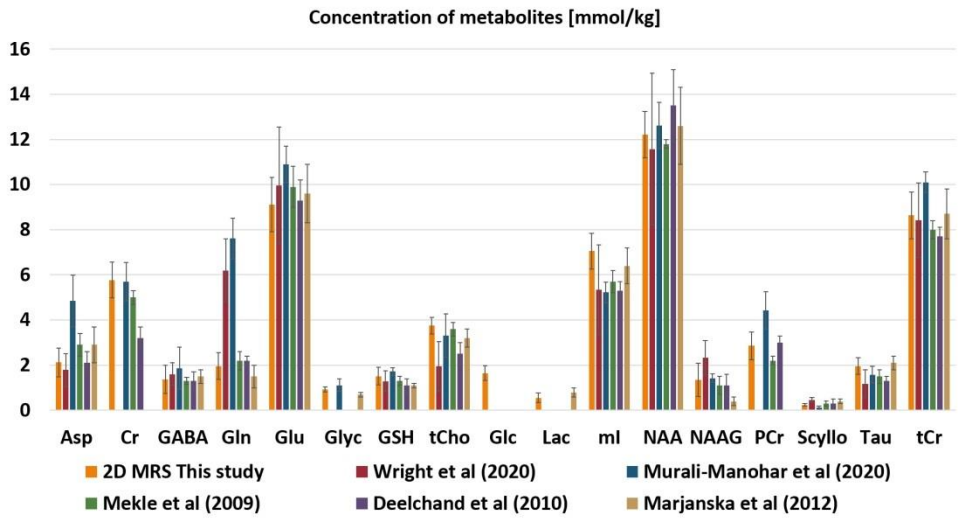

Figure 8: The figure shows the metabolite concentration values in the occipital lobe of healthy volunteers at 9.4T measured using 2D J-resolved MC semiLASER localization technique. The concentration values obtained using 2D spectral fitting for Asp, Gln and GABA are in line with previous literature. However, the previous 1D MRS studies[27,48,52] using MC semiLASER reported elevated values of these metabolites in comparison to previous literature. In conclusion, 2D MRS may perform better for the quantification of overlapped and J-coupled resonances such as Gln and GABA, and additionally also allows for the quantification of Glc and Lac.

336x187mm (150 x 150 DPI)

Metabolites	Concentration values [mmol/kg]					
	2D MRS Study (This work)	1D MRS Study 9.4 T (2021)	Murali-Manohar 9.4 T (2020)	Mekle 7T (2009)	Deelchand 9.4T (2010)	Marjanska 7T (2012)
Asp	2.13 ± 0.64	1.79 ± 1.0	4.84 ± 1.15	2.9 ± 0.5	2.1 ± 0.5	2.9 ± 0.8
Cr	5.77 ± 0.80	-	5.7 ± 0.85	5 ± 0.3	3.2 ± 0.5	-
GABA	1.37 ± 0.62	1.60 ± 0.61	1.87 ± 0.92	1.3 ± 0.15	1.3 ± 0.4	1.5 ± 0.3
Glc	1.65 ± 0.33	-	-	-	-	-
Gln*	1.96 ± 0.59	6.20 ± 0.95	7.61 ± 0.91	2.2 ± 0.4	2.2 ± 0.2	1.5 ± 0.5
Glu	9.11 ± 1.21	9.97 ± 1.07	10.9 ± 0.8	9.9 ± 0.9	9.3 ± 0.9	9.6 ± 1.3
Glyc	0.93 ± 0.11	-	1.11 ± 0.28	-	-	0.7 ± 0.1
GSH	1.51 ± 0.39	1.29 ± 0.24	1.72 ± 0.16	1.3 ± 0.2	1.1 ± 0.3	1.1 ± 0.1
Lac	0.55 ± 0.22	-	-	0.7 ± 0.1	0.5 ± 0.1	0.8 ± 0.2
mI	7.05 ± 0.79	5.35 ± 0.65	5.22 ± 0.45	5.7 ± 0.5	5.3 ± 0.4	6.4 ± 0.8
NAA	12.20 ± 1.03	11.57 ± 0.77	12.61 ± 1.02	11.8 ± 0.2	13.5 ± 1.6	12.6 ± 1.7
NAAG	1.35 ± 0.73	2.33 0.42	1.42 ± 0.19	1.1 ± 0.4	1.1 ± 0.5	0.4 ± 0.2
PCr	2.86 ± 0.61	-	4.43 ± 0.83	2.2 ± 0.19	3 ± 0.3	-
Scyllo	0.24 ± 0.06	0.46 ± 0.26	0.13 ± 0.06	0.3 ± 0.12	0.3 ± 0.2	0.4 ± 0.1
Tau*	1.96 ± 0.37	1.18 ± 0.51	1.58 ± 0.37	1.5 ± 0.3	1.3 ± 0.2	2.1 ± 0.3
tCho	3.75 ± 0.38	1.94 ± 0.85	3.31 ± 0.95	3.6 ± 0.3	2.5 ± 0.5	-
tCr	8.54 ± 1.11	8.42 ± 0.83	10.10 ± 0.46	8.0 ± 0.4	7.7 ± 0.4	8.7 ± 1.1

Table 1: Quantification results from this study in mmol/kg are reported for 16 metabolites after correcting for tissue content and water and metabolite relaxation times. T_1 and T_2 relaxation times at 9.4 T from Wright et al[27,48] and Murali-Manohar et al52 were used to account for the T1-weighting of metabolites. Additionally, results from the previous 1D MRS studies[27,48–52] are also presented for comparison. The tissue content and water and metabolite relaxation times included for these studies are briefly given in the Discussion section.

234x247mm (150 x 150 DPI)

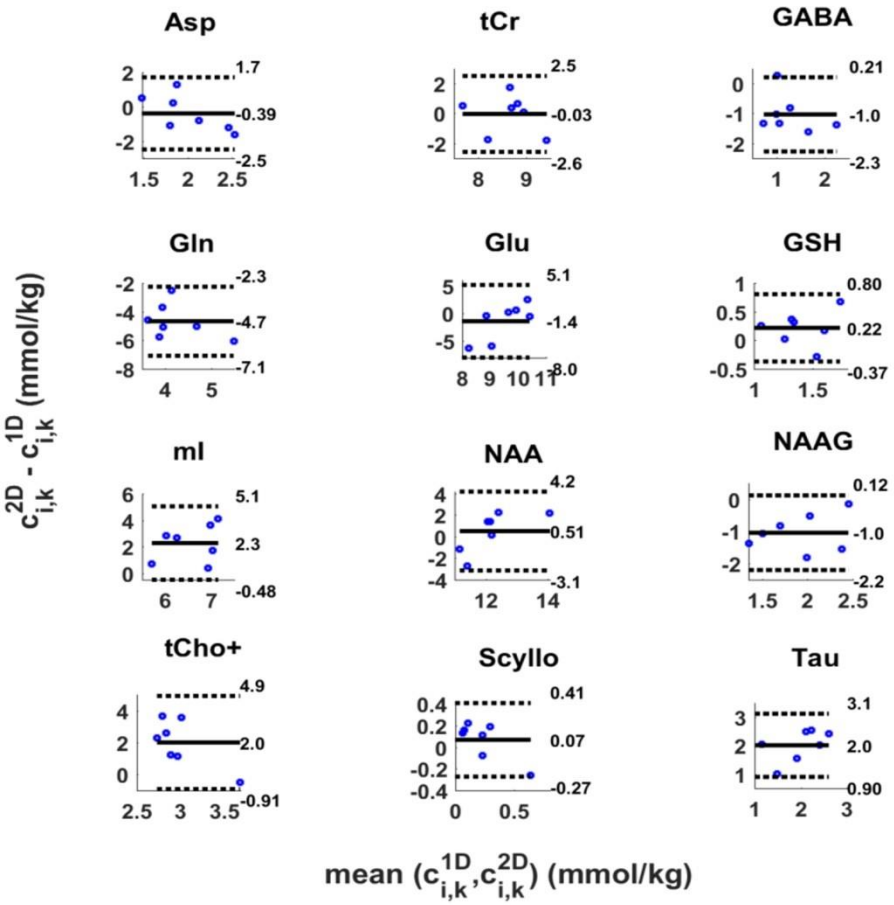

Figure 9: Bland-Altman plots[54] for 12 metabolites comparing concentration values from this study with the 1D MRS study. The center line shows the mean value of the concentrations of respective metabolite between the measurements performed using 1D and 2D MRS. The lines at the top and the bottom represent mean + 1.96 SD and mean – 1.96 SD respectively.

288x262mm (150 x 150 DPI)

Supporting information figure S1: (Top to bottom) Phantom spectrum with TE_{max} = 100, 99, and 100 ms for Δt: 2 ms (n: 50), 3 ms (n: 33), and 4 ms (n: 25) respectively. SNR is higher when Δt: 2 ms compared to 3 and 4 ms; t_1 ridges are not seen to be impacted.

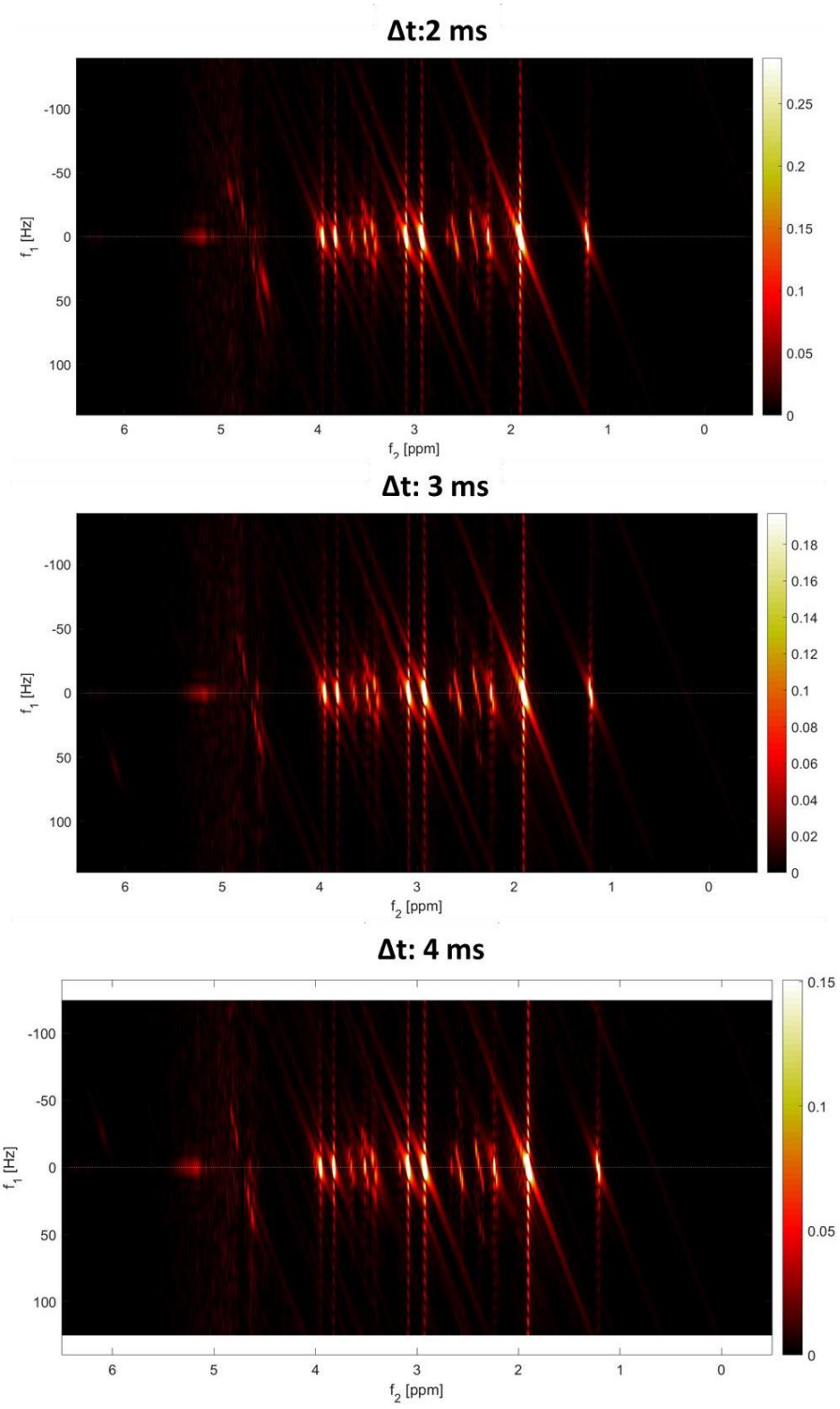

Supporting information figure S2: Box plots of metabolite concentrations in mmol/kg measured using 2D J-resolved MC semiLASER spectra. Horizontal lines inside the box plots show median values (50% quartile). The bottom and the top boundaries of the boxes indicate 25% and 75% quartiles respectively. Plus signs (+) show outlier values.